Ministry of Science and High Education of Russian Federation

Ivanovo State Polytechnic University

Jia Shuang

IMPROVEMENT OF THE DESIGN TECHNOLOGY FOR MEN'S RAGLAN COATS

Dissertation

for the degree of Candidate of Technical Sciences

Scientific specialty 2.6.16 — Technology of Light Industry Products
(Garment Pattern Design)

Scientific adviser -Doctor of Sc., Prof.
Victor Evg. Kuzmichev

Ivanovo − 2026

CONTENTS

GENERAL CHARACTERISTICS OF THE WORK

Relevance of the topic. In the context of the digital transformation of the garment industry, the traditional process of artistic and technical garment design, including model development, pattern construction, and the manufacture of a physical sample, increasingly uses the advantages of three-dimensional modelling and neural networks. To ensure the comparability of the results of physical fitting, three-dimensional virtual fitting, and images generated using artificial intelligence, a unified and reproducible system of quantitative measurements is required. Raglan-sleeve garments impose increased requirements on the accuracy of coordination between, on the one hand, construction parameters, including the configuration of the shoulder and armhole lines and the combination of design ease allowances, and, on the other hand, the volume-silhouette shape. Existing methods for constructing raglan sleeve patterns differ substantially, which, even with identical body measurements, leads to noticeable variations in sleeve shape and changes in garment fit on the figure. Therefore, the development of a digital design technology for men's raglan coats that integrates parametric pattern construction, three-dimensional virtual try-on and computer tools within a unified measurable system is a relevant scientific and technical task.

Degree of development of the topic. Digital garment design methods have been developed in the works of Russian researchers from higher education institutions, including A.N. Kosygin Russian State University (E.G. Andreeva, I.A. Petrosova, V.V. Getmantseva, and others), Saint Petersburg State University of Industrial Technologies and Design (N.N. Razdomakhin, E.Ya. Surzhenko, A.Yu. Moskvin, M.A. Moskvina), Don State Technical University (I.V. Cherunova), Kazan National Research Technological University, and Ivanovo State Polytechnic University (V.E. Kuzmichev, Xia Peng, Luo Yun, Li Yue, Yang Jiaqi, Wang Sida, and others). Scientific organizations of the People's Republic of China, including The Hong Kong Polytechnic University, Beijing Institute of Fashion Technology, Donghua University in Shanghai, and others, are conducting comprehensive research on the digitalization of artistic and industrial garment design processes. Active research is also carried out by Russian and international companies developing software for three-dimensional garment design, including ASSOL, Texel, Style3D, CLO3D, OptiTex, Marvelous Designer, and others. The application of neural networks to garment generation and virtual try-on has been examined in studies devoted to VITON, WarpDiffusion, CG-VTON, and other methods. However, the literature still insufficiently presents an integrated approach to a unified system of 2D and 3D quantitative assessment that links flat pattern drawings, two-dimensional and three-dimensional images of the human figure, and garments.

Connection with scientific programs. The research was carried out under Russian Science Foundation grant No. 25-11-00022, "Technology for Virtual Testing of

Textile Materials for 3D Garment Modeling" (2025–2027).

The aim of the research. The research aims to reduce the time required for preparation for industrial production and to improve the quality of new raglan coat models.

To achieve the aim, the following tasks were solved:

1. To develop an anthropometric database of typical male body shapes built in the form of a set of projection parameters required for generating frontal and profile silhouettes of the " body + raglan coat" system.

2. To develop a grouping of volume-silhouette shapes of raglan coats and a system of quantitative criteria for evaluating their fit on the body.

3. To improve the method for constructing raglan coats by incorporating into the pattern-making algorithm a system of equations linking pattern parameters with indicators of the designed volume-silhouette shape.

4. To develop and verify a multimodal algorithm for generating images of "body– raglan coat" systems using neural networks and to evaluate the accuracy of the generated images by comparing them with virtual and real garments.

5. To develop a direct design algorithm for raglan coats with specified indicators of volume-silhouette shape and fit criteria, as well as a reverse-engineering algorithm for reconstructing pattern details from photographs using all available digital tools, including 2D CAD, 3D CAD and neural networks.

6. To conduct industrial verification of the developed technologies and algorithms under the conditions of Chinese and Russian garment production.

The object of the research is the process of digital design of "body+ raglan coat" systems.

The subject of the research is the regularities of the influence of pattern construction parameters on the shape and fit of raglan coats in virtual and physical environments.

Research methods and tools. The study employed methods of system analysis and parametric construction of garment, body and pattern images; three-dimensional modelling and virtual fitting (Style3D version 9.0 and Rhinoceros version 7.0 software packages); analysis of multicomponent systems (Adobe Illustrator 2024 graphic editor); correlation and regression analysis (IBM SPSS Statistics version 26); statistical data processing; and prompt-engineering methods for image generation using Grok3 neural network developed by xAI.

The scientific novelty lies in the development of an integrated digital design technology for men's raglan coats that combines parametric pattern construction, three-dimensional virtual try-on and the generation of 2D and 3D images within a unified system of projection parameters. This system enables direct design from pattern-making to a specified volume-silhouette shape and reverse design from a coat

photograph to pattern-making. The following results were obtained for the first time:

1. A hierarchical system for the quantitative assessment of pattern drawings, figures, and garments based on projection parameters was proposed for the first time. The system includes criteria for bodice balance, the spatial relationship between sleeve and arm, and the grouping of volume-silhouette shapes of raglan coats.

2. Regression relationships were established between the key pattern parameters of raglan coats and fit indicators, making it possible to move from empirical forecasting to precise calculation.

3. The effectiveness of generating images of male figures and raglan coats using neural networks was substantiated. The method ensures deviations of projection dimensions of no more than 1.0 cm and surpasses traditional three-dimensional simulation in silhouette reproduction accuracy.

4. A complementary digital design algorithm was proposed, in which 3D simulation provides the coat structure and its connection with pattern drawings, whereas generation using neural networks improves photorealism and silhouette correspondence with physical prototypes.

The work corresponds to the following items of the passport of the scientific specialty:

8. Simulation modelling technologies for digital twins of fibres, yarns, materials, light industry products and human figures.

12. Anthropobiomechanical foundations and regularities in anthropometric data for constructing rational internal and external forms and structural details in the design of textile and light industry products in digital and real environments.

17. Development of methods for automation and optimization of the production of materials and textile and light industry products based on scientific forecasting, mathematical methods, neural networks, and artificial intelligence.

The theoretical significance of the research consists in the development of the scientific foundations of parametric garment design using a system of parameters as a universal measurement interface that links pattern drawings, 2D images, and three-dimensional images. The developed system of criteria and regression models deepens the understanding of relationships in the “bodu + pattern drawings + shape” system for raglan coats.

The practical significance of the completed research is as follows:

1. The obtained mathematical models make it possible to automate the correction of raglan sleeve pattern drawings at the production preparation stage.

2. The created databases of projection parameters of male figures and coats can be used to train specialized neural network models for the garment industry.

3. The developed criteria for evaluating fit and form were implemented at Polargoose Clothing Co., Ltd. (China) and at Open Joint-Stock Company “Sudar”

(Kovrov, Vladimir Region, Russia). This made it possible to shorten the preparation time for new models, reduce the number of fitting iterations from two to one, decrease the development cost of the first sample and the number of correction operations, improve quality through the introduction of quantitative fit evaluation criteria, and reduce the subjectivity of expert assessments.

Personal contribution of the author. At all stages of the research, the author, under the supervision of the scientific adviser, personally participated in setting the aim and formulating the main research tasks, planning and conducting experiments, discussing the obtained results, formulating conclusions, testing hypotheses, and preparing publication materials together with co-authors. The doctoral candidate's contribution to the published works ranges from 59% to 80%.

Provisions submitted for defense:

1. A system of indicators of volume-silhouette shape and criteria for evaluating the fit of raglan coats.

2. Methods for direct design (from patterns to shape) and reverse design (shape photograph to patterns) of raglan coats, which make it possible to obtain a volume-silhouette with specified indicators and to reconstruct part pattern drawings from a single photographic image.

3. A method for generating images of "figure – raglan coat" systems using neural networks, based on improved anthropometric databases and ensuring high reproduction accuracy while preserving the structure and shape of the coat.

The reliability of the results is confirmed by the use of a representative sample of research objects, including 23 tested sets of patterns, 230 photographs of raglan coats and 20 variants of male bodies of different fullness groups; the application of 3D simulation methods approved in scientific practice; statistical processing of measurement results at a confidence level of 95%; the high accuracy of the generated digital twins of figures and coats, with deviations of ±0.9 cm and ±2.4°; and the positive results of industrial verification of the developed models under the conditions of two real production enterprises.

Approbation of the work. The main results of the dissertation were reported and discussed at the national youth scientific and technical conferences with international participation "POISK" in 2024–2026 in Ivanovo.

Publications. Six research papers have been published on the topic of the dissertation, including two articles in peer-reviewed scientific journals included in the official list of recognized academic publications.

Structure and scope of the dissertation. The dissertation consists of an introduction, five chapters, a conclusion comprising the main findings and recommendations, a list of 139 references, and four appendices. The dissertation comprises 181 pages of main text and 38 pages of appendices and includes 77 figures

and 50 tables. The originality of the dissertation text is 97.45%.

INTRODUCTION

In the context of the digital transformation of the garment industry, the traditional process of artistic and technical clothing design, including model development, pattern construction, sample production, and post-fitting correction, is gradually expanding into a virtual and intelligent design environment. Men's raglan coats belong to garments of increased structural complexity, with their final shape depending on the coordinated interaction of the shoulder line, armhole region, sleeve construction, body morphology, and external silhouette. Consequently, the design of men's raglan coats requires highly specialized knowledge that enables simultaneous control over both pattern structure and the three-dimensional shape of the coat.

With the development of 3D virtual try-on, parametric pattern construction, digital anthropometry, and artificial intelligence, new technical conditions have emerged for designing garment structures and verifying results before physical sample production. Three-dimensional automated design systems allow pattern modeling on virtual bodies, while AI technologies can generate visual images of "body–garment" systems. To leverage these digital outputs in garment engineering, professional expertise in anthropometry, pattern design, garment shape evaluation, virtual try-on, and AI visualization must be translated into a measurable, comparable, and verifiable parameter system.

However, existing research remains limited by the disconnection of technical tools, inconsistency of evaluation criteria, insufficient linkage between pattern parameters and final garment shape, and the absence of quantitative verification for AI-generated garment images.

The objective of this study is to develop a digital design technology for men's raglan coats based on the integration of parametric pattern construction, 3Dvirtual try-on, and AI-based image generation. This objective is achieved through the creation of an anthropometric database of male bodies based on 2.5D projection parameters; the development of quantitative criteria for fit and volume-silhouette evaluation; the establishment of regression relationships between pattern and shape parameters; the construction of multimodal prompts for generating "body+coat" system images; and the validation of direct and inverse design algorithms in Chinese and Russian garment production environments.

CHAPTER 1. REVIEW OF DIGITAL TECHNOLOGIES AND ENGINEERING CHALLENGES IN RAGLAN COAT DESIGN

With the maturation of 3D modeling and virtual modeling based on CAD systems continue to develop, the traditional workflow of “pattern-driven + real sample verification” is transformed into a parallel system of “simulation + digital generation”[7,8]. Pattern-based 3D virtual try-on enables repeatedly output results under the same avatar and pose, allowing rapid structural modification and optimization according to the target silhouette, while preserving the relationship between pattern structure and garment shape[9]. Furthermore, the emergence of artificial intelligence (AI) has opened a transformative avenue for apparel design and engineering. Leveraging multimodal conditional inputs, AI can rapidly generate garment appearances at the image level and achieve transferable control over external silhouettes[10,11].

However, both digital approaches face a critical challenge: the inability to reconstruct and control the “ body+garment” system in virtual environments with high fidelity. The absence of a unified, reproducible, and quantitatively comparable measurement framework renders it difficult to validate structural and silhouette consistency across physical fitting, 3D simulations, and AI-generated outputs on a common scale. Consequently, discrepancies between virtual and real-world outcomes remain challenging to identify the source of deviations [12]. This issue is particularly pronounced in outerwear categories. The quality of an outer garment depends not only on localized fit but also more critically on the stability of its volumetric silhouette and the harmonious coordination of key structural zones. As a result, digitally generated outcomes may appear visually plausible yet still fall short of requirements in terms of quantitative validation, reproducibility, and readiness for actual production[13,14].

Raglan sleeves exhibit a characteristic feature of a seamless connection between the sleeve and bodice, requiring precise alignment among the shoulder line, armhole curve, and the outer sleeve-bodice silhouette[1,2]. Even minor adjustments in the coupled pattern structure can directly affect the bodice balance and the sleeve appearance[3]. In industrial practice, raglan sleeve pattern-making methods vary substantially[4]. Even under the same size specification, differences in pattern-making methods and digitalization routes can lead to observable variations in sleeve shape, thereby influencing both fit accuracy and silhouette stability[5,6].

To address these issues, the study develops a digital design framework for men's raglan coat by integrating pattern-based design, 3D virtual try-on, and AI-driven garment generation. The framework extends beyond traditional pattern making and fit evaluation to include virtual garment development, cross-route shape verification, AI-based silhouette generation, and the parameterized control of pattern structure. Accordingly, this chapter reviews the literature in four successive parts. First, it examines the

application of 3D CAD and virtual try-on in apparel design, with emphasis on their advantages and remaining limitations for outerwear verification. Second, it reviews the development of AI in apparel, particularly its application to garment generation and virtual try-on. Third, it discusses the engineering characteristics, pattern-making methods, and evaluation problems of raglan sleeves, which represent the core structural object of the present research. Finally, it defines the main research gaps, objectives, and technical framework of the thesis.

1.1. Application of 3D CAD in apparel design

In apparel design and product development, several 3D virtual design and try-on platforms have been widely adopted, such as Style 3D, CLO3D, OptiTex, Browzwear, and Marvelous Designer. These systems take 2D patterns as input and, after defining the avatar, posture, and fabric properties, generate 3D virtual garments and fitting results that are reproducible under identical conditions. In addition to visualizing garments, 3D CAD provides a pattern-driven environment in which garment shape, garment-body interaction, and local structural problems can be repeatedly observed and adjusted. This is especially important for outerwear with highly coupled structural regions.

However, the quality of current 3D simulations is still constrained by avatar accuracy, fabric-parameter calibration, pose setting, and the lack of unified evaluation criteria. Consequently, fitting results generated across different platforms or parameter configurations may still show noticeable discrepancies. For this reason, 3D virtual try-on remains an important but still incomplete digital route for the design and verification of men's raglan coats such as the shoulder, armhole, sleeve, and bodice areas.

Accordingly, this section reviews the main foundations of 3D-based apparel digitalization, including digital anthropometric databases and avatars, pattern-driven virtual try-on and garment-body interaction, fabric parameterization, relevant digital standards, and the remaining research gaps in 3D applications.

Digital anthropometric databases and avatars. Digital anthropometric databases and avatars provide the basic body data for 3D virtual try-on. Based on 3D body scanning and anthropometric measurements, avatars can be constructed for different body shapes and used as the body reference for virtual fit evaluation. The reliability of virtual simulation depends not only on database coverage but also on the accuracy of landmark identification, body-shape classification, and accurate reconstruction of local anatomical regions. This is particularly important in areas with complex local geometry, such as the shoulder and underarm, where local avatar errors can directly affect later garment simulation and shape evaluation.

The construction of digital avatars first depends on the acquisition of reliable 3D body data and the extraction of measurable anthropometric information. Previous studies

have shown that 3D scanning, parametric modeling, image-based reconstruction, and mobile body scanning can support the generation of digital human-body models and the extraction of key body measurements for garment design and personalized pattern development [61 – 63]. These methods improve the accessibility and coverage of body data, particularly for non-standard body shapes. However, measurement errors are still likely to occur in regions with high curvature variation, such as the neck – shoulder area, chest – back region, and upper arm. Therefore, accurate landmark-based correction remains necessary for stabilizing critical measurements in anatomically complex areas such as the shoulder and underarm.

3D anthropometric information has also been used for body-shape classification and structural grouping. Sun et al. classified upper-torso morphology, quantified neck-shoulder characteristics, and introduced spatial morphological descriptors to support pattern optimization, fit analysis, and structural adaptation [64,65,67]. These studies indicate that 3D data are used not only for modeling but also for body-type grouping. In particular, shoulder-region classification and parameterization provide data and methodological references for establishing a “sleeve+arm” system.

A further research focus concerns the accurate identification of body landmarks, the segmentation of body regions, and the reconstruction of digital human models. Studies by Chen *et al.* and Ryu *et al.* have improved landmark detection through geometric-feature analysis and automated recognition algorithms, including the recognition of difficult locations such as the axilla region [66-68]. Chi *et al.* combined scanning data, manual measurements, expert correction, and semantic information to improve reconstruction accuracy and generate more reliable 3D body models [64,69-71]. These results show that landmark accuracy directly affects avatar accuracy and, consequently, the reliability of subsequent pattern development and virtual try-on outputs. However, methods validated on a single body shape still show limited transferability across different body-type groups. Figure 1.1 shows the identification, segmentation, and reconstruction of body landmarks, as well as the correction of the basic block pattern based on body landmarks.

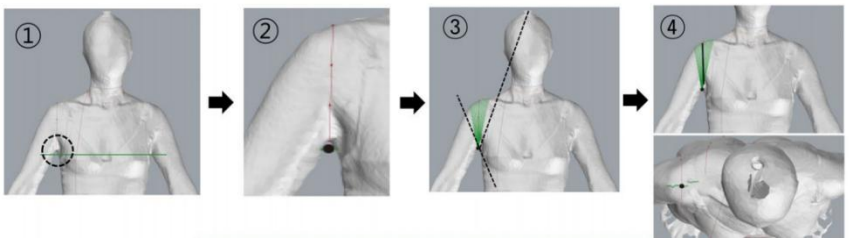

a

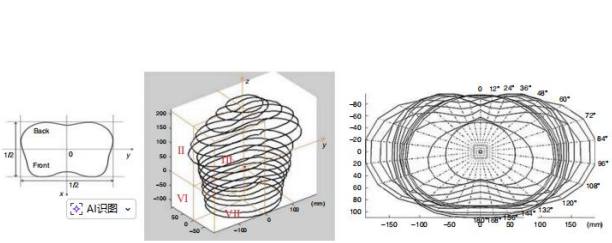

b

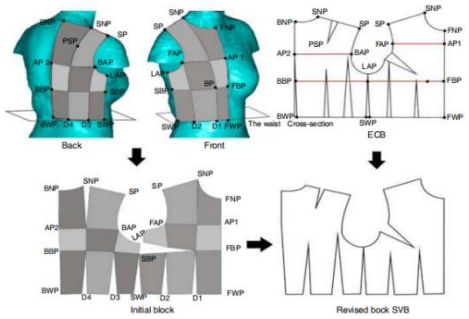

c

Figure 1.1 - Identification, segmentation, and reconstruction of body landmarks::a - armscye line and shoulder point search process [68]; b - body cross-section section in 3D coordinate system; c - 3D - to - 2D parametric pattern- making [70]; c - basic block pattern correction [64]

Many studies further applied 3D landmark detection, segmentation, and reconstruction to parametric pattern making and garment-shape model generation. In these studies, reconstructed avatar geometry is no longer treated only as the output of body modeling but also as a geometric basis for generating garment structures and 2D patterns. Kulińska *et al.* and Bao *et al.* extracted avatar landmarks and performed body-region partitioning and then used 3D surface flattening to enable 3D-to-2D parametric pattern generation[72,73]. Zhang *et al.* described garment ease and silhouette directly in a 3D environment and then used geometric parameters to generate garments in multiple sizes and styles [74,75]. Huang *et al.* further proposed a three-stage intelligent pattern-generation method, integrating avatar parameterization, ease allocation, 3D garment modeling, and 3D-to-2D pattern unfolding to produce well-fitted basic 2D patterns. Their experiments demonstrated the practical potential of this route for garment development[76].

Figure 1.2 shows the 3D-to-2D reverse-engineering route used for parametric garment pattern generation, in which 2D patterns are derived from a 3D human model with or without ease allowances.

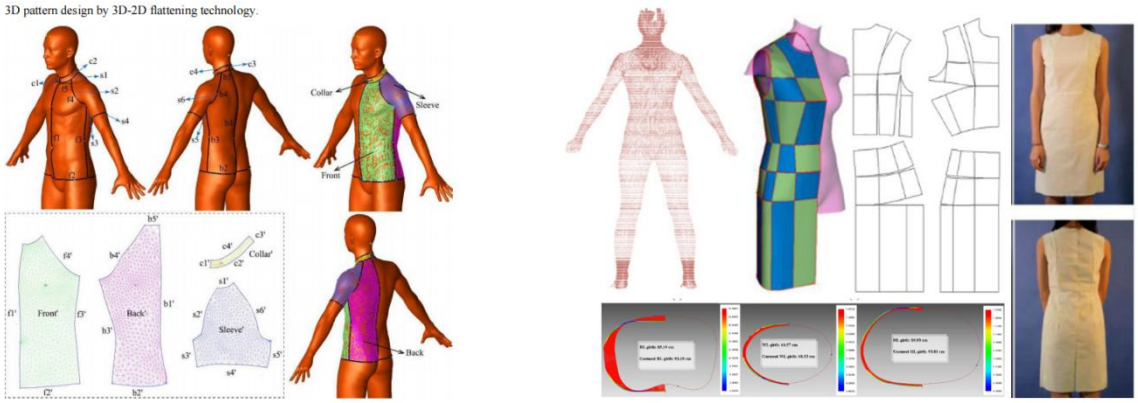

a *b*

Figure 1.2 - 3D-to-2D parametric garment pattern making: *a* - parametric pattern making without any ease allowances [59]; *b* - parametric pattern making with ease allowances at key areas(chest girth, waist girth, and hip girth) derived from cross-sectional analysis. [60]

Overall, digital anthropometric databases provide the data foundation for virtual try-on, fit evaluation, and parametric garment development. However, database coverage and avatar accuracy remain major constraints. Particularly in geometrically sensitive regions such as the shoulder and underarm, local avatar errors can be transferred into armhole-matching errors and sleeve-shape deviations, thereby reducing the reliability of subsequent virtual try-on results.

Pattern-driven 3D virtual try-on and garment–body interaction. Once digital avatars have been constructed, they can be integrated with 2D patterns in a unified virtual environment for pattern-driven 3D virtual try-on. In this process, garment structure, ease distribution, garment–body contact, and air-gap geometry can be observed, measured, and iteratively adjusted under controlled conditions. Studies by Sun *et al*. have shown that 3D virtual garment development can support a multi-stage workflow from design to evaluation and can also be used to compare discrepancies between virtual try-on outputs and physical garments [61,77,78].

A typical 3D virtual try-on workflow consists of six stages: avatar construction, 2D pattern input, digital stitching, fabric parameter assignment, try-on simulation, and fit-evaluation output. First, an avatar consistent with the research objective is selected or constructed, and the baseline posture and viewing conditions are fixed. Second, 2D patterns are imported or drafted, with sewing relations, layer hierarchy, and key construction points specified. Third, fabric parameters are assigned, and a static try-on simulation is carried out under the same posture and viewing conditions to obtain comparable virtual samples and evaluation results under unified conditions.

This process generally yields two categories of outputs: shape-related geometric outputs and fit-related simulation outputs. Shape-related geometric outputs include

volume–silhouette contours, key cross-sections, and air-gap distributions, which describe the garment's global volume silhouette and local ease allocation. Wang *et al.* have measured ease allowance directly in a 3D digital environment, established links between 2D patterns and 3D sleeve geometry, and analyzed the relationship between air gap and sleeve width under different fabric conditions [79,80,82]. These studies indicate that geometric measurements can provide direct feedback for pattern correction and help link pattern parameters to the resulting wearing space. Figure 1.3 shows the spatial relationship between 3D garment shape and the human body and the underlying 2D pattern, with particular emphasis on air-gap distribution and ease allowance.

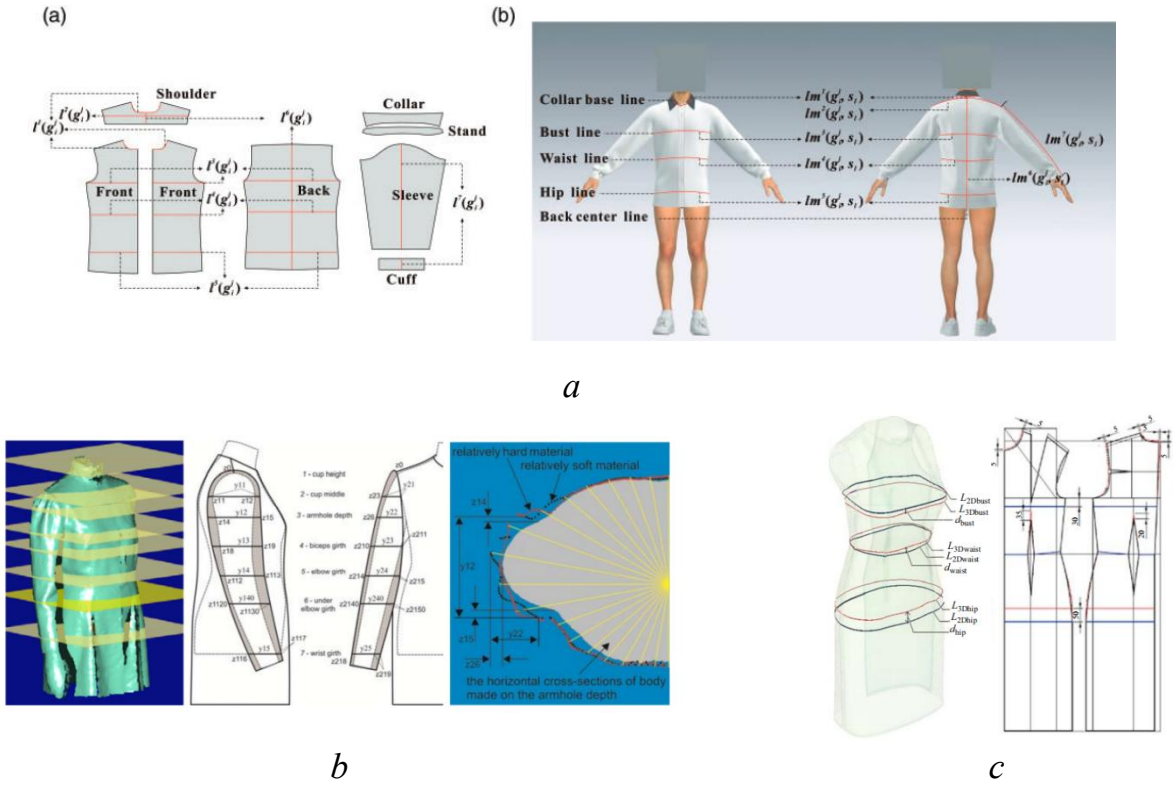

Figure 1.3 - The relationship between the 3D shape, body, and pattern: a - ease allowance measurement in the 3D digital environment. [82]; b - "arm - sleeve shape" system parameterization; *c* - 3D visualized difference of ease allowance between 2D pattern and 3D shape [81]

Fit-related simulation outputs include distributions of strain, internal tension, pressure, and contact force, and contact states, which help identify regions where excessive tightness, restricted movement, or concentrated folds. Studies by Jing *et al.* have shown that such simulation indicators can be used to evaluate the influence of construction parameters on both comfort and appearance and can further support pattern-adjustment strategies that balance comfort and appearance [82-84]. However, although these indicators are useful within a given software environment, their

definitions and outputs still depend strongly on the simulation platform and parameter settings. Figure 1.4 shows a 3D fit-evaluation example reported in previous studies, in which garment – body interaction forces are analyzed under both static and dynamic conditions.

a *b* *c*

Figure 1.4 - 3D fit verification: *a* - the influence of connection points on the raglan sleeve shape and fit [1]; b, c - Fit evaluation under 3D dynamic conditions.[82] ;

Beyond single-case simulation, virtual try-on is also used to improve efficiency in large-scale and multi-condition comparisons. Sun *et al.* established an automated avatar-modeling pipeline using Rhino and Grasshopper to generate reference lines, meshes, and intersections for an average body model, thereby reducing modeling time and improving consistency[64]. Their workflow indicates that, in large-sample and multi-condition comparisons, consistent pose, consistent conditions, and a standardized modeling protocol are essential for result comparability. Meanwhile, Islam *et al.* categorized virtual try-on studies by output format into three output types: single images, multi-pose renderings, and videos, and identified that generation quality, geometric accuracy, and generalization remain major issues[85]. These findings imply that, without an independent and unified evaluation interface, relying only on platform-internal indicators is insufficient for strict cross-method comparison.

Overall, although 3D platforms provide diverse visual and numerical outputs, differences across software in physics solvers, collision handling strategies, mesh resolution, and parameter definitions mean that even identical patterns and fabric settings may yield divergent fold patterns and air gap distributions. Therefore, platform-dependent outputs alone are insufficient to support strict cross-platform or cross-method validation. It is necessary to establish a platform-independent 2.5D projection parameter system and corresponding evaluation criteria. For raglan coats, the armhole seam–sleeve system is strongly coupled, and the shoulder–sleeve region is also the most error-sensitive zone in 3D simulation. Accordingly, this region serves as a key observation window in subsequent analysis of pattern-parameter effects and cross-route comparison based on 2.5D projection parameters.

Fabric parameterization and material simulation. Fabric parameterization and material simulation constitute another essential component of 3D garment design and virtual try-on. Once avatars and 2D patterns have been integrated in a virtual environment, the resulting garment appearance further depends on how fabric behavior is parameterized and simulated. By defining material properties such as tensile, bending, and shear properties, virtual systems can observe garment appearances, including drape geometry, fold distribution, and fit conditions. In this way, fabric simulation supports the rapid iteration of pattern structure and construction details during the design stage.

With advances in computer graphics and physical simulation algorithms, fabric simulation has gradually evolved from experience-driven visualization to physics-based prediction, improving the reproducibility of silhouette contours, fold morphology, and local fit. Major platforms such as CLO and OptiTex have integrated fabric-parameter editing and simulation modules, supporting a fast iterative loop from 2D pattern to 3D garment simulation and try-on feedback.

Previous studies explored the relationship between fabric parameters and appearance outputs from several perspectives. Xu *et al.* evaluated the accuracy of digital fabric representation through comparisons between virtual and real garments, used 3D stress-strain information to support structural adjustment and fit optimization, and developed regression-based approaches linking fabric properties, 2D patterns, and deviations in 3D virtual garments results. Lagė *et al.* have further combined virtual try-on with scanning techniques to compare appearance and ease differences between real and virtual garments under different fabric conditions [86-90].

For outerwear, and especially for garments with highly coupled structural regions, the effect of fabric simulation is even more critical. Fabric properties influence not only the overall visual appearance, but also the stability of the volume silhouette and the behavior of sensitive regions such as the shoulder, armscye, and underarm. In these areas, the bending and shear characteristics of the material directly affect air-gap morphology, fold orientation, and local fit response, thereby affecting the interpretation of pattern-parameter effects and the reliability of fit evaluation.

Therefore, in studies aimed at pattern-parameter analysis and cross-method comparison, fabric conditions cannot be treated as a secondary variable. To ensure comparability, fabric parameters must be strictly controlled; otherwise, differences caused by material behavior may be mistakenly attributed to pattern structure or digitalization route. This issue is particularly important for men’s raglan coats, in which local geometric coordination in the shoulder–sleeve region is highly sensitive to both structural and material variation. Accordingly, the present research controls fabric conditions in subsequent experiments in order to avoid introducing additional contour deviations caused by material differences.

Standards for apparel digitalization. As discussed in the preceding sections, the

reliability of 3D virtual garment results depends not only on avatar construction, pattern-driven simulation, and fabric parameterization, but also on whether the resulting measurements can be defined and interpreted in a consistent manner. Therefore, apparel digitalization standards play a critical role in converting body data and virtual outputs into comparable engineering measurements for pattern development, verification, and cross-platform evaluation. In this sense, standards provide the measurement basis for linking digital body modeling, virtual try-on, and engineering validation.

Apparel digitalization standards generally provide unified specifications for anthropometric measurement definitions, size designation, and 3D-scan data extraction. These standards ensure that body data can be transformed into usable dimensional information for garment design while remaining consistent and interoperable across different digital platforms. For research concerned with pattern accuracy and verification, this standardization is particularly important because even small differences in measurement definition or data extraction can lead to discrepancies in subsequent avatar validation and virtual try-on analysis.

In China, *GB/T 10000-2023*, *Human Body Dimensions,* provides a widely adopted anthropometric framework for the apparel industry[91]. However, this standard mainly emphasizes girth-related measurements and provides relatively limited coverage of projection-relevant widths, heights, lengths, and angle descriptors. As a result, its direct applicability to projection-based structural evaluation remains restricted, especially when the aim is to validate avatar accuracy and virtual try-on outputs in geometrically sensitive regions. By contrast, international standards such as ISO 7250-1:2017 and ISO 20685-1:2018 offer more detailed specifications for anthropometric measurement and 3D-scan data extraction, thereby supporting more rigorous cross-platform data alignment and accuracy verification [92].

However, although 3D simulation platforms such as Style 3D are capable of generating fully 3D results, industrial verification practice still widely relies on front and profile views for dimensional comparison. For this reason, 2.5D projection measurements remain more compatible with practical garment-development routines and are easier to standardize for engineering evaluation. This is particularly relevant in the present research because the visible shape and structural coordination of the men’s raglan coat are largely judged through front and profile silhouette features rather than through isolated three-dimensional coordinates alone.

Another limitation concerns the range of the dimensional variables provided by existing digital platforms. Among the 33 input parameters used by Style 3D, only a limited subset corresponds to width-related projection dimensions. In contrast, Russian standards for male body dimensions, such as GOST 31399-2009, provide a more comprehensive definition of projection-relevant body dimensions[93]. Therefore,

supplementing digital-platform measurements with projection-based dimensional specifications derived from Russian standards can provide a more operational benchmark for virtual try-on accuracy validation. This combination improves the comparability of results across platforms and also supports the development of a measurement interface that is more suitable for pattern-oriented and production-oriented analysis.

Overall, standards are not a peripheral background issue in apparel digitalization; they determine whether digital body data, simulation outputs, and subsequent evaluation results can be compared on a common basis. For this reason, the present study adopts a projection-oriented measurement logic and uses 2.5D parameters as a more standardized and operational interface for subsequent analysis. This step also prepares the transition to the remaining challenges of 3D applications, where inconsistencies in modeling, simulation, and evaluation still limit the reliability of current digital routes.

1.2. Application of AI in Apparel

3D simulation has become an important digital route in apparel design; it still faces unresolved problems in avatar adaptability, fabric simulation, dynamic interaction, and evaluation standardization. These limitations have encouraged the use of AI as another digital route in apparel.

First, AI systems for automated fashion design and recommendation, where knowledge bases or generative models support style ideation and personalized recommendation[94-95]. Second, AI-based methods for pattern generation and customization attempt to model the relationships among pattern parameters, anthropometric measurements, and user preferences, thereby enabling parametric pattern generation and individualized customization[96-98]. Third, computer-vision research on fashion detection and garment parsing, focusing on garment segmentation, human pose estimation, and garment key point detection, provides intermediate representations for structural understanding and silhouette synthesis [99]. Fourth, generation and simulation studies for virtual try-on and dynamic garment modeling, including 2D try-on synthesis, diffusion-based controllable generation, 3D reconstruction, neural simulation, and other AI-based generation methods, aiming to improve visual realism and structural consistency of garments across different bodies and poses [100-103].

The following subsection reviews AI applications in virtual try-on with particular emphasis on accuracy, controllability, and their relevance to garment shape verification.

1.2.1. Applications of AI in virtual try-on

Virtual try-on is a core application area of AI in apparel, aimed at visualizing garment fit and realistic appearance on digital human bodies, particularly with respect to garment structure, local detail, and body pose. In recent years, with advancements in AI technology, virtual try-on techniques have evolved from traditional 2D image synthesis to more complex approaches such as 3D reconstruction, generative AI, and multimodal input integration. This development has greatly expanded the technical possibilities of garment visualization, while also making issues of accuracy and structural controllability more prominent. Figure 1.5 shows the main AI routes in virtual try-on.

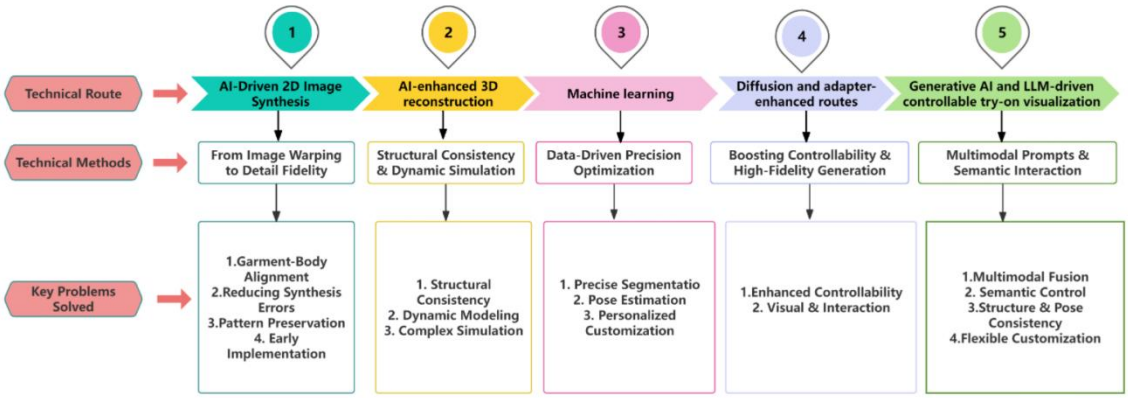

Figure 1.5 - Applications of AI in virtual try-on

As shown in 1.5, existing research can be categorized into five primary routes: AI-driven 2D image synthesis, AI-enhanced 3D reconstruction and neural simulation, machine learning optimization, diffusion and adapter-enhanced methods, and generative AI and large language model-based controlled visualization.

AI-based 2D Image Synthesis. 2D image synthesis is one of the most widely used virtual try-on solutions. It aligns a 2D garment image with the target body image through image matching and deformation, and then synthesizes the corresponding try-on result. Because this route operates directly at the image level, it provides an efficient solution for garment visualization and has been widely used in early virtual try-on research. Early methods, such as VITON, adopted a coarse-to-fine pipeline to transfer the target garment onto the target person image[104]. However, when pose changes are large or garment shapes differ substantially, these methods may produce inaccurate results, particularly around construction-sensitive areas such as the neckline, armhole, and sleeve boundary. Subsequent methods, including LA-VITON[105]and VTON-HF[106], improved garment shape retention and local detail fidelity through finer geometric matching and multi-module designs. Figure 1.6 shows the differences in garment shape and detail fidelity produced by garment transfer across different AI models.

Figure 1.6 - Differences in the detail accuracy of 2D images generated by various AI models.[104,106]

These approaches still largely rely on perceptual image-quality metrics and do not provide a direct, measurable link to garment geometry. As a result, although the generated try-on images may appear visually plausible, they may not preserve the structural features required for engineering-oriented evaluation. For structurally complex outerwear such as raglan coats, 2D image synthesis may fail to accurately maintain the raglan seam position, sleeve direction, or armhole placement. This limitation reduces its value for quantitative verification and pattern correction in production-oriented workflows.

AI-enhanced 3D reconstruction and neural simulation. Compared with 2D image synthesis, AI-enhanced 3D reconstruction and neural simulation focus on improving the garment geometry consistency and dynamic performance. Rather than operating only at the image level, these methods attempt to improve the structural correspondence between garments and the body, especially under pose variation and motion conditions. As a result, they are more directly related to the problem of maintaining geometric coherence in virtual try-on. TailorNet, for example, accelerates garment deformation prediction using neural networks and can efficiently simulate garment changes across different poses, but it suffers from over-smoothing issues, particularly in complex garment details[108]. Figure 1.7. shows an example of AI-assisted dynamic simulation, illustrating the relationship between garment structure and body motion.

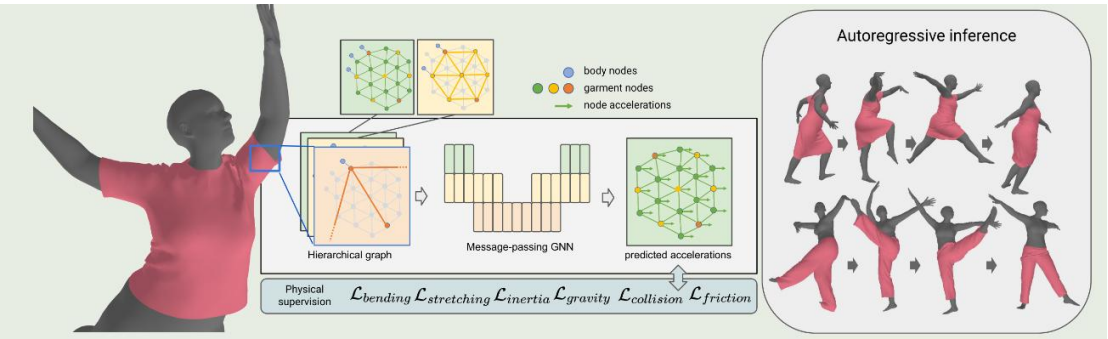

Figure 1.7 - Enhancing dynamic simulation accuracy by neural networks [110]

Grigorev et al. proposed HOOD, which uses graph neural networks with multi-level message passing to improve dynamic simulation accuracy and maintain natural structural changes during motion[110]. The manifold-aware Transformer further improves the modeling of dynamic wrinkles and local variations, enhancing fit-related behavior and structural consistency in motion scenarios[108].

However, despite these advances, 3D reconstruction and neural simulation methods still face several practical constraints. These include the need for accurate data calibration, limited generalization across different garments and body conditions, and, from the perspective of pattern engineering, difficulty in mapping predicted 3D results back to interpretable pattern parameters. Therefore, although these methods improve structural and dynamic consistency compared with image-level synthesis, they still do not fully resolve the problem of engineering-oriented verification. For raglan coats, this limitation is even more evident because their shoulder-sleeve-bodice configuration requires not only visually plausible reconstruction but also rigorous evaluation criteria capable of supporting structural analysis and pattern correction.

Machine learning. Machine learning, particularly deep learning, supports virtual try-on through intermediate tasks such as human pose estimation, garment segmentation, and keypoint detection. These models extract body- and garment-related features that serve as inputs or constraints for try-on generation. Ghodhbani *et al.* reviewed CNN-based methods in fashion parsing, pose estimation, and garment keypoint detection, showing how deep models can extract garment-relevant features[112]. Xu *et al.* used a backpropagation artificial neural network (BP-ANN) to improve pose-estimation accuracy, which can support fit optimization. Wang *et al.* and Liu *et al.* evaluated and predicted human body dimensions and garment fit using Artificial Neural Networks (ANN) and Radial Basis Function (RBF) neural networks[113-114]. Studies by Oh et al. and Kim et al. proposed low-data AI systems for multi-body-type customization using objective fit-scoring, demonstrating strong performance for individualized sizing and fit control[97,115,116]. Figure 1.8 shows the detailed workflow of using neural networks to

evaluate and predict human body dimensions and garment fit.

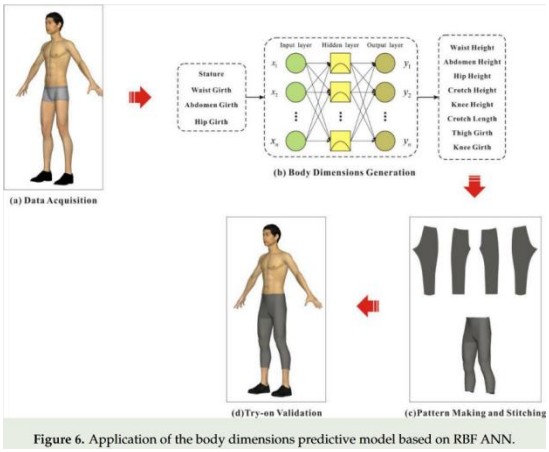

Figure 6. Application of the body dimensions predictive model based on RBF ANN.

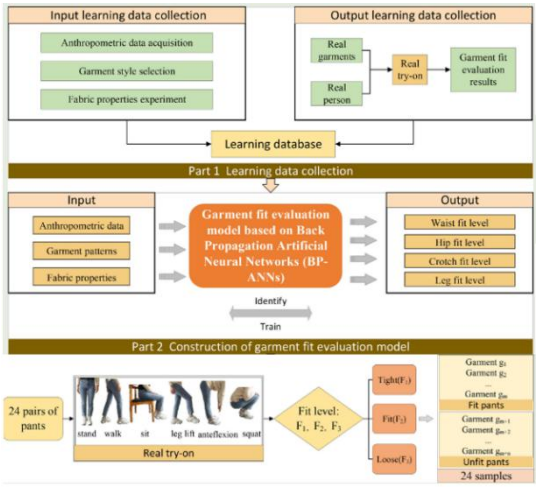

a *b*

Figure 1.8 - Evaluation and prediction of human body dimensions and garment fit by AI: *a* - human body dimensions evaluation using RBF neural networks technology for pattern making [113]; *b* - garment fit evaluation using ANN neural networks technology [114]

Machine learning models are highly dependent on the training data distribution. When body shapes, poses, garment styles, or fabric characteristics fall outside the training range, errors in key point detection and fit prediction can be amplified, making it difficult to ensure stability across different body shapes and silhouette categories. Meanwhile, the labels in many fit-prediction datasets still rely mainly on experience-based “good or bad” judgments or subjective ratings and therefore lack reproducible quantitative criteria. As a result, although machine learning can effectively support feature extraction, prediction, and intermediate optimization in virtual try-on, it still does not fully resolve the problem of standardized and engineering-oriented garment verification.

Diffusion and adapter-enhanced routes. Diffusion- and adapter-enhanced methods represent a further development of AI-based virtual try-on, with a stronger emphasis on generation accuracy and local appearance control. Compared with earlier machine-learning-based support tasks, these methods increasingly build on pretrained diffusion models and introduce explicit warping mechanisms and localized attention modules to improve garment generation quality. As a result, they have shown strong performance in maintaining silhouette stability and detail fidelity, particularly in high-resolution try-on tasks. Zhang *et al.* proposed WarpDiffusion, which combined explicit deformation with diffusion-based generation and improved try-on quality on high-resolution benchmarks[117]. Xing *et al*. used TryOn-Adapter to decouple garment

identity from person appearance and improved generation efficiency, showing potential for e-commerce applications[118]. Figure 1.9 shows the improvement in silhouette stability and detail fidelity achieved by diffusion models in garment-shape transfer on high-resolution benchmarks.

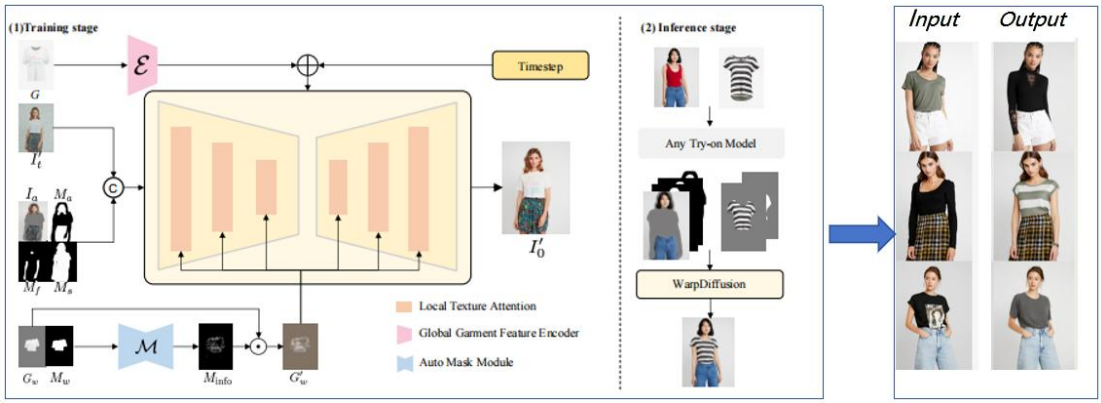

Figure 1.9 - Accuracy of garment shape generation by WarpDiffusion. [117]

However, despite these advantages, diffusion-based pipelines still optimize primarily for visual realism and typically lack measurable structural analysis. As a result, they are difficult to compare directly with engineering-oriented methods and do not resolve the problem of quantitative evaluation for structural consistency and fit adaptation [119,120].

Generative AI and controllable virtual-try-on visualization based on large language models. Advances in generative models (such as GANs, diffusion models, and Transformers) and large language models (LLMs) have enabled multimodal conditioning for virtual try-on. Frameworks such as CLIP align textual and visual representations through contrastive learning, supporting garment generation, retrieval, and editing[121]. In virtual try-on, CG-VTON combines design sketches, pose information, and text descriptions to generate controllable try-on images from concept design to visualization, improving both fit appearance and garment texture and detail rendering [107,122]. Figure 1.10 shows the workflow and results of generating controllable garment silhouettes and try-on visualization by combining generative AI with large language models.

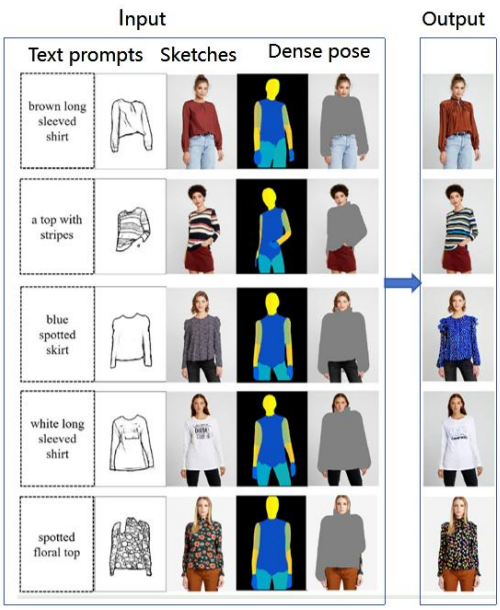

Figure 1.10 - Garment shape generation using multimodal prompts(simple text prompts + sketches + Dense pose) [122]

However, current evaluation still relies heavily on perceptual metrics, while structural deviation quantification and standardized verification protocols remain insufficient [123,124]. For structurally complex garments such as raglan coats, this limitation is particularly important because multimodal generation must ultimately be supported by measurable criteria to support engineering-oriented design and pattern analysis. Accordingly, the remaining challenges of AI applications should be understood not only in terms of generation performance but also in terms of structural consistency, quantitative verifiability, and cross-method comparability.

1.2.2. Challenges for AI applications

Several problems in AI-based virtual try-on extend beyond generation quality and include generalizability, structural consistency, dynamic adaptability, and the absence of standardized evaluation for engineering-oriented verification.

AI models depend on large-scale, high-quality training data. Data acquisition becomes particularly difficult and costly when targeting specific body shapes and complex scenarios. This limits generalization across different body shapes, styles, and dynamic conditions, and performance is often weaker for non-standard body shapes, such as extremely tall or very slim bodies.

Existing models typically perform well in static settings, but under dynamic conditions or large pose variations, they often generate wrinkles, misalignment, or unnatural shapes. The problem becomes more evident in fast motion or highly complex postures, where garment–body interaction is more difficult to represent accurately.

Distortions and detail loss still occur when complex textures and structural regions are involved. In key areas such as raglan seams and armholes, even small alignment errors may result in visually obvious and structurally meaningful inaccuracies.

A unified, standardized verification framework is still lacking. Metrics commonly used across AI methods (e.g., FID and LPIPS) cannot accurately quantify structural consistency, dimensional adaptation, or comfort-related fit. Therefore, future research should establish a unified evaluation system with measurable criteria to ensure the repeatability, comparability, and verifiability of generated garment results.

Thus, although AI-based virtual try-on and garment generation have resolved many foundational problems in visualization and controllable image synthesis, major challenges remain in data dependency, structural consistency, dynamic adaptation, generation accuracy, and evaluation standardization. These limitations indicate that AI methods alone cannot yet fully satisfy the requirements of rigorous garment shape verification and engineering-oriented design analysis. For this reason, it remains necessary to introduce measurable and structurally interpretable evaluation criteria, especially for complex garments such as men’s raglan coats. This also leads naturally to the next section, which discusses the engineering characteristics and research challenges of raglan- sleeve pattern design.

1.3. Raglan sleeve pattern-making engineering

The raglan sleeve is a particularly complex structural object in men's outerwear. Its shoulder configuration is defined by a continuous "neckline-shoulder-sleeve" zone, and this continuity directly affects comfort and the stability of the overall coat silhouette. Raglan sleeves are characterized by strong interrelationships among structural control variables; therefore, even a local correction may produce coordinated changes in front-back distribution, sleeve position, and volume-silhouette shapes. For this reason, men's raglan coats remain a long-standing problem in traditional pattern construction and require a unified quantitative system for digital design and virtual verification.

1.3.1. Pattern-making method of the raglan coat

Raglan sleeves are commonly defined as a sleeve construction in which the sleeve and bodice are connected at the shoulder through a seam line extending from the neckline or neck point to the underarm, thereby integrating the shoulder and sleeve into one structural configuration[15-16]. Unlike set-in sleeves, which rely on sewing an independent sleeve into a separate armhole, the defining raglan seam crosses the shoulder region. As a result, it changes the front–back distribution of the shoulder-

sleeve structure, as well as the front-back position and direction of the sleeve, which exerts a more direct influence on the visible silhouette.

From both functional and aesthetic perspectives, raglan sleeves accommodate upper-limb movement while shaping the outer silhouette of the garment. Specifically, the shoulder raglan seam redistributes the bodice–sleeve connection, allowing the garment to provide movement ease and maintain the intended silhouette. Accordingly, raglan sleeves are widely adopted in coats, trench coats, and casual outerwear [17-18].In application, raglan sleeves present multiple variants depending on the seam-line form. Figure 1.11 shows the shape and pattern structure of different raglan sleeve variants, including full raglan, half raglan, and locally modified raglan structures.

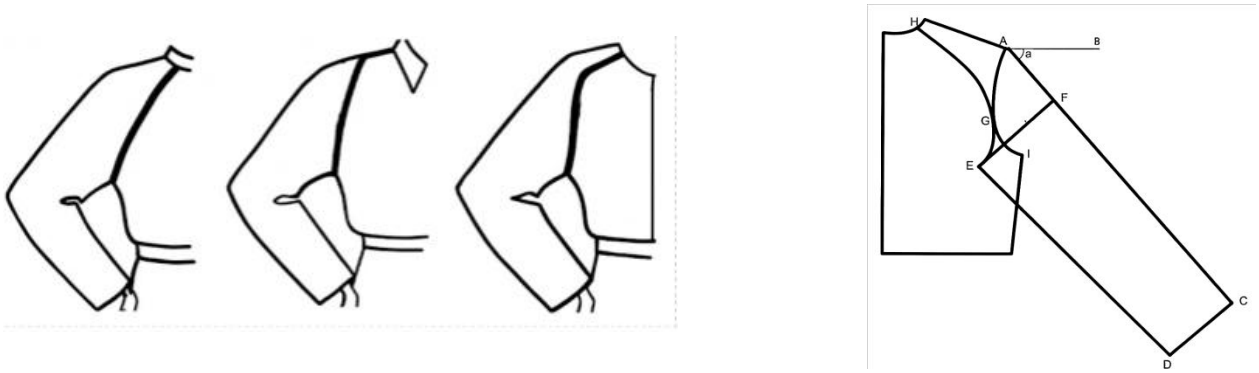

a *b* *c* *d*

Figure 1.11 - Raglan sleeve structures: *a* - full raglan; *b* - half raglan; *c* - locally modified raglan; *d* - pattern structures [19]

As shown in Figure 1.11d, the raglan-sleeve structure in conventional pattern-making is determined by several coupled elements: the angle *a* between the sleeve center line *AG* and the horizontal line *AB* defines the sleeve center line inclination, which determines the spatial positioning of the front and back sleeve panels and governs the overall sleeve morphology. The sleeve cap height *AF* and sleeve width *EF* jointly control the ease allowance at the armhole and its front and back distribution, thereby influencing the available upper-arm space. Insufficient total ease or imbalanced allocation often leads to undesirable folds and tension in the underarm (sleeve root) region. Line *HG*, which connects the bodice to the sleeve, directly shapes the external silhouette of the raglan sleeve through its position and directional curvature. In summary, under conventional pattern-making, the raglan-sleeve appearance is primarily achieved through the coordinated adjustment of the sleeve center line inclination, sleeve-cap height, sleeve width, and the bodice – sleeve connection line.

Based on these structural characteristics, three common pattern-making methods are used for raglan sleeves: direct drafting, proportional drafting, and block-based

drafting.

1) Direct drafting: This method relies on experiential rules or representative patterns. The raglan seam position, sleeve center-line direction, sleeve-cap height, and sleeve width are adjusted step by step to achieve the target appearance and fit. The main advantage is practical responsiveness to diverse body shapes and style requirements. However, because the correction process is strongly dependent on the operator, the same issue may be addressed through different modifications, and the same modification may yield different visual and fitting outcomes. As a result, reproducibility and cross-body transferability remain limited.

2) Proportional drafting: This method is based on anthropometric relations and geometric constructions. Key raglan sleeve control lines are constructed using proportions, angles, or landmark points, and sleeve direction, sleeve-cap height, and sleeve width are then determined accordingly. The main advantage is that the key variables, such as shoulder-point extension, sleeve center line inclination, sleeve-cap height, and sleeve width, can be expressed in a unified and explicit manner, which supports parameterized description and subsequent quantitative analysis. However, without a unified and reproducible evaluation framework, drafting rules alone cannot confirm structural correctness or silhouette stability.

3) Block-based drafting: this method starts from a set-in sleeve block or basic sleeve structure and retains the original armhole and sleeve-cap fitting basis. By determining the raglan seam and redistributing the shoulder-region structure into the sleeve pieces, the set-in sleeve block is transformed into a raglan sleeve. Its main advantage is clear production-oriented workflows, and partial inheritance of the fit foundation from the original block. However, the adjustment of the raglan seam position and sleeve direction still tends to depend on experiential rules. Local modifications may easily change front-back shoulder allocation and armhole matching, resulting in an unstable silhouette.

Figure 1.12 shows proportional and block-based pattern-making methods of the raglan sleeve.

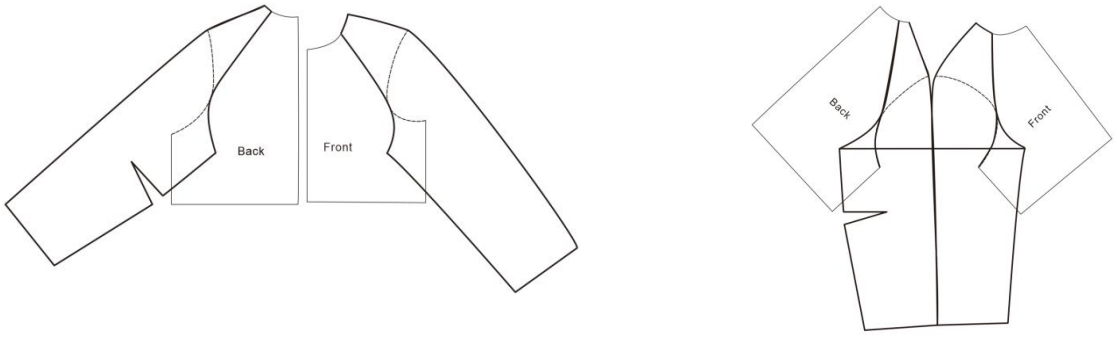

a *b*

Figure 1.12 - Pattern-making methods of the raglan sleeve: *a* - proportional drafting[20], *b* - block-based drafting[22]

In addition to differences in pattern-making method, raglan sleeves are also implemented through different sleeve-piece configurations. These configurations further influence the degree of front-back control, local shape refinement, and drafting and sewing complexity. Figure 1.13 shows the common sleeve-piece configurations of raglan sleeves, including one-piece, two-piece, and three-piece sleeves [24,22]. In general, increasing the number of sleeve pieces improves front-back allocation and local adjustment capacity, but it also increases both drafting and sewing complexity.

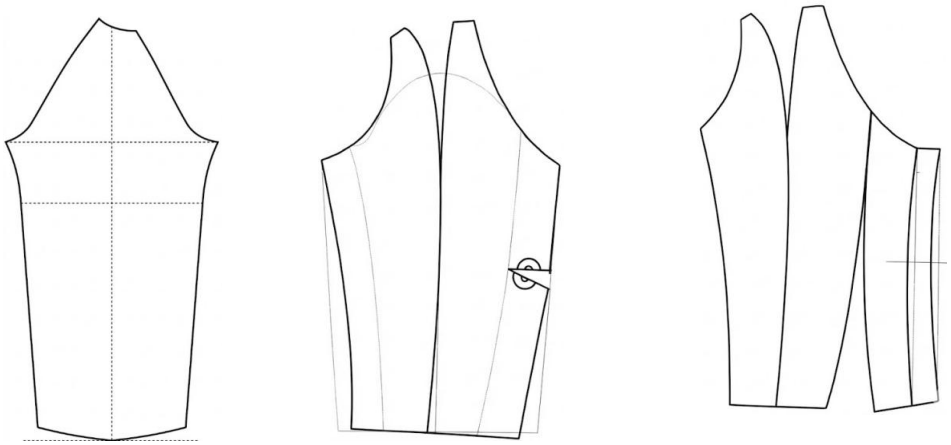

a *b* *c*

Figure 1.13 - Sleeve-piece configurations: *a* - one-piece[24], *b* - two-piece, *c* - three-piece sleeves[22]

As shown in Figure 1.13, the one-piece sleeve has a simplified structure and is used for looser or more casual silhouettes, yet it provides limited fine control over sleeve direction and armhole matching. The two-piece sleeve separates the sleeve into front and back pieces, enabling more effective distribution of ease allowance and adjustment of sleeve direction, and is therefore frequently adopted in outerwear requiring improved fit and silhouette stability. The three-piece sleeve further adds an additional piece to strengthen 3D shaping and local adjustment, making it suitable for structured outerwear or digital garment development requiring higher sleeve-line quality, armhole smoothness, and silhouette accuracy.

Overall, prior work has proposed multiple pattern-making methods for raglan sleeves, but three challenges remain for outerwear. First, key structural elements are strongly coupled, so a local adjustment can affect other structural regions and change the overall silhouette. Second, differences in blocks and body shapes amplify this instability, which makes cross-sample comparison difficult. Third, without a unified and reproducible quantitative evaluation framework, method selection and pattern correction cannot be supported by verifiable evidence.

1.3.2. Existing research on the raglan sleeve pattern design

As a sleeve-bodice integrated structure, raglan sleeve construction is influenced by various factors, including pattern-making methods, front-back bodice balance, seamline segmentation, connection points, and the spatial relationship between the sleeve and the arm. Accordingly, existing research on raglan sleeves can be reviewed from three aspects: the parameterization of pattern variables, the relationship between pattern parameters and body morphology, and the influence of pattern adjustments on wearing comfort and aesthetic performance. These three aspects together provide the main research context for understanding how raglan sleeve patterns are generated, adjusted, and evaluated in both traditional and digital design environments.

Existing studies have compared raglan-sleeve pattern-making methods and proposed parameterized models to balance comfort and aesthetic appearance. Mao *et al*. compared a traditional angle-based proportional method with a block-based fitting method and reported that the angle-based method is easy to apply and suitable for loose sleeves but has limited accuracy, whereas the block-based fitting method enables more precise matching between the armhole and the sleeve cap[26]. Although this comparison provides a basis for selecting methods for different sleeve types, it still primarily relies on empirical descriptions rather than specific numerical characterizations. Subsequent research moved beyond method comparison to the analysis of structural relationships. Zhao *et al.* established the relationship between the shoulder‑sleeve angle and bodice ease, providing both qualitative and quantitative analyses of their impact on raglan sleeve morphology[27]. Building on this line of research, Mu *et al.* and Zlatina *et al.* further developed regression models based on key pattern parameters (e.g., sleeve-center-line angle, sleeve-cap height, shoulder-point height, and armhole depth), optimizing raglan sleeve pattern design [28,29].

In addition, several studies attempted to link visual information to pattern design. Li *et al.* and Gu *et al.*constructed regression models correlating visual imagery with structural parameters, enabling automated conversion from visual information to pattern drafting and offering another approach to the quantitative digital design of raglan sleeves [30,31]. Gill *et al.* empirically compared parametric drafting with traditional CAD pattern-making methods, concluding that parametric drafting offers superior speed and accuracy in generating customized patterns[32]. A. V. Gnidenko, focusing on women's garments with sleeves of complex cuts, developed a technology for formalizing and algorithmizing the design process, in which constructional parameters, fit-quality criteria, and relationships within the "body–construction–garment" system are used as an informational basis for parametric synthesis and quality diagnosis of constructional solutions [135]. Taken together, these quantified pattern parameters and mathematical

models provide concrete data support for raglan sleeve pattern design.

The influence of individual pattern parameters on the comfort of raglan sleeves has been investigated in several studies. Wei *et al.* investigated how pattern parameters, including sleeve-cap node position and the offset of the lowest armhole point, affect the comfort and aesthetic appearance of close-fitting raglan sleeves, and further developed a CAD-based automatic generation system to efficiently produce close-fitting raglan-sleeve patterns[33]. Lou *et al.* proposed a "reverse-engineering" approach that employs regression models to analyze the impact of the pattern parameters (sleeve centerline inclination and connection point placement) on wearing comfort[34]. Liang *et al.* introduced the underarm overlap area as a quantitative metric to evaluate 3D shape and comfort, and conducted an in-depth analysis of how the set-in sleeve angle influences raglan pattern structure[35]. Figure 1.14 shows the underarm overlap area as an indicator for evaluating fit and comfort[23].

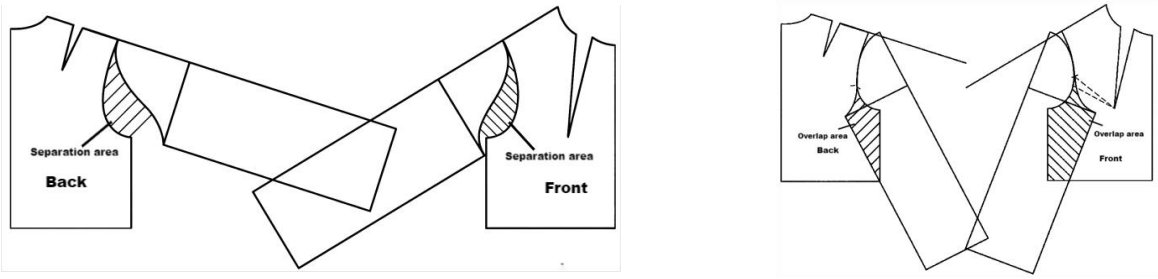

a *b*

Figure 1.14- The influence of underarm separation and overlap areas on sleeve structure: a - underarm separation area; b - underarm overlap area [27].

As shown in Figure 1.14a, a larger separation area indicates more underarm clearance and thus a looser sleeve silhouette. As shown in Figure 1.14b, a larger overlap area indicates stronger underarm compression and thus a closer fit. However, this method does not specify the boundary definition of the separation and overlap regions, nor does it provide reproducible quantitative thresholds. Consequently, fit evaluation still relies primarily on subjective judgment, making this indicator unsuitable for comparable analysis across different body shapes and volume – silhouette categories and difficult to convert into specific numerical adjustments of pattern parameters.

Due to the integrated bodice–sleeve features of the raglan pattern, comfort is typically governed by the combined effect of multiple pattern parameters. Accordingly, several studies have further investigated the combined influence of multiple pattern parameters on raglan sleeve comfort. Liu *et al.,* Huang *et al.*, and Wu *et al.* jointly analyzed the effects of several key pattern parameters, including sleeve centerline inclination, sleeve cap height, armhole depth, cuff width, sleeve width, and connection

points, on the overall silhouette and wear performance of raglan sleeves[36-38]. They proposed design strategies that optimize the interplay among these parameters to enhance both comfort and aesthetic quality. Their findings offer balanced solutions that reconcile visual appeal, wearing comfort, and manufacturing feasibility and provide concrete numerical recommendations, for instance, a sleeve centerline inclination of 45° and a sleeve cap height equivalent to B/6 (where B denotes chest circumference) for tailored blazer-type garments.

Table 1.1 shows the values of different pattern parameters associated with a good fit under different shoulder-sleeve angles.

Table 1.1 - Pattern parameter associated with good fit under different shoulder-sleeve angles

Pattern parameter,（cm , °)	shoulder–sleeve angle				
	17°	33°	40°	55°	65°
Sleeve-width ease factor	0.7	0.5	0.45	0.3	0.15
Start point of sleeve angle	3	2	1.5	1	0
Back shoulder-line to sleeve-centerline offset	10.4	7.3	5.5	3	1
Front shoulder-line to sleeve-centerline offset	10	7	5.5	3.5	1.5
Sleeve cap height	15.3	14	12.5	10.5	7.5
Distance from the back-width line to the back sleeve-joining point	1	0.5	0.5	0.5	1
Distance from front-chest-width line to front sleeve-joining point	1.2	1	1	1	0
Armhole depth drop	0	0.5	0.7	1	1.2
Back shoulder–sleeve included angle,°	61.5	48.8	41.5	34.5	25.5
Front shoulder–sleeve included angle, °	64	53.5	45.5	38.6	28.5

As shown in Table 1.1, the quantified pattern-parameter settings under different shoulder-sleeve angles are closely associated with achieving good comfort performance. This study, therefore, provides more specific numerical references for optimizing raglan-sleeve comfort.

Meanwhile, a satisfactory raglan silhouette should also be evaluated under comfort constraints. Studies conducted statistical comparisons of shoulder-shape characteristics of raglan sleeves across different silhouette classifications. Regarding

common raglan-sleeve appearance defects, particularly underarm unevenness, wrinkles, and excess ease, most research follows a three-step workflow of structural factor analysis, parameter adjustment and try-on verification[39-42]. Huang *et al.* compared one-piece and two-piece raglan sleeves across multiple body postures and analyzed how connection-point displacement affects underarm excess ease and overall silhouette quality[43]. Liu *et al.* and Zhang *et al.* further improved underarm smoothness based on structural transformation and sleeve-tube rotation principles, respectively, and validated the improvements through garment-sample verification[44-45]. Figure 1.15 shows an example in which an underarm excess-ease defect is addressed by adjusting a key pattern parameter, namely the offset of the lowest armhole point.

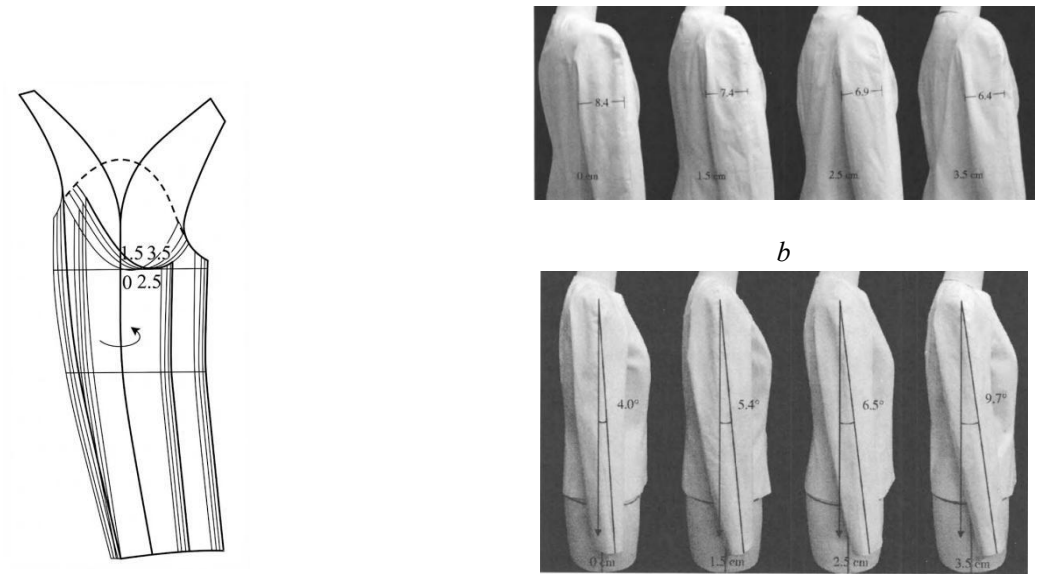

a *b* *c*

Figure 1.15 - correcting underarm unevenness by sleeve-tube rotation: *a*, structural modification; *b*, sleeve-shape rotation; *c*, sleeve forward-tilt angle [45]

As shown in Figure 1.15a, the armhole is shifted forward by 0, 1.5, 2.5, and 3.5cm. Figure 1.15b shows the resulting silhouette width in the sleeve width region under different offsets. Figure 1.15c presents the angle between the sleeve centerline and the vertical line passing through the shoulder point as a silhouette indicator for evaluating the sleeve appearance.

Overall, research on the raglan-sleeve pattern has established a methodological pathway encompassing pattern parameterization, body–garment adaptation, and silhouette performance, and has accumulated extensive structural factors, adjustment recommendations, and numerical ranges. However, several gaps remain: (1) Existing studies adjust single-pattern parameters in isolation, whereas multi-parameter coupling and feasible combination ranges are insufficiently investigated. (2) In body–garment

coupling research, body-shape characteristics are rarely used as the primary basis for defining or adjusting raglan patterns. They are more often introduced during fit evaluation and pattern modification. (3) There is a lack of standardized criteria for diagnosing common defects in the underarm region, such as fabric unevenness, wrinkles, and excess ease. Systematic correction rules linked to specific pattern adjustments are also absent.

1.3.3. Fit criteria for raglan coats

Fit evaluation is a critical component in shape and pattern optimization, providing an integrated judgment of a garment's appearance stability, wearing comfort, and overall fit quality. Traditional evaluation primarily relies on physical try-ons and expert judgment. With the advancement of digital workflows, 3D virtual try-on has been widely adopted for early-stage verification to reduce iteration costs, allowing fit performance to be repeatedly observed, documented, and quantified under relatively controlled and consistent conditions. Existing fit-evaluation criteria can be classified into two categories: subjective evaluation and objective evaluation.

Subjective evaluation involves visual inspection of an overall garment appearance under static and dynamic conditions, focusing on overall aesthetics, cross-sectional silhouettes, profile views, the placement of pattern structural lines and seam lines, and the distribution of wrinkles, bulges, and creases. In addition, some studies further incorporate psychological evaluation methods by translating the wearer's subjective perceptions, such as comfort sensation, pressure sensation, and appearance impression, into ordinal rating scales to enable quantitative scales. Subjective appearance evaluation has been formalized through region-based protocols. Monobe et al. divided a women's jacket into 31 aesthetic regions and, based on local shape, contour, wrinkles, and smoothness, rated both fit (fit/unfit/neutral) and aesthetics (attractive/unattractive/neutral)[116]. Figure 1.16 shows a schematic of local region segmentation for subjective evaluation of silhouette fit.

Figure 1.16 - Local region segmentation of a jacket for subjective scoring of silhouette fit[46]

As shown in Figure 1.16, the suit silhouette is divided into detailed regions and evaluated using a region-by-region subjective scoring scheme. This approach provides a reference for region definition and scoring workflow in raglan-sleeve evaluation. However, in a raglan sleeve, the sleeve piece is directly connected to the bodice via the raglan seam, and sleeve direction, underarm clearance, and bodice front – back balance are interdependent. Therefore, the sleeve or the bodice should not be evaluated separately; instead, the armhole – raglan seam – underarm – shoulder/back area should be assessed as an integrated region.

Kim et al. proposed a seven-dimensional evaluation scheme for different garment regions, including front-view items (fold amount, fit level, attractiveness, perceived youthfulness, slimming effect, aesthetics, and silhouette) and side-view items (waistline–bust proportion and overall appearance) (Table 1.5)[47]. Yu et al. further developed a refined fitting scale to evaluate each jacket region more precisely (Figure 1.24a)[48]. Figure 1.17 shows that the nine-point scale captures a comprehensive range of ill-fitting and well-fitting states across jacket regions.

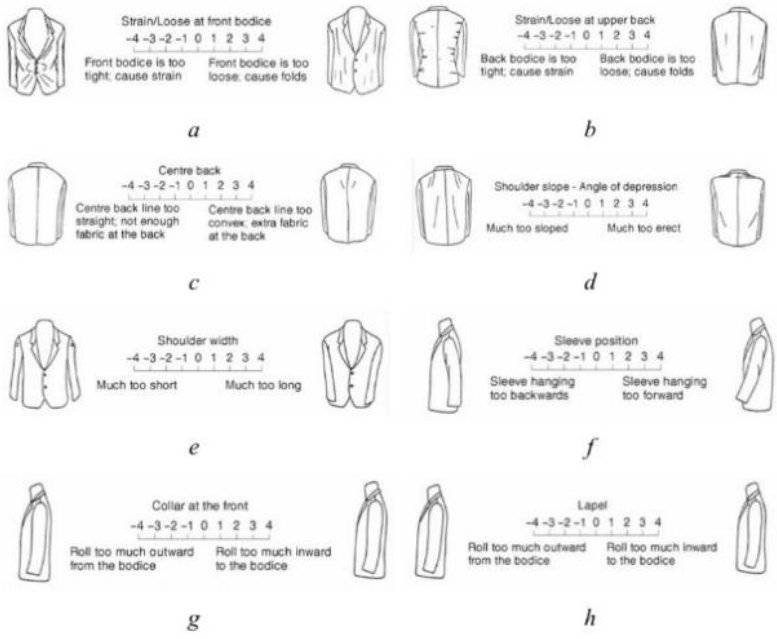

Figure 1.17 Fit evaluation schedule： a -front ; b - upper back; c- centre back d - shoulder slope; e- shoulder width; f-sleeve position; g - collar at the front; h- lapel [47]

On the other hand, comfort-based subjective evaluation examines perceived comfort under standardized postures and actions. Gu *et al.*, SAYĞILI *et al.*, and Huck *et al.* graded comfort using five arm postures to differentiate comfort levels and support comparative evaluation [49-51].

Objective evaluation relies on measurable numerical indicators, such as clothing pressure, angles, and distances. In real try-on settings, clothing pressure is widely used to identify regions that are overly tight or loose. In virtual environments, additional quantities that are difficult to measure physically—such as avatar–garment distance, ease distribution, and distortion-related metrics—can also be obtained.

Static fit evaluation for raglan sleeves is typically conducted with the wearer standing upright and arms relaxed at the sides. Key evaluation criteria include body conformity, compatibility between the sleeve cap and sleeve panel, underarm excess, and the presence of wrinkles or tension in critical zones. Static evaluation is generally performed by trained assessors using standardized protocols, with multiple ratings averaged to minimize inter-rater bias. Zhou *et al.* emphasized the importance of static fit inspection in raglan sleeve evaluation, particularly highlighting the geometric compatibility between the armscye and sleeve cap as well as the rationality of the resulting wearing posture[39]. Figure 1.18 shows three settings used for static fit evaluation.

a *b* *c*

Figure 1.18 - Static evaluation: a - the sample garment displayed on a mannequin; b - the sample garment worn by a real human body; c - the sample garment tried on a 3D avatar.

As shown in Figure 1.18, the sample garment can be evaluated under three static settings: (a) the sample garment displayed on a mannequin, used to observe the overall silhouette and structural symmetry under a standardized body baseline; (b) the sample garment worn by a real human body, used to examine how body morphology, shoulder slope, and the relaxed arm-down posture influence folds, underarm ease, and wearing balance in the sleeve region; and (c) the sample garment fitted on a 3D avatar, used to obtain a static reference under controlled pose and view constraints that is consistent with subsequent digital measurements. By comparing these three settings, a comparable static observation framework can be established, enabling rapid identification and correction of shape and fit defects.

Dynamic fit evaluation focuses on sleeve performance during body movement, such as arm raising, stretching, and crossing the arms over the chest, and mainly

examines issues such as sleeve restriction, underarm tightness, shoulder deformation, and sleeve shape stability. This evaluation can be conducted through physical try-on or 3D virtual try-on simulations. Virtual environments ensure consistent posture and viewing conditions for reliable comparison, whereas physical trials provide essential tactile feedback. Liu *et al.* investigated the influence of sleeve centerline inclination and armscye depth on dynamic comfort and quantified wearer perceptions using a structured rating scale. Crucially, dynamic evaluation requires reproducible motions and clearly defined, consistent scoring criteria; otherwise, cross-sample comparability is compromised[55]. Figure 1.19 shows four standardized arm postures adopted for dynamic fit evaluation.

a *b* *c* *d*

Figure1.19- Dynamic evaluation: *a* - Lowering; *b*-side raise，*c*-Horizontal raise; *d*-Cross arms over chest

These postures were selected to expose sleeve restriction, underarm tightness, shoulder deformation, and sleeve shape instability under repeatable movement conditions.

Building upon static and dynamic states, psychometric scales have been introduced to translate subjective experiences (comfort, pressure sensation, and visual impression) into quantifiable ordinal ratings, thereby enabling quantified evaluation of both wearing comfort and aesthetic quality. Lee *et al.* emphasised the role of consumer visual evaluation in shaping perceptions of comfort and aesthetics, advocating for the integration of visual impressions into design evaluation frameworks[56]. Liu *et al.* proposed six specific indicators for raglan sleeve comfort evaluation: underarm excess, bodice fit level, chest tightness, shoulder deformation, shoulder point pressure, and arm extension difficulty, and developed a psychological rating scale to score sample garments under both static and dynamic conditions[57].

Table 1.2 shows six psychometric indicators for evaluating garment comfort under static and dynamic conditions.

Table 1.2 - Psychometric evaluation indicators for garment comfort [19]

NO.	Evaluation item	Rating scale				
		1	2	3	4	5
①	Fit level	Very poor	Poor	Normal	Good fit	Very good
②	Underarm excess	Very much	More	Normal	Less	None
③	Chest tightness	Very tight	Tight	Normal	Loose	Comfortable
④	Shoulder deformation	Severe	Noticeable	Normal	No noticeable	None
⑤	Pressure of shoulder point	Very high	High	Normal	Low	None
⑥	Arm extension difficulty	Very difficult	Difficult	Normal	Not difficult	Easy

As shown in Table 1.2, items ① and ② correspond primarily to static evaluation: the wearer stands upright while assessors assign scores based on descriptive anchors, with higher scores indicating greater comfort. Items ③ – ⑥ mainly correspond to dynamic evaluation and are scored while the wearer performs standardized motions such as 45° arm abduction, 90° arm abduction, and arms-crossed posture; scores are assigned according to the rating descriptions and then averaged, and higher scores indicate better comfort[19]. On this basis, Zhou *et al.* further refined this approach by explicitly defining two distinct indicator systems[39]. Aesthetic indicators include the appearance of the front chest, back, and underarm regions, evaluating visual smoothness, seam alignment, and the presence of excess wrinkles or tension. Comfort indicators include sleeve-shape stability and underarm comfort, evaluated under arm-relaxed (0°) and arm-abducted (45° and 90°) conditions, with attention to restriction, tightness, or sleeve-cap deformation[37]. Composite scores are calculated as follows:

$$\text{aesthetic quality} = \text{Silhouette (front + back + underarm region)} / 3 \quad (1.1)$$

$$\text{comfort} = [\text{Underarm-region comfort (0°, 45°, 90°)} + \text{Sleeve stability (0°, 45°, 90°)}] / 6 \quad (1.2)$$

This method transforms subjective judgments into comparable aggregate scores

through indicator decomposition and formulaic aggregation, providing a more operational framework for evaluating both the fit and functionality of raglan sleeves. In this way, subjective evaluation gradually develops from intuitive visual judgment into a more structured system linking appearance observation, movement response, and composite scoring.

In addition to evaluation systems, some studies have proposed empirical pattern rules closely related to fit performance to interpret or guide structural adjustments. For example, Wu *et al.* and Liu *et al.* highlighted the critical role of front–back cuff differentiation in raglan sleeve fit, recommending that the front cuff be slightly smaller than the back to enhance cuff-edge conformity and wearing stability. They provided an empirical guideline: front cuff = total cuff width − 1 cm, back cuff = total cuff width + 1 cm [36,38]. It should be noted that such rules are primarily pattern design recommendations; in this context, they serve to elucidate the structural rationale underlying evaluation metrics and suggest potential directions for pattern modification.

Overall, current raglan sleeve fit evaluation has evolved into a dual-track system combining subjective scales and objective measurements, supported by ordinal mapping and composite scoring for quantitative expression. However, these criteria still face significant limitations in engineering applications: (1) lack of standardization in postures, motion selection, viewing angles, and rating protocols across studies, hindering result reproducibility and cross-comparison; (2) many indicators rely on subjective scoring and lack direct linkage to measurable garment data, including dimensions and shape; (3) for coats, fit quality depends not only on local conformity but also on volume–silhouette stability and coordination across key regions, whereas existing criteria tend to focus on local areas, thereby limiting reliable cross-body-shape and cross-silhouette comparison and hindering pattern-based error identification. Therefore, it remains necessary to establish a comparable and reproducible evaluation system under unified conditions to support raglan coat pattern correction, evaluation, and engineering-oriented verification.

1.3.4. Existing challenges in pattern design

Four problems limit the digital transformation of the raglan-coat design process.

First, there is insufficient adaptation to body-shape variation. Proportional drafting relies heavily on empirical rules and iterative prototyping, while block-based methods assume standardized sizing that fails to capture individual variations in shoulder slope, chest–back differential, and torso morphology. Consequently, fit and comfort fluctuate significantly across diverse body shapes [1,3].

Second, a unified approach to multiparameter interrelationships is lacking. In raglan pattern design, adjusting any single parameter, such as sleeve centerline inclination, sleeve cap height, armhole depth, connection point location, or sleeve width

distribution, simultaneously affects underarm ease, shoulder smoothness, and sleeve drape direction. As a result, isolated parameter tuning often improves one region while degrading another. Therefore, effective optimization requires coordinated analysis and validation of multi-parameter combinations under consistent evaluation conditions to derive robust, reusable adjustment rules.

Third, the traceability between pattern parameters and aesthetic outcomes remains limited. Current evaluations of raglan sleeve aesthetics rely predominantly on subjective post-try-on descriptions, such as wrinkling, tightness, and restriction, while lacking a corresponding set of repeatably measurable shape descriptors, such as displacements, angles, distances, or fold counts in key regions. Consequently, when defects occur, it is often difficult, under unified measurement conditions, to identify the defect location, quantify its magnitude, and link it to the responsible pattern structure, which reduces the interpretability and reproducibility of subsequent pattern correction.

Fourth, evaluation criteria remain non-standardized, while underarm problems persist as one of the most typical raglan sleeve defects. Most studies focus on the standing appearance; even when dynamic evaluation is included, differences in posture lead to different results, and the absence of unified evaluation standards makes findings difficult to compare[16,18,37]. Meanwhile, underarm wrinkling and poor smoothness remain among the most prevalent raglan sleeve defects. Typical remedies are experience-based local adjustments, such as shifting the lowest armhole point or adjusting armhole depth, yet their effectiveness is unstable across different body shapes, fabrics, and motion conditions[17,31].

Taken together, these challenges indicate that current raglan sleeve research still lacks a unified engineering framework capable of linking body shape, pattern parameters, measurable shape descriptors, and reproducible evaluation results. Therefore, it is necessary to establish, under unified postures and viewing conditions, a comprehensive framework comprising: (i) a measurable shape parameter system, (ii) a core set of structurally influential pattern parameters, and (iii) reproducible static–dynamic evaluation criteria, to support a traceable and verifiable validation chain from pattern refinement to production readiness for raglan coats.

1.4. Main aim and Objectives of research

Based on the unresolved challenges identified above, this research focuses on the development of a digital design technology for men’s raglan coats by integrating pattern-making, 3D virtual try-on, 2.5D projection-based measurement, and AI-assisted image generation. Previous studies have shown that 3D and AI technologies provide useful tools and data references for investigating raglan-sleeve shape and fit. However, systematic studies on men’s raglan sleeves remain limited, and several key issues are

still unresolved, including the mapping and discrepancies among 2D patterns, 3D virtual shapes, real garment shapes, and AI-generated raglan-sleeve silhouettes.

More specifically, existing Chinese male basic bodice prototypes cannot fully represent diverse Chinese male body shapes; pattern construction lacks a systematic parameterized framework linked to garment shape, which limits the quantitative adjustments of pattern parameters required for optimal shape; and unified evaluation criteria for the shape and fit of virtual and real coats are still lacking, which hinders cross-platform silhouette comparisons and complicates pattern adjustments based on silhouette analysis. Therefore, this study aims to develop a digital design technology for men's raglan coats that links body morphology, pattern parameters, 3D virtual try-on, 2.5D projection measurement, AI-assisted generation, and industrial verification within one reproducible engineering framework.

To achieve this aim, the following research objectives were formulated, as shown in Figure 1.20.

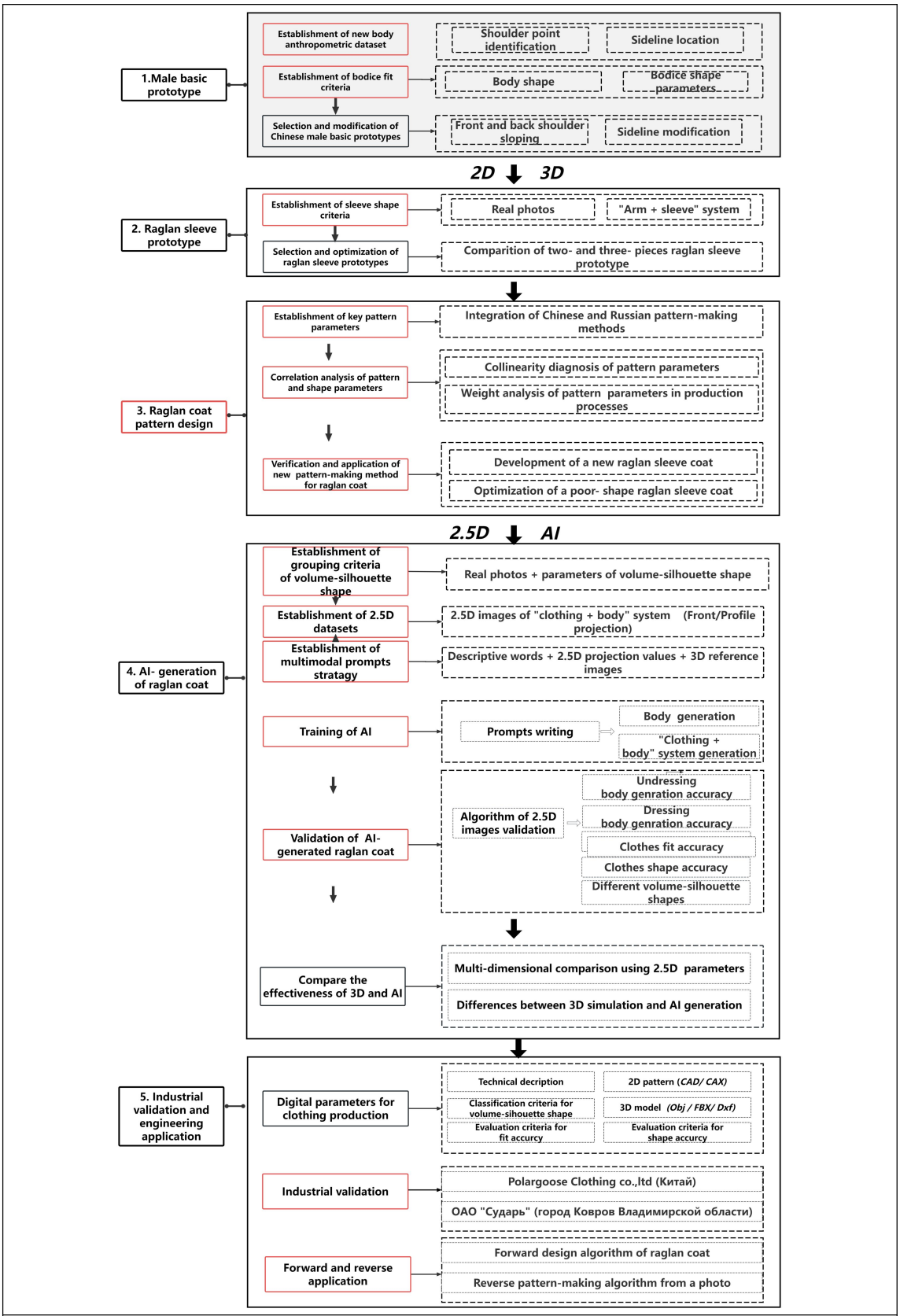

Figure 1. 20 - Framework of development of raglan coat pattern-making

1. To establish a new anthropometric database that characterizes male body morphology with shoulder point identification and sideline location. Based on typical

Chinese male body shape variations, the 3D shoulder point position is mapped to the 2D pattern to correct the front and back shoulder slopes. In addition, the front and back waist- girth allocation ratio measured in Style 3D was used to modify the sideline location for correcting the male basic prototype.

2. To establish new bodice fit criteria. The angles between the front and back center lines and the hemline, as well as the vertical distances from a horizontal reference line at the hem, are measured and adopted as quantitative shape parameters to evaluate bodice balance and overall fit.

3. To establish new raglan sleeve shape criteria. High-quality real photographs of well-fitted raglan sleeves are selected, and the spatial relationship between the body and the coat is analyzed. In the “arm+sleeve” system, the front and back spatial positions of the sleeve relative to the arm at the cuff and the elbow will be defined as key shape parameters for evaluating raglan sleeve shape.

4. To establish new key pattern parameters and a novel pattern-making method for raglan coats. Chinese and Russian pattern-making methods are integrated to derive new pattern parameters that directly and critically affect the raglan sleeve shape. The proposed parameters support coordinated front and back linkage between the raglan sleeve pieces, supporting joint optimization of the overall raglan sleeve shape.

5. To establish new grouping criteria for raglan sleeve volume–silhouette shapes. Real photographs, patterns, and air-gap information will be analyzed to define new volume–silhouette shape parameters, enabling quantitative characterization of different volume–silhouette shapes.

6. To eastablish a new 2.5D dataset, including front-view and profile-view 2.5D projection parameters of the “body + coat” system. The raglan sleeve 2.5D silhouette is quantitatively measured. These 2.5D projection parameters will serve both as AI input data and as reference data for evaluating the accuracy of AI-generated silhouettes.

7. To develop multi-modal prompting strategies. Descriptive words, 2.5D projection values, and 3D reference images are employed simultaneously to guide AI-assisted raglan coat generation. The accuracy of the AI-generated outputs, including the AI-generated body, AI-generated coat, and AI-generated undressed body, is evaluated using the established criteria of raglan sleeve shape, fit, and volume–silhouette grouping.

8. To conduct a multi-dimensional comparative evaluation of the generation accuracy of raglan coats generated by 3D simulation and AI generation. All newly developed raglan-coat design data, including 2D patterns, 3D simulations, AI prompt strategies, and the shape-fit evaluation criteria, are validated through practical testing in both Chinese and Russian garment manufacturing facilities.

CHAPTER 2. OBJECTS AND METHODS OF THE RESEARCH

This chapter establishes unified specifications for the research objects and methods, providing reproducible inputs and a unified calculation basis for the subsequent generation, measurement, and comparative analysis of the "body + coat" digital workflow. First, the research objects, including patterns, bodies, fabrics, and reference images of real raglan coats, are defined as standardized inputs for virtual try-on, AI image generation, and shape comparison under unified size, posture, and material conditions. Second, the digital workflow and software environment are specified to clarify the inputs, outputs, and data-recording rules of each processing step, covering pattern development, 3D virtual try-on rendering, contour extraction, 2.5D projection-parameter measurement, statistical analysis, and figure output. Third, the geometric parameter system for the "body + coat" system, the 2.5D projection measurement specifications, the unified measurement framework, and the statistical calculation protocol are established to support volume-silhouette grouping and quantitative evaluation of shape deviations in the subsequent chapters. Finally, the bodice fit criteria (C_B), sleeve shape criteria (C_C), and volume – silhouette grouping criteria (C_V) are developed to provide a unified basis for evaluating the subsequent generation and comparison results.

2.1.Objects of research

This section defines the research objects used as standardised input data for subsequent pattern development, virtual try-on, measurement, and comparative evaluation. Four object categories were specified, including patterns, bodies, fabrics, and reference images of real raglan coats, to ensure consistent and reproducible conditions for same-scale comparison in the following chapters.

Patterns. To establish the objective basis for optimizing raglan coat pattern-making technology, basic prototype, raglan sleeve prototypes, and various coat patterns were selected and organized for structural analysis.

These pattern objects were organized in three successive levels: basic prototypes, raglan sleeve prototypes, and complete raglan coat patterns. This arrangement makes it possible to trace the development of the raglan coat structure from the bodice foundation, through the sleeve construction logic, to the final coat pattern configuration.

Three basic prototypes, widely used in Chinese manufacturing and educational sectors, were selected as the research subjects. Specifically, the three basic prototypes, *P1, P2*, and *P3,* reflect different bodice construction rules and provide the foundational patterns for subsequent raglan sleeve design. Figure 2.1 shows three Chinese male basic prototypes, *P1*, *P2*, and *P3*.

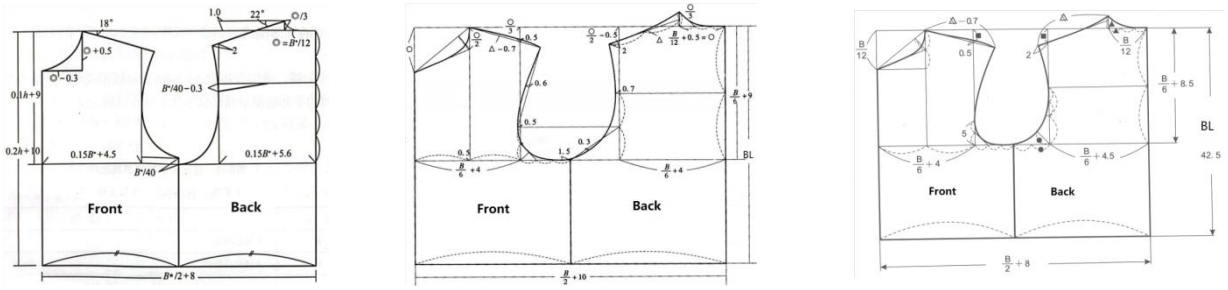

a *b* *c*

Figure 2.1 - Chinese male basic prototypes: *a* - *P1* from Donghua University block [20]; *b* - *P2* from Beijing Institute of Fashion Technology block[21]; *c* - *P3* from X. Xiong [22] (unit: *cm*)

As shown in Figure 2.1, the three prototypes are presented in the front and back pieces, with key pattern control measurements, such as the front chest width, back width, neckline, and front and back shoulder slopes, labeled. These prototypes represent typical approaches to male bodice block construction. Table 2.1 further summarizes the main pattern differences among P1, P2, and P3.

Table 2.1 - Main construction parameters of the basic prototypes P1, P2, and P3

Parameters, cm	P1	P2	P3
Chest ease	16 cm	20 cm	16 cm
Back length	0.2H + 10	Back length	42.5
Armhole depth	0.1H + 9	0.167B + 9	0.167B + 8.5
Front width	0.15B + 4.5	0.167B + 4	0.167B + 4
Back width	0.15B + 5.6	0.167B + 4	0.167B + 4.5
Front neck width	0.083B	0.083B + 0.5	Not explicitly specified
Front neck depth	0.028B	0.028B + 0.167	Not explicitly specified
Back neck width	0.083B-0.3	Not explicitly specified	Not explicitly specified
Back neck depth	0.028B+0.5	0.083B + 0.5	Not explicitly specified
Back dart	0.025B - 0.3	None	None
Front chest dart	0.025B	None	None
Shoulder slope	Front: 18°; Back: 22°	Not explicitly specified	Not explicitly specified
Note: H *denotes body height, and* B *denotes chest girth.*			

As shown in Table 2.1, the three basic prototypes differ primarily in ease of setting, bodice proportion, armhole construction, neckline treatment, dart configuration, and shoulder definition. These differences reflect distinct structural rules underlying the three prototypes and were therefore treated as important input conditions, because they

determine different initial bodice structures for subsequent prototype comparison and raglan sleeve pattern development. In particular, the difference in shoulder definition, including shoulder-point and front and back shoulder sloping construction, was considered methodologically important because it was directly relevant to the later prototype evaluation and correction procedure.

Subsequently, three raglan sleeve prototypes, *P4, P5,* and *P6,* were analyzed. These prototypes are widely applied in China and exhibit distinct differences in construction rules. They were constructed based on the same improved basic prototype in order to control the bodice condition and to identify the most suitable raglan sleeve prototype as the basis for subsequent raglan coat pattern development. Figure 2.2 shows three representative pattern-making methods for raglan sleeve prototypes in China (the original drawings are provided in Figure A.1 in Appendix A.

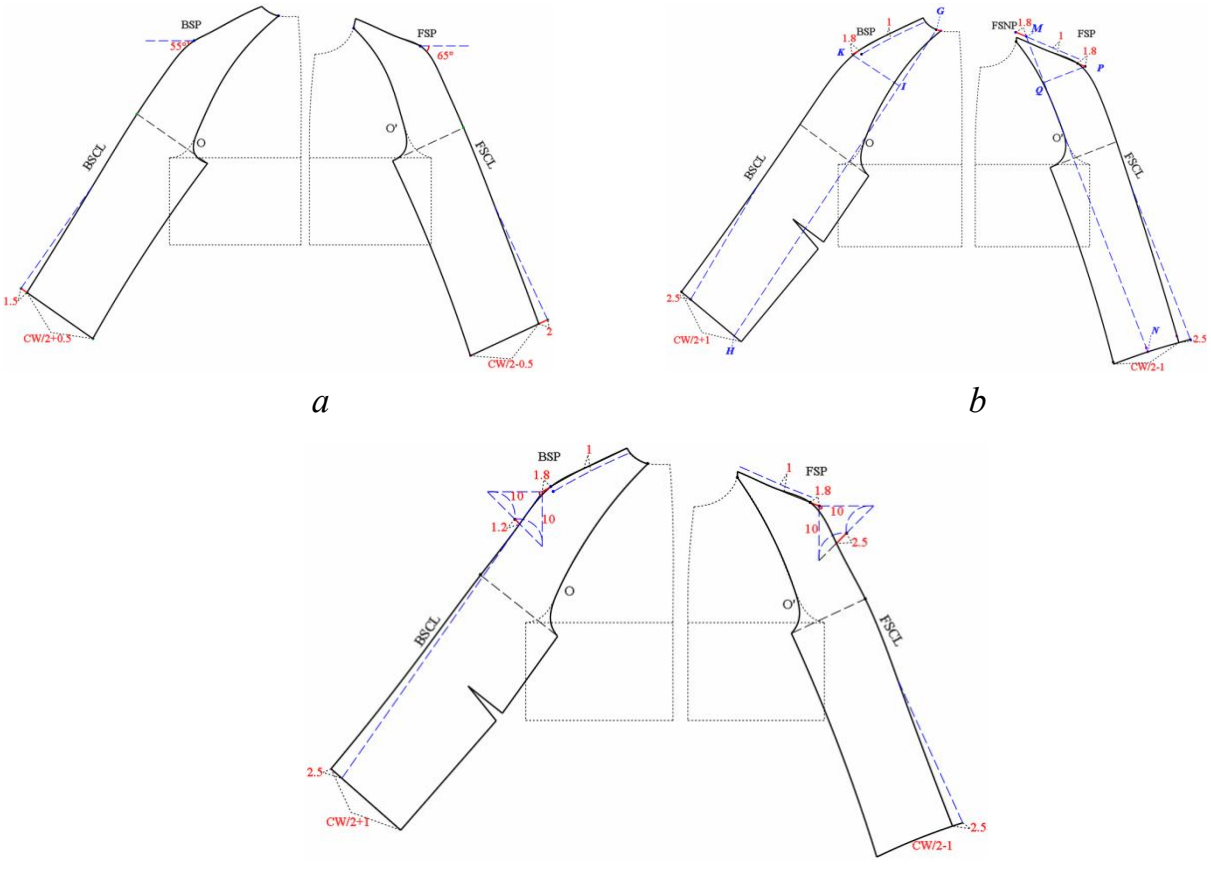

Figure 2.2 - Three raglan sleeve pattern-making methods from Chinese textbooks: *a* - Angle-method (*P4*), *b* - Parallel-method (*P5*), *c* - 10*10 Triangle-method (*P6*)

As shown in Figure 2.2, the construction rules for the three raglan sleeve prototypes differ: *P4* (Angle Method) uses the angle in the shoulder area as the main control method to define the direction of the raglan sleeve and shoulder-sleeve

distribution; *P5* (Parallel Method) controls the relationship between the sleeve seam and sleeve centerline through parallel construction and equidistant transfer; *P6* (Triangle Method) applies geometric constraints to the shoulder point position and shoulder-sleeve angle by constructing fixed-proportion triangle units at the shoulder. Table 2.2 further summarizes the key construction-rule differences among P4, P5, and P6.

Table 2.2 - Key construction-rule differences among the three raglan sleeve prototypes

Parameters, cm	*P4*	*P5*	*P6*
Slope angle of front sleeve center line,°	65°		
Slope angle of back sleeve center line, °	55°		
Distribution of front cuff width (CW)	0.5CW - 0.5	0.5CW -1	0.5CW -1
Distribution of back CW	0.5CW+ 0.5	0.5CW +1	0.5CW +1
Mutual borrowing amount of front and back shou lder lines	0	1	1
Extension of front and back shoulder line at shou lder point	0	1.8	1.8
Difference between the front and back sleeve wid th	1.6	2.1	2.5
The dart of elbow	0	1.8	1.8
Offset from the front sleeve center line at the cuff	-2	-2.5	-2.5
Offset from the back sleeve center line at the cuff	-1.5	2.5	2.5

As shown in Table 2.2, these differences are reflected mainly in sleeve center-line control, front-back cuff-width distribution, shoulder-line borrowing and extension, front-back sleeve-width difference, elbow-dart setting, and cuff-level sleeve-center-line offset. These features indicate that P4, P5, and P6 embody different structural strategies for controlling the shoulder – sleeve configuration.

23 raglan coat patterns from China were analyzed to identify and reorganize the key pattern parameters influencing the shape, and shape outcomes of different pattern-making methods in 3D virtual try-on were compared. This analysis provides a structural basis for the optimization of raglan coat pattern-making. Figure 2.3 shows two typical pattern-making methods for raglan coats.

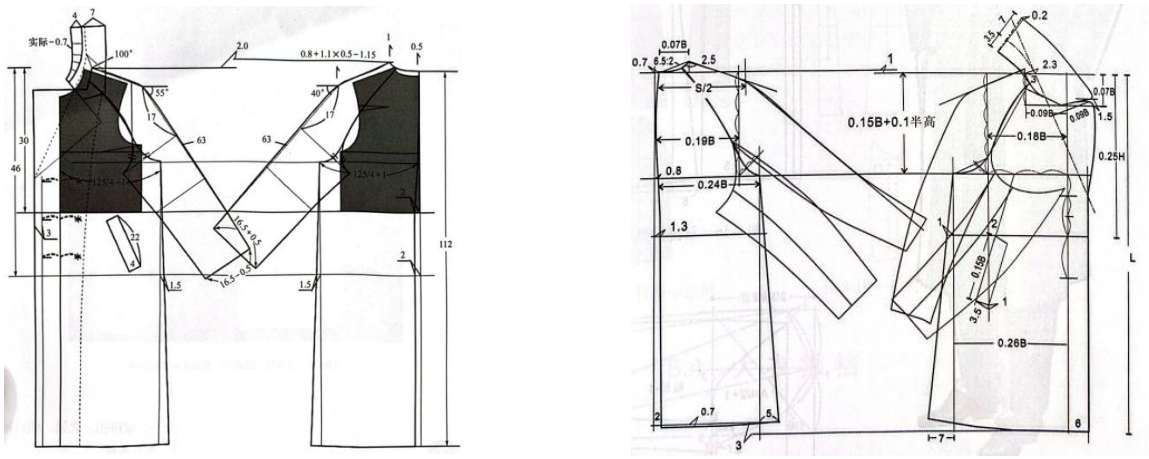

a *b*

Figure 2.3 - Raglan coat patterns: *a* - two-piece raglan sleeve drafted using the prototype method [20]; *b* - three-piece sleeve drafted using the proportional method [21]

As shown in Figure 2.3, two typical pattern-making methods are used for raglan coats: a two-piece raglan sleeve pattern developed using the basic prototype method, and a three-piece raglan sleeve pattern developed using the proportional method. These two methods are treated as representative structures within the pattern set of this study and are used to define pattern differences in sleeve panel segmentation, bodice connection, and key control positions. Therefore, they were incorporated into the subsequent pattern-parameter reorganisation and 3D comparative analysis as representative coat-structure inputs.

Bodies. In this study, a standard body form and a set of avatars with different anthropometric variants were selected. The standard body form had the following dimensions: height 182 cm, chest girth 100 cm, waist girth 84 cm, and hip girth 104 cm. These dimensional characteristics were defined according to the Chinese national standard “Sizing Systems for Garments - Men” (GB/T 1335.1-2008). For fit evaluation, 20 avatars were used, all with the same height of 182 cm, five chest-girth levels (88, 92, 96, 100, and 104 cm), and four fullness categories (Y, A, B, and C), corresponding to chest-waist differences of 22, 16, 11, and 6 cm.

Fabric. Three representative fabric samples, denoted F1, F2, and F3, were selected in this study. These fabrics represent three typical options used in coat production, namely light, medium, and heavy fabrics. Fiber composition, surface density, and thickness were recorded as reproducible parameters. Table 2.3 presents the main characteristics of F1-F3.

Table 2.3 - Property indicators of the three representative fabrics

Fabrics	Fiber content	Weight, g/m2	Thickness, mm
F1	Cotton	168	0.31
F2	Polyester	259	0.74
F3	Wool	544	1.15

These recorded attributes were used to generate digital twins in the subsequent 3D simulations.

Photos of raglan coats. Photographs of raglan coats were used to calculate projection parameters reflecting real coat shapes, including the overall silhouette, segmentation configuration in the shoulder-sleeve region, sleeve-piece direction, front-back sleeve division, fold distribution, and the spatial relationship between the sleeve and the arm. A total of 230 high-resolution photographs of premium-brand coats and real coats were collected.

2.2. Digital workflow and software environment

To ensure that the entire experimental procedure was conducted within one standardized digital workflow, nine software tools were employed, covering 2D pattern development, 3D virtual try-on, AI image generation, contour extraction, 2.5D projection-parameter measurement, geometric analysis, air-gap measurement, statistical analysis, and figure production. Rather than functioning as isolated tools, these software packages were organized into one integrated workflow linking pattern construction, virtual simulation, image generation, parameter extraction, geometric analysis, statistical treatment, and visualization. Table 2.4 shows the specific tasks and the corresponding inputs and outputs of each software tool.

Table 2.4 - Software tools and their tasks

Software information	Company	Primary tasks	Primary inputs	Primary outputs
Richpeace CAD V8	TIANJIN RICHPEACE AI CO., LIMITED (China)	2D pattern development	Pattern structure definition; dimensional parameters	2D pattern files
ET 2020	Shenzhen Buyi Technology Co., Ltd. (China)	2D garment CAD support; industrial pattern processing; preparation of pattern files for production use	Pattern pieces; structural dimensions; 2D pattern files	Edited pattern files; production-ready 2D CAD files

Style 3D V9.0	Zhejiang Lingdi Digital Technology Co., Ltd. (China)	3D virtual try-on	2D patterns; body measurements; fabric properties	Virtual body; 3D garment rendered images
Grok 3	xAI (United States)	AI image generation	Text descriptions; projection parameters; reference images	AI body images; AI coat images
Adobe Illustrator 2024	Adobe (United States)	Contour tracing; extraction of 2.5D projection parameters	Rendered images; real try-on photographs	Contour lines; 2.5D projection parameters
CorelDRAW 2020	Alludo (Canada)	Technical drawing refinement; figure and layout editing; visual annotation and diagram preparation	Vector drawings; pattern diagrams; technical figures	Edited technical figures; layout-ready illustrations; publication-ready graphics
Rhinoceros 7.0	Robert McNeel & Assoc. (United States)	Extraction of body/garment cross-sectional dimensions; air-gap measurement	3D body and garment models	Cross-sectional dimensions of body and garment; air-gap data
IBM SPSS Statistics V26	IBM (United States)	Descriptive statistics; significance testing; regression modelling	Measurement data tables	Statistical indices; test results; regression model parameters
Origin 2021	OriginLab Corporation (United States)	Statistical plotting and result visualization	Statistical result tables	Figures and charts

As shown in Table 2.4, the digital processing workflow of this study was implemented. First, patterns were drafted in Richpeace CAD V8 and ET 2020, including the basic prototypes, raglan sleeve prototypes, and raglan coat patterns, thereby forming a unified 2D pattern input library. Second, the patterns were imported into Style 3D V9.0, where body data and digitized fabric properties were combined with the 2D patterns to generate 3D avatars and virtual try-on rendered images. For both rendered images and real photographs, contour tracing was performed in Adobe Illustrator 2024, and 2.5D projection parameters were measured under unified viewpoint constraints and measurement rules in CorelDRAW 2020; a projection-parameter dataset was then established for subsequent chapters. In addition, AI body images and raglan coat images were generated using Grok 3 to provide an image source consistent with the subsequent comparative analyses. Rhinoceros 7.0 was used to extract cross-sectional dimensions of

the body and the garment and to measure the spatial air-gap between the body and the garment, thereby characterising their spatial relationship. Finally, IBM SPSS Statistics V26 was used for data analysis (including descriptive statistics and regression modelling), and Origin 2021 was used to generate statistical plots and visualisations to produce the figures required in subsequent chapters.

This integrated digital workflow ensures methodological coherence, reproducibility, and traceability across all experimental stages.

2.3. Quantitative framework of the “body + coat” system

In this section, a unified parameter system, measurement specification, and quantitative framework for the “body + coat” system were established. Specifically, anthropometric parameters, pattern parameters, and 2.5D projection parameters were defined, together with the corresponding measurement rules, deviation metrics, and statistical calculation methods. These specifications ensure the consistency and reproducibility of parameter extraction across virtual try-on, fit evaluation, and image generation and provide a unified quantitative basis for subsequent comparison and analysis across different data sources.

2.3.1 Geometric parameterization of the “body + coat” system

This subsection first defines the anthropometric parameters of the upper body and then reorganizes the key pattern parameters of the raglan sleeve to establish a unified geometric basis for subsequent prototype correction, pattern quantification, and shape analysis.

*Body Parametrization.*To locate key shoulder points and accurately calculate shoulder-slope angles, the method of the Department of Garment Design at Ivanovo State Polytechnic University was used [137]. Using avatars, vertical distances, horizontal offsets, and point-to-point distances in the neck, shoulder, and chest regions were measured. These measurements made it possible to obtain anthropometric parameters directly applicable to subsequent pattern drafting, shoulder-slope calculation, and prototype correction.

Figure 2.4 shows the measurement process, which begins with the identification of six main anatomical landmarks: shoulder-neck Point (SNP), front neck point (FNP), back neck point (BNP), shoulder point (SP), front armpit point (FAP), and back armpit point (BAP). In the measurement system, SP was further represented as the front shoulder point (FSP) and back shoulder point (BSP) according to the corresponding projection view.

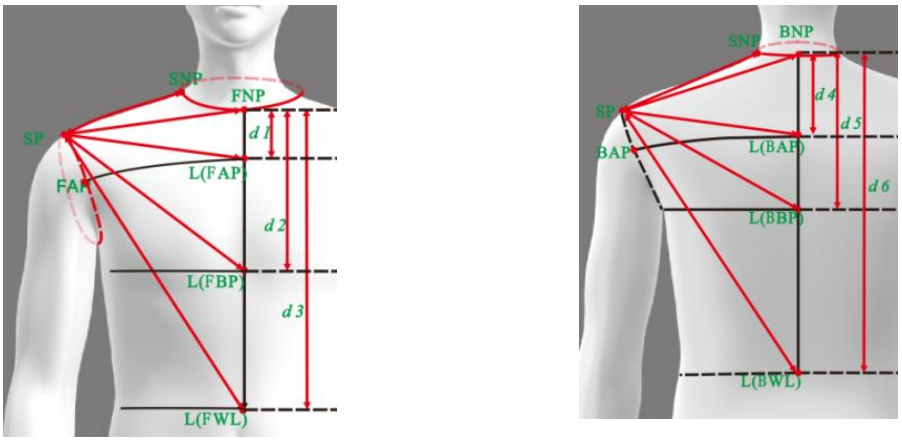

a *b*

Figure 2.4 - New body measurement scheme

Based on these landmarks, 15 geometric parameters were defined to capture the three-dimensional morphology of the upper torso. These include: vertical distances from the neck points (FNP, BNP) to reference horizontal levels (armhole, bust, waist), denoted as d1 to d6; horizontal distances from these levels to the shoulder point (SP), denoted as L(FAP)-FSP, L(FBP)-FSP, etc.; direct distances between neck and shoulder points (SNP – SP, FNP – FSP, BNP – BSP). The complete list of measurements is shown in Table 2.5.

Table 2.5 - Dimensional characteristics for upper-body parameterization

No.	Abbreviation	Measurement Position
①	SNP - SP	Distance from shoulder neck point to shoulder point
②	FNP - FSP	Distance from front neck point to front shoulder point
③	d_1	Vertical distance from front neck point to the line of front armhole point
④	L(FAP)-FSP	Distance from line of front armhole point to front shoulder point
⑤	d_2	Vertical distance from front neck point to the line of front bust point
⑥	L(FBP)-FSP	Distance from line of front chest point to front shoulder point
⑦	d_3	Vertical distance from front neck point to the line of front waist line
⑧	L(FWL)-FSP	Distance from line of front waist line to front shoulder point
⑨	BNP-BSP	Distance from back neck point to back shoulder point
⑩	d_4	Vertical distance from back neck point to the line of

		back armhole point
⑪	L(BAP)-BSP	Distance from line of back armhole point to back shoulder point
⑫	d_5	Vertical distance from back neck point to the line of back bust point
⑬	L(BBP)-BSP	Distance from line of back bust point to back shoulder point
⑭	d_6	Vertical distance from back neck point to the line of backwaist line
⑮	L(BWL)-BSP	Distance from line of back waist line to back shoulder point

As shown in Table 2.5, 15 anthropometric measurements were used to quantitatively describe the key body dimensions required for calculating the shoulder slope and garment-body balance.

Pattern parameters. Based on previous studies on raglan sleeve pattern-making technology conducted at Ivanovo State Polytechnic University[138], the Russian raglan sleeve pattern-making method *A* was adopted as the reference framework for parameter restructuring, as shown in Figure A.2 in Appendix A, under which the 23 raglan coat patterns were processed. The ease allowances for the chest, upper arm, and wrist girths were kept constant. Figure 2.5 shows the key points of the raglan sleeve pattern and the corresponding parameter-measurement scheme.

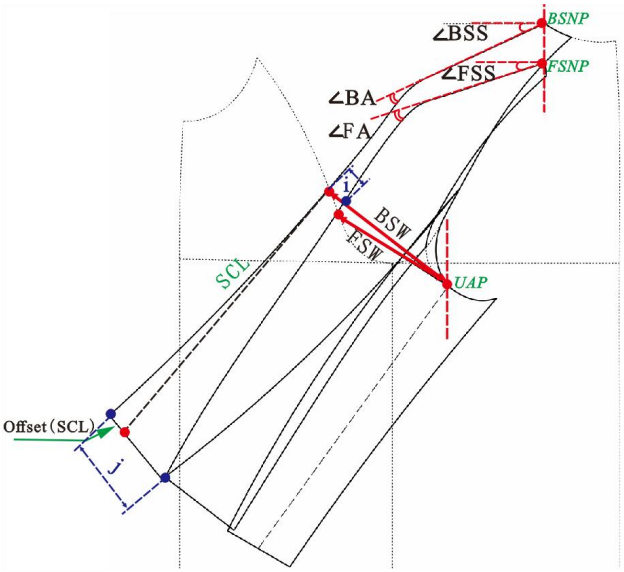

Figure 2.5 - Establishment and reorganization of pattern parameters for raglan sleeve

As shown in Figure 2.5, the alignment of the front and back underarm points (UAP) and the alignment of the front and back shoulder-neck points (FSNP and BSNP) along the same vertical line are used to establish a standardised reference, further

ensuring the consistency of all parameters. The established pattern parameters include shoulder-neck region (BSS, FSS), shoulder-sleeve angle (BA, FA), sleeve body region (back and front sleeve width, BSW and FSW), cuff region (sleeve centerline offset, Offset (SCL)), and the overlap difference between the front and back sleeve panels (i, j). These parameters define the structural configuration of the raglan sleeve at the shoulder-neck region, shoulder-sleeve junction, sleeve, and cuff, forming the basis of the raglan sleeve pattern database for this study. Table 2.6 defines the pattern parameters and their measurement schemes, and the detailed measurements are provided in Table A.1 in Appendix A.

Table 2.6- Quantification of pattern parameters (X_1–X_{14})

Index	Symbol	Measurement Scheme
X_1	∠BSS	Back shoulder sloping
X_2	∠FSS	Front shoulder sloping
X_3	Δ(∠BSS -∠FSS）	Difference between the back and front shoulder sloping
X_4	Δ（∠BSS+∠FSS）	Sum of back and front shoulder slopes
X_5	∠BA	Supplementary angle of the back shoulder line and sleeve center line (SCL)
X_6	∠FA	Supplementary angle of the front shoulder line and sleeve center line
X_7	Δ(∠BA+∠FA)	Sum of ∠BA and ∠FA
X_8	BSW	Back sleeve width
X_9	FSW	Front sleeve width
X_{10}	Δ(BSW - FSW)	Difference between back and front sleeve width
X_{11}	Offset(SCL)	Forward offset of the sleeve center line
X_{12}	i	Difference between the front and back sleeves at the arm-girth line
X_{13}	j	Difference between the front and back sleeves at the cuff
X_{14}	Δ (i-j)	Difference between i and j

Using these parameters, the raglan sleeves were quantitatively described for virtual fitting.

2.3.2. 2.5D projection parameters of the “body + coat” system

3D avatar construction is primarily based on standardized anthropometric data. However, although Style 3D provides 33 default measurements, 29 of them are

circumferential measurements, with only four measurements, including two height measurements (height, height of crotch point), one length (shoulder width), and one angle (shoulder slope). These measurements are insufficient to cover the width and posture angle information required for frontal and profile views and are inadequate for supporting the construction of detailed 2D body images. Therefore, to establish a more complete projection-based description of the human body, this study referred to the Russian anthropometric and sizing standards (GOST 17521-72 (1973) and GOST 17917-86 (2006)) and expanded the projection parameters to include height, front width, profile width, and angles, among other measurements. Figure 2.6 shows 26 projection parameters defined in the frontal and profile views, which together constitute the standardized input parameter set for AI-generated body images.

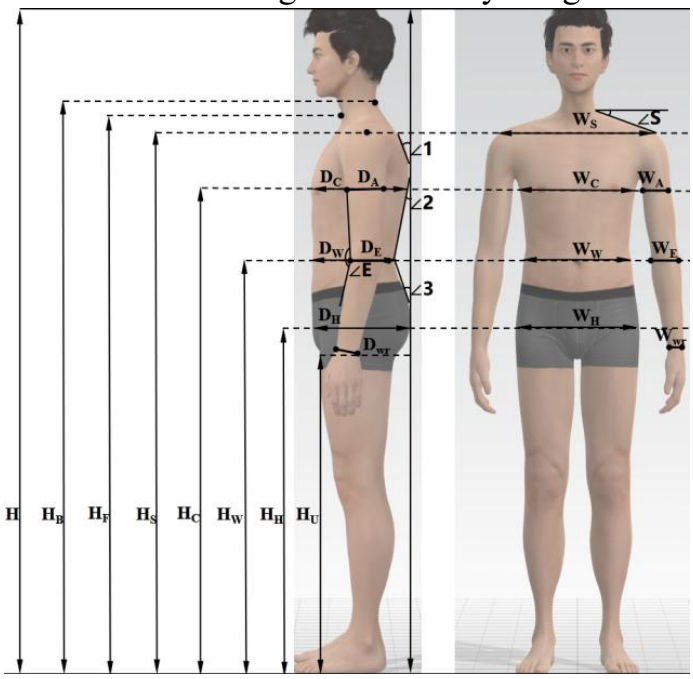

Figure 2.6 - Projection parameters of the 3D avatar in frontal and profile views

Table 2.7 shows the dimensional parameters required for AI-generated body image generation, including the default measurements (H, H_U, and W_S) and the additional projection-based dimensional parameters introduced to improve AI generation accuracy.

Table 2.7- Definition of the body-shape dimension parameters

Dimensions	Measurement Schemes	Dimensions	Measurement Schemes
H	Full body height from head to foot	W_A	Front armhole width
H_S	Height of shoulder point	W_E	Front elbow width
H_U	Height of crotch point	W_{wr}	Front wrist width

H_C	Height of chest line	D_C	Profile chest width
H_W	Height of waist line	D_W	Profile waist width
H_H	Height from the hip line	D_H	Profile hip width
H_F	Height of front neck point	D_A	Profile armhole width
H_B	Height of back neck point	D_E	Profile elbow width
W_S	Shoulder width	D_{wr}	Profile wrist width
W_C	Front chest width	∠E	Arm bending angle in profile view
W_W	Front waist width	∠1	Upper back inclination angle: angle between line from scapula (shoulder blade) to back neck point and vertical axis
W_H	Front hip width	∠2	Upper back inclination angle: angle between upper back line from shoulder blade to waist and vertical axis
∠S	Shoulder slope (front view)	∠3	Hip–waist inclination Angle: angle between line from hip point to waist point and vertical axis

The expanded parameter set enables more precise control of body posture, limb orientation, and profile balance in AI-generated body images,

Based on the above body projection parameters, a corresponding set of coat-shape projection parameters was further developed. Coat-shape parameters were defined in the same frontal and profile views so that the external coat silhouette could be accurately described and compared with body forms.

Figure 2.7 shows the comprehensive 2.5D projection parameter set extracted from the 3D virtual coat in both frontal and profile views.

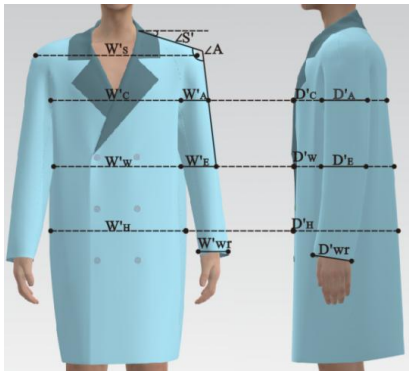

Figure 2.7 - Coat-shape projection parameters

As shown in Fig. 2.7, the projection parameters quantitatively describe the dimensions of the bodice and sleeves at key levels, including the shoulder, chest, waist, hips, armhole, elbow, and sleeve hem.

Table 2.8 shows the projection parameters of the virtual coat and their measurement schemes.

Table 2.8 - Definition of 2.5D projection parameters of the raglan coat shape

Dimensions	Measurement Schemes	Dimensions	Measurement Schemes
W'_S	Front width of bodice at shoulder level	∠A	Angle between shoulder line and sleeve center line
W'_C	Front width of bodice at chest level	D'_C	Profile distance between front and back center line at chest level
W'_W	Front width of bodice at waist level	D'_W	Profile distance between front back center line at waist level
W'_H	Front width of bodice at hip level	D'_H	Profile distance between front and back center line at hip level
W'_A	Front width of sleeve at armhole level	D'_A	Profile width of sleeve at armhole level
W'_E	Front width of sleeve at elbow level	D'_E	Profile width of sleeve at elbow level
W'_{wr}	Front width of sleeve cuff	D'_{wr}	Profile width of sleeve cuff
∠S'	Shoulder sloping		

2.3.3. Unified measurement framework

To conduct a multi-scale, quantifiable structural accuracy evaluation of the AI-generated “body + coat” system, a unified framework of vector-based deviation metrics was established across four dimensions: (i) body generation fidelity, (ii) coat shape accuracy, (iii) structural consistency of the “body + coat” system under dressing, and (iv) shape generalization ability across different volume-silhouette categories. All projection parameters used in this framework were extracted from standardized frontal and profile views, following the protocol detailed in Section 2.3.2.

Based on the 2.5D projection parameters, the present subsection defines the vector system and deviation metrics used for the subsequent quantitative comparison of real, virtual, and AI-generated outputs. Before presenting the deviation metrics, the core projection vectors and abbreviations are first defined to ensure notational consistency and interpretability.

1) Projection vectors related to the body:

RB (Real Body): the projection vectors extracted from real body measurements and

used as the true reference benchmark;

VB (3D avatar): the projection vectors directly exported from the Style 3D virtual avatar;

AIB_A, AIB_B: AI-generated body vectors produced by Grok 3 using *Method A* (text + 2.5D projection values) and *Method B* (text + 2.5D projection values + 3D reference images), respectively.

AIB_C: the projection vector of the underlying body recovered after AI-based coat removal from the dressed "body + coat" image, used to evaluate whether body morphology remains stable under AI-generated dressing.

W_R = { S, C, W, H, A, E, Wr }: the real-body projection-width vector, including shoulder width, chest, waist, hip, armhole depth, elbow width, and wrist circumference, measured from physical subjects;

W_F = { W_S, W_C, W_W, W_H, W_A, W_E, W_{wr} }: vector of the corresponding projection vector extracted from the AI - generated body by Grok 3.

Coat-related projection vectors:

RC: the projection vector of the real coat extracted from high-resolution photographs of physical garments;

VC: the projection vector of the virtual coat simulated in Style 3D;

AIC: the projection vector of the AI-generated coat produced by Grok 3;

$AIC_{S1...S4}$= { AIC_{S1}, AIC_{S2}, AIC_{S3}, AIC_{S4} }: a vector describing the projection vector of AI-generated coats with different shapes (S1, S2, S3, S4) generated using the Grok 3;

$VC_{S1...S4}$ = { VC_{S1}, VC_{S2}, VC_{S3}, VC_{S4} } is a vector describing the projection vectors for virtual coats with different shapes (*S1, S2, S3, S4*) generated using Style 3D;

$RC_{S1...S4}$ = { RC_{S1}, RC_{S2}, RC_{S3}, RC_{S4} } is a vector describing the projection vectors for real coats with different shapes (*S1, S2, S3, S4*) ;

Here, *S1(*Fit*), S2 (*Semi-fit*), S3(*Semi-loose*),* and *S4(*Loose*)* denote the four volume-silhouette categories defined in Section 2.4.3 based on chest ease and two projection-based indicators (AL sleeve width projection at the armhole line and EL sleeve width projection at the elbow line). Each sub-vector (AIC_{S1}) comprises the same 7-dimensional coat projection-width structure as W_F. This metric tests whether the generative model maintains geometric coherence when scaling across fit categories.

Based on the above vector definitions, the deviation metrics were organized into four evaluation groups:

(1) AIB generation accuracy, assessing geometric consistency between AI-generated bodies and real human subjects;

(2) AIC generation accuracy, evaluating structural alignment between AI-generated coats and physical garments;

(3) "body + coat" system consistency, testing whether the underlying body

morphology remains stable under AI-generated dressing; and

(4) silhouette generalization capability, measuring the model ' s ability to maintain shape accuracy across varying volume – silhouette categories.

All deviations are computed using projection vectors defined in Section 2.3.2. The complete set of equations is as follows:

$$\Delta_{WS\ldots Wwr} = W_F - W_R \quad (2.8)$$

$$\Delta 1 = RB - VB \quad (2.9)$$

$$\Delta 2 = RB - AIB_A \quad (2.10)$$

$$\Delta 3 = RB - AIB_B \quad (2.11)$$

$$\Delta 2' = VC - RC \quad (2.12)$$

$$\Delta 3' = AIC - RC \quad (2.13)$$

$$\Delta 4 = RB - AIB_C \quad (2.14)$$

$$\Delta 5 = AIB_B - AIB_C \quad (2.15)$$

$$\boldsymbol{\Delta}_{AIC,S1\ldots S4} = AIC_{S1\ldots S4} - RC_{\boldsymbol{S1\ldots S4}} \quad (2.16)$$

$$\boldsymbol{\Delta}_{VC,S1\ldots S4} = VC_{S1\ldots S4} - RC_{\boldsymbol{S1\ldots S4}} \quad (2.17)$$

Where: $\Delta_{WS\ldots Wwr}$ denotes the projection deviation vector of the AIB relative to the RB; $\Delta 1$ denotes the baseline error of the VB against RB; $\Delta 2$ and $\Delta 3$ denote the deviations of AIBs generated by *Method A* and Method B from RB, respectively; $\Delta 2'$ and $\Delta 3'$ measure the discrepancies between VC, AIC and the RC; $\Delta 4$ represents the deviation between the real body and the body dressing the coat, while $\Delta 5$ captures the structural shift caused by the coat overlay; $\Delta_{S1\ldots S4}$ represents the silhouette-level deviation between AI-generated and real coats across four fit categories (*S1 – S4*).

The deviation metrics defined in Eqs. (2.8-2.17) Establish a comprehensive, multi-level evaluation framework for structural fidelity in AI-generated "body–garment" systems. Together, they provide a unified basis for evaluating body-generation accuracy, coat-shape accuracy, "body+coat" consistency, and silhouette generalization under the same projection-parameter system. This framework is used in the subsequent chapters to support the quantitative comparison of AI-generated results with real-body measurements, real-coat references, and standard virtual simulations.

2.3.4. Methods of Statistical Analysis

In this study, a set of statistical and calculation methods was adopted to ensure that parameter aggregation, deviation evaluation, and comparative analysis were performed under a unified calculation protocol. The corresponding formulas are presented below according to their analytical functions.

To summarize the central tendency of each parameter, the mean value (AV) was

calculated as:

$$AV=\frac{1}{n}\sum_{i=1}^{n}X_i \quad (2.1)$$

where X_i represents an individual measurement, and n is the total number of samples.

To quantify the dispersion of measurements around the mean and thereby assess the consistency of a given silhouette feature, the standard deviation (SD) was calculated as follows:

$$SD=\sqrt{\frac{1}{n}\sum_{i=1}^{n}(X_i-AV)^2} \quad (2.2)$$

A smaller SD indicates that the majority of observations cluster closely around the mean, reflecting high uniformity in that dimension across the sample set. Conversely, a larger SD suggests greater variability. Together, AV and SD were used as the basic descriptive statistics for the subsequent quantitative analysis of body, pattern, and shape parameters.

To reflect the degree of dispersion in the data, the relative deviation (RD) is used to quantify the ratio of the fluctuation range, defined as the difference between the maximum and minimum values, to the average value of the dataset. The formula is expressed as:

$$RD=\frac{MAX-MIN}{AV} \quad (2.3)$$

Where MAX and MIN denote the maximum and minimum values in the sample, and AV is the average value of the dataset. In this study, RD is applied to evaluate the morphological variation of 95 raglan-sleeve outerwear samples at three critical cross-sectional levels: shoulder width, armhole width, and waist width. A higher RD value indicates greater relative fluctuation in silhouette dimension at a specific location, thereby reflecting a higher degree of design diversity or structural sensitivity. Consequently, RD served not only as a dispersion index but also as an analytical basis for the subsequent grouping of raglan-sleeve volume profiles.

To quantify deviations between generated or simulated coat results and real-coat references, the relative error(RE) was calculated as:

$$RE_i=\frac{X_{gen,i}-X_{RC,i}}{X_{RC,i}}\times 100\% \quad (2.4)$$

Where $X_{gen,\,i}$ denotes the projection measurement extracted from AIC or VC, and $X_{RC,\,i}$ is the corresponding measurement extracted from RC. Since RE_i preserves the sign, it indicates whether a generated or simulated silhouette overestimates ($RE_i > 0$) or underestimates ($RE_i < 0$) the real reference along each dimension. This formulation enables a more detailed evaluation of systematic distortions in AI-driven garment generation and virtual simulation, thereby supporting targeted refinement of both generative models and virtual simulation pipelines.

To assess the overall magnitude of geometric discrepancies between generated or simulated silhouettes and reference silhouettes, the mean absolute relative error (MARE) was further computed as:

$$\mathrm{MARE}=\frac{1}{n}\sum_{i=1}^{n}\left|\frac{X_{gen,i}-X_{RC,i}}{X_{RC,i}}\right|\times 100\% \qquad ((2.5)$$

where n denotes the total number of evaluated projection parameters, and $X_{gen,\,i}$ and $X_{RC,\,i}$ are defined as in Equation (2.5). To localize accuracy variation, MARE was further aggregated at two levels: (i) view-level aggregates, using frontal width parameters *W'* and profile width parameters *D';* and (ii) region-level subsets, decomposing the parameter set into bodice and sleeve subsets, with angular parameters (∠S', ∠A) reported as a separate group. Together, RE and MARE were used as the principal error metrics for evaluating local and overall shape accuracy in the generated and simulated coat images.

To evaluate the statistical reliability of the projection mean deviation (*MD*) metrics, a 95% confidence interval was calculated using the t-based classical formulation:

$$\mathrm{MD}=\mu\pm t_{\alpha/2}\cdot\frac{\sigma}{\sqrt{n}} \qquad (2.6)$$

where μ denotes the sample mean deviation, $t_{\alpha/2}$ is the two-tailed critical value at $\alpha = 0.05$, σ is the standard deviation, and n is the sample size. This formulation enabled estimation of the true mean deviation within a statistically reliable margin. Accordingly, the confidence interval was used to support the interpretation of mean-deviation results in the subsequent structural comparison.

Together, these formulas define the unified statistical and calculation protocol of this study.

2.4. New criteria

Based on the quantitative framework established in Section 2.3, three complementary evaluation criteria were developed to address these limitations and

support data-driven raglan coat design: (1) Bodice fit criteria, which assess front–back bodice balance; (2) Sleeve shape criteria, which quantify the 3D positional alignment and conformity between the raglan sleeve and the arm; (3) Volume – silhouette grouping criteria, which group raglan coat shapes into distinct morphological categories with well-defined geometric features, based on critical structural lines that directly link 2D pattern elements to 3D form, specifically, the shoulder line, armhole line, and waist line.

Together, these criteria constitute an integrated evaluation system that enables both qualitative classification and cross-modal quantitative comparison of raglan coat fit and shape across real, virtual, and AI-generated "body + coat" representations.

2.4.1. Criteria for bodice fit

To enable objective assessment of bodice balance and fit, a set of quantitative criteria was established based on 3D virtual try-ons of male basic prototypes, drawing on previous studies conducted at Ivanovo State Polytechnic University. Bodice balance C_B provides the basic structural condition for the subsequent evaluation of raglan sleeve balance.

The development of C_B includes three main steps:

1) The *P1, P2, and P3* were drafted using Richpeace CAD V8 for five chest girth sizes: 88, 92, 96, 100, and 104 cm.

2) Avatar construction. Male avatars were created to represent Chinese body-shape categories Y, A, B, and C, as defined in Section 2.1.2. The key body measurements of these avatars were set in accordance with *GB/ T 10000-2023* and the Chinese male sizing system.

3) Virtual try-on and fit analysis in Style 3D using identical fabric F1 and the same simulation settings.

Based on the results of 60 virtual fittings, different levels of bodice fit were identified. Fit differences were mainly reflected by three visible cues, including the hem alignment (d_F, d_B); the front and back centerline–hem angles (a_F, b_B); and the occurrence of surface folds (c). These indicators were then converted into four quantitative indices to characterize bodice balance and fit measurably. Figure 2.8 shows five side-view parameters (a, b, c, d_F, d_B) used to establish the bodice fit criteria, and representative examples of well-fitted and poor-fit garments used to define the bodice fit indices.

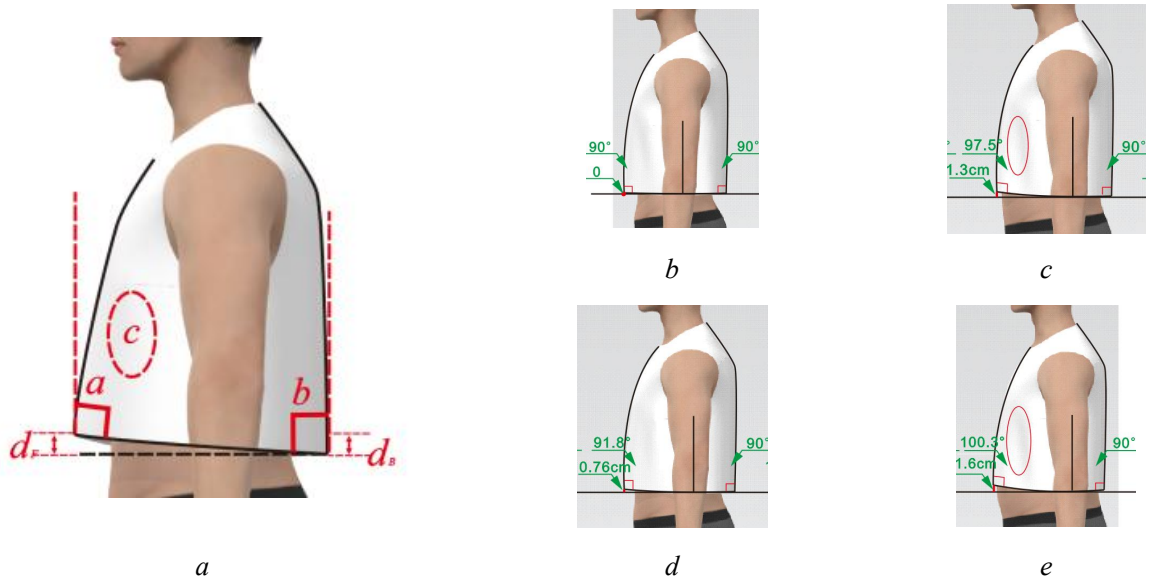

a *b* *c* *d* *e*

Figure 2.8 - Measurement scheme for evaluating bodice fit and balance in side view: *a* - the angle between FCL and the hem, *b* - the angle between BCL and the hem; *c,d,* and *e* - amount of the folds; d_F,d_B - the vertical distance between the hem and the horizontal line; *b* - good-fit sample; *c*, d, and e - poor-fit sample

Together, these parameters describe the geometric balance of the bodice and the presence of visual deformation caused by an imbalance in the bodice. The resulting perception thresholds were set at $90° \pm 2°$ for angular deviations and 0.8 cm for vertical length differences, representing the limits of visual discernibility [6]. The bodice fit criteria were defined as follows:

$$C_B = \{ a_F, b_B \in 88°...92°; c = 0; (d_F + d_B) /2 < 0.8 \text{ cm} \} \quad 2.1$$

The C_B provides an objective basis for evaluating the structural balance of the bodice and comparing prototypes *P1...P3*.

To verify the consistency and applicability of the proposed C_B under both virtual and physical try-on conditions, a virtual–real comparative experiment was further conducted under matched anthropometrics, fabric settings, and a unified measurement protocol. The four parameters of C_B were measured in both settings using the same reference lines and procedure. The process followed four main stages:

1) Selection of *TB* and the corresponding avatar construction. Based on the key dimensions and the additional body measurements defined above, a corresponding male avatar was generated in Style 3D.

2) Virtual try-on of prototypes using digital fabric. The *P1, P2,* and *P3* were virtually fitted to this avatar using three digital fabrics, *F1, F2*, and *F3* (Table 2.1 in section 2.1), respectively.

3) Physical fitting of prototype samples using real fabrics. Physical samples

based on the three prototypes were produced using the corresponding real fabrics and fitted onto real mannequins, matching the body measurements of the avatar. The resulting virtual and real samples and their parameters of C_B are presented in Figure A.3 in Appendix A. For each sample, the parameters were measured with respect to the red dotted reference lines shown in Figure A.3, using exactly the same procedure as in the establishment of C_B.

4) Comparative analysis of fit parameters. The virtual – real difference in C_B parameters was examined for each prototype under the *F1-F3* fabric conditions as shown in Table A.2 in Appendix A.

Table 2.9 shows the average values of C_B parameters for the virtual and real samples of the three prototypes.

Table 2.9 - Average values of C_B parameters for virtual (V) and real(R) samples of the three prototypes

Prototypes	Environment	Average values of parameters for three prototypes			
		a	*b*	*c*	(d_F+ d_B)/2
P1	Virtual	92.2±2.5	90.5±0.5	0	0.6±0.06
	Real	90.7±0.7	89.7±1.9	0	0.7±0.06
P2	Virtual	99.4±1.5	92.8±2.5	0	1.9±0.5
	Real	97.5±3.78	93.7±1.9	0.7±0.6	2.1±0.2
P3	Virtual	104.8±1.2	99.2±0.5	0	2.7±0.4
	Real	104.2±1.9	97.5±4.4	0.7±0.6	2.6±0.2

As shown in Table 2.9, for prototype P1, the mean differences between virtual and real values were minimal: 1.5° for aF, 0.8° for bB, 0 for c, and 0.1 cm for (dF+dB)/2. Both the virtual and real results for P1 were close to the permissible CB range, indicating relatively good bodice balance. For prototypes P2 and P3, the virtual and real results showed more substantial deviations from the CB thresholds, especially for parameter a and for (dF+dB)/2. However, the virtual and real samples showed consistent parameter trends: prototypes with more pronounced angular imbalance and greater hem-level deviation in the virtual environment also showed similar imbalance in the physical fitting results. Overall, the structural balance values and the presence of folds showed consistent evaluation trends between virtual and real samples.

These results confirmed that the proposed CB bodice fit criteria can be applied in

parallel under virtual and physical fitting conditions when different materials are used. Thus, selection of the basic prototype can be performed in the virtual environment according to the established CB criteria.

2.4.2. Criteria for sleeve shape

Accordingly, sleeve shape criteria were further developed to evaluate the spatial conformity between the raglan sleeve and the arm. The male arm exhibits slight elbow bending and a forward-tilting forearm under a natural, relaxed-hanging posture. These characteristics systematically affect the sleeve-arm spatial relationship and sleeve silhouette. Therefore, they should be quantified and incorporated into raglan sleeve pattern- making. Figure 2.9 shows two posture angles defined to parameterize these arm-shape characteristics.

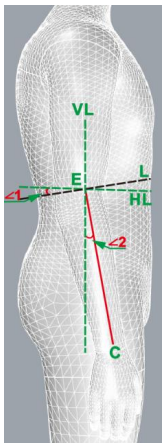

Figure 2.9 - Male arm shape: elbow bending (∠1) and forward tilt (∠2)

As shown in Figure 2.9, angle $\angle 1$ is measured as the inclination of line *L* relative to the horizontal reference line (*HL*) passing through the elbow joint, characterizing elbow bending. Angle $\angle 2$ is defined as the angle between the forearm centre line and the vertical reference line (VL), characterizing forward tilt.

To quantify the variability of these angles across body shape variations, 20 representative male avatars were generated in Style 3D using body data from the Chinese anthropometric database. For each avatar, $\angle 1$ and $\angle 2$ were measured, and the descriptive statistics, in Table A.3 in Appendix A, show that $\angle 1$ ranged from 7.3° to 13.4° (mean 8.9°, SD 1.5°), while $\angle 2$ ranged from 10.6° to 15.7° (mean 12.2°, SD 1.4°), confirming consistent elbow bending and forward tilt in the natural hanging posture. Therefore, the two angles were adopted as reference parameters for evaluating

raglan-sleeve fit in relation to arm morphology, thereby guiding the subsequent development of sleeve-shape evaluation criteria.

It was further observed that changes in raglan sleeve morphology were accompanied by systematic changes in the spatial relationship between the cuff and the arm. Accordingly, a working hypothesis was proposed: raglan-sleeve fit can be evaluated by a set of shape parameters that quantify the sleeve-arm spatial relationship, particularly the front and back cuff–arm distances and the geometric consistency of sleeve curvature. This hypothesis was tested using both real raglan sleeve photographs and 3D virtual try-on.

To establish quantitative raglan-sleeve fit criteria, high-quality photos of raglan coats from premium luxury menswear brands were selected as reference samples, incorporating various measurement indices.[10-13]. For more accurate analysis, 19 high-quality photos were further selected from the initial real-image reference set (resolution $\geq$ 1500 $\times$ 1500 px, file size $\approx$ 2.25 MB).

The selection criteria were as follows: (1) The model was in a standing position with a consistent viewing direction; (2) The arm was naturally hanging; (3) The overall sleeve shape was clearly visible, with smooth contour lines and no folds; (4) The hand was visible; (5) The air gap between the cuff and the arm was clearly visible.

Figure 2.10 shows the measurement scheme for the cuff-arm gap at the hand region and shoulder centerline offset at the upper-arm and elbow levels. Specifically, FC represents the distance between the front cuff and the hand, while BC represents the distance between the back cuff and the hand; d_A and d_E represent the distance between the shoulder centerline and the front sleeve centerline at the upper-arm line and elbow line, respectively.

a *b* *c*

Figure 2.10 - The scheme of air gaps measuring and possible position of cuff and hands: *a* - arm in the neutral position, *b* - BC=0, *c* - FC=0

As shown in Figure 2.10, three cuff–hand configurations were identified: (1) neutral position ; (2) back cuff contact (BC = 0, FC ≠ 0 ; (3) front cuff contact (FC = 0, BC ≠ 0).

Descriptive statistics show that B_C ranges from 0 to 7.2 cm (AV = 2.3 cm, SD = 1.8 cm), whereas FC ranges from 0 to 4.6 cm (AV = 2.3 cm, SD = 1.4 cm), and $|d_A-d_E|$ ranges from 0 to 0.7cm(AV = 0.3cm, SD = 0.2 cm) as shown in Table A.4 in Appendix A. Overall, descriptive statistics indicate that BC and FC share the same mean and exhibit comparable levels of dispersion, suggesting that both parameters are useful for characterize the sleeve-arm spatial relationship at the cuff, while $|d_A-d_E|$ remains tightly bounded, reflecting a highly stable geometric offset.

Based on the reference-photo measurements, virtual and real experiments were subsequently conducted to identify the key shape parameters governing raglan sleeve fit. Specifically, the effects of the FC, BC, and $|dA - dE|$ on sleeve fit were analyzed. In addition, to further enhance the geometric characterization of the sleeve–arm spatial configuration, an additional 3D descriptor, the elbow-point air gap (EC), was introduced. EC quantifies the local air-gap distance between the sleeve and the underlying arm at the elbow region and was extracted from high-fidelity 3D visualizations to capture bending-related sleeve deformations that are critical to functional fit.

Determination of the cuff-clearance parameter FC. In the previous section, three positions for the cuff-arm relationship were identified: FC = 0, FC = BC, and BC = 0. Accordingly, this section aimed to identify the configuration that best balances arm mobility and sleeve smoothness, so that the primary cuff-related shape parameter could be determined. Style 3D simulations were performed under both static and controlled arm-lift conditions. Figure 2.11 shows the parameterization used to construct the 3D virtual models.

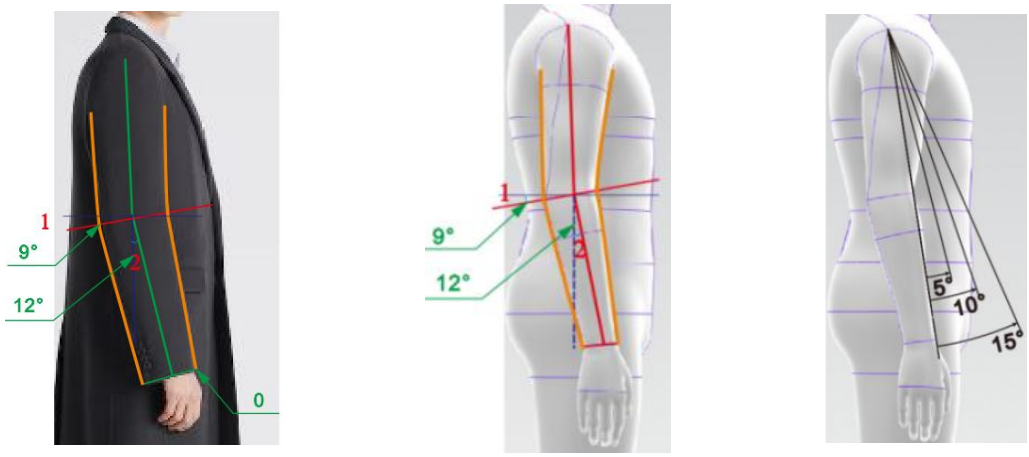

a *b* *c*

Figure 2.11 - Parameterization of the arm and sleeve: *a* - sleeve parameters, *b* - arm parameters, *c* - arm lift angle

As shown in Figure 2.11a, sleeve angle 1 between the sleeve elbow line and the horizontal line and sleeve angle 2 between SCL and the vertical line were measured from the 19 selected photographs. The average values were 9° for sleeve angle 1 and angle 2 = 12° for sleeve angle 2, and the values were applied to parameterize the sleeve-arm configuration in the virtual avatar (Figure 2.6). Dynamic evaluation was performed by prescribing four arm-lift angles (0°, 5°, 10°, and 15°) (Fig. 2.11c) to test sleeve-shape stability within an acceptable motion range. Thus, the comparison was conducted under standardized arm-morphology and movement conditions rather than under a single static posture. To evaluate the influence of the selected parameters, virtual avatars with CG ranging from 88 to 104 cm were used, incorporating coat patterns from HEILAN HOME, a Chinese menswear company specializing in men's coats.

Figure 2.12 compares sleeve appearance under the three cuff contact conditions across the four arm-lift angles, with the arm positioned inside the sleeve with FC = 0, FC = BC, and BC = 0 conditions, while the chest girth ease (E(CG)) was set to 8cm in the comparison. In this way, the comparison isolated the effect of cuff–arm configuration on sleeve-shape stability.

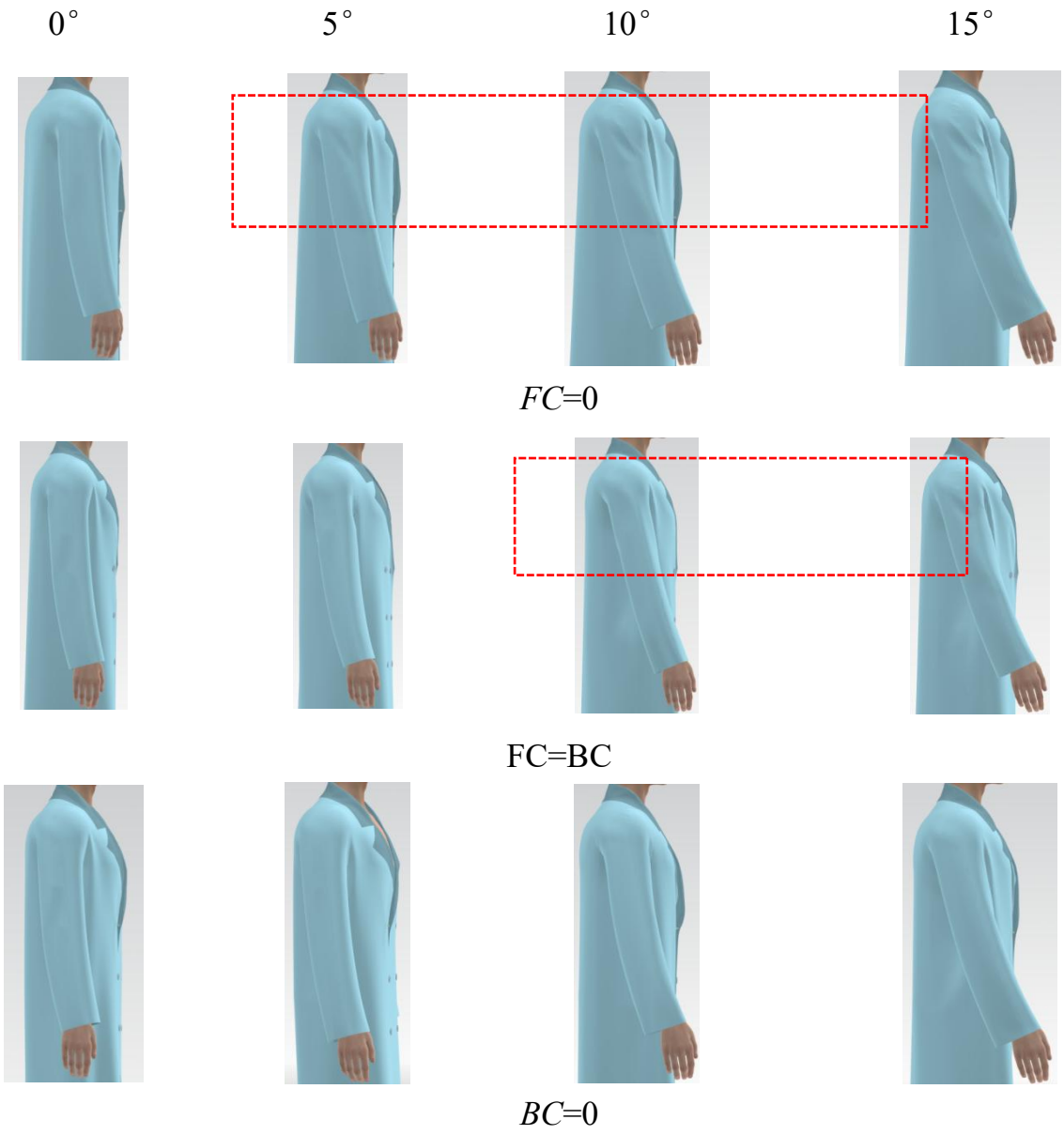

Figure 2.12 - Comparison of sleeve-shape stability under different cuff–arm configurations

As shown in Figure 2.12, when FC = 0, folds appeared in the sleeve as the arm was raised to 5°(highlighted by the red dashed box). As the arm lift angle increased to 10°and 15°, the folds gradually became more pronounced. When FC = BC, folds started to appear at an arm lift angle of 10°, and became more noticeable at 15°. When BC = 0, the sleeve maintained a smooth shape as the arm was raised from 0° to 15°, with no significant folds observed.

The results showed that when BC = 0, the sleeve remained in its optimal shape across all arm lift angles, providing the strongest adaptability for establishing the fit evaluation criteria. Therefore, BC = 0 was defined as the reference condition for the optimal " sleeve hem-arm " configuration, and FC was adopted as the main

sleeve-hem-related shape parameter in the sleeve-shape criteria; its reference range was set as 1-4.3 cm based on measurements from real photographs.

Determination of the elbow-point air-gap parameter EC. An additional parameter, the elbow-point distance, was introduced to describe the correspondence between the sleeve and the arm more completely. This parameter is based on arm morphological characteristics associated with forward forearm inclination and elbow flexion, because sleeve deformation may also occur in the elbow region even when the sleeve-hem position is acceptable.

By varying the chest-girth ease from Chinese garment-construction textbooks [19], raglan coat patterns with ease values of 12, 16, 20, and 24 cm were selected. Thus, the influence of overall coat volume on the correspondence between the sleeve and the arm at the elbow level was studied while maintaining consistency at the sleeve hem. Figure 2.13 shows the virtual fitting results of raglan coats with different ECG values. The sleeves had a smooth appearance and were therefore suitable for analysis of the elbow-point air gap.

a

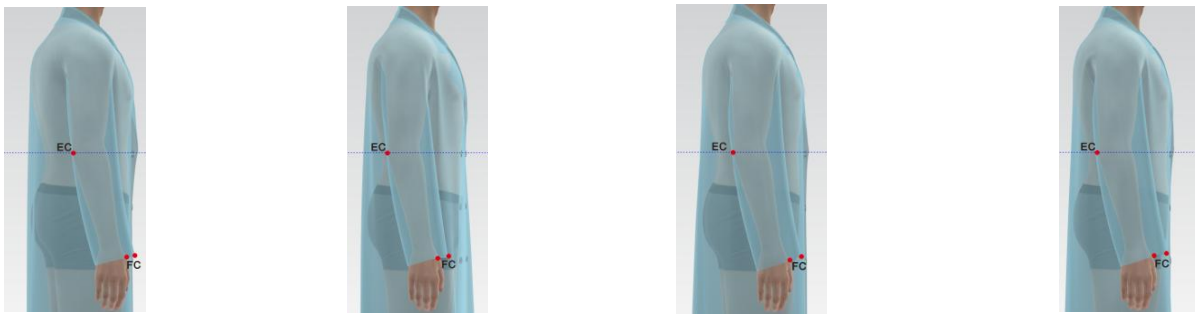

b

Figure 2.13 - Choosing second criteria *EC* for air gap between elbow point and sleeve for raglan coat with different E(CG) = 12, 16, 20， 24 cm: *a* - front silhouette of different E(CG), *b* - profile silhouette of different E(CG))

As shown in Fig. 2.13, increasing ECG changes the overall coat volume and affects the sleeve-hem position. In sleeves with a visually smooth form, the distance

between the sleeve and the arm at the elbow level remained comparatively stable. As ECG changed from 12 to 24 cm, EC remained within 0-0.3 cm, whereas FC varied from 1.0 to 4.3 cm and BC from 0 to 1.2 cm. These results show that EC has a narrower range of variation than the sleeve-hem-related distances and is therefore a stable local descriptor of the correspondence between the sleeve and the arm at the elbow level.

Therefore, EC ∈ [0, 0.3]cm was retained as the second sleeve-shape criterion, complementing FC by extending the evaluation from cuff-level clearance to elbow-level conformity

*Determination of the sleeve-curvature consistency parame*ter $|dA-dE|$. $|d_A - d_E|$ was further introduced as a parameter for evaluating the overall shape stability of the raglan sleeve.

The previous comparative analysis of prototype raglan sleeve shapes indicated that visually stable sleeve shapes corresponded to $|d_A - d_E| \in [0, 0.7]$. This observation suggested that the difference between the sleeve reference-line distances at the upper-arm and elbow levels provides a simple and intuitive descriptor of global sleeve-shape consistency. Therefore, $|d_A - d_E|$ was proposed as the third evaluation criterion for raglan sleeve shape, and its applicability was further examined through comparative analysis of virtual and real samples. Figure 2.14 shows a comparison of the raglan sleeve shape in both virtual and real samples under the conditions of $|d_A - d_E| = 1$ and $|d_A - d_E| = 0$. The front and back sleeve centerlines and the sleeve centerline are marked with red lines to clearly show the changes in sleeve shape.

Virtual Real Virtual Real

a b

Figure 2.14 - Comparison of raglan sleeve shape in virtual and real samples with different $|d_A-d_E|$ conditions: *a* - $|d_A-d_E| = 1$ cm, *b* - $|d_A-d_E| = 0$.

As shown in Figure 2.14, when $|d_A-d_E| = 1$, both the virtual and real raglan sleeves displayed visible sleeve-shape imbalance and reduced sleeve-line consistency. However, when $|d_A-d_E| = 0$, the raglan sleeve exhibited a more balanced sleeve

configuration, smoother sleeve line, and better geometric consistency between the upper-arm and elbow regions. These results indicate that smaller values of $|d_A - d_E|$ correspond to greater consistency between sleeve bending and forward inclination in the upper-arm and elbow regions, thereby producing a more stable overall sleeve silhouette. Therefore, the range $| d_A - d_E | \in [0, 0.7\text{cm}]$ was adopted as the third evaluation criterion for raglan sleeve shape.

In the final C_C system, the same measurement logic was retained, but the notation was simplified for subsequent use in the evaluation criteria. The distance from the sleeve reference line to the sleeve contour at the upper-arm level, previously denoted d_A, was designated as a; the analogous distance at the elbow level, previously denoted d_E, was designated as b. Therefore, the sleeve-line consistency parameter $| d_A - d_E |$ in the final C_C system was written as $|a - b|$, where $a = d_A$ and $b = d_E$. Based on the three stages above, the sleeve-shape criteria for the "avatar-coat" system were established as follows: FC $\in$ [1, 4.3] cm, EC $\in$ [0, 0.3] cm, and $|a - b| \in [0, 0.7]$ cm.

However, a raglan coat is evaluated as an integrated "bodice + sleeve" system. Therefore, based on the raglan sleeve shape criteria and the bodice balance criteria established in the previous section, the final raglan coat shape evaluation criteria were further formulated. In addition, through the analysis of 2D photos and 3D virtual try-on results, folds were introduced as a key shape parameter because they directly reflect local deformation caused by imbalance or mismatch between the bodice and sleeve. The front-view distance from the cuff to the back of the hand (FD) was also introduced to provide a more comprehensive description of the cuff-hand relationship. Figure 2.15 shows the shape parameters used to establish the raglan coat shape evaluation criteria, covering both bodice balance and sleeve-shape control.

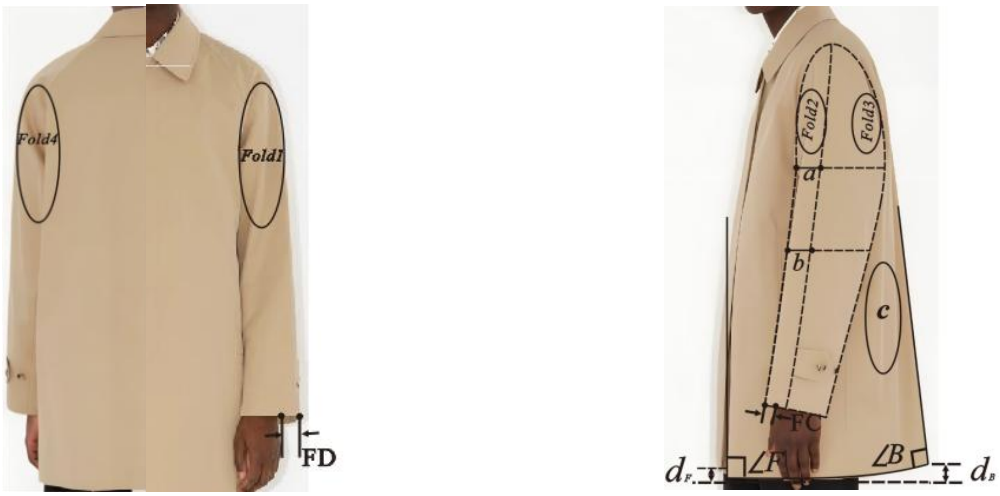

Figure 2.15 - Shape parameters used for establishing the raglan coat shape evaluation criteria (C_C)

These parameters include the front-view distance from the cuff to the back of the hand (FD), the profile-view distance from the cuff to the front arm (FC), the sleeve-line consistency parameter ｜a−b｜, and the presence of folds at specific locations on the front and back sleeve regions, namely Fold1, Fold2, Fold3, and Fold4. In the final C_C system, a and b denote the sleeve reference-line distances at the upper-arm and elbow levels, respectively; therefore, ｜a−b｜ represents the sleeve-line consistency between these two regions. The parameter c describes bodice-surface folds, whereas Folds refers to sleeve-surface folds at four defined sleeve regions.

Accordingly, the final raglan coat shape evaluation criteria (C_C) integrated both bodice-balance and sleeve-shape parameters into one unified evaluative system:

$$Cc = \{ (d_F + d_B)/2;(\angle F + \angle B)/2;\ c\ ;\ FD;\quad FC;\ |a\text{-}b|\ ;\ Folds\quad \} \tag{2.2}$$

Thus, C_C extends the previously established sleeve criteria from local sleeve–arm evaluation to the integrated assessment of the complete raglan coat system.

Table 2.10 shows the definitions, fit criteria, and acceptable intervals of the seven parameters included in C_C, thereby providing the final quantitative basis for raglan coat shape evaluation.

Table 2.10 - Definitions and acceptable intervals of shape parameters in the raglan coat shape criteria (C_C)

NO.	Parameters	Definition	Fit Criteria	Interval, unit
1	d_F	vertical offset from front hem to horizontal line	$(d_F + d_B)/2$	[0,2cm]
	d_B	Vertical offset from back hem to horizontal line		
2	$\angle F$	Angle between front center line and front hem	$(\angle F + \angle B)/2$	[88, 92°]
	$\angle B$	Angle between back center line and back hem		
3	*c*	Folds amount on bodice	c	0
4	*FD*	Distance from cuff to hand back in the front view	FD	[0.7,4.1cm]
5	*FC*	Distance from cuff to front arm in profile view	FC	[1, 4.3 cm]
6	*a*	Horizontal distance between sleeve center line and sleeve center line at upper arm	｜a-b｜	[0，0.7cm]

	b	Horizontal distance between the sleeve center line and front sleeve center line at elbow		
7	*Fold 1*	Fold on front of sleeve	Folds	[0, 1]
	Fold 2	Fold on front- side of sleeve		
	Fold 3	Fold on back-side of sleeve		
	Fold 4	Fold on back of sleeve.		

Together, these criteria form the final quantitative basis for evaluating raglan coat shape. They serve as permissible thresholds for raglan coat shape under a given silhouette condition.

2.4.3. Grouping of volume- silhouette shapes of raglan coats

Based on the previously established 2.5D projection framework, grouping criteria for raglan coat volume–silhouette were developed.

The present volume–silhouette grouping was established for raglan coats within the fabric range commonly used for autumn – winter outerwear. The selected photo samples represented garments with a medium- to heavy-weight outerwear appearance, corresponding to the autumn–winter fabric range. Under this material background, the grouping procedure focused on contour changes associated with chest-girth ease. The resulting C_V intervals therefore describe silhouette variation within a comparable autumn –winter outerwear range.

Shape parameter establishment based on pattern structure. This section proposes a real-photo-based 2.5D volume–silhouette grouping method.

A total of 230 high-quality runway photos of raglan coats were collected from fashion shows between 2010 and 2025 across multiple brands. From this dataset, 95 images were retained as analysis samples. The selection considered pose consistency, clear visibility of the front sleeve appearance, representative silhouette variation, and consistency of garment category and material range. All retained samples belonged to autumn–winter raglan coats, and their apparent thickness, overall volume, and contour expression were kept within a comparable outerwear range. Fold quantity and fold morphology on the bodice were used as auxiliary visual cues during screening to exclude samples whose material expression deviated markedly from the target autumn–winter outerwear range. Based on the observed volume–silhouette differences, the samples were preliminarily categorized into four groups: Fit, Semi-fit, Semi-loose, and Loose.

Figure 2.16 shows representative examples of these four volume – silhouette groups, demonstrating an apparent progression from a fitted to a looser silhouette.

However, although this visual grouping was intuitive, it remained descriptive and lacked measurable evidence for comparing volume and contour changes across groups.

a *b* *c* *d*

Figure 2.16 - Representative raglan coat volume–silhouette groups: *a*-Fit, *b*-Semi-fit, *c*-Semi-loose, and *d*- Loose

To convert the above visual grouping into a measurable grouping framework, a practical geometric correspondence was established between the sleeve contour observed in real photographs and its counterpart defined on the 2D pattern. Based on this assumption, four key shape parameters d_{11},d_{12}, $d_{13,}$ and $\angle A_{SS}$ are introduced as primary descriptors of volume – silhouette variation, together with their corresponding pattern parameters d_{11p}, d_{12p}, d_{13p}, and $\angle$Assp.

Figure 2.17 shows the measurement scheme of the shape and pattern parameters.

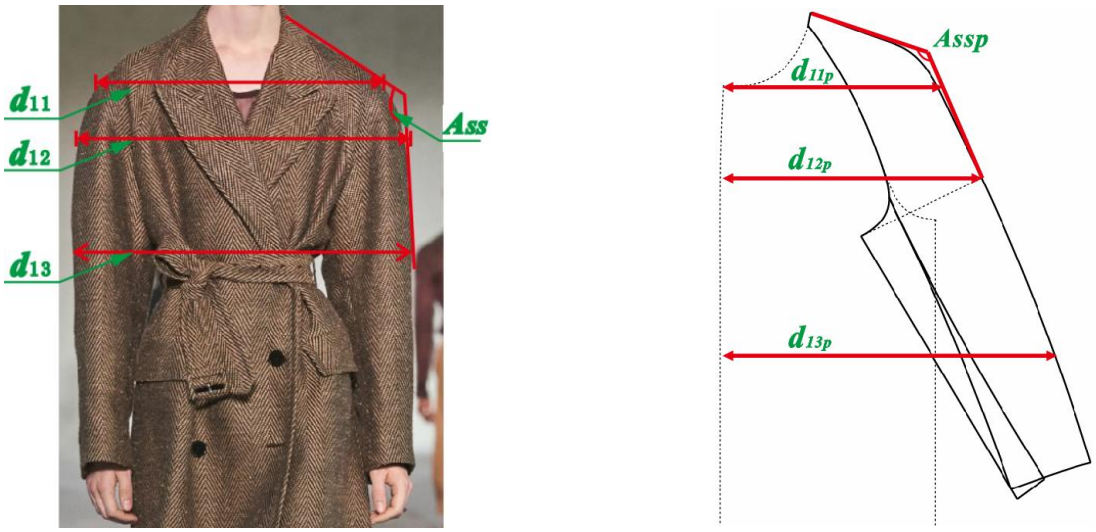

a *b*

Figure 2.17 - Measurement scheme for shape and pattern parameters: *a* - volume-silhouette shape parameters measured on real photos; *b*- corresponding pattern parameters measured at the same reference levels

Table 2.11 defines their measurement rules.

Table 2.11 - Definitions and measurement schemes of shape and pattern parameters

Parameters， cm		Measurement scheme
Shape	d_{11}	Horizontal shoulder width measured from the outermost sleeve points
	d_{12}	Sleeve width measured at the armhole level (biceps line)
	d_{13}	Sleeve width measured at the elbow level
	Ass,°	Angle between the shoulder line and the sleeve center line
Pattern	$d_{11\text{p}}$	Horizontal distance from shoulder point to front center line
	$d_{12\text{p}}$	Sleeve width at the armhole level, measured at the intersection between the shoulder-width reference line and the sleeve center line
	$d_{13\text{p}}$	Horizontal distance from sleeve center line to front center line
	Assp,°	Angle between shoulder line and front center line

Statistical data from 95 coat photographs were obtained and are presented in Table A.5 in Appendix A. The results reveal that d_{12} and d_{13} exhibit the largest relative spreads (RD= 0.47 for both), followed by d_{11} (RD=0.40) and A(SS) (RD=0.27). This indicates that the dominant variation of raglan sleeve volume–silhouette occurs mainly at the armhole and elbow levels, rather than at the shoulder level or the sleeve–shoulder

orientation. Therefore, d_{12} and d_{13} are selected as the key shape indicators for the subsequent volume–silhouette grouping. These results show that d12 and d13 capture the largest between-sample variation and therefore serve as the principal grouping parameters. In the present study, these two parameters describe the contour-width changes of autumn – winter raglan coats under different chest-girth ease levels.

Grouping of different volume-silhouette shapes. To delineate quantitative ranges of the key silhouette descriptors d_{12} at the armhole level and d_{13} at the elbow level, a two-phase workflow was developed, combining ease-based pattern evidence with cross-sectional air-gap quantification. Figure 2.18 shows the overall procedure for defining E(CG) intervals and conducting cross-sectional analysis for raglan coat silhouette grouping.

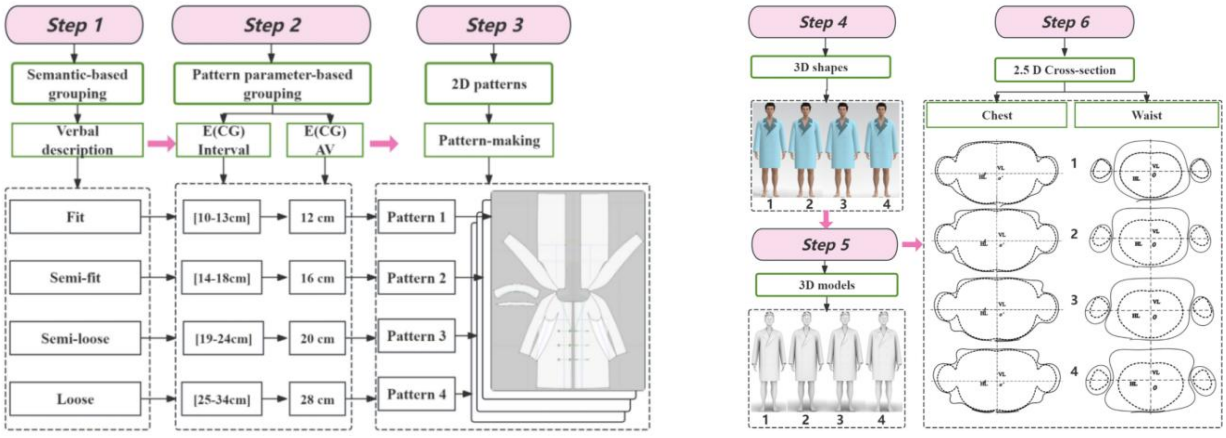

a *b*

Figure 2.18 - Workflow for defining raglan coat volume-silhouette groups: *a*- procedure for defining E(CG) intervals; *b* - procedure for 3D virtual try-on and cross-sectional analysis.

As shown in Figure 2.18, the workflow consists of two consecutive phases. In the first phase (Steps 1 – 3), silhouette groups are semantically labeled and linked to chest-girth ease values from authoritative pattern-making sources, so that stable E(CG) intervals can be established. In the second phase (Steps 4 – 6), the representative silhouette patterns are converted into 3D virtual garments, and the corresponding cross-sectional air gaps at the armhole and elbow levels are quantified to derive measurable grouping boundaries.

One 100 raglan coat draft was analyzed. The complete data set is presented in Table A.6 in Appendix A. Table 2.12 shows the agreed E(CG) ease ranges for the four volume-silhouette groups.

Table 2.12 - E(CG) intervals for different raglan coat volume-silhouette groups

E(CG),cm		Fit	Semi-fit	Semi-loose	Loose
From Making -Patterns	MIN	10	13	18	22
	MAX	13	18	25	35
	AV	**12**	**16**	**20**	**28**
From Semantic Description	*Initial Interval 1*	10...13]	12...18	18...25	22...35
	Final Interval	**[10-13]**	**[14-18]**	**[19-25]**	**[26-35]**

Next, it was determined how the four silhouette categories could be expressed through measurable silhouette widths at the armhole and elbow levels. The .dxf pattern files corresponding to the four silhouette contours were imported into Style3D (step 4). 3D virtual fitting was performed on the same avatar, and the results were saved in .obj format. These files were then imported into Rhinoceros 7.0 for extracting and measuring cross sections (step 5). Finally, cross sections were extracted at the AL and EL levels (step 6). Figure 2.19 shows the AL and EL cross sections for the four volume-silhouette groups.

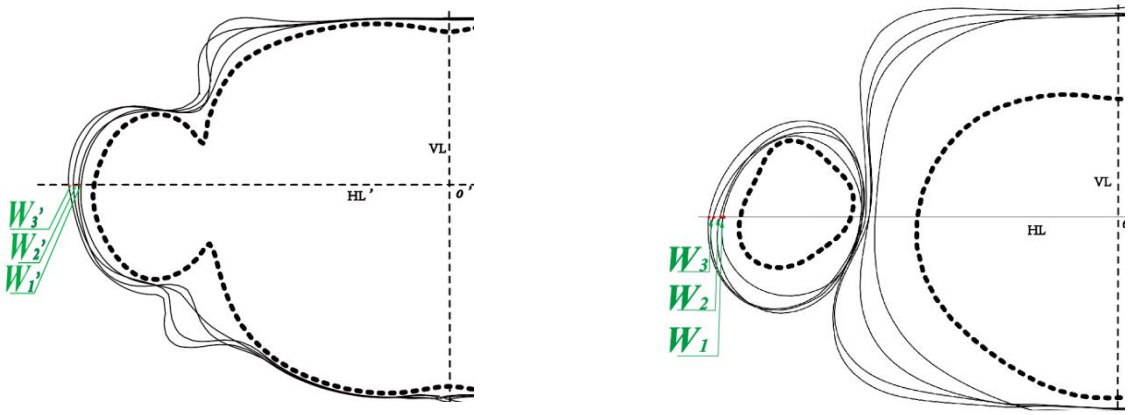

a *b*

Figure 2.19 - Cross-sections at AL and EL for the four volume–silhouette groups: a - AL cross-section; b - EL cross-section. The dashed curves represent the body contour, and the solid curves represent garment outer contours corresponding to E(CG)=12E(CG) = 12E(CG)=12, 16, 20, and 28 cm from inner to outer.

As shown in Figure 2.19, AL and EL represent the armhole-level and elbow-level cross-sections, respectively. In the AL cross-section, VL and HL were used as the vertical and horizontal reference lines, and their intersection point O was used as the alignment origin. In the EL cross-section, VL and HL′ were used as the corresponding reference lines, and their intersection point O′ was used as the alignment

origin. Based on these two origins, the body contour and the four garment outer contours corresponding to E(CG) = 12, 16, 20, and 28 cm were overlaid under the same reference coordinate system. The dashed curves represent the body contour, whereas the solid curves represent the garment outer contours from inner to outer. The full-width spacing between adjacent garment contours was used to represent the air-gap increment between neighboring volume–silhouette groups. At the AL cross-section, these increments were denoted as W1′, W2′, and W3′; at the EL cross-section, they were denoted as W1, W2, and W3.

The spacing between adjacent contours at AL and EL was recorded as full-width air-gap increments ΔW_i^{AL} and ΔW_i^{EL} (cm), where i = 1, 2, 3 correspond to Fit→Semi-fit, Semi-fit→Semi-loose, and Semi-loose→Loose, respectively. These increments represent the measurable full-width contour expansion between neighboring silhouette groups. Table 2.13 shows the resulting increments. The ΔW_i values were extracted as full-width air-gap increments from the overlaid cross-sections.

Table 2.13 - Full-width air-gap increments between adjacent silhouettes (ΔW_i, cm)

Section	ΔW_i^{AL}	E(AL)	ΔW_i^{EL}	E(EL)
Fit→Semi-fit	W_1'	0.8	W_1	1.2
Semi-fit→Semi-loose	W_2'	1.9	W_2	2.5
Semi-loose→Loose	W_3'	1.6	W_3	1.6

To reduce visual ambiguity in silhouette perception, a full-width perceptual tolerance of 1.5 cm, corresponding to ± 0.75 cm per side, was incorporated into grouping boundaries, consistent with established visual discrimination thresholds [24]. Consequently, the quantitative grouping criteria for shape parameters d_{12} *and* d_{13} are defined as follows:

$$Interval = d_{min} + \sum_{i=1}^{k} \Delta W_i \pm 1.5, k=1,2,3,\ d \in \{d_{12}, d_{13}\} \tag{2.3}$$

Where $d_{\min}$ denotes the minimum values obtained from real-photo statistics, and ΔW_i denotes the full-width air-gap of different silhouettes.

Table 2.14 shows the grouping criteria (C_V) for four volume – silhouette categories in terms of the retained key shape parameters (d_{12} and d_{13})at the armhole and elbow line.

Table 2.14 - Quantitative grouping criteria (C_V) of raglan coat volume –silhouette (cm)

Grouping basis	Shape parameter	Fit	Semi-fit	Semi-loose	Loose
Interval， cm	d_{12}	44.8...46.8	46.9...52	52.1...56.7	56.8...70
	d_{13}	46.8...50.8	50.9...57.4	57.5...62.2	62.3...73.4

As shown in Table 2.14, the final grouping criteria (C_V) define the quantitative intervals of the two retained key shape parameters, d_{12} and d_{13}, for the four raglan coat volume – silhouette categories. These intervals provide a reproducible basis for distinguishing Fit, Semi-fit, Semi-loose, and Loose silhouettes under unified 2.5D measurement conditions. Accordingly, the C_V criteria extend the previously established fit and shape evaluation system from single-silhouette assessment to the systematic classification of multiple volume – silhouette categories. Table 2.14 defines the C_V intervals for autumn–winter raglan coats within the fabric range represented by the photo data.

2.4.4. Standardized multimodal AI generation protocol for the “body + coat” system

Based on the projection-parameter system (in Section 2.3) and the evaluation criteria developed (Sections 2.4.1–2.4.3), a standardized multimodal generation protocol was further developed for the AI-driven reconstruction of the “body + coat” system. The purpose of this protocol was to ensure that the generated AI images remained controllable, comparable, and measurable under unified conditions. This protocol links the previously defined projection parameters and evaluation criteria with the subsequent AIB and AIC generation experiments by standardizing the textual, numerical, and visual inputs used in AI generation.

Table 2.15 shows the standardized multimodal prompt design scheme used for AI-generated body and raglan coat images.

Table 2.15 - Standardized prompt design scheme for generating AI images

Description aspect	Role in measurement-oriented generation	Typical elements (examples)
Body features (semantic + projection constraints)	Provide anthropometric descriptors and projection-derived geometric cues to stabilize body proportion and silhouette reconstruction.	Gender; age range; body shape descriptor; height; key length/circumference/width/angle values (cm/deg); proportional cues based on landmarks.

Pose and view control.	Lock the posture and camera view to ensure cross-sample comparability and stable projection extraction.	Standard anthropometric standing pose; neutral stance; consistent arm position; front/profile/back view (as required); full-body framing.
Clothing details (garment semantics)	Constrain garment category and structural configuration to reduce design ambiguity and stabilize body–garment interaction cues.	Garment type (raglan coat); fit level; color; collar; hem; pocket; seam/closure specification (single/double-breasted, buttons/zipper).
Fabric attributes (visual material cues)	Guide visually plausible rendering of drape and surface response, supporting fit/shape interpretation while avoiding exaggerated artifacts.	Matte/glossy; stiff/soft; thick/thin; stretchy/draped; texture/weave cues; controlled fold tendency.
Lighting constraints	Minimize shadow-induced contour distortion and improve visibility of body/garment outlines for measurement.	Soft uniform lighting; controlled direction; consistent intensity; low shadow contrast; avoid harsh highlights.
Background constraints	Remove distractions and increase contrast to facilitate subsequent silhouette/projection analysis.	Plain studio background; neutral color; no props; no extra people; no complex environment.
Realism and quality requirements	Enforce photorealistic, evaluation-friendly outputs and reduce generation noise that would bias projection measurements.	Natural skin texture; anatomically plausible muscle relief; consistent garment–body contact; physically plausible creases; avoid occlusion, extreme perspective, and visual artifacts.

Within the general framework, two input settings were defined. Method A used textual descriptions together with 2.5D projection values, whereas Method B additionally incorporated 3D-rendered reference images while retaining the same textual and geometric inputs. In both methods, pose, view, lighting, and background constraints were kept unchanged so that the generated outputs remained directly comparable in the subsequent structural and fit evaluations. The standardized protocol consisted of four main steps: preparation of body and garment inputs, construction of the multimodal prompt, AI image generation under controlled visual conditions, and post-generation measurement using the established 2.5D projection framework. On this basis, the protocol was first implemented for AIB generation and was then extended to the generation of the AI “body + coat” system.

Structured prompts for AIB generation. The body-generation process was implemented in Grok 3. The procedure included: (1) exporting standardized front-view

and side-view images of the 3D virtual body (VB) from Style 3D as .png reference images; (2) generating the corresponding front-view AI body image; and (3) generating the corresponding side-view AI body image under the same workflow conditions. In both methods, the same body-related descriptors, projection-parameter constraints, and visual-control conditions were maintained. The only controlled difference was whether 3D VB reference images were introduced as visual learning input. Table 2.16 summarizes the structured prompt design for AIB generation.

Table 2.16. Basic structure of the prompt for AIB generation

Item	Content
Role	AI-driven multimodal body image generation system
Objective	Generate realistic AI body (AIB) images of a typical male body in standardized front and side views for subsequent projection-based structural evaluation.
Primary priority	Body proportion accuracy, posture stability, and silhouette reconstruction under measurement-oriented generation, with consistent pose, view, lighting, and background across samples.
Method setting	**Method A**: textual descriptions+ projection values. **Method B**: textual descriptions+ projection values + 3D virtual body (VB) reference images.
Input parameters	**Body descriptors:** The body-related inputs included sex, body type, height, chest, waist, and a set of projection-derived width, length, and angular parameters.
	Front-view projection parameters: For the front view, these included height 182 cm, chest width 33.3 cm, waist width 29.3 cm, hip width 35.3 cm, upper arm width 9.1 cm, elbow width 8.0 cm, wrist width 6.0 cm, shoulder width 44.6 cm, shoulder slope 22.8°, arm length 60 cm, inner foot length 84.5 cm, shoulder point to foot 149.2 cm, chest to foot 131.6 cm, waist to foot 114.5 cm, and hip to foot 90.3 cm.
	Side-view projection parameters: For the side view, these included height 182 cm, chest circumference 100 cm, waist 84 cm, chest width 26.7 cm, waist width 22.7 cm, hip width 26.2 cm, upper arm width 11.4 cm, elbow width 8.9 cm, wrist width 6.5 cm, elbow angle 165.8°, front neck point to foot 150.3 cm, and back neck point to foot 157.9 cm.

Structural constraints	The generated body should be a normal and proportionate male figure standing in a basic anthropometric pose. The front view should be frontal, and the side view should be strictly lateral. The full body, including the feet, should be visible. The figure should be barefoot. Arm position should remain natural and consistent with anthropometric observation.
Stylization policy	Realistic male body appearance with black hair; form-fitting light gray leggings to reveal body contours without excessive exposure; realistic skin texture, anatomically plausible body surface, and plausible fabric–body interaction; even soft diffused lighting; pure black background for strong contour contrast.
Negative prompt	Avoid body tilt, distorted limbs, incorrect body proportions, occluded body contours, extreme perspective, inconsistent view angle, and visual artifacts.
Output	Standardized front-view and side-view AI body images under controlled visual conditions, suitable for subsequent projection extraction and comparison with real-body and 3D virtual body references.

As shown in Table 2.16, the prompt was organized as a measurement-oriented generation protocol, including the generation objective, input parameters, structural constraints, stylistic-control elements, negative constraints, and output requirements. Under this scheme, Method A tested whether textual and projection inputs alone were sufficient to reconstruct body shape and posture, whereas Method B tested whether the addition of 3D-rendered VB reference images could further improve accuracy.

Structured prompts for the AI "body + coat" system. After establishing the body-generation protocol, the multimodal prompting strategy was further extended to the generation of the AI "body + coat" system. At this stage, the aim was to ensure the geometric consistency of the generated coat with the standardized body reference and with the target volume-silhouette conditions defined earlier. Because AIC generation required stable control of the "garment-body" spatial relationship and the coat structure, Method B was used at this stage. Table 2.17 summarizes the structured prompt scheme for AIC generation.

Table 2.17 - AI prompt design for multimodal coat image generation

Item	Content
Role	AI-driven multimodal image generation system for the “body + raglan coat” configuration
Objective	Generate standardized front-view and side-view AIC images of a male figure wearing a raglan coat for subsequent projection-based structural and fit evaluation.
Primary priority	Preserve the structural configuration of the raglan coat and the garment–body relationship under measurement-oriented generation, while maintaining consistent pose, view, lighting, and background for cross-sample comparability.
Method setting	**Method B:** textual garment descriptions + 2.5D projection values + 3D-rendered “body + coat” reference images.
Visual reference input	A standardized virtual body wearing a raglan coat generated in Style 3D was used as the 3D-rendered visual reference.
Input parameters	**Garment descriptors:** The garment-related inputs included garment type (classic raglan coat), fit level (slim fit), closure mode (double-breasted and fully buttoned), fabric color (light gray), garment length, sleeve length, and a set of projection-derived structural parameters.
	Front-view projection parameters: For the front view, these included shoulder width 48.8 cm, chest width 37.1 cm, waist width 37.0 cm, hip width 37.6 cm, sleeve width 48.8 cm, elbow width 21.3 cm, wrist width 18.4 cm, scapular-region projection angle 42.9°, angle between shoulder line and sleeve center line 125.3°, sleeve length 62 cm, and coat length approximately 100 cm.
	Side-view projection parameters: For the side view, these included shoulder width 48.8 cm, chest width 33.9 cm, waist width 35.0 cm, hip width 35.4 cm, sleeve width 18.9 cm, elbow width 17.9 cm, wrist width 15.7 cm, sleeve length 62 cm, and coat length approximately 100 cm.
Structural constraints	The generated coat should be a classic raglan-sleeve coat with a sleeve-to-neckline connection. The male figure should have black hair, be 182 cm tall, have a normal build, be barefoot, and stand in a basic anthropometric pose with arms hanging naturally along the sides and feet kept close together. The front view should be frontal, and the side

	view strictly lateral. The full body should be visible. The coat should remain buttoned with all double-breasted buttons fastened, and the cuffs should be approximately at the wrist.
Stylization policy	Realistic garment appearance with light-gray fabric; clear garment–body interaction; visually stable slim-fit silhouette; black wall background; evaluation-oriented realism rather than decorative stylization. The general visual controls inherited from the shared multimodal framework included soft uniform lighting, reduced shadow interference, plain background, and photorealistic output quality suitable for silhouette and projection analysis.
Negative prompt	Avoidance of visible or excessive sleeve folds, occlusion, extreme perspective, inconsistent view angle, and visual artifacts.
Output	Standardized front-view and side-view AIC images under controlled visual conditions, suitable for subsequent projection extraction and comparison with real and 3D-simulated coat references.

As shown in Table 2.17, the AIC prompt retained the same measurement-oriented organization as the AIB prompt, but additionally introduced garment-specific control of raglan-coat structure, garment-body relationship, sleeve characteristics, and silhouette-related parameters. Under the shared constraints of pose, view, lighting, and background, the generated AIC images could be directly compared with real-coat images and virtual-coat images under the same projection-based measurement conditions. By combining textual garment descriptions, projection-parameter values, and 3D rendered reference images within a unified protocol, the prompt design improved control over the coat contour, the “sleeve – arm” relationship, and volume – silhouette reproduction.

Overall, the standardized multimodal prompting protocol established in this subsection provided a controlled and reproducible pathway for generating AIB and AIC images under unified geometric, visual, and measurement constraints.

Conclusion of Chapter 2

1. A new upper body measurement scheme was developed to accurately identify and reconstruct key anatomical points according to Russian anthropometric and garment-sizing principles, including shoulder points and side seam location, thereby improving the shoulder and side seam structure accuracy of the basic prototype. Based on the body morphology, representative Chinese basic prototypes were optimized to

provide a reliable bodice foundation for raglan-sleeve pattern-making.

2. A hierarchical quantitative evaluation system for the integrated“bodice-sleeve” framework was developed, comprising three tiers of criteria: bodice balance fit evaluation C_B, raglan coat shape evaluation C_C, and volume-silhouette grouping criteria C_V. These criteria were derived from bodice balance, arm posture characteristics, and volume – silhouette differences, including forward tilt and elbow bending of the arm. The system enables the adaptability of raglan coat structures to be assessed across different body shapes and silhouette categories, ensuring geometric balance, sleeve – arm conformity, and shape stability between the bodice and sleeve. The framework provides structured guidance for subsequent pattern optimization, shape verification, and accuracy-oriented raglan coat development.

3. A structured 2.5D “body + coat” projection-parameter dataset was constructed. Under standardized posture and angle conditions, key body dimensions and angles of both front and side projections were systematically defined and measured to form a structured and comparable 2.5D dataset. This dataset serves as a bridge connecting 2D patterns, 3D shapes, and AI-generated images, providing a unified data benchmark for subsequent AI-driven generation and virtual-real consistency evaluation.

4. A measurement-oriented multimodal prompting strategy was formulated for AI-assisted generation of the “body + coat” system. The strategy defines the input structure based on textual descriptions, 2.5D projection values, and 3D-rendered reference images, thereby providing a standardized basis for the generation experiments in Chapter 4. Together with the C_B, C_C, and C_V criteria, this protocol supports the subsequent evaluation of AI generation accuracy, fit consistency, and volume-silhouette generalization.

CHAPTER 3. DEVELOPMENT AND IMPROVEMENT OF THE RAGLAN COAT CONSTRUCTION

On the basis of the measurable evaluation system established above, Chapter 3 develops an engineering-oriented workflow for designing and improving coat patterns. Specifically, Section 3.1 selects a male basic bodice prototype through virtual fittings across several body-shape categories. The selected prototype is then verified for body types Y, A, B, and C using body-type-specific parameters of shoulder slope and side-seam position. Section 3.2 compares alternative raglan-sleeve prototypes to identify the raglan-sleeve construction that better corresponds to arm morphology. Section 3.3 investigates raglan-coat pattern drawings and identifies key parameters and their corresponding shape parameters. Through this procedure, constructional changes are transformed into quantitative rules for predicting and optimizing coat shape.

3.1. Basic bodice prototypes

3.1.1. Selection of basic bodice prototypes

For the subsequent raglan-sleeve pattern development, three standard basic prototypes (*P1, P2,* and *P3*) were evaluated through virtual try-ons on 20 male avatars representing diverse body shapes, yielding 60 standardized samples (3 prototypes × 5 chest girths × 4 body shapes). All samples were simulated in Style 3D using an identical woven fabric (*F1*) and consistent physical parameters. Each sample was assessed against the four parameters (*a, b, c,* $(d_F + d_B)/2$) of bodice fit criteria C_B (Section 2.4.1) and classified as "good fit" or "poor fit" per predefined thresholds.

Figure 3.1 shows the overlapped side-view contours of the 20 virtual try-ons for *P1...P3,* respectively.

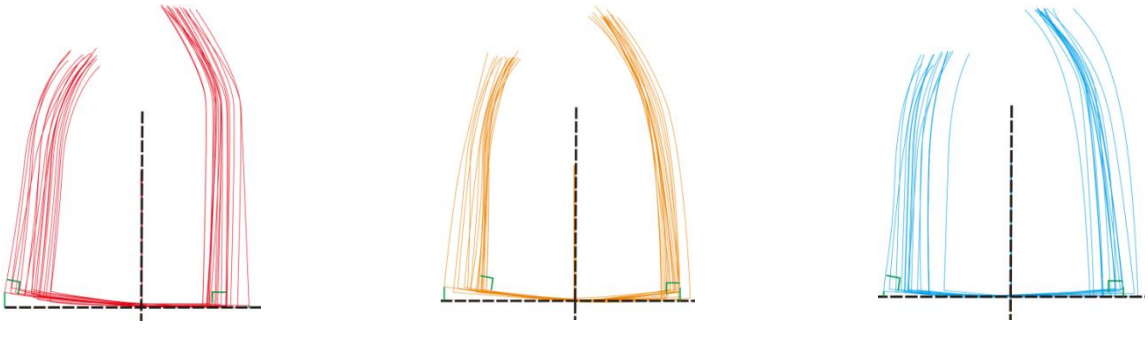

a *b* *c*

Figure 3.1 - Overlaid contours of the 20 virtual try-ons for basic prototypes: *a* - *P1*, *b* - *P2*, *c* -*P3*

As shown in Figure 3.1, the side-view contours of all samples were overlaid and aligned along the side seam as a common reference line. Table 3.1 shows the total number of samples that satisfied the threshold for each C_B parameter. Detailed distributions for parameters of C_B appear in Table A7 - A10 in Appendix A.

Table 3.1 - C_B parameter-pass counts across prototypes based on 20 virtual try-on samples

Parameters	Number of bodices with a good fit		
	P1	*P2*	*P3*
a	10	3	6
b	16	12	9
c	10	4	3
$(d_F + d_B)/2$	11	7	10
Cumulative pass amount	47 (58.5 %)	26 (32.5 %)	28 (35 %)

Note: Values represent the number of samples satisfying the threshold for each C_B parameter. For each prototype, the maximum cumulative count was 80, calculated as 20 virtual try-ons × 4 C_B parameters. Percentages were calculated relative to these 80 parameter-level evaluations.

As shown in Table 3.1, P1 achieved the highest cumulative CB pass rate at 58.5%, outperforming P2 and P3. Therefore, P1 was selected as the basic prototype for the subsequent development of raglan-coat patterns. However, the remaining cases that did not satisfy the criteria indicated that prototype P1 still did not provide optimal fit for all selected body types, confirming the need for further modification.

3.1.2. Improvement of the bodice basic prototype

These deficiencies of P1 were mainly associated with two structural regions that directly affect bodice balance: shoulder configuration and the position of the side seam. Therefore, the subsequent modification focused on the FSS, BSS measurements, and the BWG: FWG ratio for the four body types.

Prototype P1 was modified through a multi-stage process combining 3D body modelling, anthropometric measurements, and 2D pattern adjustment. First, 20 standardized male avatars were generated in Style 3D according to the Chinese male size system. Second, the key anatomical landmarks, including the FSP, BSP, SNP, and the BWG: FWG ratio. Based on these measurements, P1 was redrafted in Richpeace V8.0 by adjusting the shoulder slope and side-seam position in the flat pattern. Finally, a

virtual try-on was performed to evaluate the modified bodice according to the bodice-fit C_B.

The shoulder region was selected for prototype modification because it directly affects bodice balance, comfort, and overall fit. In the original *P1*, the total shoulder slope was preset at 40° (front 18° and back 22°). However, this fixed configuration did not accurately represent the shoulder morphology of many contemporary Chinese male body types, as shown in Figure 3.1.

To establish body-type-specific shoulder slope, a graphical-analytical measurement method was developed. This method enabled quantitative locate FSP, BSP, and SNP, and to calculate the inclination angles of the shoulder cuts. Figure 3.2 shows the scheme used to determine the positions of the shoulder lines.

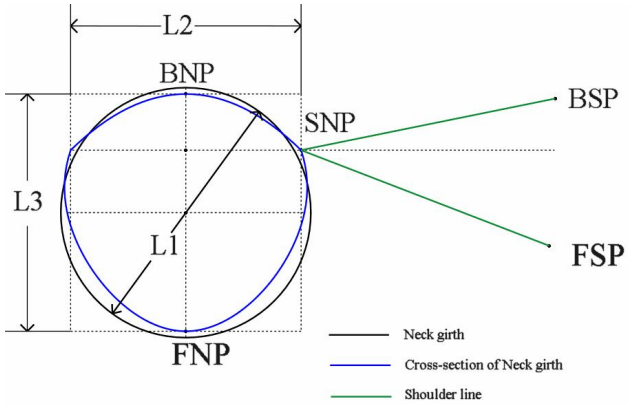

Figure 3.2 - Construction of the neck section and localization of FNP, BNP, and SNP (L1-L3)

As shown in Figure 3.2, the neck section is modelled as an ellipse to represent the anatomical characteristics of the neck. Given the neck girth (NG), the diameter *L1* was calculated as $L1=NG/\pi$. To account for anterior-posterior elongation and lateral compression observed in 3D avatars, the transverse diameter *L2* was set to *0.95L1,* and the anteroposterior diameter *L3* to *1.05L2*. This elliptical model was then divided into four equal sectors, with SNP positioned at a back-to-front ratio of 1:3 along the neckline.

Quantitative measurements were taken at 15 key body regions. The spatial positions of FSP and BSP were projected onto a 2D plane, enabling geometric quantification of their relationship to SNP. Figure 3.3 shows the geometric procedure used to localize the shoulder points and to compute the FSS and BSS.

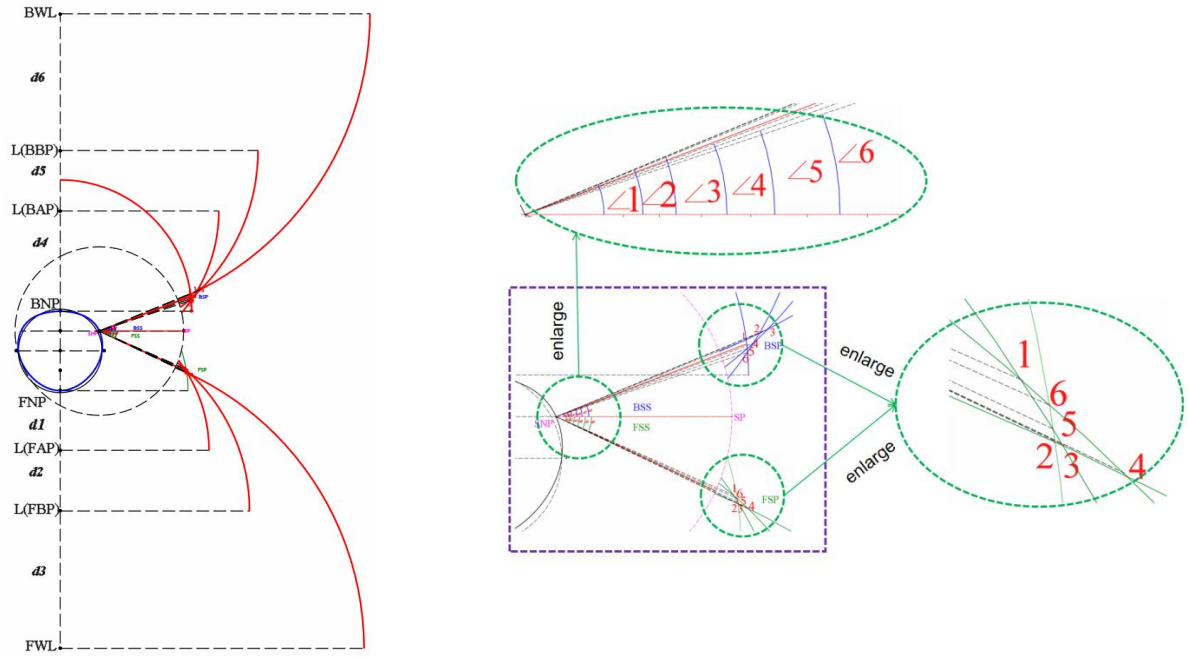

a *b*

Figure 3.3 - Graphical-analytical scheme for determining FSS and BSS: *a* - circle-based intersection solutions constrained by measured distances; *b* - enlarged views of the six candidate intersection points (Points 1–6) used to estimate shoulder slope angles.

Based on the six measured dimensions (③, ⑤, ⑦, ⑩,⑫,⑭), the landmark positions L(BAP), L(FAP), L(BBP), L(FBP), L(BWL), and L(FWL) were located on the front and back center lines in the 2D plane. Eight dimensions (②, ④, ⑥, ⑧, ⑨,⑪,⑬, ⑮), the distances from FNP, BNP, L(BAP), L(FAP), L(BBP), L(FBP), BWL, and FWL to SP were computed (Figure 2.8*a*). Circles were constructed using these distances as radii. This procedure yielded six candidate points (Points 1–6) for the front and six for the back, corresponding to candidate 3D locations of the FSP and BSP, respectively.

After the candidate shoulder points were determined, the shoulder slope was calculated by constructing line segments from SNP to Points 1–6 (in Figure 2.8 b) for each avatar. The included angle between each segment and the horizontal reference line SNP–SP (dashed line in Fig. 2.7) was defined as the SS. The final SS for each avatar was obtained by averaging the six angles. The same procedure was applied to all 20 avatars.

To support prototype modification for different body types, the anthropometric measurements were grouped based on the Y, A, B, and C body types. Two critical geometric parameters were identified as the key determinants of bodice fit: (1) shoulder slope configuration, quantified by BSS and FSS, and (2) lateral body partitioning, defined by the FWG and BWG, and their BWG: FWG ratio. Table 3.2 shows the mean

values of these parameters for the four body types, with the full dataset provided in Table A.11 in Appendix A.

Table 3.2. Body-type-specific anthropometric parameters used for bodice modification

Body-type	AV				BWG:FWG
	BSS, °	FSS, °	BWG, cm	FWG, cm	（%）
Y	21.3±1.8	25.0±1.2	17.5±1.8	19.5 ± 1.5	47.2：52.8
A	22±1.2	25.5±0.6	18.4 ± 1.9	21.6 ± 1.3	46：54
B	22.6±1.7	25.8±0.9	19.9 ± 1.8	23.1 ± 1.5	46.4：53.6
C	22.9±1.5	26.1 ±0.7	20.9 ± 1.7	24.4 ± 2.3	46.2：53.8

As shown in Table 3.2, the combined BSS+FSS angle ranges from 46.3±2.2° for the Y-type body to 49.0±1.7° for the C-type body, which exceeded the fixed shoulder slope of the P1 prototype by 6.3°-9.0°, corresponding to 15.7-22.5%. These results indicate that the original prototype underestimated the shoulder configuration of contemporary Chinese male body types. Therefore, the shoulder parameters of P1 were modified according to the mean BSS and FSS values of the corresponding body Y, A, B, and C types.

Another critical factor is the body side line position, which determines the front and back partition of waist girth. The BWG: FWG ratio varied across different body shape categories, indicating that the original 1:1 front – back waist-girth partition in P1 was not suitable for all body types. Therefore, FWG and BWG were quantified to support accurate side-seam repositioning. Figure 3.4 shows the identification of the body side line and the partitioning of waist girth into FWG and BWG across body-type categories.

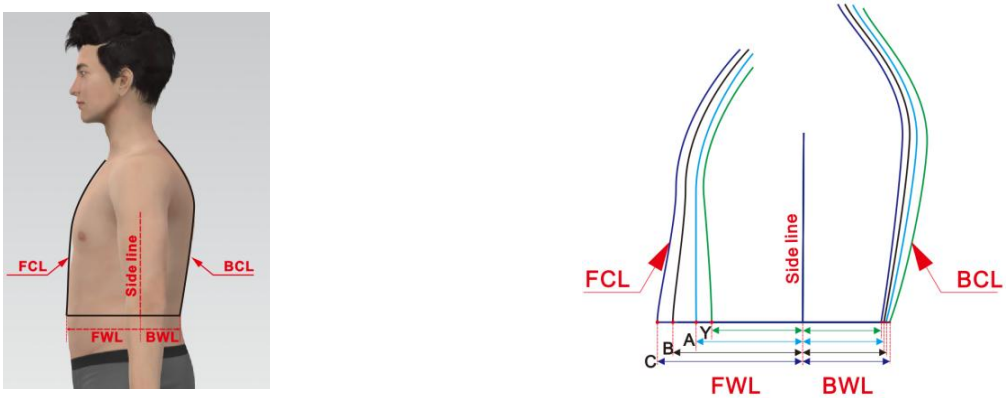

a *b*

Figure 3.4 - Body side-line identification and waist-girth partitioning: a- the body side line on the avatar; b- side contour overlay across body-type categories(Y, A, B, and C)

As shown in Figure 3.4, after alignment to the body side line, the front waist line (FWL) and back waist line (BWL) differ across body shapes, indicating an uneven front –back distribution of waist girth. As shown in Table 3.2, the BWG: FWG ratio ranged from 46.0:54.0 to 47.2:52.8 (Table A.12 in Appendix A), which deviated from the original 1:1 front-back partition used in prototype P1. Based on the body-type-specific modification rules established above, P1 was modified separately for the Y, A, B, and C body types. Figure 3.5 shows the original Donghua bodice prototype P1 and the corresponding shoulder-line and side-seam adjustments applied to each body type.

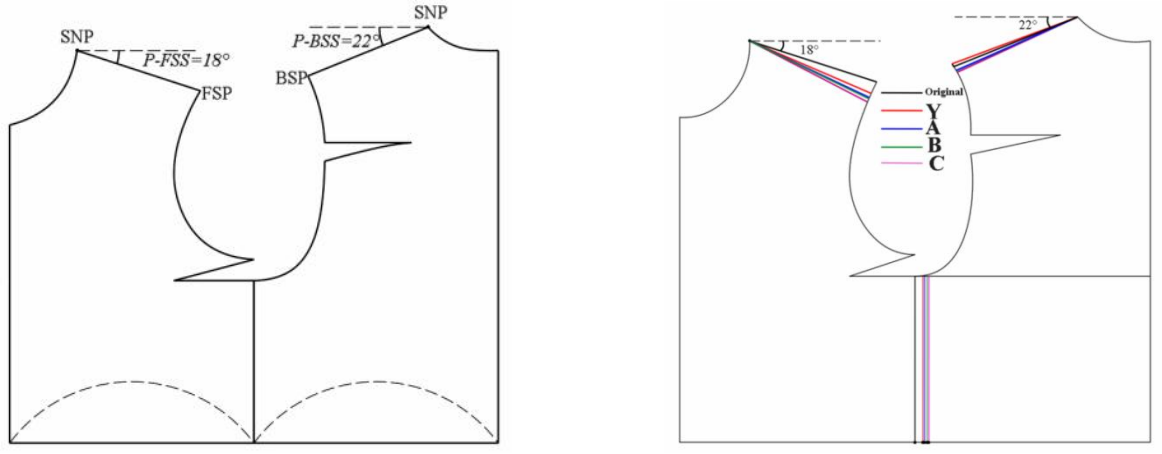

a *b*

Figure 3.5 - Modification of prototype P1: *a* - original prototype P1, b - shoulder-line and side-seam adjustments for the Y, A, B, and C body types

To evaluate the effect of the proposed prototype modification, virtual try-ons were conducted on the 20 avatars. Figure 3.6 shows the side contours of the bodice before and after modification for the four body types.

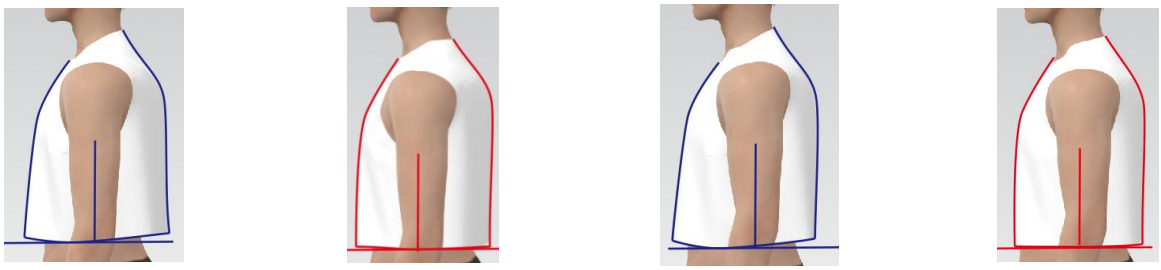

a *b*

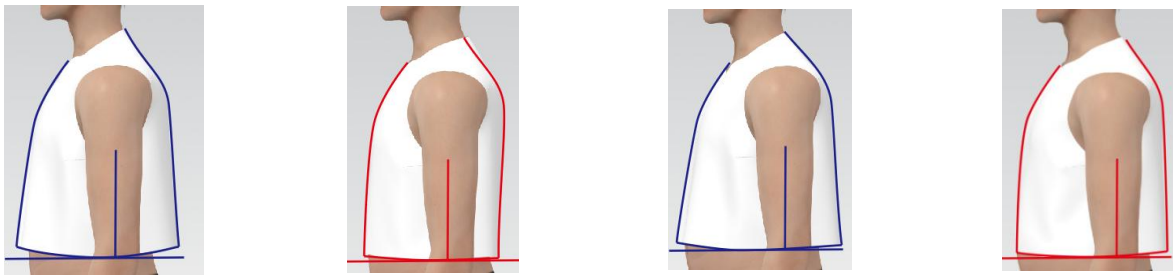

c *d*

Figure 3.6. - Side-view silhouettes before and after bodice-block modification across body-type categories: a - Y; b - A; c - B; d - C; blue outline—prototype *P1*; red outline—corresponding modified prototype

As shown in Figure 3.6, compared with P1, the modified prototypes substantially improved the bodice-fit indicators for all four body types. According to the measurements (Table A.13, Appendix A), the number of passed cases for the CB fit parameters were 19, 18, 20, and 19, respectively, corresponding to 95%. Compared with the original P1 prototype (58.5%), the modified prototypes showed a marked improvement in bodice fit, confirming the effectiveness of the proposed modification strategy.

3.2. Raglan sleeve prototype

3.2.1. Comparison of raglan sleeve prototypes

Comparison of 2D patterns. In the naturally relaxed lowered position, the male arm is characterized by forward inclination and flexion at the elbow. These two features directly affect the spatial relationship between the arm and the sleeve and, therefore, should be reflected in sleeve pattern design. Based on these morphological characteristics, the 2D pattern shapes of three two-piece raglan sleeve prototypes, P4, P5, and P6, were compared.

The forward tilt of the arm can be represented in the 2D pattern by the relative forward shift between two structural reference lines: the sleeve centre line (SCL) and the sleeve side seam line (SSL). To ensure comparability, two alignment conditions were used: SCL - alignment and SSL - alignment. Forward tilt is quantified by the forward offset between SCL and SSL, while elbow bending is quantified by the forward angle of the back sleeve induced by the elbow dart. Figure 3.7 shows the overlay results under the two alignment conditions, highlighting their mapped forward-tilt and bending features in 2D pattern geometry.

P4 *P5* *P6*

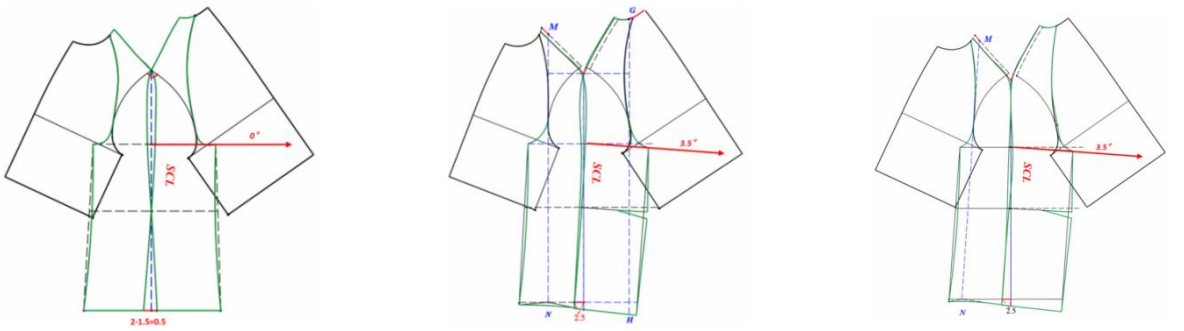

a

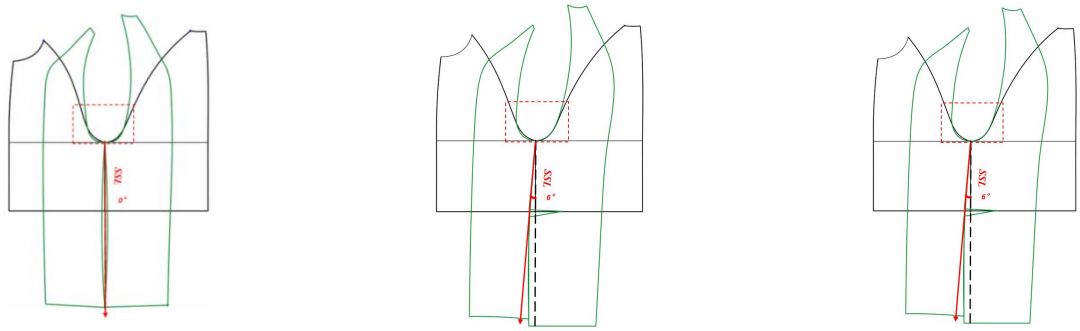

b

Figure 3.7 - Comparison of three raglan sleeve prototypes, *P4*, P5, and P6, with SCL and SSL alignments: *a,* SCL alignments; *b,* SSL alignments

As shown in Figure 3.7a, under the SCL-aligned condition, the forward offsets of the SCL and SSL were 0.5 cm for *P4*, 2.5 cm for *P5*, and 2.5 cm for *P6*; meanwhile, P5 and P6 produced a 3.5° back-sleeve forward angle through elbow darting, whereas *P4* remained at 0°. As shown in Figure 3.7 *b,* under the SSL-aligned condition, the forward angles of the SSL were 0° for *P4*, 6° for *P5*, and 6° for P6. Therefore, P5 and P6 showed stronger forward-tilt and bending representation than P4. However, P6 was preferred over P5, because it achieved consistent matching of the front and back armhole curves (see Table 2.18). Comparing with the arm-morphology angles $\angle 1 = 8.9° \pm 1.5°$ and $\angle 2 = 12.2° \pm 1.4°$described in section 2.4.2, P6 performed better among the three raglan sleeve prototypes.

Table 3.3 - Comparison of 2D pattern - structure parameters

2D pattern - shape parameters	*P4*	*P5*	*P6*
Forward offset of SCL, cm	0.5	2.5	2.5
Forward angle of back sleeve, degree	0	3.5	3.5
Forward angle of SSL, degrees	0	6	6
Matching curves at front armhole	N	N	Y
Matching curves at back armhole	N	N	Y

As shown in Table 3.3, P6 provided the most consistent 2D pattern geometry among the three prototypes. Nevertheless, the comparison of the two-dimensional patterns also showed that the representation of forward inclination in P6 was still lower than the measured values of arm morphology.

Comparison of 3D raglan sleeve shapes. The comparison of two-seam patterns showed that they did not fully provide the required spatial relationship between the sleeve and the arm. Therefore, the three two-piece raglan-sleeve prototypes were further assessed in 3D using the raglan-coat shape criteria (C_C) established in Section 2.4.2. To quantify the spatial relationship between the sleeve and the arm and the stability of the sleeve surface under identical simulation conditions, three 3D shape indicators were selected: Folds, for evaluating sleeve-surface smoothness; FC, for describing the spatial relationship between the sleeve and the arm at the cuff; and $|a_s - b_s|$, for evaluating the consistency of sleeve direction in the upper-arm and elbow regions. Figure 3.8 shows the measurement scheme for these parameters.

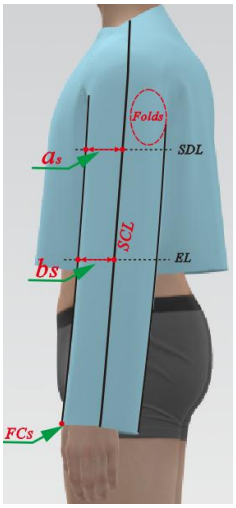

Figure 3.8 - Definition of 3D raglan-sleeve shape parameters for quantifying sleeve–arm spatial relationship and forward-tilt consistency (*FCs,* a_s, b_s, *Folds*).

Figure 3.9 shows the comparative counts for P4, P5, and P6. The complete measurement results for all chest-girth and body-type combinations are reported in Tables A.14 - A.17 in Appendix A.

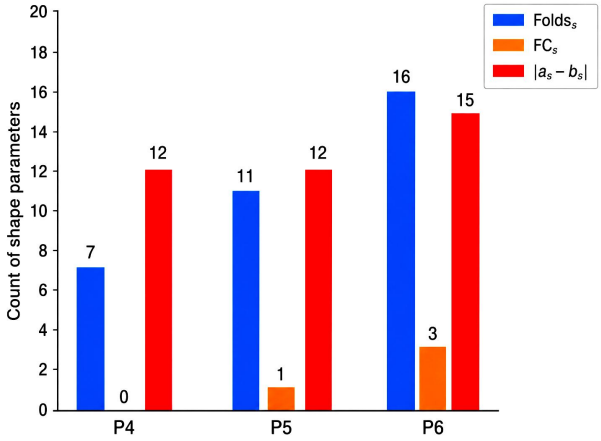

Figure 3.9 - Numbers of samples satisfying the 3D raglan-sleeve shape criteria for prototypes P4, P5, and P6

As shown in Figure 3.9, P6 demonstrated the best overall performance among the three prototypes with the highest number of samples satisfying the three criteria. The detailed measurements (Tables A.15.... A.17 in Appendix A) showed the same tendency, with P6 exhibiting the lowest mean fold count (AV = 0.2), the largest mean FC (AV = 0.5 cm). These results indicate that P6 provided the most stable spatial relationship under the combined constraints of forward tilt and elbow bending; therefore, it was selected as the baseline for subsequent development.

However, when evaluated according to the CC criterion, the FC values for P6 remained below the requirement for good shape (FC in [1.0, 4.3] cm). This means that although P6 performed best in relative terms, its sleeve still insufficiently represented the required forward-inclination clearance in the cuff area.

3.2.2. Improvement of the raglan sleeve prototype

Two modification strategies were developed for prototype P6 on the basis of the quantified arm morphology, particularly its forward tilt and elbow bending. The first strategy retained the original two-piece sleeve structure and resulted in a modified prototype, denoted as P6(m). In this method, the sleeve centre line (SCL) was shifted further forward, and the elbow dart was enhanced to strengthen the forward rotation of the back sleeve and improve conformity to the natural forward tilt of the arm. The second strategy converted P6 into a three-piece raglan sleeve, denoted as P7, by introducing an additional under-sleeve panel. This reconstruction enabled the lower

sleeve to rotate more freely, thereby improving conformity to both forward tilt and elbow bending while reducing folds in the underarm region. These two strategies were designed to compare whether the FC deficiency could be solved through parameter adjustment within the original two-piece structure or whether a structural reconstruction was required.

Figure 3.10 shows the structural modifications adopted in these two methods.

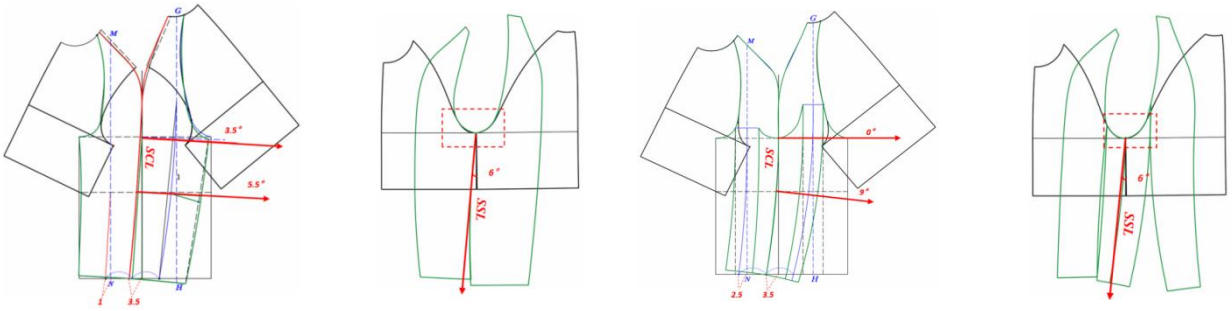

a *b*

Figure 3.10 - Pattern modification strategies for prototype P6: *a* - P6（m）- two-piece sleeve; *b* - *P7* - three-piece sleeve

As shown in Figure 3.10, the two-piece modification P6(m) was achieved by increasing the forward offset of the SCL to 3.5 cm and applying a 9° forward rotation to the back sleeve, corresponding to the average elbow-bending angle obtained from arm morphology. This adjustment produced a 3.5 cm forward displacement at both the sleeve-cap base and the elbow level. By contrast, the three-piece modification P7 redistributed the forward rotation through the added under-sleeve structure. The principal forward tilt was applied at the back elbow with a 9◦ rotation, producing a more effective forward displacement of the lower sleeve, while the side-seam forward rotation remained unchanged at 6◦ . Compared with the two-piece refinement, the three-piece reconstruction provided greater structural flexibility for accommodating the natural curvature of the arm.

To evaluate the effectiveness of these two modification strategies, the 3D sleeve shapes of P6, P6(m), and P7 were comparatively assessed using 20 standardized virtual try-on samples under identical posture, fabric, and simulation settings. The sample set covered five chest-girth sizes and four representative body-type categories, yielding 20 comparable body cases for each prototype. The evaluation followed the same 3D sleeve-shape criteria used in Section 3.2.1, including Folds, FC, and $|a_s - b_s|$, so that the modified prototypes could be directly compared with the original baseline P6. The comparative validation results are summarized in Table 3.4, whereas the complete measurement results for all samples are provided in Appendix A (Tables A.18–A.21).

Table 3.4 - Comparative validation results of prototypes P6, P6(m), and P7 across 20 standardized virtual try-on samples

Parameters	*P6*	*P6(m)*	*P7*
Folds	16	16	18
FCs	3	6	19
$\|a_s - b_s\|$	15	15	18
Total satisfied criterion count	34	37	55
Overall satisfaction rate	56.7%	61.7%	91.7%

As shown in Table 3.4, Relative to the original prototype P6, the modified two-piece sleeve P6(m) showed a limited but clear improvement, with the total number of satisfied cases increasing from 34 to 37 and the overall satisfaction rate increasing from 56.7% to 61.7%. The most notable gain was observed in FC, where the number of samples satisfying the criterion increased from 3 to 6. However, the three-piece prototype P7 showed a substantially greater improvement across all criteria. It achieved 18 cases with Folds = 0, 19 cases satisfying the FC criterion, and 18 cases satisfying the $|a_s - b_s|$ tolerance. This yielded a total of 55 satisfied cases and an overall satisfaction rate of 91.7%, markedly higher than those of both P6 and P6(m). These results demonstrate that, while the two-piece refinement improved the original prototype to some extent, the three-piece reconstruction provided a much more stable and effective structural response to the arm's forward tilt and bending.

To visually support the quantitative tendencies, Figure 3.11 shows representative 2D and 3D comparisons of the original prototype P6 and the two modified prototypes, P6(m) and P7, in order to visually confirm the tendencies observed in the summarized validation results.

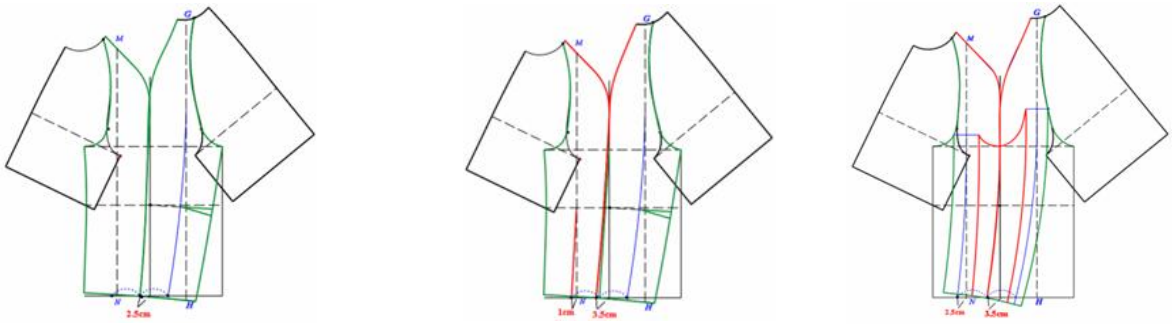

a *b* *c*

Figure 3.11 - Representative 2D pattern geometry and corresponding 3D sleeve-shape comparison of the three prototypes: (a) P6; (b) P6(m); (c) P7.

As shown in Figure 3.11, the comparisons show a progressive improvement from P6 to P6(m) and then to P7. With increasing structural conformity, the sleeve exhibits a clearer forward rotation, fewer underarm irregularities, and a more coherent bending response, approaching the natural posture of the arm. In particular, P7 shows the most stable alignment in both the upper and lower sleeve regions. This advantage can be attributed to the additional geometric freedom provided by the three-piece construction, which allowed the sleeve shape to respond more effectively to the quantified arm morphology.

3.3. Development of the Raglan coat construction

This section aimed to identify the key pattern parameters governing raglan coat shape, determine their effective value ranges, and establish a quantitative relationship between pattern and shape parameters.

3.3.1. Evaluation of the simplified condition for virtual try-on

In the preceding experiments, the raglan coat was constructed on the basis of the bodice and sleeve in order to examine the effect of excluding the collar, lining, and facing. Therefore, the subsequent analyses in this study mainly adopted virtual try-on as the principal method for shape verification. A real raglan coat normally includes complete structural components such as the collar, lining, and facing. In virtual try-on, these additional components increase modeling and process-simulation complexity and may introduce extra simulation noise. Accordingly, the subsequent virtual analyses were conducted under a simplified structural condition in which non-critical details were omitted. Before adopting this condition, however, it was necessary to determine whether the omission of the collar, lining, and facing would significantly affect the evaluation of

the main shape features.

To address this issue, a comparative experiment was conducted under real-garment conditions using two versions of the same raglan coat structure. In one version, the collar, lining, and facing were fully retained; in the other, these components were removed, while the main structure required for shape evaluation was preserved. The outer fabric was a medium-thickness grey cotton fabric, so that any shape differences caused by the presence or absence of these components could be clearly observed. The lining was made of a conventional woven polyester lining fabric (80 g/m²).

Figure 3.12 shows the back, front, and side-view comparison of the raglan coat with and without the collar, lining, and facing (the red boxes highlight the local regions where slight differences can be observed). In addition to the back, front, and side views, front- and side-view contour overlays were extracted to examine whether the omission of these structural details altered the principal silhouette boundary.

a b c d e

Figure 3.12. Comparison of raglan-coat shape with and without the collar, facing, and lining: (a) back view; (b) front view; (c) side view; left—with the collar, facing, and lining; right—without these components; (d) front-view contour overlay; (e) side-view contour overlay. Black outline—without the collar, facing, and lining; red outline—with these components.

As shown in Figure 3.12a - c, the visual comparison shows that the raglan-coat shape remained highly similar under the two conditions, namely with and without the collar, facing, and lining. Figure 3.12d - e further indicates that the main silhouette boundaries in the front and side views remained highly consistent.

To support this visual observation, SSIM analysis was performed using the corresponding back, front, and side views. Global grayscale SSIM was used to evaluate overall visual similarity, including local grayscale and texture differences. Silhouette mask SSIM was calculated from binary garment masks to focus on external contour similarity and reduce the influence of local visual details[125]. Table 3.5 shows the

SSIM-based comparison of visual structural consistency between the raglan coats with and without the collar, facing, and lining. The complete analysis process and detailed results are presented in Tables A.25 – A.28 in Appendix A.

Table 3.5. SSIM-based comparison of raglan-coat shape with and without the collar, facing, and lining.

View	Global grayscale SSIM	Silhouette mask SSIM	Main difference region
Back view	0.775	0.885	Back neck
Front view	0.806	0.883	Collar, lapel
Side view	0.766	0.887	Shoulder neck region and sleeve arm space
Mean	0.782	0.885	Local upper-body details

As shown in Table 3.5, the global grayscale SSIM values were 0.775, 0.806, and 0.766 for the back, front, and side views, respectively, indicating a relatively high level of overall image-structure similarity. More importantly, the silhouette mask SSIM values reached 0.885, 0.883, and 0.887, respectively, confirming that the principal external contour of the raglan coat was largely preserved after removing the collar, facing, and lining. The lower grayscale SSIM values, compared with the silhouette mask SSIM values, indicate that the differences were mainly caused by local visual details rather than by changes in the overall garment outline. These local differences were concentrated in the shoulder–neck region and the collar and lapel area. Such regions were directly affected by the presence of the collar and facing, while the sleeve body, bodice contour, side silhouette, and lower hem remained structurally stable. Although slight differences were observed in the shoulder–neck transition, they did not alter the principal side silhouette or the cuff-level sleeve–arm relationship used in the subsequent evaluation. Therefore, the omission of the collar, lining, and facing had a limited influence on the visual details of the upper garment but did not substantially affect the evaluation of sleeve forward tilt, bodice balance, or the overall raglan-coat silhouette.

Therefore, to simplify the experimental procedure, reduce simulation noise in the virtual environment, and allow the subsequent analyses to focus more directly on the relationship between pattern structure and garment shape, the collar, lining, and facing were omitted in the later virtual try-on experiments. This simplified condition was then adopted as the unified experimental setting for the subsequent pattern-parameter analysis and shape evaluation.

3.3.2. Weight analysis of pattern parameters

All data samples were normally distributed.

Statistical analyses and collinearity diagnosis of pattern parameters. Table 3.6 shows the Pearson correlation coefficients between the pattern variables (X) and shape variables (Y). Significant terms ($p < 0.05$) identify pattern variables that were sensitive to shape variation and thus provided direct evidence for selecting key pattern variables.

Table 3.6 - Pearson correlations between pattern variables (X) and shape variables (Y).

Correlation Coefficient	Y1	Y2	Y3	Y4
X1	.901**	-0.298	-0.154	-0.01
X2	.526*	.457*	0.058	0.33
X3	.926**	-0.057	-0.106	0.135
X4	.595**	-.493*	-0.168	-0.165
X5	-0.169	.601**	0.137	.747**
X6	0.337	-.485*	-0.179	-.878**
X7	0.161	.535**	0.016	.915**
X8	-0.008	0.32	0.28	-0.041
X9	0.06	0.202	-.648**	-0.105
X10	-0.073	0.034	.899**	0.083
X11	-0.063	0.948**	0.003	.538**
X12	-0.09	-0.035	.956**	0.032
X13	-0.013	0.112	.873**	0.087
X14	0.031	0.187	.770**	0.112
Note: Pearson's r (two-tailed). $p < 0.05$ (*), $p < 0.01$ (**). $n = 23$.				

As shown in Table 3.6, the correlation analysis produced four main findings. First, X1, X2, X3, and X4 were significantly correlated with Y1, indicating that the front and back shoulder slopes and their combined relationships affected the spatial configuration of the front and back sleeve panels and further changed the relative spatial relationship between the sleeve and the arm at the cuff level. Second, the shoulder–sleeve connection angle parameters (X_5, X_6, and X_7) showed strong significant correlations with the fold indicator Folds (Y4), indicating that the angular configuration of the shoulder–sleeve connection region played a critical role in determining sleeve-surface smoothness. Third, Offset(SCL) (X_{11}) showed a highly significant positive correlation with FC (Y_2) ($r = 0.948$, $p < 0.01$), indicating that the offset(SCL) directly affected the spatial relationship between the sleeve and the arm at the cuff level. Fourth, the forward displacement of the sleeve. Fourth, X_9, X_{10}, and X_{12}–X_{14} were

significantly correlated with Y3, indicating that the front–back distribution and displacements at the upper-arm and cuff levels were key factors influencing sleeve posture and the overall silhouette. X8 shows weak correlations with shape parameters. Overall, 13 structural parameters were found to have significant correlations with shape parameters.

However, it should be noted that Pearson correlation only reflects the linear relationship between pairs of variables and does not account for interdependence among structural variables. Therefore, the statistically shape-sensitive variables identified through Pearson correlation analysis still require further multicollinearity examination before regression modelling. In a raglan coat, the front sleeve panel, back sleeve panel, bodice, and collar are structurally continuous and interconnected. As a result, a change in one structural parameter may lead to simultaneous changes in other related parameters, which is an important source of multicollinearity. Accordingly, this section adopts a correlation-matrix screening method to evaluate multicollinearity among the 13 structural parameters identified above, with the aim of identifying redundant parameters, reducing repetitive explanations, and stabilizing variable selection and parameter interpretation in the subsequent regression models.

Table 3.7 shows the correlation matrix, showing the Pearson correlation coefficient between the 9 effective pattern parameters.

Table 3.7 - Collinearity Diagnosis of Pattern Parameters

	X_1	X_2	X_3	X_4	X_5	X_6	X_7	X_9	X_{10}	X_{11}	X_{12}	X_{13}	X_{14}
X_1	1												
X_2	0.106	1											
X_3	.884**	-0.371	1										
X_4	.902**	.525*	.595**	1									
X_5	-0.365	0.331	-.498*	-0.169	1								
X_6	.516*	-0.247	.599**	0.335	-.902**	1							
X_7	0.018	0.325	-0.136	0.157	.742**	-0.38	1						
X_9	0.093	-0.037	0.104	0.065	-0.209	0.222	-0.104	1					
X_{10}	-0.0	-0.0	-0.04	-0.0	0.183	-0.1	0.09	-.714	1				

	7	38	5	76		91	4	**					
X_{11}	-0.303	.455*	-.497*	-0.062	.600**	-.483*	.535**	0.206	0.033	1			
X_{12}	-0.064	-0.089	-0.016	-0.094	0.117	-0.136	0.039	-.677**	.972**	-0.035	1		
X_{13}	-0.005	-0.028	0.01	-0.017	0.06	-0.021	0.094	-.545**	.864**	0.115	.923**	1	
X_{14}	0.028	0.008	0.024	0.027	0.024	0.044	0.119	-.436*	.747**	0.19	.820**	.977**	1

As shown in Table 3.7, a correlation coefficient of $|r| > 0.8$ indicates a strong correlation and suggests that multicollinearity may exist among the variables. To ensure the stability of the coefficients in the subsequent regression analysis, redundant parameter groups were identified based on Table 3.7 to guide variable reduction before modelling. The correlations among the structural parameters can be clearly summarized into four groups: the shoulder-slope angle parameter group (X_1–X_4) ($|r| = 0.595–0.901$), the shoulder–sleeve angle parameter group X_5–X_7 ($|r| = 0.535–0.601$), the front–back sleeve distribution parameter group X_9, X_{10}, and X_{12}–X_{14} ($|r| = 0.770–0.956$), and the cuff-offset parameter Offset(SCL) (X_{11}). The first three groups constitute three structurally related parameter groups, indicating different degrees of variable redundancy. This means that some redundant parameters can be excluded without losing key information, and representative variables can be selected from these groups to reduce variable redundancy before regression modelling. The fourth parameter, namely the cuff-offset parameter Offset(SCL) (X_{11}), is relatively independent of the other parameters and shows an extremely strong correlation with the shape parameter Y2 ($r = 0.948$), indicating that it directly affects the spatial relationship between the sleeve and the arm at the cuff level. Although parameters can be screened according to the strength of correlation coefficients, due to the specific structural characteristics of the raglan sleeve, different parameters have different weights in the pattern-making process, and statistical correlation itself cannot fully reflect the actual functional role of each parameter in the pattern-making process. Therefore, the weights of the structural parameters need to be further analysed by combining collinearity diagnosis with the actual production process.

Weight analysis of pattern parameters in the production process. To further analyze the weight of these structural parameters, a subjective analysis was conducted based on the industrial raglan sleeve pattern-making process. By combining both Chinese and Russian pattern-making methods for raglan sleeves, the entire pattern-making process was summarized.

Table 3.8 shows Steps 1-7 of the raglan sleeve pattern-making process, from the determination of BSNP and FSNP to the under-sleeve side seam line difference. Each step incorporates specific pattern and shape parameters, all of which were thoroughly analyzed.

Table 3.8 - Weight analysis of pattern parameters in the production Process

Step	Pattern-Making Processes	Parameters		
		Pattern		Shape
1	Determination of FSNP, BSNP	\	\	\
2	Determination of SP (Shoulder sloping)	Δ(∠BSS-∠FSS)	X_3	\
		Δ(∠BSS+∠FSS)	X_4	Y_4
3	Determination of SCL (Sleeve Center Line)	∠BA	X_5	Y_4
		∠FA	X_6	Y_2,Y_4
		Δ(BA + FA)	X_7	Y_4
4	Determination of SH (Sleeve Height)	\	\	\
5	Determination of SW (Sleeve Width)	FSW	X_9	Y_1， Y_3
		Δ (BSW - FSW)	X_{10}	
6	Determination of CW (Cuff width)	Offset (SCL)	X_{11}	Y_2,Y_4
7	Determination of Under-Sleeve Seam	i	X_{12}	Y_1,Y_3
		j	X_{13}	Y_1,Y_3
		Δ(i-j)	X_{14}	Y_3

As shown in Table 3.8, the weight hierarchy is as follows:

$X_1, X_2, X_3, X_4 > X_5, X_6, X_7 > X_9, X_{10} > X_{11} > X_{12}, X_{13}, X_{14}$

This hierarchy reflects the sequential dependence of the pattern-making steps in the industrial raglan-sleeve design process. First, the shoulder-slope configuration parameters ∠BSS and ∠FSS ($X_1 - X_4$) have the highest weight. This indicates that shoulder-slope angles are the most critical parameters in raglan-sleeve pattern-making, determining the overall fit and alignment between the sleeve and the body. Second, the next most influential parameters are the shoulder–sleeve angles $X_5 - X_7$, which further improve sleeve fit and alignment, particularly in relation to the outer contour of the arm. Third, the sleeve-width difference parameters X_9 and X_{10} and Offset(SCL) X_{11} are important parameters because they directly affect the coordination between the sleeve shape and the natural morphology of the arm. Finally, the under-sleeve side-seam differences $X_{12} - X_{14}$ contribute to the overall formation of the sleeve shape, and the

position of the under-sleeve seam also affects the distribution relationship between the large and small sleeve panels.

Combining the collinearity analysis results (Table 3.7) with the production-process-based weight analysis (Table 3.8), four variable-reduction steps were conducted:

(1) X_1–X_4 showed relatively strong correlations. Considering their high weight in the pattern-making process, X_3 and X_4 jointly determine the distribution relationship between the front and back shoulder slopes and have a critical influence on the shoulder-slope shape; therefore, both parameters need to be retained.

(2) X_5 – X_7 showed strong correlations. Among them, X_7 had a stronger correlation with the fold indicator Y_4 ($|r| = 0.915$) than X_5 ($|r| = 0.747$) and X6 ($|r| = 0.878$) (Table 3.6). Therefore, X_7 was retained;

(3) X_9 and X_{12}–X_{14} were located in Step 5 and Step 7 of the pattern-making process, respectively, with relatively low weights, and were highly redundant with X_{10}. Therefore, X_9 and X_{12}–X_{14} were excluded, while X_{10} was retained;

(4) Offset(SCL) X_{11} was a relatively independent parameter located in Step 6 of the pattern-making process. It is a key parameter for evaluating shape in the previously established shape criteria and shows a strong correlation with the shape parameter Y2 ($r = 0.948$), indicating that it directly affects the forward-tilt shape of the sleeve. Therefore, X11 was retained.

Finally, five key structural parameters with the greatest influence on raglan-sleeve shape were selected: X_3, X_4, X_7, X_{10}, and X_{11}. However, it should be noted that a certain degree of collinearity exists between X_3 and X_4, and the correlation coefficient of X_4 ($r = 0.902$) is higher than that of X_3 ($r = 0.884$). Therefore, in the subsequent regression modelling, X4 was included in the regression equation as a key structural parameter, while X_3 was retained as an auxiliary parameter to constrain the distribution relationship between the front and back shoulder slopes. Subsequently, in Section 3.3.3, these five retained parameters were controlled within the observed ranges, and the resulting sleeve shapes were evaluated according to the established criteria to verify their effects on shape. Thereafter, these retained parameters were used in controlled variation tests to determine the influence strength of each parameter on raglan-coat shape and to establish their practical effective value ranges.

3.3.3. Validation of the influence of key pattern parameters on raglan coat shape

The five key quantifiable pattern parameters identified in Section 3.3.2, namely X_3, X_4, X_7, X_{10}, and X_{11}, were numerically characterized as $\Delta(\angle BSS - \angle FSS)$, $\Delta(\angle BSS + \angle FSS)$, $\Delta(\angle BA + \angle FA)$, $\Delta(BSW - FSW)$, and Offset(SCL), respectively.

The observed value ranges of these parameters were first obtained from the 23 raglan-sleeve patterns. These ranges provided the numerical basis for the subsequent controlled variation tests.

Table 3.9 shows the quantification of the key pattern parameters, measured across the 23 raglan-sleeve patterns. They were extracted using the standardized measurement scheme described in Figure 2.4 in Section 2.3.1. The complete dataset is provided in Table A.20 in Appendix A.

Table 3.9 - Quantification of key pattern parameters

Parameter	X_3, °	X_4, °	X_7, °	X_{10}, cm	X_{11}, cm
AV	4.5	45.2	53.8	2.6	1.6
Max	12.4	54	83.9	8.3	3.5
Min	-4.5	33.2	22.3	-0.7	0

Based on the descriptive statistics, the impact of key sleeve pattern parameters on raglan coat shape was verified using Style 3D. The sleeve quality was judged by the established criteria. Folds = 0 was used as the primary pass condition for sleeve-surface quality, while FD, FC, and |a − b| were used to interpret sleeve–arm configuration and alignment.

The impact of key sleeve pattern parameters on raglan coat Shape. Table 3.10 shows the effects of key pattern parameters on the raglan-sleeve shape.

Table 3.10 - Impact of key pattern parameters on raglan sleeve shape. The complete visual results are provided in Table A20 in Appendix A.

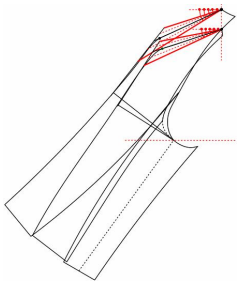				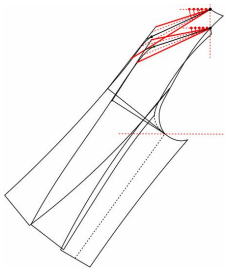		
X_4 [33°...54°]		33	53	X_3 [-4.5°...12.4°]	-3	6
Fit Level	FD	4.5	2.7	FC	2	1.3
	Folds	2	0	Folds	2	0

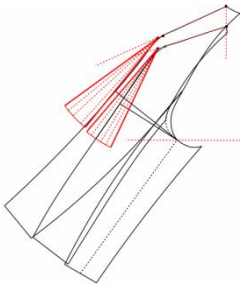				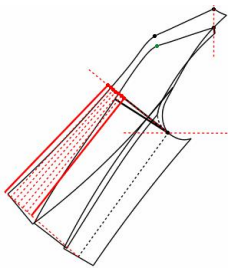		
X_7 [22.3°...72.4°]		54	66	X_{10} [-0.7...8.3cm]	-0.5	5
Fit Level	FD	5.7	3.1	|a-b|	2.2	0.7
	Folds	2	0	Folds	2	0
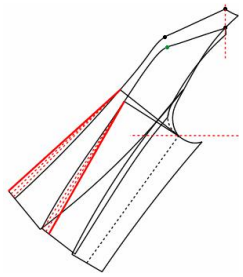						
X_{11} [0...3.5cm]		0		3.5		
Fit Level	FC	0		1.8		
	Folds	2		0		

As shown in Table 3.10, these parameters were progressively adjusted, and the resulting sleeve fit and appearance were analyzed through 3D virtual try-ons using the same criteria (FD, FC, $|a-b|$ and Folds). The following key pattern parameters were tested:

(1) When X_4 was in the range of [40°, 54°], the sleeve fitted the arm most closely, with no visible folds. Whereas at 61°, folds reappeared (Folds = 1); therefore, 61° was treated as an over-range test point rather than part of the good-shape interval, and 40°–54° was retained as the practical range;

(2) X_3 controlled the sleeve–arm configuration: when it increased from −3° to 6°, FC decreased from 2.0 cm to 1.3cm and Folds reduced from 2 to 0, whereas folds reappeared at 9°. Therefore, the favourable interval was 0°- 6°;

(3) X_7 affected sleeve conformity; a good sleeve surface (Folds = 0) was obtained at 60° - 72°;

(4) X_{10} influenced sleeve shaping; when it was within 2.5-7.5 cm, the sleeve aligned more stably with no visible folds;

(5) The forward displacement of the sleeve centre line at the cuff (X_{11}) improved

alignment with the arm forward tilt; within 1.5 - 3.5 cm, folds were eliminated, and the best result in this test occurred at Offset(SCL) = 2 cm.

Overall, the stepwise adjustment results in Style 3D confirmed that Folds = 0 could be consistently achieved when the parameters were controlled within the following ranges: X_3 within 0°-6°, X_4 within 40°–54°, X_7 within 60°-72°, X_{10} within 2.5-7.5 cm, and X_{11} within 1.5–3.5 cm. These results identified the effective value ranges of the key sleeve pattern parameters and confirmed their direct influence on raglan-coat shape. Therefore, these validated ranges were used in subsequent sections to evaluate single-parameter and multi-parameter adjustments under the same evaluation criteria.

The impact of key bodice pattern parameters on the raglan coat Shape. In addition to sleeve-related variables, bodice pattern parameters also affect raglan-coat shape through their influence on bodice balance and sleeve appearance. Therefore, this part further examined the effect of bodice ease design, including the location, proportion, and magnitude of chest ease, on the resulting raglan-coat shape.

1. *Bodice parameters.* Figure 3.13 shows three bodice parameters are considered: (i) the different E(CG) values; (ii) chest ease distribution location across the front bodice (L(*F*)), back bodice (L(*B*), and armhole-related regions (L(*A*)); (iii) chest ease distribution proportion of chest ease on the bodice: front width (FW), armhole width (AHW), and back width (BW).

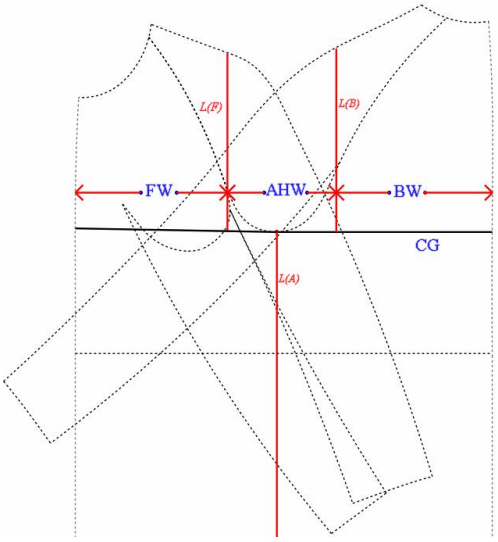

Figure 3.13 - Definition of bodice $E_{(CG)}$ parameters for validation

To comprehensively assess the bodice $E_{(CG)}$, three commonly used ease-allocation schemes were identified across FW – AHW – BW:33.3:33.3:33.3, 16.7:33.3:50, and 14.2:33.3:52.5. These schemes (marked as ①–③ in Figure 2.27) were used as standardized levels for validation. The sleeve pattern remained constant, and only the bodice chest ease design was varied. These three ratios were obtained by

normalizing the E(CG) allocation of each of the 23 patterns into FW – AHW – BW portions; the distribution clustered into three dominant schemes, which were adopted as the standardized levels (①–③) for validation.

2. *Effects of E(CG) distribution location and proportion.* In the first test, E(CG) was set to 16 cm, with a basic block pattern providing 8 cm ease. An additional 8 cm ease was added. Two placement options were compared: ease at AHW (armhole area) and ease at FW/BW (front/back width).

Table 3.11 shows the representative effects of $E_{(CG)}$ distribution location (AHW, FW/BW) and allocation proportions (② at L(A), *L(F),* and *L(B)* , $E_{(CG)}$=16cm, including the corresponding 2D patterns, 3D fitting views, and fit level (Good (G) / Not Good (NG). And the full results for ①–③proportions under both distribution locations are provided in Table A.21 in Appendix A.

Table 3.11 - Representative effects of $E_{(CG)}$ distribution location and allocation proportion on raglan-coat sleeve shape ($E_{(CG)}$=16 cm)

2D pattern		3D shape	Fit level
Ease distribution	Ease proportion		
②16.7:33.3:50	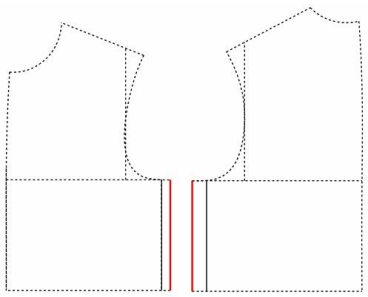	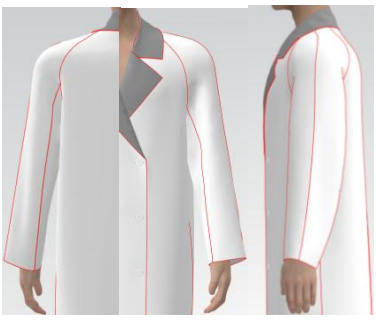	*NG*
AHW （ *L(A)* ）			
② 16.7:33.3:50	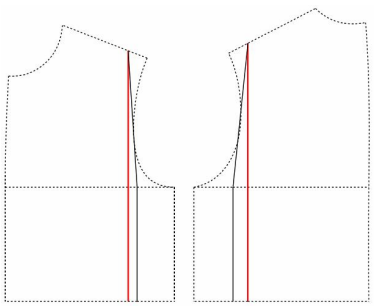		*G*
FW - BW （ *L(F) / L(B)* ）			

As shown in Table 3.11, adding ease at AHW resulted in visible folds for all three allocation schemes, and the sleeve forward tilt showed no clear difference among proportions ①– ③. Folds were mainly concentrated near the small-sleeve area, indicating an unstable sleeve appearance. In contrast, adding ease at *L(F)* and *L(B)* reduced folds and made the sleeve appearance sensitive to the allocation proportion. Proportion ② (evenly distributed between FW and BW) produced a smoother sleeve surface and a clearer forward-tilt feature.

These findings demonstrate that bodice ease design also acts as a controlling factor in raglan-coat shape and must therefore be considered together with sleeve pattern parameters.

3. *Effects of different E(CG)*. Based on the comparisons above, proportion ② was adopted for further testing, representing a non-uniform allocation with a higher proportion assigned to the back width. With this distribution allocation kept constant, $E_{(CG)}$ was varied across multiple values (12 cm, 16 cm, 20 cm, 28 cm) to examine its influence on the raglan sleeve shape. The sleeve pattern remained unchanged for all cases.

Table 3.12 - Effects of different E(CG) on raglan-coat sleeve shape (FW – BW; distribution proportion 16.7:33.3:50)

Ease position	3D shape			
FW/BW	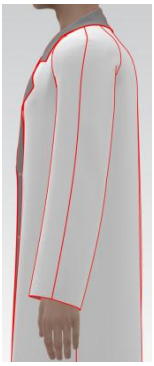		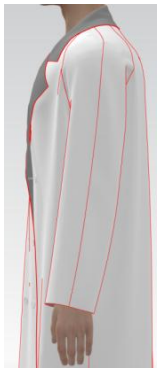	
E(CG),cm	12	16	20	28
Fit Level	G	G	G	NG

As shown in Table 3.12, the fit level remained Good (G) for E(CG) from 12 to 20 cm, but became Not Good (NG) at 28 cm. Meanwhile, larger E(CG) progressively weakened the sleeve's forward tilt and bending appearance, even though the sleeve pattern was unchanged.

These results confirm that the magnitude of chest ease is itself a controlling factor in raglan-coat shape. Under the same ease-allocation location and proportion, a smaller E(CG) produced a more pronounced forward-tilt appearance, whereas excessive E(CG) weakened the sleeve's shape characteristics.

To further visualize the combined effect of chest-ease proportion and E(CG) value under the FW/BW distribution condition, Table 3.13 shows representative sleeve-shape appearances across three allocation proportions and four E(CG) levels.

Table 3.13. Integrated visual comparison of raglan-coat sleeve shape under different chest-ease proportions and E(CG) values with the FW/BW distribution condition

Proportion of chest ease, %	Chest ease of different shapes, cm			
	Fit	Semi-fit	Semi-loose	Loose
	12	16	20	28
33.3:33.3:33.3				
16.7:33.3:50	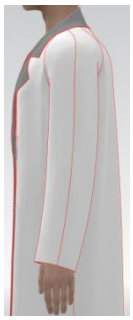	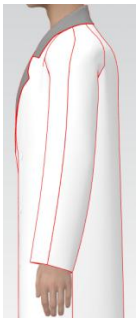		
14.2:33.3:52.5				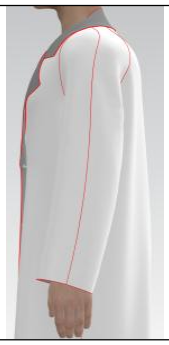

As shown in Table 3.13, both the proportion of chest ease and the value

of E(CG) influenced the visual expression of raglan-coat sleeve shape. Under the FW/BW distribution condition, some combinations maintained a clear forward-tilt and bending appearance, whereas others weakened the sleeve’s structural expression. In particular, the sleeve shape remained relatively stable at lower and moderate E(CG) values, while excessive ease reduced the clarity of the intended raglan-sleeve configuration. These visual comparisons are consistent with the quantitative evaluation presented in the previous subsections and further confirm that bodice ease design must be considered together with sleeve pattern parameters in the control of raglan-coat shape.

4. *Validation of the optimized pattern set for shape enhancement.* Additional adjustment tests were conducted to determine whether the validated parameter ranges could be used to improve raglan-coat shape in practice. This section verifies the practical effectiveness of the optimized parameter set through two complementary strategies: (a) single-parameter adjustment, used to confirm the isolated shape contribution of each key term, and (b) multi-parameter coordination, to test whether the good sleeve shape can be achieved more stably through coupled adjustments.

Table 3.14 shows representative results of single-parameter adjustment, comparing the raglan-coat shape before and after each pattern-parameter correction. The complete comparison, including both virtual and real validation results, is provided in Table A.24 in Appendix A.

Table 3.14 - Improvement of key pattern parameters for raglan sleeve shape

No.	①		②		③	
Pattern parameters	Δ(FSS＋BSS），°		Δ(BA＋FA)，°		Δ（BSW-FSW）,cm	
	32	47	54	66	0	3
Real shape						
Fit level	NG	G	NG	G	NG	G
No.	④		⑤		⑥	
Pattern parameters	Offset(SCL)，cm		E(CG) Distribution，cm		E(CG) Values, cm 16.7:33.3:50	
	0	2	33.3:33.3:33.3	16.7:33.3:50	8	16

Real shape						
Fit level	NG	G	NG	G	G	G

As shown in Table 3.14, the blue and red lines on the pattern represent the structural lines before and after the adjustments, respectively. The red lines on the 3D model highlight the key shape lines, demonstrating the coat shape changes resulting from the parameter adjustments. Based on the established optimal shape ranges for the raglan sleeve, the original pattern parameters were adjusted.

By comparing the virtual and real garment models, it was found that adjusting the pattern parameters within the optimal range significantly improved the fit and appearance of the raglan sleeve. This confirmed the effectiveness of the established pattern parameter ranges in achieving an optimal shape and highlighted the significant impact of key pattern parameters on sleeve shape. On the basis of single-parameter optimization, a collaborative adjustment of multiple pattern parameters was explored to achieve the optimal raglan sleeve shape. Using the same body measurements and 2D pattern, the raglan coat was produced with real fabric (100% cashmere), and the optimization schemes for all pattern parameters were gradually integrated.

After the single-parameter effects had been confirmed, Figure 3.16 further shows the collaborative multi-parameter optimization process, in which key parameters were progressively combined to improve the raglan-sleeve shape from Not good to Good.

Figure 3.14 - Real sample of raglan coat with the effect of pattern parameters adjustments: a -initial; b - Optimized sample

The results confirmed that an optimal raglan sleeve shape was achieved when

key pattern parameters were adjusted within the identified value ranges, demonstrating that raglan-sleeve shape could be effectively improved by adjusting key structural parameters.

3.3.4. Regression optimization for shape improvement

The regression models established in this section were developed under representative fabric conditions for autumn/winter outerwear, including cotton- and wool-based fabrics used in both real and virtual experiments. Within the tested fabric range (approximately 300-600 g/m ²), the resulting raglan-coat shapes consistently preserved the required forward-tilt and bending characteristics. Although slight numerical variations were observed across different fabrics, the shape responses remained within the validated good-shape intervals. Therefore, fabric was not introduced as an explicit predictor in the regression equations, but was treated as a controlled application condition. The resulting models may thus be regarded as applicable to this representative range of autumn/winter coat fabrics rather than to a single specific material.

Regression model development. Based on the 23 pattern datasets, four key pattern parameters were selected as predictors: X_4, X_7, X_{10}, and X_{11}. Four sleeve-shape criteria were used as response variables: Y_1, Y_2, Y_3, and Y_4. Simple regression equations were derived to estimate each shape criterion as follows:

$$Y1 = -8.98 + 0.242 \cdot X4 \qquad R^2 = 0.857 \qquad (3.1)$$

$$Y2 = -1.48 + 1.658 \cdot X11 \qquad R^2 = 0.898 \qquad (3.2)$$

$$Y3 = -0.35 + 0.140 \cdot X10 \qquad R^2 = 0.808 \qquad (3.3)$$

$$Y4 = -5.02 + 0.0838 \cdot X7 \qquad R^2 = 0.837 \qquad (3.4)$$

These equations provide practical estimates of Y_1 -Y_4 from the selected pattern parameters and were used to guide parameter adjustment toward the good-fit ranges established in the previous sections. The regression equations were used as quantitative links between pattern parameters and sleeve-shape criteria. Together with the established good-shape intervals and the verified effective ranges of pattern parameters, they formed a constraint-based optimization framework for raglan-sleeve pattern design and shape improvement.

Regression model validation. Independent raglan-sleeve patterns [10- 23] were selected. Both two-piece and three-piece sleeve constructions were tested (Table 3.16). For each construction, the initial pattern parameters (X_4, X_7, X_{10}, and X_{11}) were measured. The parameters were then adjusted using the regression equations, with reference to the optimal fit value ranges established in the previous sections.

Table 3.15 shows the good-fit ranges and the initial and modified values of the key pattern parameters for both sleeve constructions. Overall, the regression-guided modification drove the pattern parameters toward the verified good-fit ranges, providing a quantitative basis for parameter adjustment.

Table 3.15 - Comparison of pattern parameters before and after modification

Pattern parameters	X_4	X_7	X_{10}	X_{11}
	Δ（∠BSS+ ∠FSS）	Δ(∠BA+∠FA)	Δ(BSW - FSW)	Offset(SCL)
Interval	[40°...54°]	[60°... 72°]	[2.5... 7.5]	[1.5...3.5]
Two-piece				
Initial	46.7	33.6	8.3	0
Modified	46.7	72	2.5	2
Three-piece				
Initial	53.9	83.6	11.4	3
Modified	50	72	5	3

Note: X3 (BSS−FSS) was not included as a regression predictor in Table 3.14, but was retained as an auxiliary constraint for distributing the target X4 (BSS+FSS) into individual BSS and FSS values during pattern reconstruction.

Figure 3.15 shows the corresponding 2D patterns and 3D try-on results before and after modification for the two-piece and three-piece sleeves.

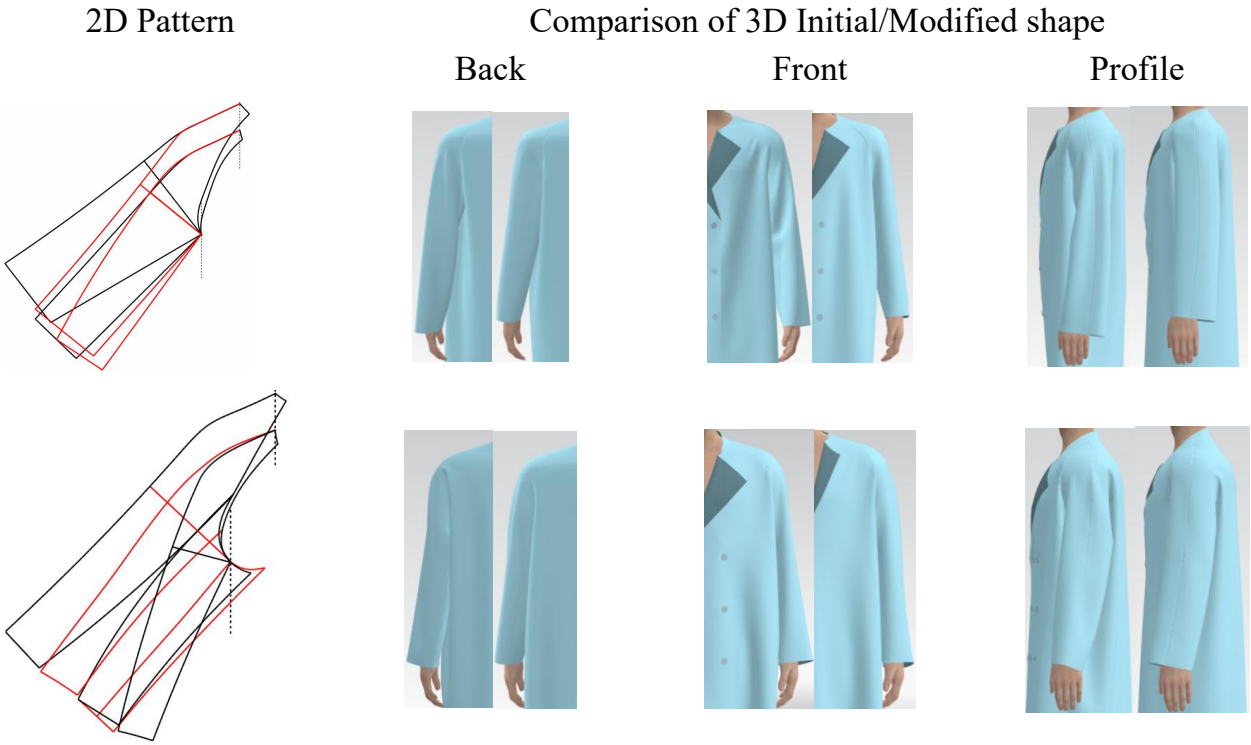

Figure 3.15 - 2D patterns and 3D shape before and after modification for the two-piece and three-piece sleeves. *Note: Initial pattern: black line; modified pattern: red line*

As shown in Figure 3.15, in the initial patterns, the sleeve appearance showed clear fit problems, including visible folds and an imbalanced sleeve posture under the front/back/profile views. Following the regression-guided adjustments, the sleeve shape improved significantly, with the surface becoming smoother and the sleeve fitting closer to the body.

Table 3.16 compares the predicted shape criterion values (Y_1 - Y_4) calculated from the regression model with the measured values from the 3D shapes.

Table 3.16 - Comparison of Initial and Modified 3D Shapes Based on Regression Model

	NO.		Y_1-FD	Y_2-FC	Y_3-$\lvert\Delta(a-b)\rvert$	Y_4-Folds
Two - pieces	Initial	3D Measured	4.5	0.6	0.5	4
		Equation	3.6	0.4	0.1	3
	Modified	3D Measured	3.0	0.5	0.6	0
		Equation	4.5	2.3	0.5	0.4
	Difference		1.5	1.8	0.1	0.4
Three - pieces	Initial	3D Measured	5.4	0.8	0.2	2
		Equation	2.8	3.2	1	0
	Modified	3D Measured	3.5	3.0	0	0
		Equation	4.1	3.2	0.2	0.4
	Difference		0.6	0.2	0.2	0.4
Good fit range			0.7... 4.1cm	1... 4.3cm	0... 0.7cm	0...1
1ST step：Whether Y_4 is 0 if yes，compare Y_3, Y_2, Y_1. If NO, ending						

As shown in Table 3.16, Y_4 (Folds) was used first as the priority criterion in the evaluation. When Y_4 is within the acceptable range [0, 1], folds on the sleeve surface are limited to an acceptable level. Y_1, Y_2, and Y_3 were then compared to determine whether they satisfied the good-fit criteria. In the modified cases, both sleeve types showed an obvious reduction in folds, and the Y_4 values measured from the 3D virtual-fitting results decreased to the range [0, 1]. This indicates that pattern adjustments based on the regression equations effectively improved sleeve-surface smoothness.

Further comparison showed that certain differences in Y values remained for the two-seam sleeve. Specifically, the differences for Y_1 and Y_3 were less than 1 cm, whereas the largest difference was observed for Y_2 and reached 1.3 cm. This indicates that, after adjustment using the regression equations, the spatial relationship between the sleeve and the arm at the cuff did not fully reach the good-fit range. After modification,

the three-seam sleeve satisfied all good-fit criteria, indicating a more stable effect of structural adjustment. This result is consistent with the analysis of differences between raglan sleeves presented in Chapter 2 and further confirms the structural validity and methodological significance of selecting the three-seam sleeve construction as the subsequent research object.

Conclusion of Chapter 3

1. An optimization method for the basic prototype was developed based on the precise localization of key anatomical landmarks. This method significantly enhanced the individualized fit accuracy of the basic block, providing a stable foundation for all subsequent raglan sleeve development. It provides a reliable optimization pathway for pattern design, improving both comfort and aesthetic appearance.

2. Critical raglan-sleeve pattern parameters were reorganized and standardized to improve pattern-making methodology and optimize sleeve morphology. Four decisive parameter groups governing the shape were identified: the position and distribution of chest-girth ease, the distribution of front and back shoulder sloping, the angle between the shoulder line and sleeve center line, and the offset of the sleeve center line at the cuff. By adjusting these parameters within verified angular and dimensional ranges in combination with the same silhouette target, a more stable and reproducible improvement in raglan-sleeve shape can be achieved.

3. A parameterized control framework was developed to link 2D patterns and 3D shapes. Through statistical analysis and regression modeling, the mapping relationship between 2D pattern parameters and 3D shape parameters influencing raglan-sleeve morphology was clearly defined. The parametric design framework based on this relationship shifts the pattern optimization process from trial-and-error to precise data-driven control, significantly improving pattern design efficiency and shape predictability.

CHAPTER 4. AI - DRIVEN DIGITALIZATION OF RAGLAN COAT DESIGN

This chapter introduces an AI-driven generation and evaluation framework for the "body+coat" system. However, as the design task extends from pattern construction to image-level generation and cross-route comparison, the limitations of relying only on 2D pattern-making and 3D virtual try-on become more evident. Therefore, AI-driven digitalization is introduced as an additional route for generating, comparing, and refining raglan coat images under measurable 2.5D projection constraints.

The aim of this chapter is to present an AI-driven algorithm for generating and evaluating raglan coat images by integrating projection parameters, 3D reference images, and multimodal prompting strategies.

4.1. Overall framework of the AI-driven digitalization

Figure 4.1 shows the overall framework of the AI-driven digitalization framework for generating the "body+coat" system.

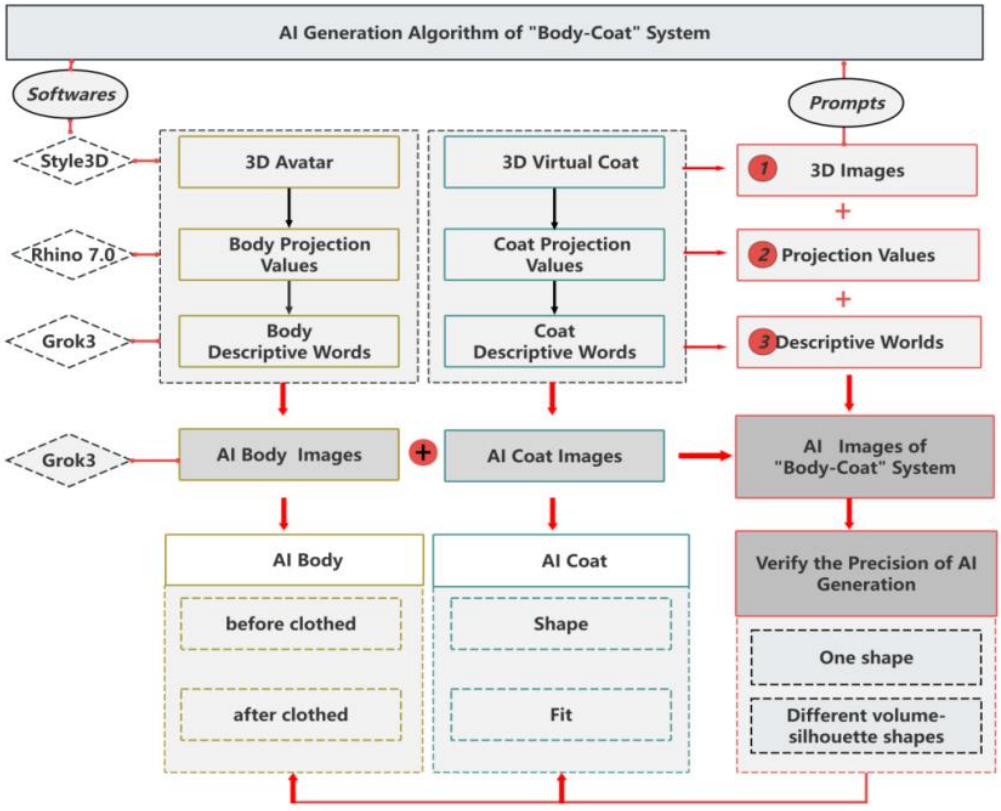

Figure 4.1 - AI-driven generation and verification framework for the "body–raglan coat" system

As shown in Figure 4.1, the framework integrates Style 3D, Rhino 7.0, and Grok3, projection-based parameterization, and structured multimodal prompting. The prompts for body and coat generation include three modules: three-dimensional reference images, projection measurements, and descriptive text.

The workflow consists of three stages.

1) AIB generation is conducted. The VB is constructed in Style 3D from key anthropometric dimensions and imported into Rhino 7.0 to extract additional frontal and profile projection measurements. These projection values, together with body descriptive text and 3D reference images, form the multimodal prompt to Grok 3 for generating AIB images.

2) AIC generation is performed. Using the same VB, a 2D raglan coat pattern is developed and simulated in Style 3D to obtain the VC. The VC is then transferred to Rhino 7.0 to label and measure coat projection parameters at key girth levels (shoulder, chest, waist, hip, armhole, elbow, cuff), capturing both volume-silhouette descriptors and fit-relevant dimensions. These projection values, 3D coat images, and coat descriptive texts constitute the Grok 3 prompt for generating AIC images.

3) Verification of the AI-generated “body + coat” system. AIB structural fidelity is evaluated against RB and VB. AIC accuracy is examined in terms of projection deviation and fit performance, and the stability of the generated body structure after coat overlay is further assessed. The framework is then extended to different volume-silhouette categories and fabric descriptors to evaluate its generalization ability.

To ensure direct comparability among the subsequent experiments, the objects, prompting schemes, projection parameters, and deviation metrics established in Chapter 2 are applied consistently in the following sections.

4.2. Generation and verification of AI-generated images

The purpose of this section is to verify the structural accuracy of the images. AIB is compared with RB and VB, and AIC is compared with the real coat (RC) and the virtual coat (VC). The specification of the typical body (TB) is used as the control basis.

4.2.1. Accuracy verification of AI- generated bodies

The AIB generation results were evaluated from three aspects: visual generation quality, image stability under repeated generation, and intertemporal stability of the generated image.

AIB generation. A comparative experiment was conducted using TB according to

the multimodal generation process described in Section 2.3.2. Figure 4.2 shows RB, VB, and AIB images generated by Methods A and B under the same TB specification. These body representations were used to quantify the geometric consistency between AI-generated bodies and the scanned reference under identical pose and viewing constraints.

a *b* *c* *d* *e*

Figure 4.2 - Comparison of RB, VB, and AIB: *a* - real scanned body, *b* - 3D avatar, *c* - AI body using *Method A*, *d*-AI body using *Method B*,*e*- AI body after coat overlay

Generation stability. Before the main validation, an additional cumulative convergence analysis was conducted based on 30 consecutively generated AIB outputs to evaluate the adequacy of the sample size for repeated generation. The results showed that the cumulative means, dispersions, and deviations from the real body changed markedly from n=5 to n=15 and then approached a stable plateau, with only marginal fluctuations observed from n=20 to n=30 (Table B1-B2 and Figure B1-B2 in Appendix B). These results indicated that the stabilization point occurred at n=15...20. Therefore, 20 consecutively generated valid AIB images were retained as a conservative and sufficient formal sample size.

To evaluate the repeatability of AIB generation, 20 AIBs were generated on 14 March 2025 using identical multimodal prompts according to Method B (Table 2.14). The projection deviations between the selected AIBs and the real body (RB) were calculated using Eq. (2.8) and are presented in Table B.4 in Appendix B. In virtual try-on systems, a deviation of no more than 1.0 cm is generally regarded as an acceptable tolerance threshold [139]. The results showed that Grok 3 maintained deviations within ±1.0 cm for all seven projection parameters, while most deviations were concentrated within ±0.5 cm.

Figure 4.3 shows the proportions of samples falling within the deviation thresholds of ≤1.0 cm and ≤0.5 cm for different body regions.

Figure 4.3 - Proportion of AIB samples within the projection-deviation thresholds for body parameters: ΔW_S, ΔW_C, ΔW_W, ΔW_H, ΔW_A, ΔW_E, and ΔW_{Wr}. Here, ΔWs...wr = W_{AIB} - W_{RB}, where WS is shoulder width, W_C is transverse chest diameter, W_W is transverse waist diameter, W_H is transverse hip diameter, W_A is transverse upper-arm diameter, W_E is transverse elbow diameter, and W_{Wr} is transverse wrist diameter.

As shown in Figure 4.3, more than 90% of the samples for W_S, W_C, W_W, W_E, and W_{Wr} remained within the ±1.0 cm range. Moreover, W_S, W_C, W_W, and W_E also showed more than 50% of samples within ±0.5 cm, indicating relatively high local accuracy in body regions that are critical to garment balance and fit. Most body regions exhibited mean deviations within approximately ±0.2– 0.6 cm, together with relatively narrow confidence intervals, reflecting limited variability among repeated generations. Although W_{Wr} showed a lower proportion within the ±0.5 cm interval, it remained within the acceptable ±1.0 cm tolerance, thereby preserving the structural integrity of this relatively delicate anatomical region. These results confirm that the proposed multimodal prompt can support high-accuracy AIB generation at the level of projection measurement and is therefore applicable to subsequent generation and verification of the virtual “body - coat” system.

To further verify whether the fixed multimodal prompt remained reliable under model iteration over time, an additional 20 AIBs were generated on 22 April 2026 using the same multimodal prompt and the same generation settings. The mean ± SD values of the seven projection parameters obtained on the two dates were then compared. Detailed data are presented in Table B.5 of APPENDIX B. The mean differences ranged from 0.02 to 0.30 cm, with an average absolute difference of 0.16 cm across the seven parameter sets. For six of the seven parameters, the mean difference did not exceed 0.24 cm, indicating good cross-time consistency and stability at the projection measurement level. AW showed the largest shift (0.30 cm), suggesting that this parameter was relatively more sensitive to cross-time generation variation than the other body-width parameters. However, even this difference remained well below the engineering tolerance threshold of 1.0 cm.

Taken together, these results indicate that the fixed multimodal prompt did not guarantee image-identical outputs across different generation dates, but it did maintain stable anthropometric measurements at the projection-parameter level. Therefore, the prompt can be regarded as temporally stable for measurement-based AIB generation and suitable for subsequent comparative analysis in this study.

Accuracy verification of AIB generation. The 26 key body projection parameters were divided into four types (in Table B.6 in Appendix B): heights (H, H_S, H_C, H_U, H_W, H_H, H_F, H_B), front widths (W_S, W_C, W_W, W_H, W_A, W_E, W_{Wr}), profile widths (D_C, D_W, D_H, D_A, D_E, D_{Wr}), and angles (∠E, ∠1， and ∠3). Deviations were computed between RB and the three comparative models: VB, AIB_A, and AIB_B using Eqs. (2.9), (2.10), and (2.11) in Section 2.3.3. For each group, *MD* was calculated: MD_H (heights), MD_W (front widths), MD_D (profile widths), and MD_A (angles).

The comparative analysis revealed that AIB_B showed the best overall accuracy among the three comparative models. The MD_H and MD_A groups showed the lowest deviation (−0.6 ± 0.9 cm; 0.7 ± 4.5°), whereas AIB_A exhibited greater underestimation −1.5 cm. AIB_B also demonstrated stable performance in MD_W and MD_D, whereas AIB_A showed greater bias and variability. Despite larger overall errors in the angle parameters, AIB_B maintained the narrowest deviation range, indicating that the incorporation of 3D reference images improved the reconstruction of posture-sensitive body geometry, especially the angular features related to arm posture. Figure 4.4 shows bar charts comparing the projection deviations across all 26 parameters grouped into Heights, Front widths, Profile widths, and Angles.

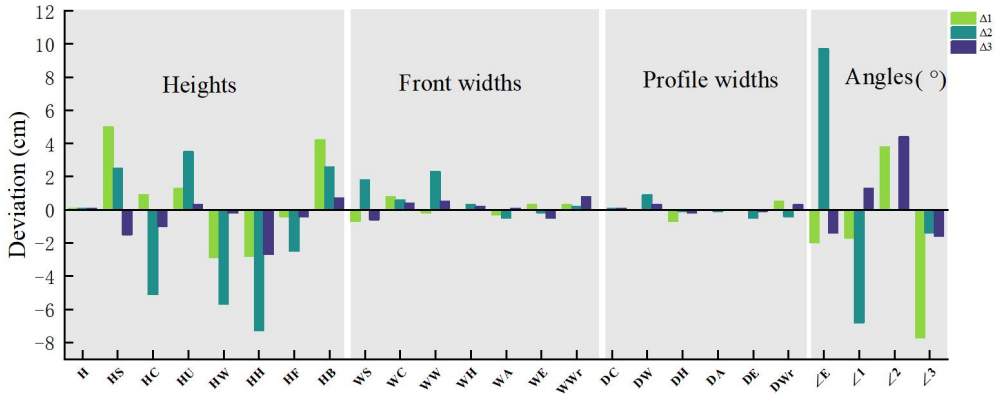

Figure 4.4 - Projection deviation comparison across RB, VB, AI_A, and AIB_B

As shown in Figure 4.4, *Method B* (Δ3) consistently achieved lower projection deviations than *Method A* (Δ2) across most dimensions. For height-related parameters (H–H_B), *Method B* remained within ±1.0 cm, while key front and profile widths (D_C, D_W) and posture-sensitive back angles (∠1, ∠3) stayed within ± 0.5 cm and ±1.5°,

respectively. In contrast, *Method A* exhibited larger deviations and instability, particularly for W_E, D_E, and ∠S, indicating that text and projection constraints alone are insufficient.

Overall, the results demonstrate that AIB generation was repeatable and cross-time stable. Among the tested generation routes, the AIB_B image showed the best overall agreement with RB and VB. Method B was adopted as the baseline configuration for subsequent AIC generation and "body−coat" verification experiments, with AIB_B serving as the verified AI-generated body baseline.

4.2.2. Generation and verification of the "body+coat" system

The "body+coat" system was generated on the verified AIB_B baseline and standardized *Method B* prompting settings. The generated AIC outputs were evaluated against RC and VC references using the projection-based criteria established in Chapter 2. In addition, body-structure consistency before and after coat overlay was verified by comparing the pre- and post-clothing body projections.

*AIC generation and visual comparison. U*sing *Method B*, the virtual coat VC generated in Style3D based on the standard VB was used as the 3D reference image and input into Grok 3 for AIC generation. The front view was generated using Prompts 5 and 6 with Steps 1 and 2, while the profile view was generated using Prompts 7 and 8 with Steps 3 and 4. To verify the structural accuracy of AIC, a comparative analysis was conducted against RC with identical dimensions. The high-accuracy AIB_B generated in the previous step was used as the basis for the AIC generation (see Figure 2.6 in Section 2.1). Figure 4.5 shows the visual comparison of AIC, VC, and RC under the representative "body+coat" system.

a *b* *c*

Figure 4.5 - Visual comparison of VC, AIC, and RC under the representative "body+coat" system: a - VC, 3D-simulated raglan coat; b - AIC, AI-generated raglan coat; c - RC, real raglan coat worn by the model.

As shown in Figure 4.5, VC, AIC, and RC were compared in front and profile views. VC showed the pattern-driven 3D simulation reference, AIC represented the multimodal AI-generated output, and RC served as the real reference. The AIC demonstrated visual consistency with RC, particularly in terms of coat length, sleeve shape, collar structure, and overall silhouette. Additionally, compared to RC, AIC had a smoother surface. Key structural features such as shoulder curvature, sleeve outline, and garment outline remained visually consistent with RC.

Projection-parameter and fit verification of AIC. To further evaluate the structural accuracy, detailed AIC projection parameters were measured and analyzed using Eqs. (2.14) and (2.15). The projection deviations of AIC and VC relative to RC as the reference are presented in detail in Table B.7, Appendix B.

The 19 key coat projection parameters were divided into three categories: front widths (W'_C, W'_W, W'_H, W'_A, W'_E, W'_{Wr}, W'_S), profile widths (D'_C, D'_W, D'_H, D'_A, D'_E, D'_{Wr}), and angles ($\angle S'$, $\angle A$). Both local and overall structural deviations were evident between the AIC and VC. The differences were minor in front width, with *MD*'$_W$ of VC (−0.7 cm) and AIC (−0.4 cm), indicating similar performance. However, profile widths of VC exhibited a large deviation (−4.6 ± 1.0 cm), particularly in lateral and sleeve regions, while AIC significantly reduced the deviation to −1.0 ± 1.1 cm, demonstrating notably higher fidelity in side shaping. The angular parameters revealed even larger differences: VC exhibited considerable instability (–3.7 ± 15.2°), while AIC maintained a much narrower deviation (–0.9 ± 3.2°).

Figure 4.6 shows bar charts comparing AIC and VC using RC as the reference across all 19 parameters. The results were grouped into front widths, profile widths, and angles.

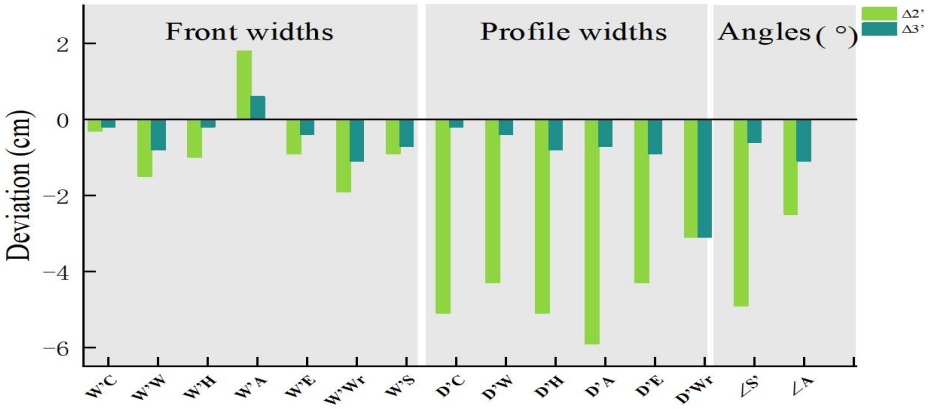

Figure 4.6 - Projection deviation comparison between VC and AIC, grouped by front widths, profile widths, and angles

As shown in Figure 4.6, AIC showed lower projection deviation than VC, particularly in profile-width and angular parameters. For key frontal parameters such as W'$_C$,

W'_W, and W'_S, AIC deviations remained within 1.0 cm, whereas the corresponding VC deviations exceeded 1.5 cm. The angular parameters (∠S', ∠A) also showed smaller deviations (≤ 1.1°) in AIC. The largest differences were observed in the lateral parameters: the AIC, D'_C, and D'_H deviations ranged from 0.2 to 0.8 cm, whereas the corresponding VC deviations reached up to 5.1 cm. These results indicate that, under the tested representative configuration, the multimodal AI generation route achieved closer projection-level agreement with RC than the pattern-driven 3D simulation route.

In addition to geometric deviation, the fit quality of the raglan coat was further evaluated using the seven fit criteria adopted from previous studies. Table 4.2 shows the verification results based on these criteria by comparing the AIC with the RC and VC.

Table 4.1 -Fit verification of AIC under the representative "body+coat" system

Fit Criteria	Coat dimensions			Differences between RC and		Interval	I or O
	RC	VC	AIC	VC	AIC		
				Δ2'	Δ3'		
$(d_F+ d_B)/2$，°	1.2	2.5	3	1.3	1.8	[0... 2]	O
$(\angle F+\angle B)/2$, °	91	89	92	2	2	[88...92]	I
c	0	0	1	0	1	0	O
FC, cm	3.3	2.0	3.8	1.3	0.5	[0.7...4.1]	I
PC, cm	3	1.8	2.2	1.2	0.8	[1...4.3]	I
|a-b|	0	0	0.7	0	0.7	[0，0.7]	I
Folds	0	0	1	0	1	-	O
Note: I = within the acceptable interval; O = outside the acceptable interval. The status refers to AIC.							

As shown in Table 4.1, the key observations were as follows:

1) Bodice balance indicators. AIC slightly exceeded the upper tolerance limit ($(d_F+ d_B)/2$= 3.0 cm > 2.0 cm), indicating a slightly front-back balance deviation. However, $(\angle F+\angle B)/2$ remained within the interval [88, 92°], indicating that the vertical balance remained within the acceptable range.

2) Sleeve balance. Both FC and PC values remained within their respective intervals ([0.7... 4.1] cm and [1.0... 4.3] cm), indicating acceptable sleeve-body spatial conformity.

3) Sleeve-arm alignment. |a–b| = 0.7 cm closely reached the upper limit, but still indicated acceptable alignment with a natural arm posture.

4) Fold formation. The fold count for AIC was 1 compared with 0 for RC and VC. This slight increase suggested minor structural irregularities, likely due to the sensitivity of AI to complex drape zones. However, it did not affect the overall fit quality.

Overall, the AIC satisfied most of the predefined fit criteria, while localized deviations remained in bodice balance and fold formation. Therefore, the generated sample should be interpreted as a mostly acceptable AIC output with minor local fit defects, rather than as a completely defect-free result. This distinction is important because the subsequent fit-defect diagnosis and AI-assisted refinement section further examine how such localized imperfections can be identified and corrected.

Structural accuracy and stability of AIBc. To assess whether the body structure remained consistent after the coat overlay, Grok3 was used to regenerate AIBc from the "body+coat" system after removing the coat. The pre- and post-clothing body projections were then compared; specifically, AIBc was compared with RB and AIB_B using Eqs. (2.11), (2.12), and (2.13). Category-level MD for $\Delta 3$ (RB−AIB_B), $\Delta 4$ (RB−AIBc), and $\Delta 5$ (AIB_B −AIBc) were grouped into heights, front widths, profile widths, and angles; the complete parameter-wise deviations are provided in Table B.7 in Appendix B.

The *MD* indicated good structural stability and consistency between the pre-dressed AIB_B and post-dressed AIB_C. Deviations in height (MD_H), front width (MD_W), and profile width (MD_D) remained small, suggesting that coat overlay introduced only limited changes to the overall geometric structure of the generated body. Slight increases in angular deviations were observed, which were the expected changes in shoulder and back angles due to the garment's ease allowance after dressing. Despite these local changes, AIB_C maintained a high level of anatomical consistency and geometric stability, providing a reliable foundation for fit evaluation and layered garment modeling.

The morphological stability of AIBc was further inspected at the parameter-group level by visualizing deviation trends. Figure 4.7 shows the deviation trends across Δ3, Δ4, and Δ5, grouped into heights, front widths, profile widths, and angles.

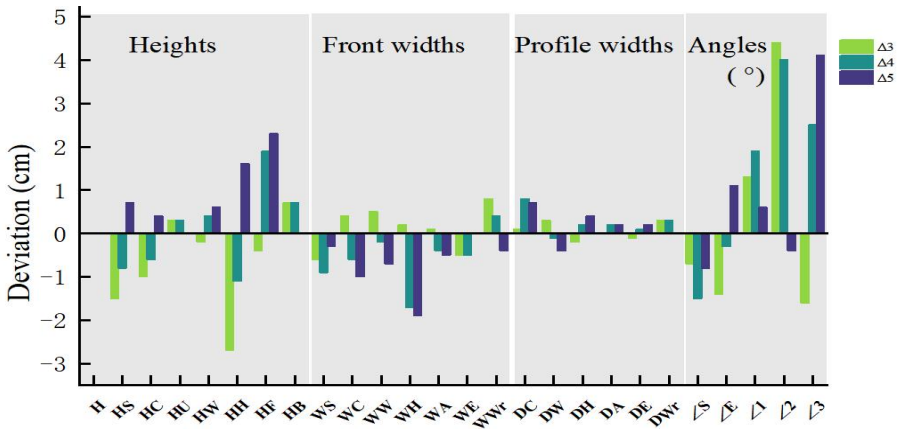

Figure 4.7 - Projection deviation trends of AIB_C against RB and AIB_B, grouped by heights, front widths, profile widths, angles

As shown in Fig. 4.7, Δ3 reflects the difference between RB and AIB_B, showing moderate and consistent deviations across the key dimensions. Δ4 followed a trend similar to Δ3, indicating the adequacy of AIB_C relative to the real body. Notably, Δ5 remained the smallest for almost all parameters, confirming that the dressing and coat-removal processes had a minimal influence on the AIB morphology. These results confirmed that the proposed Grok3 multimodal "body+coat" generation framework maintained strong anatomical consistency.

Overall, the representative "body+coat" verification demonstrated that Method B could generate an AIC with good projection-level agreement with RC and VC, while preserving body similarity.

4.3. Verification of the AI generalization ability across different volume-silhouette shapes from different fabrics

To examine the applicability of the developed scheme, this section extends the generation task to four predefined volume–silhouette categories. Additionally, Method B is evaluated in this section from four aspects: volume – silhouette generation, projection-parameter accuracy, compliance with the raglan-coat shape criteria CC, and robustness to fabric-category descriptors.

4.3.1. AI Generation of a coat with different volume-silhouette shapes

The chest-ease allowance and corresponding volume–silhouette descriptors were varied. The accuracy was subsequently evaluated using the raglan coat shape criteria C_C from Chapter 2.

Figure 4.8 shows the AICs corresponding to four predefined volume-silhouette categories, namely S1, S2, S3, and S4, with average chest ease allowances of 12 , 16 , 20 , and 28cm, respectively. The figure presents the frontal views (S1-F to S4-F) and profile views (S1-P to S4-P) of four silhouette categories - Fit, Semi-fit, Semi-loose, and Loose.

S1-F S2-F S3-F S4-F S1-P S2-P S3-P S4-P

Figure 4.8 - AICs generated under four different volume-silhouette shapes

As shown in Figure 4.8, the generated AICs exhibited a clear visual progression from the fitted silhouette to the loose silhouette. The overall coat width, side contour expansion, and coat volume gradually increase. The results indicate the visual feasibility of AIC generation with different volume-silhouette parameters. Detailed measurement results for the parameters of all four coats are provided in Figure B.3 of APPENDIX B.

The results showed smooth monotonic increases in both descriptors from S1 to S4, and all values remained within the predefined interval ranges of their corresponding target silhouette groups. This indicates that the gradation of coat volumes was accurately reproduced.

A comparative analysis was conducted to evaluate the different shape accuracy of the AICs. The analysis included two data sources: (1) VCS $_{S1...S4}$ generated by Style3D and (2) AIC$_{S1...S4}$ generated by Grok 3. The deviation $\Delta_{S1...S4}$ =AIC$_{S1...S4}$ - VC$_{S1..S4}$ was calculated using the deviation equation defined in Chapter 2, where i represents S1, S2, S3, or S4. The aggregated MD results were grouped into front widths (MD_W), profile widths (MD_D), and angles (MD_A), while the complete parameter-wise deviations for each silhouette group are provided in Table B.9 in Appendix B.

The results indicate that the projection deviations were acceptable for all four coat forms. Overall, *S3* showed the smallest overall deviation, indicating the most stable AI performance for the medium-volume silhouette. In contrast, S1 and S4 showed relatively larger deviations, indicating that very fitted or highly voluminous silhouettes may introduce greater projection variation. Figure 4.9 shows the projection - deviation comparison between AIC$_{s1...s4}$ and VC$_{s1...s4}$

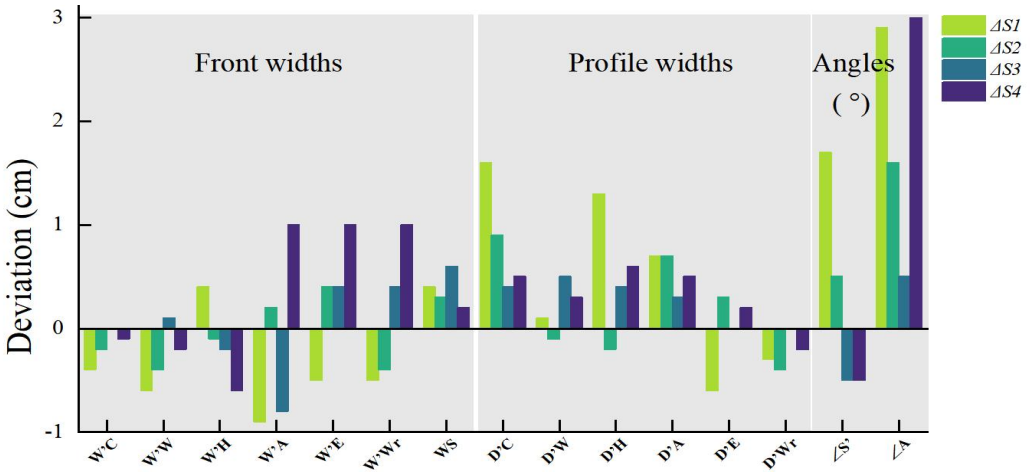

Figure 4.9 - Projection deviation comparison between AIC and VC across four silhouette categories (*S1–S4*)

Figure 4.9 demonstrates the structural accuracy of the proposed AI generation system. The stable accuracy observed across all silhouette forms confirms the ability of this method to create structurally reliable and geometrically consistent raglan coat images under different style conditions.

Table 4.2 shows the fit evaluation results using the seven established criteria.

Table 4.2 - Fit evaluation results for different volume-silhouette shapes

Fit Criteria	*S1*	*S2*	*S3*	*S4*
$(d_F + d_B)/2$	2.8	2.1	3	2
$(\angle F + \angle B)/2$	94	92	90.5	93
c	0	0	0	0
FC	2	2.6	2.4	4.7
PC	2.1	1.8	2.0	3
$\lvert a-b \rvert$	0.5	0.3	0.6	0
Folds	1	1	1	1
Note: Grey-shaded cells indicate values located within the predefined acceptable intervals.				

As shown in Table 4.2, the 18 grey-shaded cells indicate values located within the predefined intervals, accounting for 64.3%. The remaining 10 indicators showed limited deviations from the target criteria: the deviations of the linear indicators did not exceed 1.0 cm, the angular deviations remained within 2°, and the fold-related deviations were limited to one visible fold. Most deviations were observed in S4.

Thus, generating AIC with different volume-silhouette shapes confirms the ability of AI to reliably generate objects with different sets of quantitative parameters.

4.3.2. Influence of fabric type on AI-generated coat silhouettes

This section uses three types of autumn-winter fabrics. Figure 4.10 presents raglan coats made from three fabrics with a chest ease of 16 cm.

F1	F2	F3	F1	F2	F3

Figure 4.10. AI-generated raglan coats in three fabric types at the 16 cm chest-ease level

As shown in Figure 4.10 and Figure B.4 of APPENDIX B, among the three materials, the wool fabric F3 generally produced a clearer contour, whereas the cotton fabric F1 tended to show softer transitions in the sleeve and bodice regions. The polyester samples F2 appeared smoother and more uniform. These observations indicate that fiber composition affects visual impression more strongly than the overall silhouette trend determined by chest ease.

Differences between fabrics are summarized in Tables B.10-B.11 of APPENDIX B. Overall, frontal widths remained relatively stable. In contrast, profile widths showed more pronounced fluctuations, indicating greater sensitivity of the side contour to fabric-related drape expression. The largest changes were observed in the angular parameters.

Overall, the inter-fabric comparison shows that changing the fabric category does lead to measurable shifts in projection parameters; however, these shifts were mainly concentrated in local regions rather than in the overall silhouette structure. Importantly, differences between fabrics were generally smaller than the structural progression caused by increasing chest ease. Therefore, fabric variation should be interpreted as a factor influencing local contour response and visual expression, rather than as a dominant factor redefining the overall volume-silhouette trend.

Although differences between fabric types were observed for several parameters, it was necessary to determine whether these differences were significant for the developed volume-silhouette grouping. Therefore, the applicability of the established intervals under changes in fabric type was evaluated by changes in descriptors d12 and d13, which were calculated for the three selected fabric types and four predefined chest-ease levels. Figure

4.11 shows the d12 and d13 curves for AI-generated raglan coats made from cotton, polyester, and wool. Detailed values are given in Table B.12 of APPENDIX B.

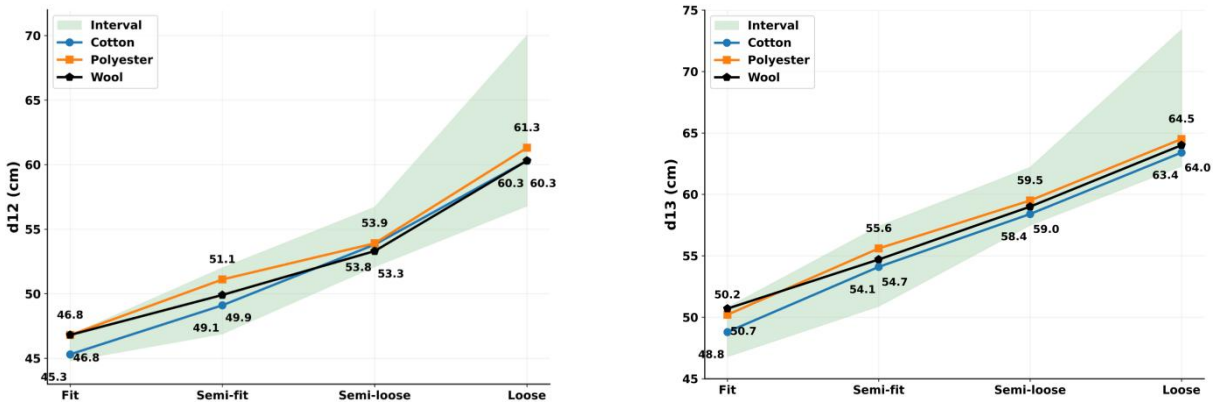

a *b*

Figure 4.11 - Verification of the robustness of volume-silhouette grouping for AI-generated raglan coats made from three fabric types using integrated projection descriptors d12 and d13 at four chest-ease levels: a - d12, characterizing silhouette width in the chest and armhole region; b - d13, characterizing silhouette width in the waist and elbow region. The lines show descriptor values for cotton, polyester, and wool fabrics, and the green shaded area indicates the predefined interval ranges of the corresponding volume-silhouette categories Fit, Semi-fit, Semi-loose, and Loose.

As shown in Figure 4.11, for all three fabric types, d12 and d13 increase monotonically from S1 to S4, indicating stable and consistent volume-silhouette response dynamics with increasing chest ease. This result suggests that, within the selected fabric types, the AI-generated silhouettes maintain the specified proportions. It also indicates that differences between fabric types exist but do not change the silhouette-grouping result.

4.4. Comparison of 3D simulation and AI generation results

This section compares RC, VC, and AIC to verify structural deviations, compliance with fit criteria, and volume-silhouette form. Four raglan coats S1-S4 with chest ease values of 12, 16, 20, and 28 cm, respectively, were selected for comparison. The coat images were generated in Grok 3 using multimodal prompt B. The 3D images were generated in Style3D.

Figure 4.12 presents RC, AIC, and VC images in frontal and profile views for S1-S4.

Figure 4.12- Visual comparison of RC, AIC, and VC across four volume – silhouette conditions in frontal and side views: *S1-S4* correspond to $E_{(CG)}$ = 12,16,20, and 28 cm chest ease; *a* - RC, *b* -AIC, *c* - VC

As shown in Figure 4.12, as chest ease increases, the overall coat width increases for all image-acquisition methods. Based on this qualitative observation, a rigorous parametric evaluation was conducted.

To summarize the magnitude of deviation regardless of direction, the mean absolute relative error (MARE) was calculated using Equation (2.6). To improve interpretability, projection parameters were divided into subsets: frontal bodice, side bodice, frontal sleeve, and side sleeve. Angular parameters were treated as a separate group. Table 4.3 shows the

parameters for all defined groups. Detailed data are presented in Table B.13 of APPENDIX B.

Table 4.3 - Aggregated MARE (%) for AIC and VC

Evaluation level	Group		parameters	MARE(%)	
				AIC	VC
Region-level subsets	Front bodice	Frontal "shoulder-chest-waist-hips" contour	W'_S, W'_C, W'_W, W'_H	1.6	4.7
	Side bodice	Profile "chest-waist-hips" contour	D'_C, D'_W, D'_H	2.4	2.4
	Front Sleeve	Frontal "armhole-elbow-sleeve hem" contour	W'_A, W'_E, W'_{wr}	3.9	12.1
	Side Sleeve	Profile "armhole-elbow-sleeve hem" contour	D'_A, D'_E, D'_{wr}	2.8	9.2
View-level aggregates	Front width	Complete frontal contour of bodice and sleeve	W'_S, W'_C, W'_W, W'_H, W'_A, W'_E, W'_{wr}	2.6	7.9
	Side width	Complete profile contour of bodice and sleeve	D'_C, D'_W, D'_H, D'_A, D'_E, D'_{wr}	2.6	5.8
Additional groups	Angle	Shoulder angle and angle between the shoulder region and sleeve	∠S', ∠A	3.4	12.3
Overall level	Total	All projection parameters	All parameters	2.8	7.6

Figure 4.13 shows the grouped comparison of MARE between AIC and VC based on the hierarchical parameter groups in Table 4.5 and provides a direct visual summary of inter-method differences.

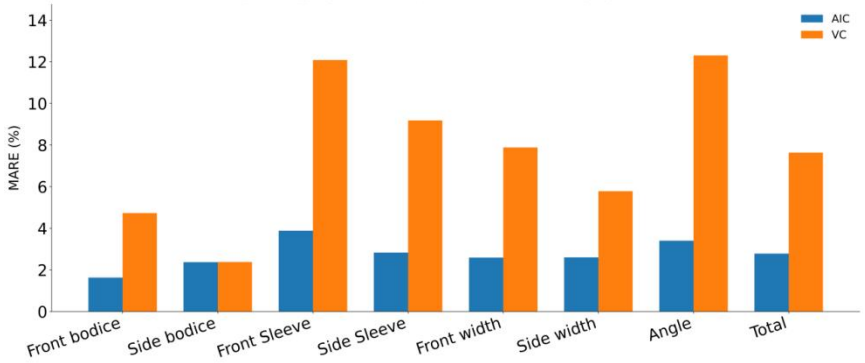

Figure 4.13 - MARE comparison between AIC and VC

As shown in Figure 4.14, AIC demonstrated lower aggregated MARE values than VC for all parameter groups.

Taken together, Figure 4.13, Table 4.3, and Figure 4.14 confirmed the main difference between AIC and VC in favor of AIC.

Table 4.4 shows the main differences between VC and AIC.

Table 4.4 - Comparative interpretation of VC and AIC

Aspect	VC (3D virtual try-on)	AIC (AI generation)
Main concentration of deviations	Sleeve-related parameters: contour regions defined by the shoulder and armhole	Lower overall projection deviations; residual variability in folds, textures, and local contour details
Probable influencing factors	Local mismatch between avatar and real body; air-gap distribution; fabric, solver, collision, and seam-processing effects	Strength of multimodal constraints; absence of explicit pattern/assembly priors
Advantage	Structural traceability and interpretability from pattern to simulation to contour	Projection-level silhouette fidelity under controlled conditions
Limitation	Sensitive to simulation settings and physical parameterization	Less stable in high-frequency appearance details, especially folds, textures, and local surface variations

Overall, VC and AIC demonstrated complementary characteristics. VC was based on patterns and simulation, making it more controllable, reproducible, and structurally interpretable; however, its sleeve parameters were more sensitive to

simulation settings and physical parameterization. AIC showed closer correspondence to RC in 2.5D projection measurements, although the appearance of folds and other local surface details was less stable. These results clarify the different roles of VC and AIC in image-level digitalization and provide the basis for a complementary 3D+AI workflow.

Table 4.5 shows the positioning of VC, AIC, and the evaluation algorithm within the complementary 3D+AI digital process.

Table 4.5 - Structure of the 3D+AI digitalization process

Module	VC (3D virtual try-on)	AIC (AI generation)	Unified 2.5D evaluation
Main role	Pattern- and simulation-based structural reference	Enhances projection-level silhouette agreement	Ensure the same measurement and comparison across RC/VC/AIC
Key inputs	Body baseline + pattern + fabric/simulation settings	Prompt + 2.5D projection parameters + 3D reference images + controlled pose/view/lighting/background	Same 2.5D parameters + RE/MARE
Main output	Interpretable structure and physically plausible drape	Image-level silhouette fidelity relative to RC	Quantitative benchmarking across RC/VC/AIC
Best application	Pattern development, structural verification, repeatable simulation	Reducing virtual–real discrepancy; fast image-level refinement	Error localization, method comparison, cross-silhouette evaluation

4.5 Identification and elimination of fit defects

This section verifies the ability of AI to generate fit defects and investigates the possibility of eliminating them through iterative prompt-based refinement.

During the verification of the AIC, it was found that not all predefined fit criteria were satisfied. The main deviations were associated with bodice balance and the occurrence of folds. Defect identification was therefore treated as a diagnostic process based on the developed evaluation criteria.

To enable the identified defects to be used for subsequent prompt refinement, the detected defects were annotated on the selected AIC coat image. Table 4.6 presents the main defects, the diagnostic scheme, and the corresponding directions for prompt correction to prevent these defects in subsequent generations.

Table 4.6. Visual diagnosis of AI-generated fit defects and directions for prompt correction

Defect name	Defect image	Diagnostic basis	Prompt-adjustment direction
Bodice balance defect	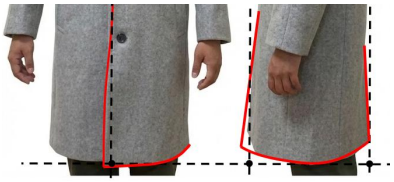	The center-front line is uneven and non-vertical, and the hemline deviates from the good-shape reference line, indicating insufficient front–back bodice balance and front-center stability.	Emphasize a straight, stable, and vertically continuous center-front line; maintain a clean and balanced frontal contour; avoid center-front irregularity and hemline deviation.
Sleeve-body balance defect		The distance between the front cuff and the arm is insufficient, and the sleeve-body spatial relationship is uncoordinated, indicating deviations in cuff position, sleeve-line direction, or sleeve–arm alignment.	Moderately increase the cuff–arm distance; improve the sleeve–arm spatial relationship; maintain the overall alignment between the sleeve and the body; and avoid stiffness in the cuff region.
Surface-contour irregularity		Visible folds and local contour fluctuations appear on the bodice, sleeve, or back surface, indicating insufficient surface smoothness.	Reduce local folds; smooth the bodice, sleeve, and back surfaces; stabilize the local contour while maintaining the target silhouette category.

In Table 4.6, black dashed lines denote reference lines of good shape, and red solid lines denote defective contour lines observed in the original AIC sample. The deviation between them provides the visual basis for describing local defects.

The general prompt structure used for iterative refinement and defect correction is presented in Table B.14 of APPENDIX B.

According to the three types of defects identified in Table 4.8, refinement was performed in four steps. Figure 4.14 shows the original defective sample and the iterative-refinement results under different strategies.

Figure 4.14 Original defective sample and iterative refinement results generated based on the defect diagnosis results in Table 4.8: Original; ① center-front regularization; ②+③ sleeve centerline refinement and fold reduction; ②+④ sleeve-line refinement and cuff–arm spatial adjustment; ②+③+④ integrated refinement.

As shown in Figure 4.14, the selected prompt-modification strategy improved the appearance of the coat from left to right: the verticality of the front edge was restored successively (Figure 4.14a), visible folds on the bodice and sleeve surfaces were removed with improvement of the sleeve structure (Figure 4.14b), and the sleeve position in the profile view and the spatial relationship between the sleeve hem and hand were improved (Figure 4.14c). The integrated refinement (Figure 4.14d) showed an overall effect expressed by a clearer forward-inclination tendency of the sleeve line, a more natural transition in the elbow region, fewer local folds, and good sleeve fit in the profile view. Table 4.7 presents the changes in indicators.

Table 4.7 - Verification before and after defect-oriented correction of the selected AIC sample

indicator	Before correction	After correction	After-Before	Target / criterion	Result
Center-front regularity	locally less regular	more regular and more stable	/	straighter and more stable front center line	Improved
Sleeve folds	visible	less visible	/	reduced folds	Improved
Sleeve-surface smoothness	weak	smoother	/	smoother sleeve surface	Improved

Cuff–arm spatial relation	not ideal	still not ideal	/	larger and more natural spacing	Partially improved
$((d_F+d_B)/2)$,cm	5.5	2.3	-2.2	[0…2]	Improved
((∠F+∠B)/2),°	126	94	-32	[88…92]	Improved
c	4	0	-4	0	Corrected
FD, cm	1.9	1.7	-0.2	[0.7...4.1]	Maintained
FC, cm	2.5	2.2	-0.3	[1...4.3]	Improved
|a-b|,cm	0.5	0.2	-0.3	[0...0.7]	Improved
Folds	4	1	-3	[0...1]	Corrected
d12, cm	52.5	51.8	-0.7	[46.9...52]	Corrected
d13, cm	58	57.2	-0.8	[50.9...57.4]	Corrected

Table 4.7 shows that after the iterations, the defects were corrected, which was confirmed visually and quantitatively. The results show that local fit defects in AI-generated raglan coat images can be diagnosed using predefined indicators and interval rules and can be corrected through prompts.

Conclusion of Chapter 4

1. An AI-oriented digitalization system was developed within a unified interface using projection measurements of the “body + coat” system, including Style3D, Rhinoceros 7.0, and Grok 3. This system enabled physical coats, 3D virtual images, and AI-generated images to be compared on a common scale.

2. A unified evaluation scheme was formed. This scheme used MD, confidence intervals, relative error (RE), and MARE to evaluate structural deviations in key regions of the body and coat.

3. The practical applicability of the proposed system was verified by generating and validating AIB and AIC “body-coat” images. Comparisons of AIB and AIC with RB, VB, RC, and VC confirmed the structural adequacy of AI-generated images of bodies and raglan coats.

4. The proposed criteria for evaluating coat fit quality can be used to evaluate AI-generated raglan coat images.

5. The complementary roles of 3D simulation and AI generation were identified. Their complementary characteristics confirmed the feasibility of combining 3D and AI within a unified algorithm for the digital transformation of the design process, in which 3D simulation provides the structural reference and AI generation improves the silhouette solution of images.

CHAPTER 5. VERIFICATION AND ENGINEERING APPLICATION OF THE PROPOSED METHOD FOR DESIGNING RAGLAN COATS

This chapter verifies the practical applicability of the proposed raglan coat design method. The verification covers two core pathways: forward design, in which the garment shape is generated from pattern structure, and reverse reconstruction, in which the pattern structure is reconstructed from target silhouette information, in which the structure of the garment pieces is restored through analysis of an existing volume-silhouette shape.

The unified validation framework includes three main forms of evidence: (1) virtual try-on validation; (2) physical sample production; and (3) quantitative comparative analysis based on the established Cc shape evaluation criteria and 2.5D projection parameters. In addition, the production-preparation efficiency of the proposed method was evaluated through a comparison of development links, time consumption, cost, and fitting rounds. Figure 5.1 shows the overall framework of the forward and reverse raglan coat design algorithms.

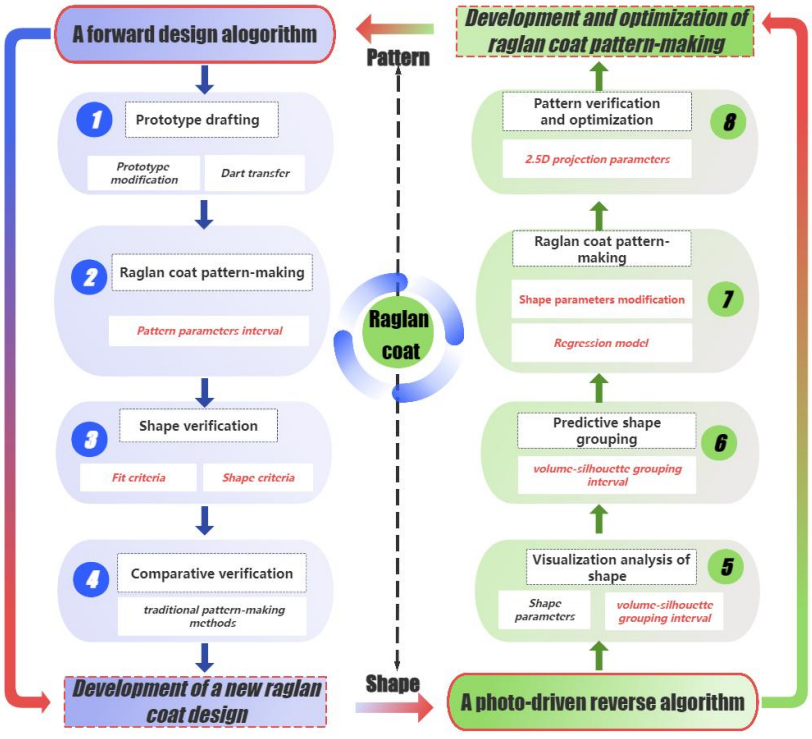

Figure 5.1 - Framework of the forward and reverse design algorithms for the raglan coat

As shown in Figure 5.1, the left side (① – ④) illustrates the forward design pathway, in which the raglan-coat shape is generated from the basic prototype through

pattern development, shape verification, and comparison with the traditional method. The right side (⑤-⑧) illustrates the image-driven reverse design pathway.

5.1. Validation of the forward design algorithm

In this section, the forward design algorithm is verified through the development process from "pattern drawings to form." The verification includes selecting the characteristics of the coat volume-silhouette form, constructing the pattern drawings according to the established rules, producing a physical coat sample, and conducting virtual simulation. The resulting virtual and physical samples were evaluated using the established Cc form criteria.

5.1.1 Database for pattern construction

A men's raglan coat was selected for validation. Figure 5.2 shows the technical sketch of the target coat.

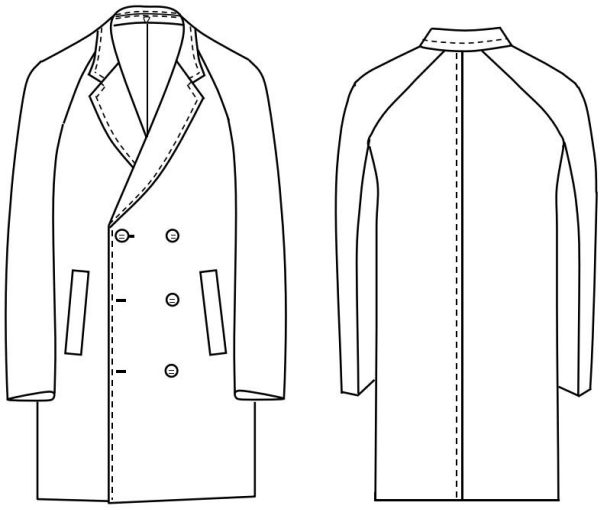

Figure 5.2 -Technical sketch of the target raglan coat

As shown in Figure 5.2, the selected coat is double-breasted and has a classic turn-down collar with lapels. The main specifications of the coat were as follows: coat length 100 cm, chest line width 52 (full girth 126 cm), shoulder width 48 cm, sleeve length 61 cm, cuff width 17 cm, stand collar height 4 cm, and lapel width 7 cm. The chest girth of the standard figure is 100 cm, and the corresponding chest ease was set at 26 cm. According to the previously established classification system for volume-silhouette form, the coat belongs to the Semi-loose category.

The initial database for pattern construction included: (1) the basic prototype; (2) the developed construction method for a three-seam raglan sleeve; (3) the design

characteristics of the coat model; and (4) the key pattern parameters with allowable ranges corresponding to the selected shape.

5.1.2 Forward pattern-making algorithm

The overall workflow consists of two main stages. The first stage is the construction of the model pattern based on the basic prototype, including prototype adjustment and dart transfer. The second stage is the construction of the raglan-sleeve coat patterns.

Prototype drawing. Table 5.1 shows the algorithm of prototype drawing, including the determination of the reference lines and the construction of the front and back bodice outlines.

Table 5.1 - Procedure for constructing the basic prototype, cm

No.	Pattern construction item	Segment	Equations	Drawing	Calculated results, cm
1	Waist line	100-108	$0.5(CG+E_{(CG)})$	Draw a horizontal line from 100 to 108	54
2	Back center line	100-10	/	Draw a vertical line from 100 to 10.	47
3	Front center line	100-18	/	Draw a vertical line from 100 to 18.	39
4	Armhole depth	10-90	*0.1*height+9*	Determine point 90	27.2
5	Chest line	90-98	/	Draw a horizontal line through 90 to intersect the front center line.	54
6	Back width	90-92	0.15*CG + 5.6	Draw a perpendicular from 92 to 98–90.	20.6
7	Front width	96-98	0.15*CG + 4.5	Draw a perpendicular from 96 to 98–90.	19.5
8	Sideline and modification	104-94 104’-94’	/	Point 104 is located at the midpoint of 100–108. Bisector of 100-108 move back	2
9	Back shoulder	02-01-23	/	Draw a line through 01 at	22°

	sloping			an angle to the horizontal line 01–02.	
10	Front shoulder sloping	16-17-35	/	Draw a line through 17 at an angle to the horizontal line 17–16.	18°
11	Back shoulder sloping modification	16-17-35’	/	According to different body-shape characteristics.	25°
12	Chest dart width	94-84	0.025*CG-0.3	Take the value upward along the extension of 104–84.	2.2
13	Scapular dart	62-52	0.025*CG	Draw through 52 and 62, tangent to 92–02.	2.5
14	Front neck width	10-11	*0.08*CG*	Draw a horizontal line leftward through 10.	8.3
15	Front neck depth	00-01	0.33*10-11	Draw a vertical line upward through 11 to 01.	2.8
16	Back neck width	48-47	10-11 - 0.3	Draw a horizontal line leftward through 48.	8
17	Back neck depth	48-18	10-11 + 0.5	Draw a vertical line upward through 48	8.8
18	Back shoulder line	01-23	/	Take 2 cm from 22 to obtain point 23.	15.3
19	Front shoulder line	17-35	01-23 - 0.7	Draw the shoulder line from point 17.	14.6
20	Back armhole curves	23-94	/	Draw a smooth curve from 32 through 52 and 62 to 94′.	25
21	Front armhole curves	35-84’	/	Draw a smooth curve from 32 through 76 to 84′.	24.3
22	front dart distribution at front center line	48-108	/	At the midpoint of the front center line /48-108/	0.7
23	front dart distribution at neckline	/48-17/	/	At the midpoint of the neckline curve /48-17/	0.5
24	front dart	94’-84’	0.025*CG- 1.5	Take the value upward	1

	distribution at armhole			from 94′	
25	Back dart distribution at shoulder line	10-90’	/	At the midpoint of /10-90’/, take in	0.5
26	Back dart distribution at back center	01-23	/	At the midpoint of / 01-23 /	1
27	Back dart distribution at armhole	62-52’	0.025CG-1.5	Point 51 is the midpoint of 50–52; draw dart lines 51–52 and 51–62.	1

Figure 5.3 shows the drawing schemes at different stages of construction.

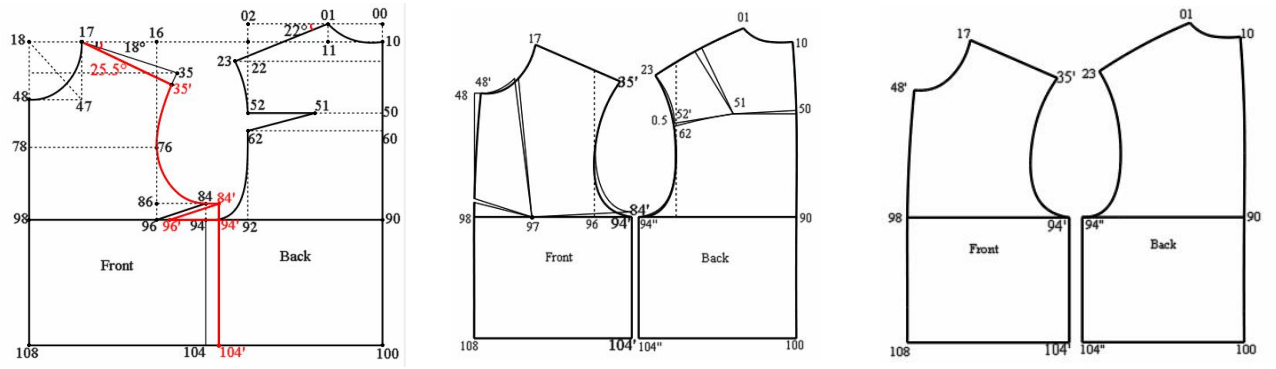

a *b* *c*

Figure 5.3 - Schemes for construction and adjustment of the basic prototype: a - construction of the basic prototype and adjustment of shoulder inclination and side-seam position; b - transfer of bust and waist darts according to virtual-fitting results; c - finally adjusted basic prototype for subsequent construction of the raglan-sleeve coat patterns.

As shown in Figure 5.3, the construction process includes the construction of the basic prototype and adjustment of the shoulder-line inclination and side-seam position (Figure 5.3a), transfer of the bust and waist darts to different positions (Figure 5.3b), and verification of the finally adjusted prototype, which serves as the basis for subsequent construction of the raglan-sleeve coat patterns (Figure 5.3c).

Construction of the raglan-sleeve coat pattern. Table 5.2 shows the algorithm for constructing the raglan-sleeve coat patterns.

Table 5.2- Algorithm for constructing raglan-sleeve coat patterns

No.	Pattern construction item	Segment	Equations	Drawing	Calculated result, cm
1	Back neckline point	10’	10-10’	10 downward value	0.5
2	Front neckline point	48’’	48-48’’	48 downward value	2
3	Back SNP	17’	17-17’	17 along shoulder line	1
4	Front SNP	01’	01-01’	01 along shoulder line	1
5	Front chest ease	96’-96’’	0.33* ($0.5E_{(CG)}$-8))	Widen the front chest width 36’-96.’	3
6	Back ease	92’-92’’	0.67* ($0.5E_{(CG)}$-8)	Widen the back width:	6
7	Chest line	92’-94’’, 96’-94’	/	Rotate 23’-94’’, 5’-94’’around 16,36	/
8	armhole depth	94’ - 940’, 94’’ - 40’’	0.17* ($E_{(CG)}$-8)	Increase prototype armhole depth	3
9	Back raglan width	17-27	/	Draw along the front neckline from 17.	2
10	Front raglan width	01-12	/	Draw along the back neckline from 01.	4
11	Front and back raglan lines	12 - 940’’, 27 - 940’	/	Draw arc 27-940’,12-940.’’	/
12	Sleeve width line	S30 - S38	/	Draw 96’-940, 92’-940 on the same horizontal line, draw the curves 35’-940, 940-23	43.5
13	Sleeve center line	00 - S54	/	Draw midpoint 00 of 35’-23, draw a vertical line downward.	27.2
14	Sleeve cap height	940 - S10	0.83* 00-940	Sleeve cap height	21.7
15	Front sleeve angle line (straight)	S10 - S30	35’ - 940’-1	Front armhole	29.5
16	Back sleeve angle line (straight)	S10 - S38	23-940’’-0. 5	Back armhole	32
17	Front and back connecting	S22， S26	0.17* 00-940	Draw a horizontal line through S20 to intersect	

	points			the front and back armhole lines.	
18	Front/ back sleeve center line	S12-S52 , S16 - S56	/	Draw the midpoint S52, S56 of S50 - S54, S54 - S58	/
19	Front sleeve cap arc	S10 - S30	/	Take S12 - S52 as the symmetry axis and make arc S30 - S35'' and 35' - 940	/
20	Back sleeve cap arc	S38 - S10	/	Take S16 - S56 as the symmetry axis and make arc 23 - 940 and 23'' - S38.	/
21	Front sleeve armhole	940-35'	15：1.2	Sleeve center line offset along S34-S43 tilt ratio ， 940-35'is symmetric to 35''-S30	15cm, 1.2cm
22	Front and back sleeve center line division	S10' - 54', S10''- 54''	/	Separate sleeve center line S10- S54	/
23	Front/back sleeve raglan line	S27- S22 - S30, S12 - 26 - S38	/	Draw the arc through the connection points S22 and S26	/
24	Front and back shoulder slope sum	∠1+∠2	40°...54°	Draw horizontal lines through 01 and 02; the angle between the shoulder slope and the horizontal line	47
25	Front and back shoulder-sleeve angle sum	∠3+∠4	60°... 72°	The angle between the shoulder line and the sleeve center line	*62*
26	Difference between the front sleeve and back sleeve width	S34 - S34'' - S34 - S34'	2.5... 7.5	The difference between the front and back sleeve-width line	*6.5*
27	Sleeve center line offset at cuff	S54''- 40'' S54'- 540'	0...3.5	The offset of the sleeve center line at the cuff	*3.2*
28	Sleeve center line offset	S34- 54'		S34 - S54 offset forward by S54 - S54'	3
29	Front sleeve center line	S230- 520		S230 - S52 offset forward	2

30	Back sleeve center line	S270- 58''		S270 - S560 offset forward	2
31	Cuff width	S520- 560	0.5*Cuff width	Cuff width line	16
32	Front/back sleeve side seam	S23 - S50',S27- S58'	S50'- S520	Parallel to S230 - S520,S270 - S58''	3.5
33	Under sleeve sleeve side seam	S23'- 50'', S27'- 58''	S58'-S560	Parallel to S230 - S520, S270 - S58''	2.5
34	Under sleeve armhole arc	S23'- S34- S27	/	Draw under sleeve	/

Figure 5.4 shows the drawing schemes at different construction stages.

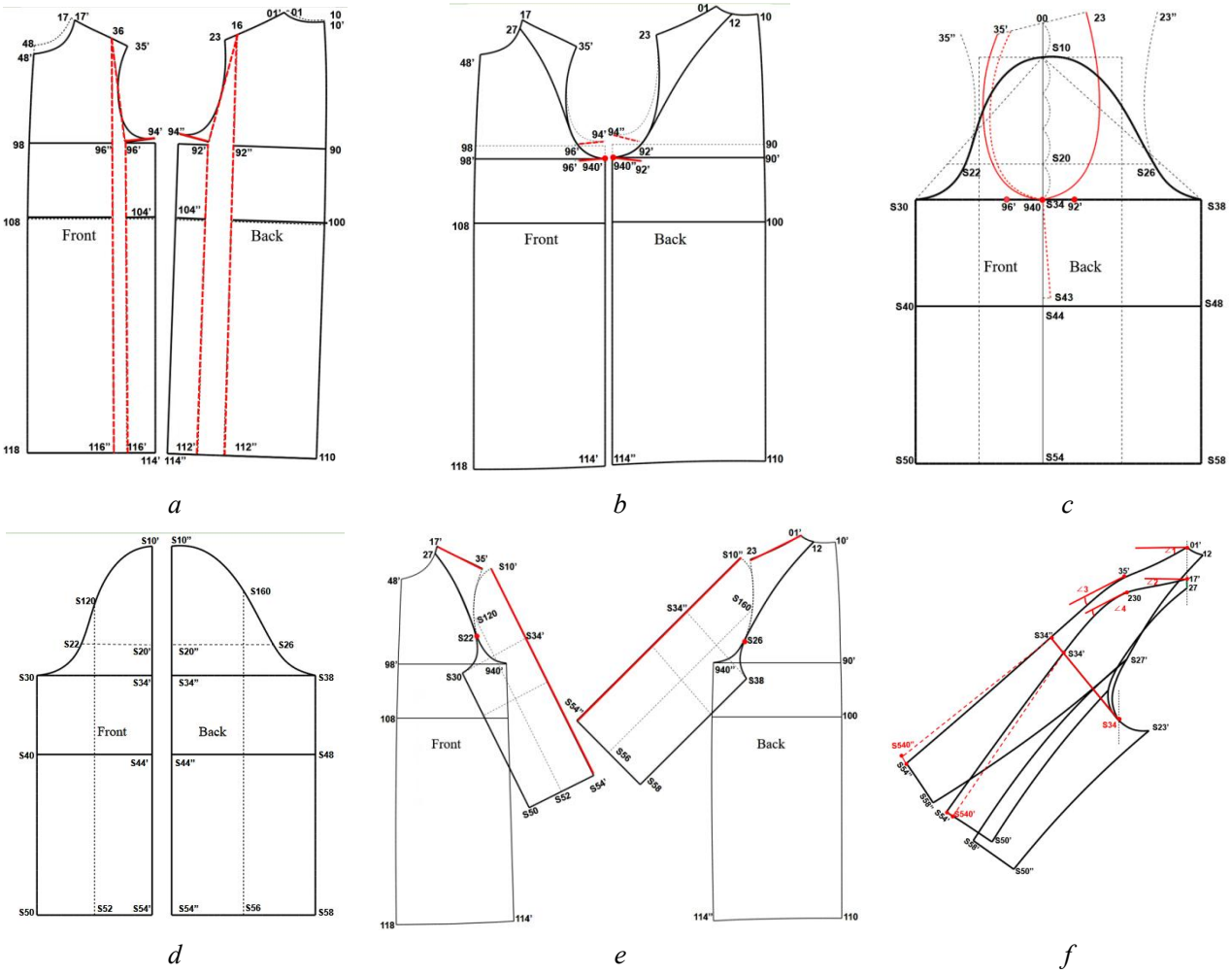

a *b* *c*

d *e* *f*

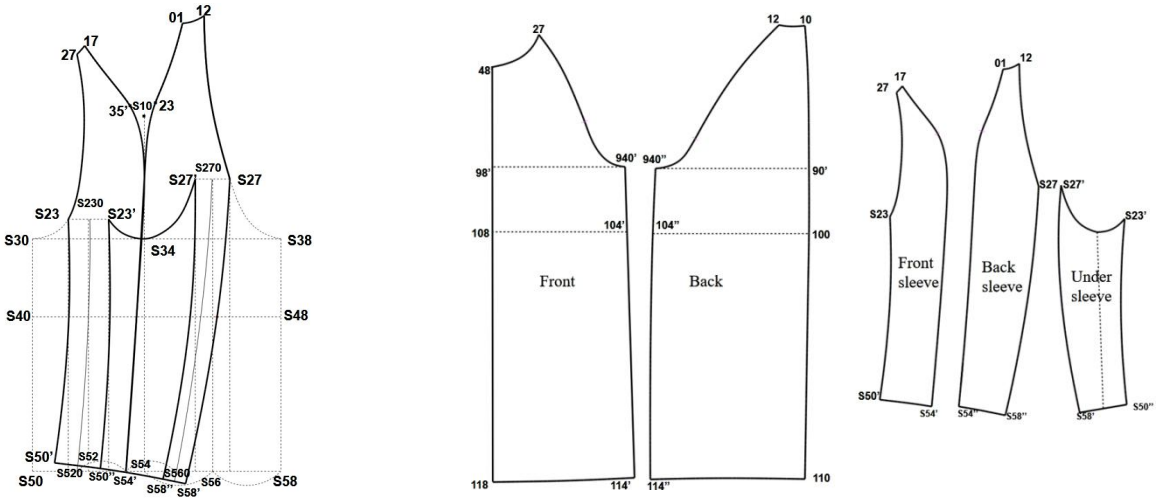

g *h*

Figure 5.4 - Key steps of the forward pattern-making algorithm for the raglan coat: a-basic prototype drafting; b-g, raglan sleeve and bodice pattern drafting; h - final bodice and sleeve patterns.

To evaluate the engineering advantages of the proposed pattern-construction method, it was compared with a traditional method widely used in contemporary Chinese textbooks [140]. The detailed construction procedure for the traditional method is presented in Table C.1 of Appendix C.

5.1.3. Physical sample validation

To evaluate the engineering feasibility, the pattern drawings obtained using the proposed method were transferred to two garment enterprises: Polargoose Clothing Co., Ltd. (China) and OAO “Sudar” (Kovrov, Vladimir Region, Russia). The corresponding industrial validation documents are provided in Appendix C.

To control the influence of material when validating the physical samples, all garments in this section were produced from the same fabric. A Melton wool fabric was used (60% wool, 20% viscose, and 20% polyester). Figure 5.5 shows the raglan-sleeve coat form obtained during physical fitting based on the proposed design algorithm.

Figure 5.5 - Physical raglan-sleeve coat obtained using the proposed pattern-construction algorithm

As shown in Figure 5.5, the physical sample generated using the proposed forward pattern-making algorithm presents an acceptable sleeve–arm spatial relationship in the front, side, and back views. In the front view, the raglan sleeves maintain a clear and relatively balanced spatial distance from the arms on both sides. The underarm region presents a relatively smooth appearance, and the sleeves form sufficient local space around the arms, indicating that the sleeve width and armhole structure support the spatial extension around the arms. In the side view, the sleeve follows the natural forward tilt of the arm, while a certain space is maintained between the sleeve and the front side of the arm. The arm is positioned relatively stably within the sleeve space. This indicates that the sleeve-centerline direction and the cuff-level spatial relationship present the expected sleeve–arm configuration features. In the back view, the shoulder–sleeve transition and back sleeve panels appear relatively smooth, and the back sleeve panel, underarm region, and lower sleeve line present a continuous external shape.

Thus, this physical sample confirms a satisfactory fit quality.

5.1.4. Validation of the two construction methods

Figure 5.6 shows the virtual try-on results generated using the traditional method (drafting steps in Table C.6 in Appendix C) and the proposed method.

a *b* *c*

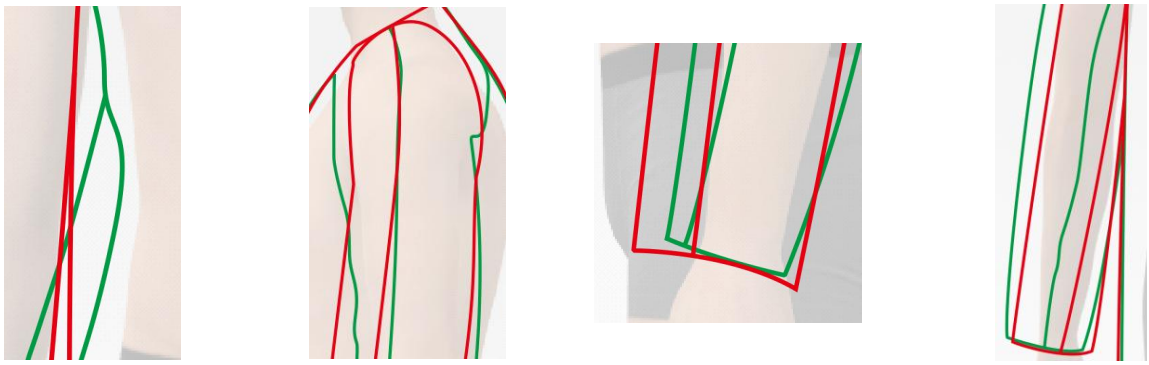

d *e* *f* *g*

Figure 5.6 Shape comparison of virtual try-on results between the traditional and the proposed pattern-making methods: a...c- front, back, and side views; d...g- contour comparison at key locations. Green lines indicate the traditional method; red lines indicate the proposed method.

As shown in Figure 5.6, the coat constructed by the traditional method exhibits deformations in the underarm area, along the back centerline, and along the front and back sleeve seams. The sleeve fold is especially evident in the side view, where the spatial gap between the front sleeve fold and the arm at the sleeve bottom is minimal.

Table 5.4 shows the comparative analysis of the real and virtual coat forms obtained using the traditional and proposed pattern-construction methods.

Table 5.4 - Comparative analysis of real and virtual forms obtained by the traditional and proposed pattern-construction methods

Fit Criteria	Interval	Comparison of traditional, new, and real results				
		Virtual		Real	Δ (New −Traditional)	Δ (Real–New)
		Traditional	New			
$(d_F + d_B)/2$	0...2 cm	0.7	1.5	2	0.8	0.5
$(\angle F + \angle B)/2$	88...92°	94.2	92.5	91.9	1.7	0.6

c	0	0	0	0	0	0
FD	0.7...4.1cm	4.4	3.1	3.8	1.1	0.7
FC	1...4.3cm	0.4	3.6	3.8	3.2	0.2
$\lvert a\text{-}b \rvert$	0...0.7cm	1.4	0	0	1.4	0
Folds	0...1	4	0	0	4	0

As shown in Table 5.4, the physical fitting result obtained using the proposed method satisfied all seven criteria. The deviations between the physical and virtual results did not exceed 0.7 cm for the linear parameters and 0.6° for the angular parameter, indicating good consistency between the virtual and physical forms under the conditions of this experiment. In comparison, the traditional method satisfied only two criteria.

5.2. Validation of the reverse algorithm of pattern-making

In this study, the reverse pattern-construction algorithm was validated through two interrelated tasks: reconstructing pattern drawings from form and adjusting pattern drawings to transform an unsatisfactory coat form into a high-quality one.

5.2.1. Object for the reverse algorithm

To validate the proposed reverse pattern-making algorithm under the condition that only a raglan coat photograph is available, a men's raglan-sleeve coat with clearly traceable industrial origin was selected as the validation object. The coat was produced and released to the market in 2025 by Ningbo Marriott Garment Co., Ltd. (China). The figure dimensions corresponded to the standard figure defined in the previous sections. Figure 5.7 shows the analysis scheme for the selected raglan coat.

Figure 5.7 - Photo-based analysis of the target raglan coat: blue dotted lines indicate localized shape defects; red solid lines indicate the measured shape parameters.

As shown in Figure 5.7, an initial visual diagnosis of the coat was first performed to locate and mark the defective areas. The shape was then measured according to the established Cc form-evaluation criteria. These parameters constitute the input basis for reverse reconstruction of the pattern drawings and provide quantitative support for subsequent form diagnosis and parametric correction. The reference form in Figure 5.7 shows a pronounced bodice imbalance at the lower front edges, inconsistency between the sleeve centerline and the front sleeve fold, and sleeve folds.

5.2.2. Algorithm for reverse generation of pattern-making

The reverse design algorithm is based on three foundations established in the previous sections: (1) the grouping intervals for coat volume–silhouette shapes; (2) the corresponding E(CG) and its distribution for the given group; and (3) the pattern–shape regression models, which map shape parameters Y to the key pattern parameters X.

From the implementation perspective, the reverse algorithm consists of two computational routes. Route A reconstructs the shape using parameters measured from the photograph and directly substitutes them into the regression equations to calculate the corresponding pattern parameters. Route B generates a corrected shape through targeted adjustment: form parameters indicating an unsatisfactory shape state are first corrected to representative target values within the allowable intervals for good shape and are then used in the regression equations. Table 5.5 shows the reverse design workflow for “photograph -> pattern drawings” reconstruction and correction-based generation. Table 5.5 shows the reverse engineering workflow for photo-to-pattern reconstruction and target-corrected generation.

Table 5.5 - Reverse design algorithm for pattern reconstruction

Route	Procedure	Input / Target value	Equation / Rule	Output
A	Determine volume–silhouette category	d12c, d13c	Volume–silhouette grouping interval	Silhouette category
A	Determine $E_{(CG)}$ and ease distribution	Identified volume–silhouette category	Representative value + optimal distribution ratio	E(CG) and front–back ease allocation
A	Extract shape parameters and diagnose shape	FDc, FCc, a_c, b_c, Folds	Shape criteria *Cc*	Photo-derived Y values and diagnostic decision

A/B	Set target fold level and derive shoulder–sleeve angle	Measured Y4 or target Y4 selected ∈ 0...1	Y4 = -5.02 + 0.0838 X_7	X_7
A/B	Set target sleeve-centerline consistency and derive shoulder slope	Measured Y3 or target Y3 selected ∈ 0...0.7 cm	Y3 = -0.35 + 0.140 X_{10}	X_{10}
A/B	Derive sleeve-centerline offset	Measured Y2 or target Y2∈ 1.0...4.3 cm;	Y2 = -1.48 + 1.658 X_{11}	X_{11}
A/B	Derive the sleeve-width difference	Measured Y1 or target Y1∈ 0.7...4.1 cm;	Y1 = -8.98 + 0.242 X_4	X_4
Output	Generate reverse patterns	$E_{(CG)}$, X_4, X_7, X_{10}, X_{11}	Optimized prototype as a structural template	Route A and Route B reverse-generated raglan coat patterns
Note: Route A uses the measured Y values extracted from the photograph to reconstruct the photographed shape. Route B uses target Y values selected from the acceptable good-shape intervals to generate the corrected shape. Y1 - FDC, Y2 - FCC, Y3 - |ac − bc|, Y4 - FoldsC; X10 - Δ(BSW − FSW), X11 - Offset(SCL), X4 - Δ(∠BSS + ∠FSS), X7 - Δ(∠BA + ∠FA).				

In Route A, the Y values measured from the photograph are used to calculate the structural parameters of the coat patterns. In Route B, the Y values identified as defective are first corrected to target values within the good-form intervals and are then used to calculate the pattern parameters intended for the generation of the corrected form.

In this case, d12c and d13c were measured from Figure 5.7 as 52.5 cm and 58.0 cm, respectively. According to the established volume – silhouette grouping intervals, the photographed raglan coat was classified as Semi-loose. Therefore, the applicable chest-ease interval was determined as E(CG) ∈ 19...25 cm. A representative value of E(CG) = 24 cm was then selected for reverse pattern generation. Based on the front – back ease-allocation rule established in the previous sections, the corresponding front and back pattern-width allowances were calculated as 3.5 cm and 4.5 cm, respectively. After the volume – silhouette category, total chest ease, and front – back ease allocation had been determined, the remaining shape parameters Y_1 – Y_4 were further used to derive the key pattern parameters X through the regression equations. The Y and X

values for the two routes are presented in Table 5.6.

Table 5.6 - Shape-parameter inputs and reverse-calculated pattern parameters under two calculation routes

Shape parameter	Photo-measured Y	Route A		Route B	
		Y is used for reconstruction	calculated X	Y is used for corrected generation	calculated X
Y_1 - FD_C	4.0	4.0	$X_4 = 53.7$	4.0	$X_4 = 53.7$
Y_2 - FC_C	3.0	3.0	$X_{11} = 2.7$	3.0	$X_{11} = 2.7$
Y_3- $\lvert a_c - b_c \rvert$	1.0	**1.0**	$X_{10} = 9.6$	**0.4**	$X_{10} = 5.4$
Y_4 - $Folds_C$	2	**2**	$X_7 = 83.8°$	**0.5**	$X_7 = 65.9°$

As shown in Table 5.6, Route A uses the photo-measured values of Y1, Y2, Y3, and Y4 to calculate the corresponding pattern parameters. This route therefore preserves the shape characteristics observed in the photograph. Route B retains the measured values of Y1 and Y2 because they are within the acceptable intervals, while Y_3 and Y_4 are replaced by target values to correct sleeve-centerline inconsistency and fold formation. As a result, Route B produces a different set of key pattern parameters, especially X4 and X7. Figure 5.8 shows the reverse-generated patterns and the corresponding key-parameter inspection under the two calculation routes.

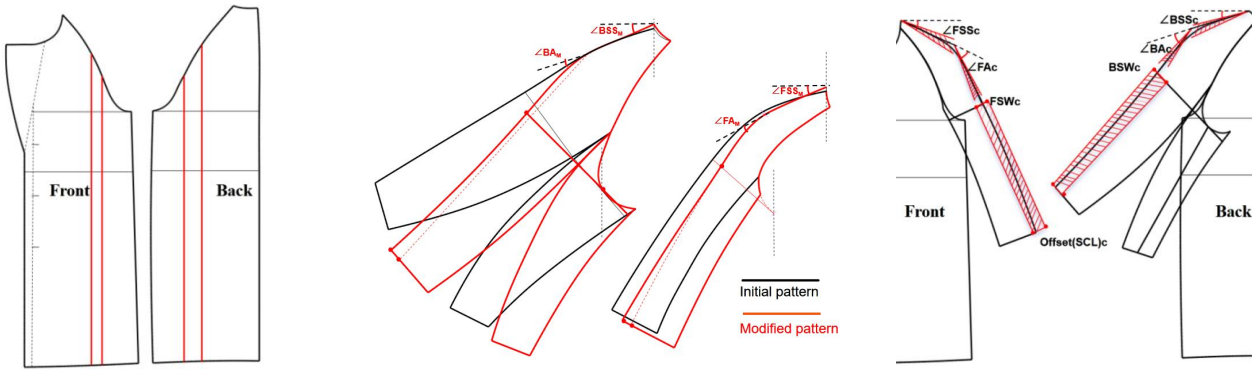

a *b* c

Figure 5.8 - Reverse-generated patterns and key-parameter inspection under two calculation routes: a - generated bodice pattern; b - sleeve pattern comparison between Route A and Route B; c - key pattern parameters of the Route B pattern located within the target interval ranges.

As shown in Figure 5.8a, the bodice pattern was generated according to the E(CG) value and the front–back pattern-width allowance derived from the Semi-loose volume–silhouette category. Figure 5.8b compares the sleeve patterns generated under Route A and Route B. Compared with Route A, the Route B sleeve pattern shows an adjusted shoulder–sleeve angle and sleeve-centerline configuration, reflecting the target correction of Y_3 and Y_4.

Figure 5.8c further shows the key control pattern variables for Route, including the shoulder-slope-related angle, shoulder – sleeve angle, sleeve-width difference, and sleeve-centerline offset. The Route B pattern satisfies the target interval requirements for the key pattern parameters, including X_4, X_7, X_{10}, and X_{11}.

Therefore, the two reverse-generated patterns provide different validation objects for the following section. Route A is used to examine whether the proposed reverse workflow can reconstruct the photographed shape, while Route B is used to evaluate whether target-corrected shape parameters can improve the poor-shape features and generate a corrected raglan coat shape under virtual and physical validation conditions.

5.2.3 Virtual and physical validation

To evaluate the effectiveness of the reverse algorithm, the two raglan coat patterns obtained in Section 5.2.2 were validated under virtual and physical conditions. The validation was carried out from three aspects: (1) visual comparison of virtual and physical silhouettes to evaluate folds and local deformation; (2) verification of the key shape parameters to determine whether they belong to the good-form intervals; and (3) verification that the corrected form generated by Route B retained its membership in the Semi-loose category.

In the virtual validation, the patterns were imported into Style3D V9.0 for 3D simulation. A digital fabric with the same material properties as the real fabric used for the physical sample was applied in the simulation to maintain consistency between the virtual and physical validation conditions. Meanwhile, a physical sample was produced based on the Route B pattern. Figure 5.9 shows the virtual and physical fitting results of the raglan coats generated from the reconstructed patterns.

a

b

Figure 5.9 - Virtual validation of the two reverse-generated routes and physical validation of the target-corrected pattern: a - virtual try-on results; b - physical fitting results; front, side, and back views. Note: In the virtual validation, the Route A reconstructed shape is shown on the left and the Route B corrected shape is shown on the right. In the physical validation, the original sample shown in Figure 5.7 is shown on the left, and the Route B corrected sample is shown on the right.

As shown in Figure 5.9, the comparison between Route A and Route B indicates that the corrected pattern improved several local shape defects, particularly folds in the underarm areas of the front and back sleeve parts. The forward inclination of the sleeve became more distinct, the sleeve surface lines became smoother, and the spatial relationship between the sleeve and the arm became more stable. These results indicate that target correction of the defective Y parameters improved the sleeve-centerline consistency and fold-control performance of the generated raglan coat. In the Route A result, sleeve folds and local deformation were retained to a certain extent. Table 5.7 shows the corresponding measured values of shape parameters.

Table 5.7 - Quantitative comparison of sleeve shape parameters for Route A and Route B

Fit Criteria	Interval	Comparison of Initial and Modified Shapes		
		Initial	Modified	Δ (Initial-Modified)
$(d_F + d_B)/2$	0...2cm	4.9	2.0	2.9
$(\angle F + \angle B)/2$	88...92°	109.5	91.3	18.2
c	0	2	0	2
FD	0.7...4.1cm	3.4	1.7	1.7
FC	1...4.3 cm	4.0	2.2	1.8
$\lvert a-b \rvert$	0...0.7 cm	1.5	0	1.5
Folds	0	4	0	4

As shown in Table 5.7, the Route A reconstructed shape retained several shape defects observed in the photo-based reference shape, including obvious bodice imbalance, sleeve-centerline inconsistency, and visible sleeve folds. In contrast, all key shape parameters of the Route B corrected shape were located within the good-shape intervals. The value of $(d_F + d_B)/2$ decreased from 4.9 cm to 2.0 cm, and $(\angle F + \angle B)/2$ decreased from 109.5° to 91.3°, indicating improved bodice balance. The value of $|a - b|$ decreased from 1.5 cm to 0 cm, and the number of folds decreased from 4 to 0, indicating improved sleeve-centerline consistency and fold control. These results confirm that the target-corrected Y parameters can be effectively converted into pattern parameters capable of improving the final raglan coat shape.

To further evaluate the reproduction accuracy of the overall volume–silhouette, the 2.5D projection parameters of the Route B corrected garment were compared with those of the photo-based reference shape. The d12 and d13 parameters were measured for both shapes, with differences of 0.4 cm and 0.7 cm, respectively. These small differences indicate that the Route B corrected shape maintained the same Semi-loose volume–silhouette category as the photo-based reference shape while improving local defects.

A detailed comparison of the front and side 2.5D parameters between the photo-based reference shape and the Route B corrected coat is provided in Table C.5 in Appendix C. Based on the MD analysis, the Route B corrected shape showed high accuracy in reproducing the overall volume–silhouette, especially in the front-width and side-width dimensions, with average deviations of 0.2 ± 0.8 cm and -0.7 ± 1.1 cm, respectively. The deviations in the sleeve-related region were relatively larger, mainly because the shoulder slope and shoulder–sleeve relationship were intentionally adjusted during Route B correction to resolve the sleeve imbalance and fold problems observed in

the photo-based reference shape. Therefore, these local deviations reflect necessary structural adjustments for shape improvement rather than uncontrolled silhouette distortion.

Overall, the photo-driven reverse design algorithm can achieve pattern reconstruction. The validation results indicate that the reverse-generated corrected patterns eliminated form defects while preserving the shape category.

5.3 Evaluation of Engineering efficiency at the production preparation stage

The evaluation of production-preparation efficiency focused on the representative task of forward construction, because this task includes the complete workflow: model analysis, prototype preparation, development of raglan-coat pattern drawings, verification, correction, and approval of the first sample. Constant coat-assembly operations were not included in the main efficiency indicator because they do not directly depend on the logic of pattern generation.

The comparison was conducted using the same initial data. The traditional route was represented by the textbook-based process for constructing a raglan coat pattern and subsequent post-fitting correction, whereas the proposed route used the validated parameter intervals, chest-ease distribution rules, virtual try-on verification, and targeted correction procedure established in the previous chapters. The indicators were calculated according to the definitions of development links, stage-based time costs, and estimated cost composition listed in Tables C.3 - C.5 in Appendix C.

Table 5.8. Comparative evaluation of engineering efficiency between the traditional and proposed methods

Indicator	Traditional method	Proposed method	Reduction, %	Note
Key development links	12	7	41.7	manually adjusted links
Pattern-development time, h	19	9	52.6	style analysis + drafting + checking
Fitting-correction time, h	24	12	50.0	physical fitting-based modification
Total development time, h	43	21	51.2	excluding fixed garment assembly
Pattern-development fee, RMB	400	200	50.0	estimated
First-sample development cost, RMB	800	500	37.5	estimated, same material assumption
Number of fitting rounds	2	1	50.0	from two rounds to one round

As shown in Table 5.8, the proposed method reduced both the number of key manually adjusted development links and the development resources required for first-sample confirmation. These results indicate that the engineering advantage of the proposed method is reflected in both shape-control performance and a more efficient development workflow.

Specifically, the proposed method reduced all major production-preparation indicators, including key development links, pattern-development time, fitting-correction time, total development time, fitting rounds, and estimated costs. The most evident improvements were observed in pattern-development time and total development time, both of which were reduced by more than half. The number of fitting rounds also decreased from two to one. These results indicate that the efficiency improvement was mainly achieved by replacing repeated empirical adjustments with parameter-guided drafting, virtual checking, and targeted correction.

The estimated cost comparison showed the same tendency. Under the same style and material assumptions, the proposed method reduced both the pattern-development fee and the cost of first-sample development, mainly because fewer manual correction steps and fewer fitting rounds were required. Therefore, the proposed method improves shape controllability, reproducibility, engineering efficiency, and cost-effectiveness at the production-preparation stage for raglan-sleeve coats.

Detailed definitions of the key development links, the stage-based time estimation, and the estimated cost composition are provided in Tables C.2 – C.4 in Appendix C.

In addition to the quantitative efficiency indicators, engineering readiness for production implementation was also examined through industrial validation. The corrected CAD pattern files and the corresponding technical package were submitted for checking by two garment companies, Polargoose Clothing Co., Ltd. (China) and OAO “Sudar” (Kovrov, Vladimir Region, Russia). The validation included checking the drawings, matching the seam connections between the bodice and sleeve, assessing cutting and sewing feasibility, and verifying the clarity of the information for production preparation. The industrial validation records are presented in Figures D.1-D.2 of Appendix D. These validation results provided additional evidence of the engineering feasibility of the proposed method for designing raglan-sleeve coats.

Overall, the efficiency comparison shows that the proposed method has practical value for production preparation because it converts several experience-dependent operations into parameter-guided and verifiable procedures. In the tested forward development task, the reduction in development stages, time costs, corrective fittings, and estimated cost demonstrates that the method can shorten first-sample confirmation while ensuring the required quality.

Conclusions of Chapter 5

1. A production-oriented verification framework for raglan coat pattern design was established. Under controlled and reproducible conditions, virtual try-on, physical sample production, Cc shape criteria, and projection parameters assessment were integrated.

2. The forward design algorithm was validated for the development of a new raglan coat pattern. The proposed method ensured stable silhouette control and demonstrated consistency between virtual simulation and physical fitting results, showing better performance in key shape parameters than the traditional pattern-making method.

3. The photo-driven reverse algorithm was validated for pattern reconstruction and target-corrected shape generation. Given only a raglan coat photo, the algorithm preserved the volume–silhouette grouping, regression-based back-calculation of pattern parameters based on regression models, and performed targeted correction according to the specified criteria for good fit.

4. Engineering feasibility was confirmed through industrial validation. The generated pattern files were submitted to two independent garment companies in China and Russia, and the resulting sampling and feedback confirmed the correctness of the pattern calculations and manufacturability.

5. The proposed bidirectional design method for raglan coats improved shape controllability, reproducibility, and efficiency at the production preparation stage. Compared with the traditional method, the proposed method reduced the number of manual corrections by 41.67%, the total development time by 51.16%, and the estimated first-sample development cost by 37.5%.

CONCLUSION

RESULTS OF THE COMPLETED RESEARCH

1. A digital design technology for men ' s raglan coats was improved by integrating parametric pattern construction, 3D virtual fitting, and the generation of 2D and 3D images within a unified system of projection parameters. The system includes knowledge bases related to human body shapes, pattern drawings of garment parts, the volumetric-silhouette shapes of coats, and rule bases related to fit criteria.

2. A direct algorithm for designing raglan coat patterns was developed and practically validated. The algorithm is based on regression equations that link the established intervals of pattern parameters and volumetric-silhouette shapes of coats with predefined fit indicators. Its application reduces the number of fitting trials and decreases the estimated development cost by 38%.

3. A reverse design algorithm from coat image to pattern drawings was developed and verified. The algorithm is based on the identification of the volumetric-silhouette shapes of the coat, the reverse calculation of pattern parameters, and their targeted correction, followed by the generation of corrected pattern drawings that prevent the occurrence of fit defects.

4. A set of quantitative criteria was developed for the first time and verified for the objective evaluation of bodice fit, raglan coat fit, and the grouping of volumetric-silhouette forms. The proposed criteria made it possible to achieve a 95% proportion of high-quality coats across a wide range of sizes.

5. A correlation analysis of raglan coat patterns was conducted, which made it possible to identify the key parameters controlling the indicators of volumetric-silhouette form.

6. A multimodal strategy for using neural networks to generate high-precision images of human figures and coats was developed and experimentally validated. The mean absolute percentage error (MAPE) for AI-generated coat images was 2.8%, which is significantly lower than the 7.6% obtained from pattern-based 3D simulation. The differences between real human body images and neural-network-generated body images did not exceed ± 1.0 cm and $\pm 2.5°$. The proposed strategy functions as a universal measurement interface, ensuring quantitative comparability among real objects, 3D models, and images generated by neural networks.

7. A complementary "3D simulation + neural network" algorithm was proposed for the digital design of raglan-sleeve coats. The 3D simulation provides structural traceability and maintains a direct link with pattern drawings, whereas neural networks provide higher accuracy in reproducing projection parameters and a closer correspondence between the generated silhouette and real garment samples.

8. The engineering effectiveness and industrial feasibility of the developed technology were confirmed. Positive industrial testing reports from Polargoose Clothing Co., Ltd. (China) and OJSC "Sudar" (Russia) confirmed the manufacturability of the proposed method and demonstrated a 51.2% reduction in the overall development time.

RECOMMENDATIONS AND PROSPECTS FOR FURTHER RESEARCH

1. The results of this research are recommended for implementation in light industry enterprises to improve the development process of outerwear models. They are also recommended for integration into the educational process for bachelor's and master's degree programs in the field of light industry product design.

2. A promising direction for further research is the extension of the developed technology to other types of upper-body garments, such as jackets and blazers, as well as to other sleeve constructions. Another promising direction is integration with CAD systems to create modules for automated pattern generation and pattern diagnostics.

3. The methodology of image generation using neural networks may be further developed for the creation of dynamic 4D digital twins that account for material behavior and changes in coat shape during movement. It may also be extended to reverse-engineering methods for the automatic generation of pattern drawings based on garment images.

SYMBOLS AND ABBREVIATIONS

a	—	Distance from the sleeve contour to the reference line at the upper-arm level
a_F	—	Verticality indicator of the front profile contour
AHW	—	Armhole width
AIB	—	AI-generated body
AIB_A	—	AIB generated by Method A: text + 2.5D projection values
AIB_B	—	AIB generated by Method B: text + 2.5D projection values + 3D reference images
AIB_C	—	Body reconstructed after removing the coat from the “body + coat” image.
AIC	—	AI-generated coat
$AIC_{S1...S4}$	—	AIC in volume-silhouette categories S1–S4
AL	—	Armhole level; cross-section along the armhole line
Assp	—	Angle between the shoulder line and the sleeve center line at the shoulder point
av	—	Average value
b	—	Distance from the sleeve contour to the reference line at the elbow level
BAP	—	Back underarm angle
b_B	—	Verticality indicator of the back profile contour
BC	—	Back clearance: distance from the back side of the arm to the back sleeve contour at the sleeve hem in the profile view
BNP	—	Back neck point
BSNP	—	Back shoulder-neck point
BSP	—	Back shoulder point
BSS	—	Back shoulder-slope line
X_8—BSW		Width of the back part of the sleeve
BW	—	Back width
BWG	—	Back waist width
c	—	Number of folds on the bodice; fold-presence indicator
d_{11}	—	Horizontal shoulder width measured through the outermost sleeve points
d_{11p}	—	Angle between the shoulder line and the sleeve center line
d_{12}	—	Composite descriptor of silhouette width in the chest and armhole region
d_{12p}	—	Horizontal distance from the shoulder point to the front center line
d_{13}	—	Composite descriptor of silhouette width in the waist and elbow

		region
d_{13p}	—	Sleeve width at the armhole level at the intersection of the shoulder-width reference line and SCL
d_B	—	Deviation of the back hemline from the horizontal line
D'_C, D'_W, D'_H, D'_A, D'_E, D'_{Wr}	—	Profile projection depth parameters of the outer coat contour
D_C, D_W, D_H, D_A, D_E, D_{Wr}	—	Profile projection depth parameters of the body
d_F	—	Deviation of the front hemline from the horizontal line
E(CG)	—	Chest-girth ease
EC	—	Air gap between the sleeve and the arm at the elbow point
EL	—	Elbow level; cross-section along the elbow line
FAP	—	Front underarm angle
Y_2 -FC	—	Front clearance: distance from the front side of the arm to the front sleeve contour at the sleeve hem in the profile view
Y_1 - FD	—	Distance from the back of the hand to the side contour of the sleeve in the front view
FNP	—	Front neck point
Fold 1–Fold 4	—	Number of folds in four sleeve regions
Y_4 - Folds		Total number of folds on the sleeve
FSNP	—	Front shoulder-neck point
FSP	—	Front shoulder point
FSS	—	Front shoulder-slope line
X_9 - FSW		Width of the front part of the sleeve
FW	—	Front width
FWG	—	Front waist width
G	—	Chest girth
G / NG	—	Fit evaluation: good/unsatisfactory
H, H_S, H_C, H_U, H_W, H_H, H_F, H_B	—	Projection height parameters of the body
X_{12} - i	—	Difference between the front and back parts of the sleeve along the upper-arm girth line
X_{13} - j	—	Difference between the front and back parts of the sleeve at the sleeve-hem level
L(A)	—	Area related to the armhole
L(B)	—	Back bodice area
L(F)	—	Front bodice area
MARE	—	Mean absolute relative error
MD	—	Mean deviation

MD_A	—	Mean deviation of angular parameters
MD_D	—	Mean deviation of profile depths
MD_H	—	Mean deviation of height parameters
MD_W	—	Mean deviation of frontal widths
X_{11} - Offset(SCL)	—	Forward displacement of the sleeve center line
RB	—	Real body; vector of its projection parameters
RC	—	Real coat; vector of its projection parameters
$RC_{S1...S4}$	—	Real coats in volume-silhouette categories S1...S4
RD	—	Relative deviation
RE	—	Relative error
S1...S4	—	Set of volume-silhouette categories: S1 Fit, S2 Semi-fit, S3 Semi-loose, S4 Loose
SCL	—	Sleeve center line
SD	—	Standard deviation
SNP	—	Side neck point
SP	—	Shoulder point
UAP	—	Underarm point
VB	—	Style3D virtual avatar; vector of its projection parameters
VC	—	Style3D virtual coat; vector of its projection parameters
$VC_{S1...S4}$	—	Virtual coats VC in volume-silhouette categories S1–S4
W1′...W3′	—	Full-width air-gap increments at the AL level
W1...W3	—	Full-width air-gap increments at the EL level
W'_C, W'_W, W'_H, W'_A, W'_E, $W'_{Wr, W'S}$	—	Frontal projection width parameters of the outer coat contour
WF = {W_S, W_C, W_W, W_H, W_A, WE, WWr}	—	Projection vector of widths of the AI-generated body
WR = {W_S, W_C, W_W, W_H, W_A, W_E, W_{Wr}}	—	Projection vector of widths of the real body
W_S, W_C, W_W, W_H, W_A, W_E, W_{Wr}	—	Frontal projection width parameters of the body
Y_1–Y_4	—	Sleeve shape variables: FD, FC, |a-b|, and Folds
Y_3 - |a-b|	—	Absolute difference between distances a and b; indicator of sleeve-curvature consistency
∠1	—	Angle between the sleeve elbow line and the horizontal line
∠2	—	Angle between SCL and the vertical line
∠A	—	Angular parameter of the outer coat contour
∠B	—	Angle between the back center line and the back hemline
X_5 - ∠BA	—	Angle between the back shoulder line and the center line of the back sleeve part

X_1 -∠BSS	—	Inclination angle of the back shoulder line
∠E, ∠1, ∠3	—	Angular parameters of body posture and shape
∠F	—	Angle between the front center line and the front hemline
X_6 -∠FA	—	Angle between the front shoulder line and the center line of the front sleeve part
X_2 -∠FSS	—	Inclination angle of the front shoulder line
∠S′	—	Angular parameter of the outer contour of the coat shoulder region
X_7 -Δ(∠BA+∠FA)	—	Sum of the back and front shoulder-sleeve angles
X_4 -Δ(∠BSS+∠FSS)	—	Sum of the back and front shoulder angles
X_3 -Δ(∠BSS-∠FSS)	—	Difference between the back and front shoulder angles
X_{10} -Δ(BSW-FSW)	—	Difference between the widths of the back and front sleeve parts
X_{14} - Δ(i-j)		Difference between parameters i and j
Δ1	—	Deviation between RB and VB
Δ2	—	Deviation between RB and AIBA
Δ3	—	Deviation between RB and AIBB
Δ4	—	Deviation between RB and AIBC
Δ5	—	Deviation between AIBB and AIBC
Δ6	—	Deviation between VC and RC
Δ7	—	Deviation between AIC and RC
$\Delta_{AIC,S1...S4}$	—	Deviation between AIC and RC in categories S1...S4
$\Delta_{VC,S1...S4}$	—	Deviation between VC and RC in categories S1...S4
ΔW_i^{AL}	—	Generalized full-width air-gap increment between adjacent volume-silhouette groups at the AL level
ΔWi^{EL}	—	Generalized full-width air-gap increment between adjacent volume-silhouette groups at the EL level

Note. The indices S, C, W, H, A, E, and Wr denote the shoulder, chest, waist, hip, armhole or upper-arm, elbow, and wrist levels, respectively; the prime symbol (′) denotes parameters of the outer coat contour. The symbol Δ indicates a difference or deviation, and ∠ denotes an angular parameter.

REFERENCES

1. Aldrich, W. Metric Pattern Cutting for Menswear / W. Aldrich // Wiley-Blackwell, 2011. – 208 p.

2. Armstrong, H.J. Patternmaking for Fashion Design / H.J. Armstrong // Pearson Education, 2009. – xi, 819 p.

3. Zhang, J. Research on the fit raglan sleeve based on the armhole depth and the connection point between body and sleeve / J. Zhang, M. Zhao // International Journal of Clothing Science and Technology, 2021, 33(5), pp. 774–795. doi: 10.1108/IJCST-07-2020-0105.

4. Fujii, C. Effects of combinations of patternmaking methods and dress forms on garment appearance / C. Fujii, M. Morooka, S. Yamada // AUTEX Research Journal, 2017, 17(3), pp. 277–286. doi: 10.1515/aut-2016-0020.

5. Hakeem, F. Expand and Compare the Use of Different Digital Fashion Technologies in Simulation Three-Dimensional Structured Designs: PhD dissertation / F. Hakeem // LSU Doctoral Dissertations, 2023. doi: 10.31390/gradschool_dissertations.6100.

6. Dai, X. Fabric mechanical parameters for 3D cloth simulation in apparel CAD: A systematic review / X. Dai, Y. Hong // Computer-Aided Design, 2024, 167, 103638. doi: 10.1016/j.cad.2023.103638.

7. Baria, B. Transformative effect of 3D sampling technology for the ready-made garment industry: a review / B. Baria, M.A. Shahid, A. Misra, M.B. Hoque, M.M. Rahman, M.D. Hossain, D. Das // Textile Research Journal, 2025, p. 00405175251360399. DOI: 10.1177/00405175251360399.

8. Liu, X. Research on improving the efficiency of garment sample production process based on virtual simulation technology / X. Liu, N. Zhong // AIVRID 2025: 2025 International Conference on Artificial Intelligence, Virtual Reality and Interaction Design. DOI: 10.1145/3777730.3777792.

9. Zangue, M. Virtual fit and physical fit: virtual material and garment calibration / M. Zangue, B. Promayon, S. Bouterf, A. Magnenat-Thalmann // 3DBODY.TECH 2020 – 11th International Conference and Exhibition on 3D Body Scanning and Processing Technologies. DOI: 10.15221/20.21.

10. Zhu, L. TryOnDiffusion: A Tale of Two UNets / L. Zhu, D. Yang, T. Zhu [et al.] // Proceedings of the IEEE/CVF Conference on Computer Vision and Pattern Recognition (CVPR), 2023. DOI: 10.1109/CVPR52729.2023.00447.

11. Morelli, D. LaDI-VTON: Latent Diffusion Textual-Inversion Enhanced Virtual

Try-On / D. Morelli, A. Baldrati, G. Cartella, M. Cornia, M. Bertini, R. Cucchiara // Proceedings of the 31st ACM International Conference on Multimedia (MM ’23), Ottawa, ON, Canada, October 29–November 3, 2023, pp. 8580–8589. DOI: 10.1145/3581783.3612137.

12. Islam, T. Deep Learning in Virtual Try-On: A Survey / T. Islam [et al.] // IEEE Access, 2024, 12, pp. 29475–29502. DOI: 10.1109/ACCESS.2024.3368612.

13. Shim, H. Quantitative analysis of fabric parameters affecting 3D garment simulation / H. Shim, N. Cho, S. Ku, J. Lee, G. Cho // ACS Omega, 2022, 7(46), pp. 42150–42162. DOI: 10.1021/acsomega.2c06302.

14. Hu, Y. Dynamic garment pressure and air gap thickness for multi-layer clothing system / Y. Hu, X. Li, Y. Li, X. Cheng, D. Yang // Textile Research Journal, 2019, 89(19–20), pp. 4148–4161. DOI: 10.1177/0040517519826930.

15. Kazlacheva, Z. A study on pattern making of sleeves with curved shoulders / Z. Kazlacheva // IOP Conference Series: Materials Science and Engineering, 2021, 1031(1):012024. https://doi.org/10.1088/1757-899X/1031/1/012024

16. Lee, E.-J. Visual image evaluation of 3D virtual clothing with raglan sleeves for plus-size women / E.-J. Lee // The Research Journal of the Costume Culture, 2025, 33(1), pp. 111–127. https://doi.org/10.29049/rjcc.2025.33.1.111

17. Lee, Y.-J. A Study on Based on the Possibility of Quantitative Analysis using Virtual Clothing Simulation according to Raglan Sleeve Pattern Types / Y.-J. Lee // Korean Journal of Human Ecology, 2012, 21(2), pp. 299–314. https://doi.org/10.5934/KJHE.2012.21.2.299

18. Yi, K.-H. A comparative study on the raglan-sleeve patterns according to the construction factors (II): Focused on the evaluation of the developed sleeve pattern / K.-H. Yi // Journal of the Korean Society of Costume, 2003, 53(8), pp. 1–10.

19. Liu, J. Research on women’s fitting raglan sleeve structure design [Master’s thesis, Donghua University], 2014.

20. Zhang, W.B. Clothing structure design // Beijing: China Textile & Apparel Press, 2006, pp. 36, 37.

21. Liu, R.P. Principles and application of men’s clothing paper pattern design // Beijing: China Textile Press, 2017, pp. 35, 36.

22. Xiong, X. The world’s classic clothing design and paper pattern // Nanchang: Jiangxi Fine Arts Publishing House, 2007, pp. 122–123.

23．Zhao, X. Research on correlation of raglan sleeve modeling and sleeve angle / X. Zhao // Wool Textile Journal, 2017, 45(11), pp. 42–46.

24．Huỳnh Thị Kim Phiến. Giáo trình thiết kế trang phục IV [M]. Tp. Hồ Chí Minh: Đại học Sư phạm Kỹ thuật Tp. HCM, 2007. 64 p.

25．Kuzmichev, V. Clothing Design in the Era of Artificial Intelligence / V. Kuzmichev // Journal of Computer and Communications, 2025, 13(5), pp. 121–136. https://doi.org/10.4236/jcc.2025.135008

26．Mao, X.L. Brief analysis of the adaptation method between raglan sleeve and garment body / X.L. Mao // Guangdong Canye, 2018, 52(11), pp. 115–117.

27．Zhao, X. Research on correlation of raglan sleeve modeling and sleeve angle / X. Zhao, T. He // Wool Textile Journal, 2017, 45(11), pp. 42–46.

28．Hong, M. A study on raglan sleeve based on inclination of sleeve centre line and bust ease / M. Hong // Unpublished report, 2015.

29．Kazlacheva, Z. A study on pattern making of sleeves with curved shoulders / Z. Kazlacheva // IOP Conference Series: Materials Science and Engineering, 2021, 1031(1):012024. https://doi.org/10.1088/1757-899X/1031/1/012024

30．Li, Y. Sablina, E. Devising the up-to-date method pattern making of female apparel with raglan sleeve / Y. Li, V.E. Kuzmichev, E. Sablina // Journal of Wuhan University of Science and Engineering, 2004, 17(6), pp. 1–6.

31．Gu, B., Su, J., Liu, G., Xu, B. Pattern alteration of women’s suits based on ease distribution / B. Gu, J. Su, G. Liu, B. Xu // International Journal of Clothing Science and Technology, 2016, 28(2). https://doi.org/10.1108/IJCST-07-2015-0083

32．Gill, S., Hayes, S., Conlon, J. Evolving pattern practice, from traditional patterns to bespoke parametric blocks / S. Gill, H. Al, S. Hayes, J. Conlon // International Journal of Fashion Design, Technology and Education, 2023, 17(2), pp. 144–161. https://doi.org/10.1080/17543266.2023.2260829

33．Wei, J. A study on the structural design method of fitting raglan sleeves for women’s wear and the automatic generation system for pattern (Unpublished master's thesis) / J. Wei // Donghua University, 2011.

34．Lou, Y.F. Wei, J.L. Research on the parameters of women's fitting raglan sleeve / Y.F. Lou, Z.F. Zhang, J.L. Wei // Journal of Wuhan Textile University, 2014, 27(2), pp. 39–41.

35．Liang, Z.Y. Analysis of sleeve setting angle parameters for fitted raglan sleeves / Z.Y. Liang, Z.H. Yin // Liaoning Silk, 2023, (2), pp. 33–35.

36．Liu, N. Study on the form-fitting raglan sleeve comfort based on sleeves and pieces join point position / N. Liu, X. Ren // Journal of Henan Institute of Engineering (Natural Science Edition), 2015, 27(4), pp. 22–25, 34.

37．Huang, W.W. Dress fit raglan sleeve structure design research / W.W. Huang // Textile Reports, 2017, pp. 64–65.

38．Wu, G.D. Discussion on the structure design and application of two-piece raglan sleeve / G.D. Wu // China Science & Technology Overview, 2018, (24), pp. 58–59.

39．Zhou, X. The relationship between armhole depth of raglan sleeve and its shape / X. Zhou, L. Zhou // Textile Science and Technology Progress, 2017, (5), pp. 48–51.

40．Kim, H. A Study on the Changes of Power Shoulder Shape in Contemporary Fashion / H. Kim, S.J. Bae // Journal of Fashion Business, 2016, 20(1), pp. 157–172. https://doi.org/10.12940/JFB.2016.20.1.157

41．Park, J. A study on the shoulder composition methods of power shoulder jackets and corresponding details / J. Park, J. Lee // The Research Journal of the Costume Culture, 2021, 29(3), pp. 388–405. https://doi.org/10.29049/rjcc.2021.29.3.388

42．Lee, S.-B. Body compensation image on power shoulder raglan sleeve jacket according to the shoulder height and width / S.-B. Lee, M.-A. Suh, M.-K. Uh // The Research Journal of the Costume Culture, 2015, 23(1), pp. 117–125. https://doi.org/10.7741/RJCC.2015.23.1.117

43．Huang, Y. Study on the position of body-sleeve juncture in raglan sleeve / Y. Huang // Journal of Zhejiang Fashion Institute of Technology, 2011, (4), pp. 21–24.

44．Liu, M.H. Research on pattern-making for close fitting raglan sleeve based on set-in sleeve / M.H. Liu, Y.X. Zhao // Journal of Beijing Institute of Clothing Technology, 2013, 33(1), pp. 7–15.

45．Zhang, D. Based on the sleeve rotation principle of women's fitting raglan sleeve structure design / D. Zhang, Y. Liu // Journal of Beijing Institute of Clothing Technology, 2016, 36(3), pp. 9–14.

46．Monobe, A. Effect of the difference between body dimensions and jacket measurements on the appearance of a ready-made tailored jacket / A. Monobe, K. Kim, M. Takatera // International Journal of Clothing Science and Technology, 2017, 29(5), pp.

627–645.

47. Kim, K.O. Effect of bust line position on appearance of upper garment / K.O. Kim, M. Sakaguti, M. Takatera // IOP Conference Series: Materials Science and Engineering, 2017, 254, p. 172014.

48. Yu, W.M. Assessment of garment fit / W.M. Yu, K.W. Yeung, Y.L. Lam // Proceedings of HKITA and CTES Conference on Hand-in-hand Marching into the 21st Century, 1998, pp. 1125–129.

49. Gu, B. Individualizing women's suit patterns using body measurements from two-dimensional images / B. Gu, G. Liu, B. Xu // Textile Research Journal, 2017, 87(6), pp. 669–681.

50. Sayğili, B. Determination of Body-Clothing Pattern Fit Problems In Men's Jacket and Pattern Proposal / B. Sayğili, Ş. Çivitci // Journal of Textile & Apparel/Tekstil ve Konfeksiyon, 2015, 25(3), pp. 270–279.

51. Huck, J. Protective overalls: Evaluation of clothing design and fit / J. Huck, O. Maganga, Y. Kim // International Journal of Clothing Science and Technology, 1997, 9(1), pp. 45–61.

52. Guo, M.N. Pressure and comfort perception in the system "female body–dress" / M.N. Guo, V.E. Kuzmichev // AUTEX Research Journal, 2013, 13(3), pp. 71–78.

53. Lage, A. Virtual try-on technologies in the clothing industry. Part 1: Investigation of distance ease between body and garment / A. Lage, K. Ancutiene // The Journal of The Textile Institute, 2017, 108(10), pp. 1787–1793.

54. Liu, K. Wearing comfort analysis from aspect of numerical garment pressure using 3D virtual-reality and data mining technology / K. Liu, J. Wang, Y. Hong // International Journal of Clothing Science and Technology, 2017, 29(2), pp. 166–179.

55. Liu, R. Creative structure of split raglan sleeve / R. Liu // China Textile Leader, 2017, (9), pp. 77–78.

56. Lee, E.-J. Visual image evaluation of 3D virtual clothing with raglan sleeves for plus-size women / E.-J. Lee // The Research Journal of the Costume Culture, 2025, 33(1), pp. 111–127. https://doi.org/10.29049/rjcc.2025.33.1.111

57. Liu, N. Study on the form-fitting raglan sleeve comfort based on sleeves and pieces join point position / N. Liu, X. Ren // Journal of Henan Institute of Engineering (Natural Science Edition), 2015, 27(4), pp. 22–25, 34.

58. Jing, Z. Research on the fit raglan sleeve based on the armhole depth and the

connection point between body and sleeve / Z. Jing, Z.M. Hua // International Journal of Clothing Science and Technology, 2021, 33(5), pp. 774–795. https://doi.org/10.1108/IJCST-07-2020-0105

59．Kazlacheva, Z. A study on pattern making of sleeves with curved shoulders / Z. Kazlacheva // IOP Conference Series: Materials Science and Engineering, 2021, 1031(1):012024. https://doi.org/10.1088/1757-899X/1031/1/012024

60．Liu, J. Research on women's fitting raglan sleeve structure design [Master's thesis, Donghua University], 2014.

61．Shi, H. Duan, T. Advances in personalized modelling and virtual display of ethnic clothing for intelligent customization / H. Shi, J. Yu, T. Duan // Autex Research Journal, 2024, 24(1). https://doi.org/10.1515/aut-2023-0040

62．Gu, B. 3D female upper body modelling based on 2D images / B. Gu, M. Kawysar, Z. Zhong, J. Jin // International Journal of Clothing Science and Technology, 2020, 32(4), pp. 471–482. doi: 10.1108/IJCST-03-2019-0042.

63．Idrees, S. Mobile 3D body scanning applications: a review of contact-free AI body measuring solutions for apparel / S. Idrees, S. Gill, G. Vignali // The Journal of The Textile Institute, 2023, 115(7), pp. 1161–1172. doi: 10.1080/00405000.2023.2216099.

64．Sun, K. Automation of 3D average human body shape modeling using Rhino and Grasshopper Algorithm / K. Sun, H. Kyung // Fashion and Textiles, 2021, 8(1). doi: 10.1186/s40691-021-00249-6.

65．Wang, T. Automatic recognition and 3D modeling of the neck-shoulder human shape based on 2D images / T. Wang, B. Gu // International Journal of Clothing Science and Technology, 2021, 33(5), pp. 796–810. doi: 10.1108/IJCST-05-2020-0079.

66．Chen, Y., Hou, Q., Hong, Y. &Gao, W. (2023). Automatic Identification of Wrist Position in a Virtual Environment for Garment Design. Autex Research Journal, 23(2), 253-265. https://doi.org/10.2478/aut-2021-0054

67．Sun, J. Body shape classification and block optimization based on space vector length / J. Sun, Q. Cai, T. Li, L. Du, F. Zou // International Journal of Clothing Science and Technology, 2019, 31(1), pp. 115–129. doi: 10.1108/IJCST-07-2018-0089.

68．Ryu, E.J. Automatic extraction of upper body landmarks using Rhino and Grasshopper algorithms / E.J. Ryu, H.K. Song // Fashion and Textiles, 2022, 9(1), p. 36. doi: 10.1186/s40691-022-00302-y.

69．Chi, C. Bruniaux, P., Tartare, G., Jin, H. A new parametric 3D human body

modeling approach by using key position labeling and body parts segmentation / C. Chi, X. Zeng, P. Bruniaux, G. Tartare, H. Jin // Textile Research Journal, 2022, 92(19–20), pp. 3653–3679. doi: 10.1177/00405175221089688.

70. Xia, M. Quantitative analysis of the relationship between the Male body shape and block pattern based on the three-dimensional human model / M. Xia, H. Lu, X. Xu, L. Zhang // Textile Research Journal, 2024, 94(3–4), pp. 323–340. doi: 10.1177/00405175231204375.

71. Song, D., Kankanhalli, M., Liu, A. Image-Based Virtual Try-On: A Survey / D. Song, X. Zhang, J. Zhou, W. Nie, R. Tong, M. Kankanhalli, A. Liu // International Journal of Computer Vision, 2024, 133(5), pp. 2692–2720. doi: 10.1007/s11263-024-02305-2.

72. Kulińska, M. Block pattern design system using 3D zoning method on digital environment for fitted garment / M. Kulińska, M. A, P. Bruniaux, X. Zeng // Textile Research Journal, 2022, 92(23–24), pp. 4978–4993. doi: 10.1177/00405175221114164.

73. Bao, C. 3D interactive garment parametric pattern-making and linkage editing based on constrained contour lines / C. Bao, Y. Miao, B. Gu, K. Liu, Z. Liu // International Journal of Clothing Science and Technology, 2021, 33(5), pp. 696–723. doi: 10.1108/IJCST-09-2020-0137.

74. Zhang, J. Upper garment 3D modeling for pattern making / J. Zhang, N. Innami, K. Kim, M. Takatera // International Journal of Clothing Science and Technology, 2015, 27(6), pp. 852–869. doi: 10.1108/IJCST-01-2015-0003.

75. Luo, X. 3D sweater garment style generation based on 3D anthropometric characteristic parameters / X. Luo, D. Li, J. Yuan // Journal of Engineered Fibers and Fabrics, 2024, 19, 15589250231222620. doi: 10.1177/15589250231222620.

76. Huang, H. Block pattern generation: From parameterizing human bodies to fit feature-aligned and flattenable 3D garments / H. Huang, P. Mok, Y. Kwok, J. Au // Computers in Industry, 2012, 63(7), pp. 680–691. doi: 10.1016/j.compind.2012.04.001.

77. Sun, N. Innovative Application of Modularized Virtual Interaction Design Technology in Clothing Design / N. Sun, T. Sun, B. Cao, X. Mu // Applied Mathematics and Nonlinear Sciences, 2024, 9(1). doi: 10.2478/amns-2024-1190.

78. Ren, X. Research on 3D simulation design and dynamic virtual display of clothing flexible body / X. Ren, S. Niu, X. Huang // Autex Research Journal, 2024, 24(1). doi: 10.1515/aut-2023-0042.

79. Kochanova, N. Development of pattern block shaping in accordance with the real sleeve-in shapes / N. Kochanova, V. Kuzmichev, D.C. Adolphe // Proceedings of the 3rd

International Conference on 3D Body Scanning Technologies, Lugano, Switzerland, 16–17 October 2012, pp. 343–347. doi: 10.15221/12.343.

80. Lagė, A. Virtual try-on technologies in the clothing industry. Part 1: Investigation of distance ease between body and garment / A. Lage, K. Ancutiene // The Journal of The Textile Institute, 2017, 108(10), pp. 1787–1793. doi: 10.1080/00405000.2017.1286701.

81. Lagė, A. Virtual try-on technologies in the clothing industry: Basic block pattern modification / A. Lagė, K. Ancutienė // International Journal of Clothing Science and Technology, 2019, 31(6), pp. 729–740. doi: 10.1108/IJCST-11-2018-0140.

82. Wang, Z. Prediction of garment fit level in 3D virtual environment based on artificial neural networks / Z. Wang, J. Wang, X. Zeng, S. Sharma, Y. Xing, S. Xu, L. Liu // Textile Research Journal, 2021, 91(15–16), pp. 1713–1731. doi: 10.1177/0040517520987520.

83. Jing, Z. Research on the fit raglan sleeve based on the armhole depth and the connection point between body and sleeve / Z. Jing, Z.M. Hua // International Journal of Clothing Science and Technology, 2021, 33(5), pp. 774–795. doi: 10.1108/IJCST-07-2020-0105.

84. Teyeme, Y. Fit and Pressure Comfort Evaluation on a Virtual Prototype of a Tight-Fit Cycling Shirt / Y. Teyeme, B. Malengier, T. Tesfaye, S. Vasile, L. Van // Autex Research Journal, 2023, 23(2), pp. 153–163. doi: 10.2478/aut-2021-0057.

85. Islam, T. Deep Learning in Virtual Try-On: A Comprehensive Survey / T. Islam, A. Miron, X. Liu, Y. Li // IEEE Access, 2024, 12, pp. 29475–29502. doi: 10.1109/ACCESS.2024.3368612.

86. Xu, X. Color analysis and performance optimization of 3D virtual simulation knitted fabrics / X. Xu // Autex Research Journal, 2025, 25(1). doi: 10.1515/aut-2025-0030.

87. Lagė, A. Virtual try-on technologies in the clothing industry. Part 1: Investigation of distance ease between body and garment / A. Lage, K. Ancutiene // The Journal of The Textile Institute, 2017, 108(10), pp. 1787–1793. doi: 10.1080/00405000.2017.1286701.

88. Jagelčáková, L. Virtual fit evaluation for optimization of garment component's parameters / L. Jagelčáková, E. Tokarčíková // Applied Sciences, 2024, 14(5), p. 2122. doi: 10.3390/app14052122.

89. Lagė, A. Virtual try-on technologies in the clothing industry: basic block pattern modification / A. Lagė, K. Ancutienė // International Journal of Clothing Science and Technology, 2019, 31(6), pp. 729–740. doi: 10.1108/IJCST-11-2018-0140.

90. Lagė, A. Pukienė, R., Lapkovska, E., Dāboliņa, I. Comparative Study of Real and

Virtual Garments Appearance and Distance Ease / A. Lagė, K. Ancutienė, R. Pukienė, E. Lapkovska, I. Dāboliņa // Materials Science, 2020, 26(2), pp. 233–239. doi: 10.5755/j01.ms.26.2.22162.

91．GB/T 10000-2023. Human dimensions of Chinese adults. Beijing: Standards Press of China, 2023.

92．ISO 7250-1:2017. Basic human body measurements for technological design — Part 1: Body measurement definitions and landmarks. Geneva: International Organization for Standardization, 2017.

93．GOST 31399-2009. Classification of standard men's figures by height, sizes and full-bodied groups for projection of clothes. Moscow: Standartinform, 2011.

94．Choi, W. Developing an AI-based automated fashion design system: reflecting the work process of fashion designers / W. Choi, S. Jang, H.Y. Kim, Y. Lee, S. Lee, H. Lee, S. Park // Fashion and Textiles, 2023, 10(1), article 39. doi: 10.1186/s40691-023-00360-w.

95．Wu, X., & Li, L. (2024). An application of generative AI for knitted textile design in fashion. The Design Journal, 27(2), 270-290. https://doi.org/10.1080/14606925.2024.2303236

96．Yin, N. Ching, W. A novel approach in predicting virtual garment fitting sizes with psychographic characteristics and 3D body measurements using artificial neural network and visualizing fitted bodies using generative adversarial network / N. Yin, P. Wai, A. Pun, K.Y. C., W. Ching // Heliyon, 2023, 9(7), e17916. https://doi.org/10.1016/j.heliyon.2023.e17916

97．Oh, J. Automatic generation of parametric patterns from grading patterns using artificial intelligence / J. Oh, S. Kim // International Journal of Clothing Science and Technology, 2023, 35(6), pp. 889-903. https://doi.org/10.1108/IJCST-07-2022-0102

98．Danner, M. AI-assisted Pattern Generator for Garment Design / M. Danner, E. Brake, G. Kosel, Y. Kyosev, K. Rose, M. Rätsch, H. Cebulla // Communications in Development and Assembling of Textile Products, 2024, 5(2), pp. 195–206. https://doi.org/10.25367/cdatp.2024.5.p195-206

99．Ghodhbani, H. You can try without visiting: a comprehensive survey on virtually try-on outfits / H. Ghodhbani, M. Neji, I. Razzak, M. A // Multimedia Tools and Applications, 2022, 81(14), pp. 19967–19998. https://doi.org/10.1007/s11042-022-12802-6

100．Chenghu, D. Multi-Pose Virtual Try-On Via Self-Adaptive Feature Filtering / C. Chenghu, F. Yu, M. Jiang, X. Wei, T. Peng, X. Hu // ICASSP 2022, pp. 2544–2548. https://doi.org/10.1109/ICASS*P43*922.2022.9747847

101．He, W. VTON360: High-fidelity virtual try-on from any viewing direction / W. He, X. Sun, Y. Shen, J. Yu, C. Lu // Proceedings of the IEEE/CVF Conference on Computer Vision and Pattern Recognition (CVPR), 2025. https://doi.org/10.1109/CVPR.2025

102．Rombach, R. High-resolution image synthesis with latent diffusion models / R. Rombach, A. Blattmann, D. Lorenz, P. Esser, B. Ommer // Proceedings of the IEEE/CVF Conference on Computer Vision and Pattern Recognition (CVPR), 2022, pp. 10684–10695. https://doi.org/10.1109/CVPR52688.2022.01044

103．Li, X. Dress-1-to-3: Single image to simulation-ready 3D outfit with diffusion prior and differentiable physics / X. Li, C. Yu, W. Du, Y. Jiang, T. Xie, Y. Chen, Y. Yang, C. Jiang // ACM Transactions on Graphics, 2025, 44(4), pp. 1–16. https://doi.org/10.1145/3731177

104．Han, X. VITON: an image-based virtual try-on network / X. Han, Z. Wu, Z. Wu, R. Yu, L.S. Davis // Proceedings of the IEEE/CVF Conference on Computer Vision and Pattern Recognition (CVPR).

105．Lee, H.J. LA-VITON: a network for looking-attractive virtual try-on / H.J. Lee, R. Lee, M. Kang, M. Cho, G. Park // Proceedings of the IEEE/CVF International Conference on Computer Vision Workshops, 2019. http://openaccess.thecvf.com/content_ICCVW_2019/html/CVFAD/Lee_LA-VITON_A_Network_for_Looking-Attractive_Virtual_Try-On_ICCVW_2019_paper.html?ref=https://githubhelp.com

106．Du, C. VTON-HF: High Fidelity Virtual Try-on Network via Semantic Adaptation / C. Du, F. Yu, Y. Chen, M. Jiang, X. Wei, T. Peng, X. Hu // 2021 IEEE 33rd International Conference on Tools with Artificial Intelligence (ICTAI), pp. 224–231. https://doi.org/10.1109/ICTAI52525.2021.00038

107．Zhou, P. Text-driven 3D human generation via contrastive preference optimization / P. Zhou, X. Shen, Y. Hu // arXiv preprint arXiv:2502.08977, 2025. https://doi.org/10.48550/arXiv.2502.08977

108．Patel, M. TailorNet: Predicting clothing in 3D as a function of human pose, shape and garment style / M. Patel, S.K. Ramakrishnan, V. Jampani, C. Theobalt // Proceedings of the IEEE/CVF Conference on Computer Vision and Pattern Recognition (CVPR), 2020, pp. 7365–7375. https://doi.org/10.1109/CVPR42600.2020.00739

109．Xu, H. Research on T-shirt-style design based on Kansei image using back-propagation neural networks / H. Xu, R. Ren, H. Chen // Autex Research Journal, 2023, 24(1). https://doi.org/10.1515/aut-2023-0007

110．Grigorev, A. HOOD: hierarchical graphs for generalized modelling of clothing

dynamics / A. Grigorev, M.J. Black, O. Hilliges // 2023 IEEE/CVF Conference on Computer Vision and Pattern Recognition (CVPR), pp. 16965–16974. https://doi.org/10.1109/cvpr52729.2023.01627

111. Li, P. Sorkine-Hornung, O. Neural Garment Dynamics via Manifold-Aware Transformers / P. Li, Y. T., T. Levent, D. Ceylan, O. Sorkine-Hornung // Computer Graphics Forum, 2024, 43(2). https://doi.org/10.1111/cgf.15028

112. Ghodhbani, H. A. You can try without visiting: a comprehensive survey on virtually try-on outfits / H. Ghodhbani, M. Neji, I. Razzak, M. A // Multimedia Tools and Applications, 2022, 81(14), pp. 19967–19998. https://doi.org/10.1007/s11042-022-12802-6

113. Wang, Z. Estimating human body dimensions using RBF artificial neural networks technology and its application in activewear pattern making / Z. Wang, J. Wang, Y. Xing, Y. Yang, K. Liu // Applied Sciences, 2019, 9(6), p. 1140. https://doi.org/10.3390/app9061140

114. Liu, K. Garment fit evaluation using neural networks technology / K. Liu, R. Wang, X. Hao, C. Zhu, S. Zhou, X. Zeng, X. Tao, P. Bruniaux, J. Wang // Journal of the Textile Institute, 2024, 115(4), pp. 562–572. https://doi.org/10.1108/00405000.2023.2201526

115. Li, T. GarTrans: Transformer-based architecture for dynamic and detailed garment deformation / T. Li, Z. Qiao, Z. Li, R. Shi, Q. Zhu // Computational Visual Media, 2025, pp. 1–18. https://doi.org/10.26599/CVM.2025.9450448

116. Deng, M. AI-driven innovation in ethnic clothing design: an intersection of machine learning and cultural heritage / M. Deng, Y. Liu, L. Chen // Electronic Research Archive, 2023, 31(9), pp. 5793–5814. https://doi.org/10.3934/era.2023295

117. Zhang, X. WarpDiffusion: Efficient diffusion model for high-fidelity virtual try-on / X. Zhang, X. Li, M. Kampffmeyer, X. Dong, Z. Xie, F. Zhu, H. Dong, X. Liang // arXiv preprint arXiv:2312.03667, 2023. https://doi.org/10.48550/arXiv.2312.03667

118. Xing, J. TryOn-adapter: Efficient fine-grained clothing identity adaptation for high-fidelity virtual try-on / J. Xing, C. Xu, Y. Qian, Y. Liu, G. Dai, B. Sun, Y. Liu, J. Wang // arXiv preprint arXiv:2404.00878, 2024. https://doi.org/10.48550/arXiv.2404.00878

119. Raut, A. Generative AI in vision: A survey on models, metrics and applications / A. Raut, S. Sengupta, A. Sharma, R. Banerjee // arXiv preprint arXiv:2401.02658, 2024. https://doi.org/10.48550/arXiv.2401.02658

120. Bie, F. Renaissance: A survey into AI text-to-image generation in the era of large models / F. Bie, Y. Yang, Z. Zhou, A. Ghanem, M. Zhang, Z. Yao, X. Wu, C. Holmes, P.

Golnari, D.A. Clifton, Y. He, D. Tao, S.L. Song // arXiv preprint arXiv:2309.00810, 2023. https://doi.org/10.48550/arXiv.2309.00810

121. Radford, A. Learning transferable visual models from natural language supervision / A. Radford, J.W. Kim, C. Hallacy, A. Ramesh, G. Goh, S. Agarwal, I. Sutskever // Proceedings of the 38th International Conference on Machine Learning (ICML), 2021, 139, pp. 8748–8763.

122. Lei, H. CG-VTON: Controllable Generation of Virtual Try-On Images Based on Multimodal Conditions / H. Lei, X. Zhao, Y. Liang, Y. Cao // IET Image Processing, 2025, 19(1). https://doi.org/10.1049/ipr2.70144

123. Shim, G. GaussianMotion: End-to-end learning of animatable Gaussian avatars with pose guidance from text / G. Shim, S. Lee, J. Choo // arXiv preprint arXiv:2502.11642, 2025. https://doi.org/10.48550/arXiv.2502.11642

124. Cui, Y. FashionGAN: Display your fashion design using conditional generative adversarial networks / Y. Cui, Y. Song, C. Feng, Y. Yao, L. Lu, M.H. Yang // Computer Graphics Forum, 2018, 37(7), pp. 67–78. https://doi.org/10.1111/cgf.13573

125. Kim, J. StableVITON: Learning Semantic Correspondence with Latent Diffusion Model for Virtual Try-On / J. Kim, G. Gu, M. Park, S. Park, J. Choo // Proceedings of the IEEE/CVF Conference on Computer Vision and Pattern Recognition, 2024, pp. 8176–8185. DOI: 10.1109/CVPR52733.2024.00781.

126. Xu, Y. OOTDiffusion: Outfitting Fusion Based Latent Diffusion for Controllable Virtual Try-On / Y. Xu, T. Gu, W. Chen, A. Chen // Proceedings of the AAAI Conference on Artificial Intelligence, 2025, 39(9), pp. 8996–9004. DOI: 10.1609/aaai.v39i9.32973.

127. Zhao, X. UniFashion: A Unified Vision-Language Model for Multimodal Fashion Retrieval and Generation / X. Zhao, Y. Zhang, W. Zhang, X.-M. Wu // Proceedings of the 2024 Conference on Empirical Methods in Natural Language Processing, 2024, pp. 1490–1507. DOI: 10.18653/v1/2024.emnlp-main.89.

128. Wang, Z. Image quality assessment: From error visibility to structural similarity / Z. Wang, A.C. Bovik, H.R. Sheikh, E.P. Simoncelli // IEEE Transactions on Image Processing, 2004, 13(4), pp. 600–612. https://doi.org/10.1109/TIP.2003.819861

129. Цзя Шуан. Антропометрическое обоснование градации лекал / Цзя Шуан, В.Е. Кузьмичев // Молодые учёные – развитию национальной технологической инициативы (ПОИСК – 2024) : сборник материалов национальной (с международным участием) молодёжной научно-технической конференции. – Иваново : Ивановский государственный политехнический университет, 2024. – С. 735–739.

130. Цзя Шуан. Оптимизация и валидация чертежей пальто покроя реглан / Цзя

Шуан, В.Е. Кузьмичев // Молодые учёные – развитию национальной технологической инициативы (ПОИСК – 2025) : сборник материалов национальной (с международным участием) молодёжной научно-технической конференции. – Иваново : Ивановский государственный политехнический университет, 2025. – С. 530–534.

131. Цзя Шуан. Алгоритм сравнительного анализа базовых чертежей конструкций для мужской одежды / Цзя Шуан, В.Е. Кузьмичев // Известия высших учебных заведений. Технология текстильной промышленности. – 2025. – № 2 (416). – С. 205–215. – DOI 10.47367/0021-3497_2025_2_205.

132. Кузьмичев, В.Е. Применение искусственного интеллекта в индустрии моды / В.Е. Кузьмичев, Цзя Шуан, Инь Чжидуань // Известия высших учебных заведений. Технологиятекстильнойпромышленности. – 2025. – № 3 (417). – С. 66–78. – DOI 10.47367/0021-3497_2025_3_66.

133. Цзя Шуан. 2,5D-система проекционных параметров для оценки точности формы пальто покроя реглан, сгенерированных с использованием ИИ /Цзя Шуан, В.Е. Кузьмичев // Молодые учёные – развитию национальной технологической инициативы (ПОИСК – 2026) : сборник материалов национальной (с международным участием) молодёжной научно-технической конференции. – Иваново : Ивановский государственный политехнический университет, 2026. – С.683-687.

134. Цзя Шуан.Сравнительный анализ прототипов рукава реглан/ Цзя Шуан, В.Е. Кузьмичев // Молодые учёные – развитию национальной технологической инициативы (ПОИСК – 2026) : сборник материалов национальной (с международным участием) молодёжной научно-технической конференции. – Иваново : Ивановский государственный политехнический университет, 2026. – С.666-673.

135. Гниденко, А.В. Формализация и алгоритмизация процесса проектирования женской одежды с рукавами сложных покроев: диссертация кандидата технических наук / А.В. Гниденко // Ивановская государственная текстильная академия, Иваново, 2008, 171 с.

136. Кузьмичев, В.Е. Разработка конструктивно-антропометрического обеспечения процесса конструирования одежды / В.Е.Кузьмичев, И.В.Жукова, Н.А.Сахарова // Известия вузов. Технология текстильной промышленности, 2022, №6(402), с.143-148

137. Кузьмичев, В.Е. Основы теории системного проектирования костюма / В.Е. Кузьмичев, Н.И. Ахмедулова, Л.П. Юдина // Москва, Юрайт, 2025, 260 с.

138. Xie, H. Structure-consistent customized virtual mannequin reconstruction from 3D scans based on optimization / H. Xie, Y. Zhong // Textile Research Journal, 2020, 90(7–8), pp. 937–950. doi: 10.1177/0040517519883957.

139. Bai, J. L., & Wang, X. M. Practical Garment Industrial Pattern Making [M]. Beijing: Beijing Institute of Technology Press, 2020: 45-48.

APPENDIX A.

Supplementary Materials on the Construction, Parameterization, and Verification of Raglan Coat Pattern-making

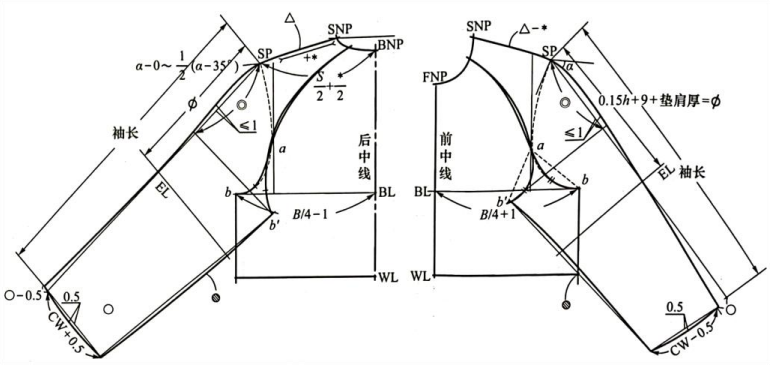

a

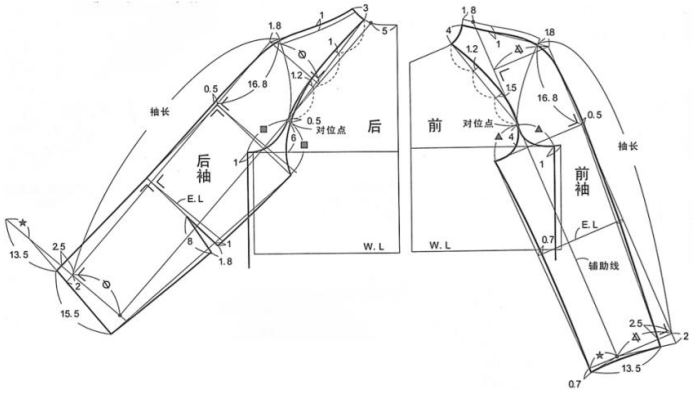

b

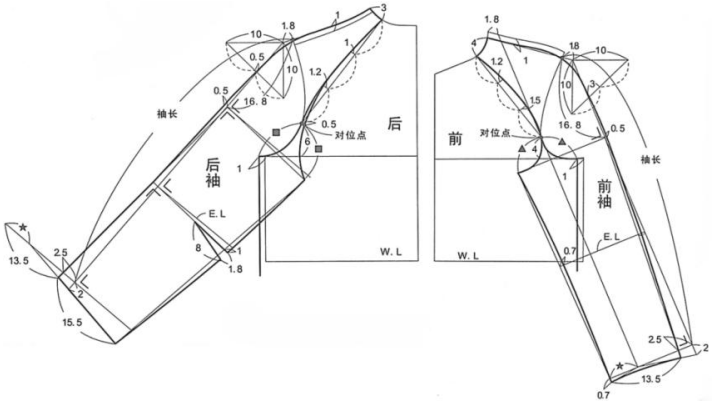

c

Figure A.1 - Raglan sleeve Pattern-making method from Chinese teaching-book: P4, P5, P6

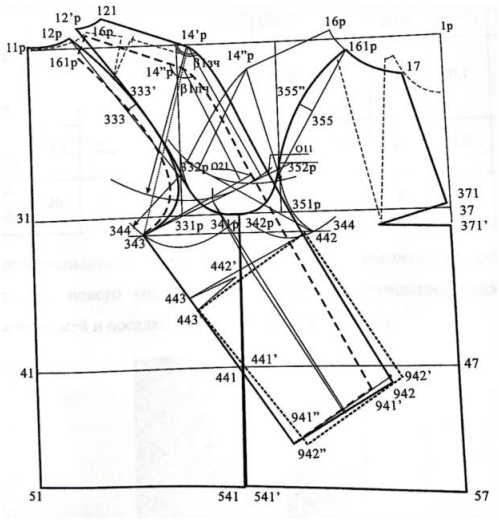

Figure A.2 - Russian raglan sleeve pattern-making method

Figure A.3. - Virtual (V) and real (R) samples of three prototypes, *P1, P2, P3*, made on fabrics F (F1, F2, F2).

Table A.1 - The specific quantification of pattern (X1–X14) and shape (Y1–Y4) parameters

No.	X1	X2	X3	X4	X5	X6	X7	X8	X9	X10	X11	X12	X13	X14	Y1	Y2	Y3	Y4
1	31.9	24.8	56.6	7.1	30.2	39.5	69.7	21.5	18.0	3.5	2.5	1.2	-3.0	-4.2	4.7	2.7	0.1	1.0
2	28.2	24.1	52.3	4.1	27.0	45.0	72.0	22.6	20.9	1.7	2.8	2.6	9.0	6.4	3.7	3.1	0.2	1.0
3	31.9	25.1	57.0	6.9	11.6	53.9	65.5	25.5	23.8	1.7	1.5	1.8	4.0	2.2	4.8	1.0	0.2	0.5
4	31.4	21.6	53.0	9.7	6.9	53.1	60.0	26.8	27.5	-0.7	1.5	-0.6	-3.9	-3.3	3.8	1.0	0.0	0.0
5	28.5	20.0	48.5	8.4	34.5	37.5	72.0	24.8	20.1	4.7	1.5	5.0	11.6	6.6	2.8	1.0	0.3	1.0
6	33.0	20.6	53.5	12.4	0.1	59.9	60.0	23.9	24.1	-0.2	1.5	0.0	5.7	5.7	4.0	1.0	0.0	0.0
7	33.0	21.0	54.0	11.9	3.3	57.2	60.5	27.1	21.7	5.4	1.5	5.2	12.5	7.3	4.1	1.0	0.3	0.0
8	32.4	24.1	56.5	8.3	25.2	45.8	71.0	27.2	20.8	6.4	3.4	5.6	17.0	11.4	4.7	4.1	0.4	1.0
9	30.7	24.0	54.6	6.7	20.9	48.2	69.1	27.1	21.7	5.4	3.1	5.6	17.0	11.4	4.2	3.6	0.4	1.0
10	26.6	30.7	57.3	-4.1	24.6	44.6	69.2	24.4	23.0	1.4	3.4	1.2	6.1	4.9	4.9	4.1	0.2	0.8
11	21.0	22.1	43.1	-1.1	22.0	46.9	68.9	26.6	20.8	5.8	3.4	5.1	15.1	10.0	1.5	4.1	0.4	0.7
12	21.0	22.1	43.1	-1.1	22.2	46.8	69.0	26.6	20.8	5.8	3.4	5.1	15.1	10.0	1.5	4.1	0.4	0.8
13	31.4	20.6	52.0	10.8	5.2	59.9	65.1	24.7	24.4	0.3	1.5	0.5	2.0	1.5	3.6	1.0	0.0	0.4
14	18.3	22.8	41.1	-4.5	22.0	41.3	63.3	21.7	18.3	3.4	1.5	3.4	5.1	1.7	1.0	1.0	0.3	0.5
15	22.9	25.8	48.7	-2.9	22.2	40.2	62.4	24.0	23.0	1.0	3.1	0.4	2.3	1.9	2.8	3.6	0.1	0.5
16	30.7	24.0	54.6	6.7	25.7	45.3	71.0	27.8	27.8	0.0	3.4	-0.7	1.8	2.5	4.2	4.1	0.0	1.0
17	30.8	24.4	55.3	6.4	26.0	45.1	71.1	28.2	28.2	0.0	3.4	-0.4	-1.3	-0.9	4.4	4.1	0.0	1.0
18	21.0	22.1	43.1	-1.1	21.9	47.1	69.0	26.6	26.6	0.0	3.4	-0.5	-2.5	-2.0	1.5	4.1	0.0	1.0
19	29.9	20.0	49.9	9.8	13.2	51.1	64.3	22.4	22.4	0.0	2.1	0.0	1.7	1.7	3.1	2.0	0.0	0.5
20	27.9	21.9	49.8	6.1	12.5	48.7	61.2	28.2	19.9	8.3	1.5	7.9	17.1	9.2	3.1	1.0	0.7	0.1
21	18.7	18.7	37.3	0.0	24.5	39.9	64.4	27.0	25.0	2.0	2.8	1.9	3.9	2.0	0.1	3.1	0.1	0.4
22	21.0	22.1	43.1	-1.1	22.0	40.4	62.4	26.6	25.4	1.2	2.8	1.2	3.2	2.0	1.5	3.1	0.2	0.0

23	29.0	24.0	53.0	5.0	22.0	40.4	62.4	27.8	23.4	4.4	3.5	4.8	13.6	8.8	3.8	4.3	0.3	0.0
Min	18.3	18.7	37.3	-4.5	0.1	37.5	60.0	21.5	18.0	-0.7	1.5	-0.7	-3.9	-4.2	0.1	1.0	0.0	0.0
MAX	33.0	30.7	57.3	12.4	34.5	59.9	72.0	28.2	28.2	8.3	3.5	7.9	17.1	11.4	4.9	4.3	0.7	1.0
AV	27.3	23.0	50.1	4.5	19.2	47.0	66.2	25.6	23.0	2.8	2.5	2.5	6.7	4.2	3.1	2.7	0.2	0.5

Table A.2 - Parameter measurements(*a, b, c,* and $(d_F+d_B)/2$) of real (R) and virtual (V) samples for three prototypes

Prototype	Fabric		*a,* °	*b*， °	*c, amount*	$(d_F+d_B)/2$， cm
P1	F1	V	90.8	90	0	0.6
		R	90.2	88.1	0	0.7
	F2	V	90.7	90.6	0	0.6
		R	91.5	90	0	0.6
	F3	V	95.1	91	0	0.7
		R	90.5	91.8	0	0.7
P2	F1	V	98	92.5	0	1.5
		R	96.6	95.6	1	2.1
	F2	V	101	90.5	0	1.7
		R	101.6	93.7	1	1.9
	F3	V	99.1	95.4	0	2.5
		R	94.2	91.8	0	2.3
P3	F1	V	104.5	99.6	0	2.3
		R	104.8	100.1	1	2.4
	F2	V	103.9	99.4	0	2.8
		R	102.1	92.5	1	2.8
	F3	V	106.2	98.7	0	3
		R	105.7	100	0	2.7

Table A.3 - Descriptive statistics for arm shape angles

Index	∠1, degree				∠2， degree			
CG	Y	A	B	C	Y	A	B	C
88	13.4	9.5	7.3	9.1	15.7	11.1	10.6	11.6
92	10.5	9.3	7.7	8.9	15.6	11.9	12.2	11.7
96	9.2	8.8	8.2	10.0	12.6	12.2	12.5	12.9

100	8.0	7.9	9.8	9.6	12.2	11.3	12.9	11.1
104	7.9	7.9	7.8	7.7	11.5	11.2	11.2	10.8
MIN	7.9				12.2			
MAX	13.4				15.7			
AV	8.9				12.2			

Table A.4 - Descriptive Statistics for cuff shape in 19 photos

	BC	FC
1	3.5	0
2	2.3	1.9
3	0.5	1.1
4	1.3	3.2
5	4.3	1.5
6	0	4.6
7	2.4	4
8	0.8	0.8
9	0.9	0.6
10	0.9	1.5
11	1.6	0.8
12	1	2.7
13	0	4.1
14	1.9	3.8
15	7.2	1.8
16	2.8	1.7
17	5.1	2.6
18	2	3.5
19	1.6	3.5
MIN	0	0
MAX	7.2	4.6
AV	2.3	2.3
SD	1.8	1.4

Table A.5 - The total interval ranges from the shape parameters of 95 photos (cm)

	SP	AL	EL	Angle (Shoulder-Sleeve)
1	41.8	46.8	48	124
2	42.6	49.6	50.8	119.2
3	46	55.2	57	119
4	42	57.6	59	132.3

5	40.6	44.8	46.8	123.5
6	43.8	51.2	55	126.7
7	42.2	52.4	55.8	121.4
8	43.8	48	49.4	123.7
9	40	46	48.8	124.3
10	45.4	54	58.2	127.3
11	42.8	46.4	47.8	140.2
12	44.8	50	55.2	130.7
13	41.4	47.6	49.2	121.3
14	44.2	46.6	46.8	126
15	53.4	47.2	47.2	120.9
16	44	54.4	59	120.9
17	46.6	60	62.8	127.9
18	46.8	54	56.8	118.7
19	48.9	48	50.8	123.6
20	47.2	52.8	57	132.5
21	41.6	47.4	48.6	121.3
22	46.8	53.4	55.8	127.6
23	45	47.6	50.6	118.8
24	43.4	52.2	57	118.6
25	47	57.2	57.6	120.5
26	45	51	52	125.7
27	48.8	56.8	58.2	131.2
28	47.8	58.4	64.4	126.4
29	42.8	50.6	53	136.2
30	47.2	55	61.8	126.8
31	43	52.4	55.2	127.5
32	49	53.4	58.8	126.7
33	48.6	55	58	113
34	48.2	58.4	60.4	131.4
35	42	47.8	52.4	131.6
36	41	44.8	47	135.7
37	43	56	61.6	128
38	46.8	58	61.8	123.3
39	43.2	48.4	51.4	122.7
40	43.8	54	56	124.2
41	47	51	54	125.3

42	46.4	55.4	60	126.8
43	45.4	56.8	60.8	127.8
44	39.4	48.8	55	120
45	46.4	50.8	54.2	126.5
46	44	56.2	60	119.9
47	45.6	54.2	56.4	128.6
48	42.4	50.2	54	125.2
49	46	60.2	64	120.9
50	41	49.4	51.4	125
51	40.8	46	47.6	123.6
52	42.8	49	51.6	130.4
53	46	50.8	53	129.4
54	43.6	51	53	120.8
55	41.4	46	49.6	120.8
56	43.8	48.4	52.6	126.3
57	49.6	49.2	52.4	121.2
58	44	55.2	59	132
59	46	54	60	127.2
60	42.4	48.6	50.6	128.1
61	44.8	49.2	52	120.2
62	45.6	54	57.8	121
63	46	55.4	59.4	131.5
64	48.6	58	63.8	124.7
65	45.2	59.6	67	132.6
66	45	55.6	61.8	106.2
67	51	66.4	71.6	118.6
68	46	54	55	122.7
69	48.2	58.2	62.8	123.7
70	41.6	50.2	56.6	128
71	44.6	51.6	55.6	118.3
72	47.2	51.2	55	126.9
73	47.8	50	51.4	126
74	46.2	55.6	58.8	116.8
75	51.4	58.8	62.2	129.2
76	48.8	57.6	62.8	124.8
77	46.6	54.2	58.8	127.5
78	46.4	55.4	58.4	129.7

79	47.2	56	61.2	118
80	48.6	56.8	61	119.3
81	57.8	70	73.4	130.2
82	52.2	64	67	116
83	47.2	56.8	63.2	120.4
84	50.8	61	63.4	129.7
85	48.6	56.4	57.6	131.1
86	49.2	56.4	60.2	120.2
87	45	52	55.2	122
88	47.8	55.8	60.2	130
89	54.4	49	52	119
90	50	63	66.2	117.3
91	53	55.6	60.2	119.2
92	45.4	48.6	51.8	137
93	48.8	58.2	61.6	125.5
94	50.4	55.6	56.4	117.8
95	48	52	54	125
AV	45.9	53.3	56.6	124.8
MAX	57.8	70	73.4	140.2
MIN	39.4	44.8	46.8	106.2
RD	0.40	0.47	0.47	0.27

Table A.6 - E(CG) of 100 raglan-sleeve coat patterns from Chinese pattern-making teaching textbooks

NO.	Fit	Semi-Fit		Semi - Loose	Loose	
1	10	14	18	18	31	24
2	13	14	16	19	26	30
3	/	16	18	19	21	26
4	/	13	18	20	24	26
5	/	13	18	20	26	27
6	/	15.5	18	20	26	27
7	/	15.5	14	20	26	30
8	/	14.5	18	20	26	22
9	/	14.5	18	20	28	25
10	/	15.5	18	21	21	32
11	/	18	16	22	21	30
12	/	13	18	18	30	35

13	/	13	18	18	28	26
14	/	15	18	18	28	26
15	/	15	16	20	28	26
16	/	15	18	20	34	26
17	/	15	18	20	34	28
18	/	14	18	25	25	30
19	/	16	14	23	28	30
20	/	14	/	/	32	32
MIN	10	13		18	22	
MAX	13	18		25	35	
AV	12	16		20	28	

Table A.7 - Comparative analysis of parameter *a*

CG, cm	*P1*				*P2*				*P3*			
	Y	A	B	C	Y	A	B	C	Y	A	B	C
88	-2.5	-2	2.8	2.6	0	2	2	2	0.3	-0.3	4.4	3
92	-1.3	1.6	0.8	1	3.1	2.1	-3.2	3.1	0.4	2.6	-1.4	-1.7
96	1.2	-0.3	0	-1.2	3.6	3.1	2.5	2.7	1.5	2.2	3.2	2.5
100	2.1	-2.9	-3.5	2.6	3.2	4	2.7	0.5	2.9	2.8	-2.2	2.1
104	1.9	1.0	2.1	2.6	3.5	4.7	0.5	0.9	3.1	2.3	-1.5	1.6
Av	1.8				2.0				2.1			

Table A.8 - Comparative analysis of the parameter *b*

CG, cm	*P1*				*P2*				*P3*			
	Y	A	B	C	Y	A	B	C	Y	A	B	C
88	0	0	0	2	-1.4	-2.7	1.4	2	0.3	-0.3	4.4	2
92	0.1	0	0.4	2.3	2.7	2.8	-1.4	2.4	0.4	2.6	-1.8	2.4
96	0	0	0.2	0	0.7	-3.2	1.0	2.8	1.5	2.2	3.2	2.5
100	0.4	0	0	0	0.7	0.5	3.1	0.4	2.9	2.8	-1.2	1.1
104	0	0	2.3	2	0.4	0.5	1.6	1.2	3.1	2.3	-1.5	1.6
Av	0.5				1.6				2			

Table A.9 - Comparative analysis of the parameter *c*

CG, cm	*P1*				*P2*				*P3*			
	Y	A	B	C	Y	A	B	C	Y	A	B	C
88	2	1	2	1	2	2	2	2	0	0	2	1
92	0	0	0	1	0	0	1	1	2	2	2	1
96	0	0	0	0	1	1	0	1	2	2	2	3

100	0	2	2	2	2	2	2	2	3	0	2	2
104	0	0	1	2	0	1	2	2	2	3	2	2
Av	0.2				0.9				1.3			

Table A.10 - Comparative analysis of the parameter $(d_F + d_B)/2$

CG, cm	*P1*				*P2*				*P3*			
	Y	A	B	C	Y	A	B	C	Y	A	B	C
88	0.2	0.8	1	1	0.3	0.4	0.5	0.5	0.8	0.8	0.6	0.7
92	0.7	1	1.1	1.2	0.6	0.7	0.9	0.9	0.8	0.8	1	1.1
96	0.8	0.2	0.2	0.4	1	1.3	1.3	1.1	1.2	0.8	1.8	1
100	0.7	0.8	1.2	1.3	0.8	1.1	1.4	1.8	0.6	0.7	0.9	1.3
104	0.5	0.6	1.1	2	1.8	1.8	1.9	1.6	0.6	0.9	1.1	0.9
Av	0.8				1.1				0.9			

Table A.11 - BSS and FSS for typical 3D avatars

		CG	BSS, degree	FSS, degree
1	Y	88	24.9	27.3
2		92	21.1	24.9
3		96	20.3	24.6
4		100	20.1	24.4
5		104	19.9	23.9
AV			**21.3**±1.8	**25.0**±1.2
6	A	88	23.1	26.1
7		92	21.9	25.2
8		96	21.2	24.9
9		100	20.8	24.8
10		104	20.2	24.7
AV			**22**±1.2	**25.5**±0.6
11	B	88	24.9	27.3
12		92	23.6	26
13		96	22.2	25.5
14		100	21.6	25.1
15		104	20.6	25.1
AV			**22.6**±1.7	**25.8**±0.9
16	C	88	23.5	25.0
17		92	20.5	26.0
18		96	24.2	26.7

19		100	23.7	26.3
20		104	22.5	26.3
AV			**22.9±1.5**	**26.1 ±0.7**

Table A.12 - Front and back waist girths (FWG/BWG) and BWG: FWG ratio for typical avatars

		CG	BWG	FWG	BWG:FWG（%）
1	Y	88	15.4	17.6	46.7:53.3
2		92	16.5	18.5	47.1:52.9
3		96	16.9	20.1	45.7:54.3
4		100	18.8	20.3	48.1:51.9
5		104	19.8	21.2	48.3:51.7
AV			17.5±1.8	19.5 ± 1.5	47.2：52.8
6	A	88	16.4	19.6	45.6:54.4
7		92	16.9	21.1	44.5:55.5
8		96	18.2	21.8	45.5:54.5
9		100	19.6	22.4	46.7:53.3
10		104	20.9	23.1	47.5:52.5
AV			18.4 ± 1.9	21.6 ± 1.3	46：54
11	B	88	17.7	21.3	45.4:54.6
12		92	18.4	22.6	44.9:55.1
13		96	20.5	22.5	47.7:52.3
14		100	21.4	23.6	47.6:52.4
15		104	21.7	25.3	46.2:53.8
AV			19.9 ± 1.8	3.1 ± 1.5	46.4：53.6
16	C	88	18.8	21.7	46.4:53.6
17		92	19.6	22.5	46.6:53.4
18		96	21.5	24.5	46.7:53.3
19		100	22.1	25.9	46.0:54.0
20		104	22.7	27.2	45.5:54.5
AV			20.9 ± 1.7	24.4 ± 2.3	46.2：53.8

Table A.13 - Detailed measurement results of bodice-fit criteria for the body-type-specific modified prototypes

CG, cm	*a*				*b*				*c*				$(d_F + d_B)/2$			
	Y	A	B	C	Y	A	B	C	Y	A	B	C	Y	A	B	C
88	-1.5	-2	1.9	1.6	0	0	0	1.2	0	0	0	0	0.2	0.8	0.5	0.6
92	-1.3	1.6	0.8	1	0.1	0	0.4	1.3	0	0	0	0	0.7	0.7	0.8	0.8
96	1.2	-0.3	0	-1.2	0	0	0.2	0	0	0	0	0	0.8	0.2	0.2	0.4
100	2	-2.9	-1.5	1.6	0.4	0	0	0	0	0	2	0	0.7	0.8	0.7	0.6
104	1.9	1	1.8	1.6	0	0	2.3	2	0	0	0	0	0.5	0.6	0.8	1.2
Av	1.7				0.4				0.7				0.8			
	19				18				20				19			

Table A. 14 - Folds comparison of 3D shape for different prototypes and body shapes

Folds, amount	*P4*				*P5*				*P6*			
	Y	A	B	C	Y	A	B	C	Y	A	B	C
88	0	0	2	0	0	0	0	0	0	0	0	0
92	0	0	0	0	0	0	0	0	0	0	1	0
96	1	1	0	2	0	0	0	0	0	0	0	0
100	0	0	1	0	0	0	0	1	0	0	1	0
104	2	1	1	2	0	1	1	1	0	0	1	1
AV	0.6				0.2				0.2			

Table A.15 - FC comparison of 3D shape for different prototypes and body shapes

FC, cm	*P4*				*P5*				*P6*			
	Y	A	B	C	Y	A	B	C	Y	A	B	C
88	0	0	0	0	0.3	0.3	0.3	0	0.5	0.5	0.5	0.5
92	0	0	0	0	0.3	0.6	0.4	0.3	0.4	0.5	0.4	0.4
96	0	0	0	0	0.5	0.5	0.7	0.4	0.5	0.6	0.5	0.7
100	0	0.4	0.5	0.3	0.3	0.3	0.3	0.3	0.4	0.6	0.7	0.4
104	0.6	0	0	0.3	1.1	0.4	0.4	0.5	0.6	0.3	0.5	1.3
AV	0.1				0.4				0.5			

Table A.16 - a_s-b_s=0 comparison of 3D shape for different prototypes and body shapes

a_s-b_s=0	*P4*				*P5*				*P6*			
Y-yes, N-no	Y	A	B	C	Y	A	B	C	Y	A	B	C
88	Y	Y	Y	N	N	Y	Y	N	Y	Y	Y	N
92	Y	Y	Y	Y	Y	Y	Y	Y	Y	Y	Y	Y
96	N	Y	Y	N	Y	Y	N	Y	Y	Y	Y	Y

100	Y	N	Y	N	N	Y	Y	N	Y	Y	N	Y
104	Y	N	N	N	Y	N	N	N	Y	N	N	N
Y-amount	12				12				15			

Table A.17 - Complete measurement results of fold counts for P6(m) and P7 across 20 standardized virtual try-on samples

folds，*amount*	P6(m)				P7			
	Y	A	B	C	Y	A	B	C
88	0	0	1	0	0	0	0	0
92	0	0	0	0	0	0	0	0
96	0	0	0	0	0	0	0	0
100	0	1	1	0	0	0	0	1
104	0	0	0	1	0	0	0	1
AV	0.2				0.1			

Table A.18 - Complete measurement results of FC values for P6(m) and P7 across 20 standardized virtual try-on samples

***FC**, cm*	P6(m)				P7			
	Y	A	B	C	Y	A	B	C
88	1.5	1.2	0.8	0.7	1.5	1.2	1.4	1.2
92	1.2	0.5	0.4	0.9	1.2	1.3	1	1.4
96	1.2	0.8	0.5	0.4	1.2	1.5	1.5	1.2
100	0.4	0.6	1	0.4	1.3	1.5	1	1.2
104	1.0	0.5	0.6	0.3	1.0	1.3	1.7	0.5
AV	0.7				1.3			

Table A.19 - Table A.20 - Complete measurement results of $|a_s - b_s|$ values for P6(m) and P7 across 20 standardized virtual try-on samples

$\|a_s - b_s\|$，*cm*	P6(m)				P7			
	Y	A	B	C	Y	A	B	C
88	0.1	0.2	0.4	0.5	0	0.1	0.1	0.2
92	0	0	0.3	1.2	0	0	0.3	0.4
96	0.3	0.2	0.3	1	0.3	0.2	0.3	0.5
100	0.2	0	0.3	1	0.2	0	0.3	0.9
104	0.3	0.6	1.0	1.2	0.3	0.6	0.7	1.2

AV	0.5	0.3

Table A.20 - the validated working ranges for key sleeve pattern parameters (Style 3D perturbation tests)

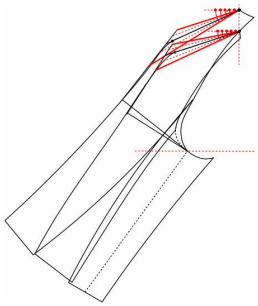						
Δ(∠BSS+∠FSS) [33°...54°]		33	40	47	54	61
Fit Level	FD	4.5	3.7	3.4	2.7	1.5
	Folds	2	0	0	0	1
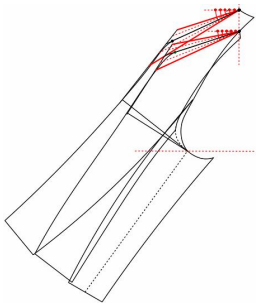			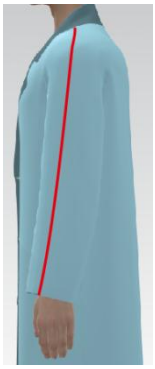	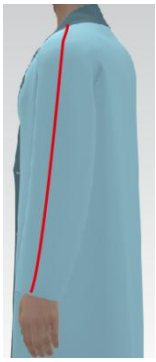	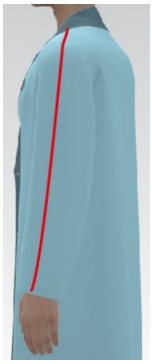	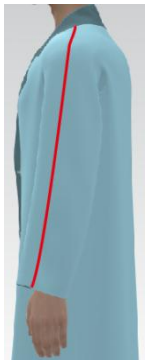
Δ(∠BSS -∠FSS) [-4.5°...12.4°]		-3	0	3	6	9
Fit Level	FC	2	1.8	1.5	1.3	1
	Folds	2	0	0	0	1
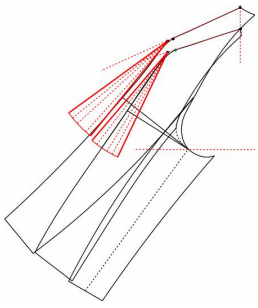						
Δ(∠BA+∠FA) [22.3°...72.4°]		54	60	66	72	84
Shape Level	FD	5.7	4.0	3.1	2.7	2.1
	Folds	2	0	0	0	1

c						
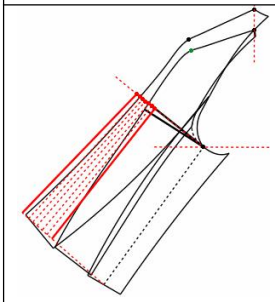						
Δ(BSW-FSW) [-0.7...8.3cm]		-0.5	2.5	5	7.5	9.5
Fit Level	|a-b|	2.2	0.3	0.7	0.5	0.5
	Folds	2	0	0	0	2
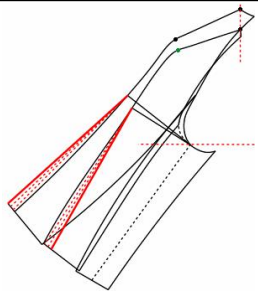						
Offset(SCL) [0...3.2cm]		0	1.5	2.5	3.5	
Fit Level	FC	0	0.3	0.7	1.8	
	Folds	2	0	0	0	

Table A. 21 - Effects of E(CG) distribution location and allocation proportion on raglan-coat sleeve shape ($E_{(CG)}$=16 cm)

2D pattern		3D shape		Fit level
Ease distribution	Ease proportion			
AHW （ *L(A)* ）				
① 33.3:33.3:33.3	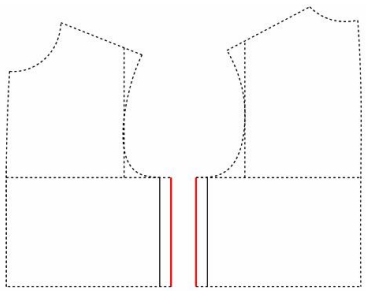		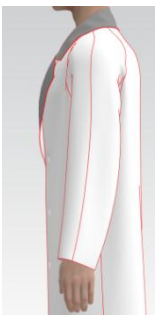	*NG*

② 16.7:33.3:50	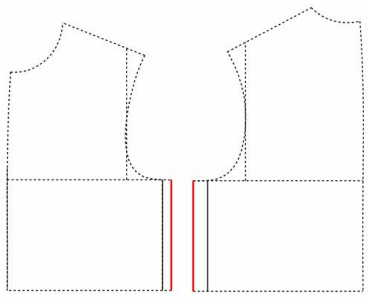	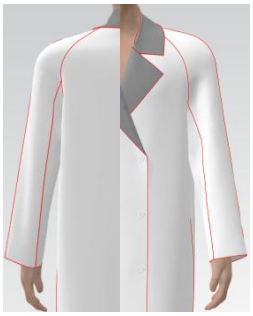		*NG*
③ 14.2:33.3:52.5	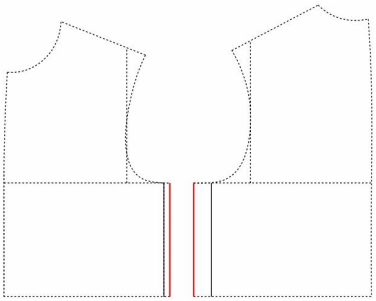			*NG*
FW - BW （ *L(F) / L(B)* ）				
① 33.3:33.3:33.3	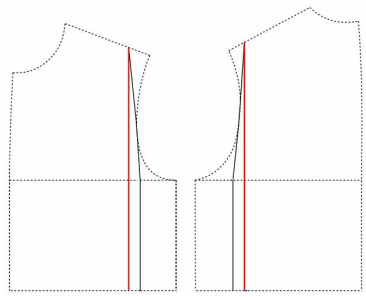			*NG*
② 16.7:33.3:50	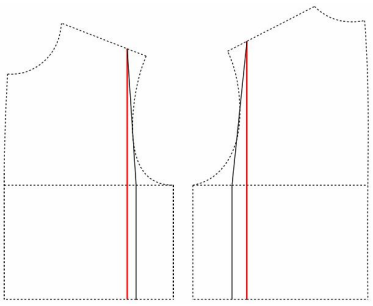	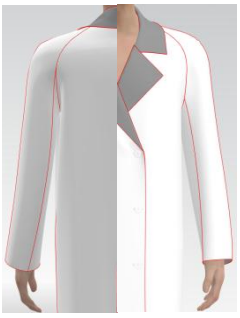		*G*
③ 14.2:33.3:52.5	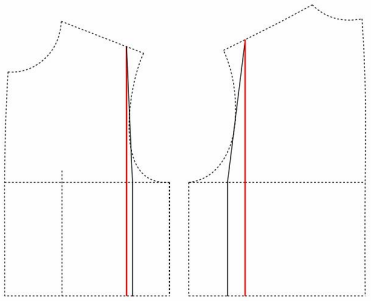		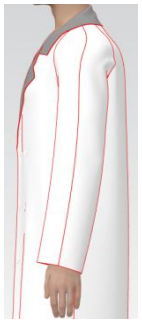	*NG*

Table A.22 - Optimization of key pattern parameters for raglan sleeve shape

Pattern Parameters		3D shape		Real shape		Optimization of Pattern （Red line）
		Before	After	Before	After	
①	Δ(FSS＋BSS），°					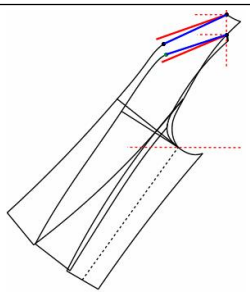
Good-fit Interval		32	47	32	47	[40...54]
Fit level		NG	G	NG	G	
②	Δ(BA＋FA)，°					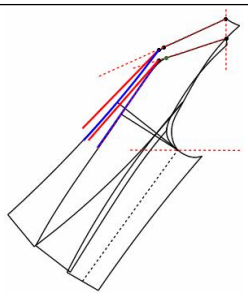
Good-fit Interval		54	66	54	66	[60...72]
Fit level		NG	G	NG	G	
③	Δ（BSW-FSW）,cm					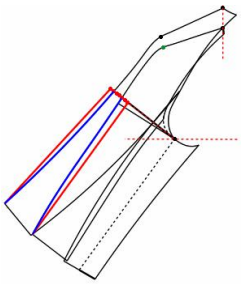
Good-fit Interval		0	3	0	3	[2.5...7.5]
Fit level		NG	G	NG	G	
④	Offset(SCL)，cm					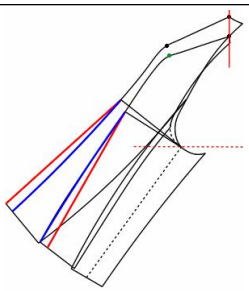
Good-fit Interval		0	2	0	2	[0...3.5]
Fit level		NG	G	NG	G	

⑤	E(CG) Distribution，cm					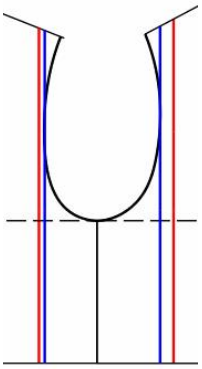 27.5:17.5:55
Good-fit Interval(%)		33.3:33.3:33.3	27.5:17.5:55	33.3:33.3:33.3	27.5:17.5:55	
		NG	G	NG	G	
⑥	E(CG) Values, cm					
		12	20	12	16	
		G	G	G	G	

Table A.24 - Image preprocessing and SSIM calculation procedure for the simplified-structure assessment

Step	Operation	Purpose
1	Image pair selection	The raglan coat with the collar, facing, and lining was compared with the same coat without these components.
2	View separation	Back, front, and side views were analyzed separately to avoid mixing view-dependent shape differences.
3	Foreground cropping	The garment area was cropped from the original image to reduce the influence of the background.
4	Size normalization	The paired images in each view were resized to the same image dimensions before SSIM calculation.
5	Grayscale conversion	The images were converted into grayscale images for global grayscale SSIM calculation.
6	Binary garment mask extraction	Garment masks were extracted to calculate silhouette-level SSIM and reduce the influence of local texture and lighting.

7	Edge and regional analysis	Edge- and region-based SSIM values were calculated to identify the main areas of local visual difference.
8	Result synthesis	The view-specific results were summarized in Table 3.5 to evaluate whether the simplified structure preserved the principal raglan-coat silhouette.

Table A.25 - Detailed SSIM results for the front-view comparison with and without the collar, facing, and lining

Analysis item	SSIM value	Main affected region	Interpretation
Global grayscale SSIM	0.806	Overall front view	The two front-view images showed relatively high overall image-structure similarity.
Garment-region grayscale SSIM	0.825	Main visible garment area	After reducing the influence of the background, skin, and inner garment, the front garment structure showed higher similarity.
Silhouette mask SSIM	0.883	External front contour	The main front-view external contour was largely preserved.
Contour-edge SSIM	0.902	Front garment boundary	The main garment boundary, sleeve boundary, and hem contour remained highly consistent.
Shoulder–neck region SSIM	0.779	Neckline and upper shoulder	Local differences were caused by the collar and upper neckline structure.
Upper sleeve–armhole region SSIM	0.743	Upper sleeve and raglan transition	The upper sleeve and shoulder transition showed local differences due to shadow and structural-edge changes.
Sleeve body–cuff region SSIM	0.813	Sleeve body and cuff	The sleeve body remained relatively consistent, with minor differences in cuff and hand position.
Front bodice region SSIM	0.879	Main front bodice	The front bodice contour and vertical surface showed high structural consistency.
Lower hem–bodice region SSIM	0.903	Lower front bodice and hem	The lower garment region was highly similar under the two structural conditions.

Table A.26 - Detailed SSIM results for the side-view comparison with and without the collar, facing, and lining

Analysis item	**SSIM value**	**Main affected region**	**Interpretation**
Global grayscale SSIM	0.766	Overall side view	The two side-view images showed a relatively high level of overall image-structure similarity, although local visual differences were visible.
Silhouette mask SSIM	0.887	External side contour	The principal side-view silhouette was largely preserved.
Edge / structural-line SSIM	0.83	Side outline and sleeve boundary	The side contour and sleeve boundary remained relatively consistent.
Shoulder–neck / upper-sleeve region SSIM	0.78	Shoulder, neck, and upper sleeve	Local differences were mainly caused by the collar and shoulder–neck transition.
Sleeve body–cuff region SSIM	0.789	Sleeve body and cuff	Minor differences were observed in the sleeve–arm spatial relationship and cuff area.
Lower hem–bodice region SSIM	0.936	Lower side bodice and hem	The lower side contour and hem region showed very high similarity.

Table A.27 - Detailed SSIM results for the back-view comparison with and without the collar, facing, and lining

Analysis item	SSIM value	Main affected region	Interpretation
Global grayscale SSIM	0.775	Overall back view	The two back-view images showed a relatively high level of overall image-structure similarity.
Silhouette mask SSIM	0.885	External back contour	The main back-view external contour was largely preserved after removing the collar, facing, and lining.
Edge / structural-line SSIM	0.868	Back outline and sleeve boundary	The main garment boundary remained consistent, although local edge differences were visible.

Shoulder – neck / back-collar region SSIM	0.772	Back neck and collar area	The visible difference was mainly caused by the presence or absence of the collar.
Raglan sleeve – shoulder transition SSIM	0.71	Back shoulder and upper sleeve	The shoulder – sleeve transition was locally affected by collar-related thickness and shadow changes.
Sleeve body – cuff region SSIM	0.717	Sleeve body and cuff	Differences were observed in sleeve shadow and hand position, but the sleeve outer contour remained stable.
Back bodice region SSIM	0.831	Main back bodice	The back bodice surface and vertical structure showed relatively high consistency.
Lower hem – bodice region SSIM	0.827	Lower back bodice and hem	The lower body and hem region showed limited shape variation.

APPENDIX B.

Results of Accuracy and Robustness Verification for AI Generation of the "Body + Coat" System

Table B.1 - Cumulative mean ± SD of the seven projection parameters at different sample-size levels

Parameter	Real body	n = 5	n = 10	n = 15	n = 20	n = 25	n = 30
W_S	44.6	44.74 ± 0.64	44.88 ± 0.56	44.84 ± 0.56	44.72 ± 0.51	44.84 ± 0.59	44.86 ± 0.51
W_C	33.30	33.80 ± 0.27	33.46 ± 0.67	33.51 ± 0.75	33.54 ± 0.68	33.55 ± 0.68	33.6 ± 0.63
W_W	29.50	28.54 ± 0.79	29.06 ± 0.83	29.19 ± 0.74	29.17 ± 0.73	29.18 ± 0.73	29.19 ± 0.74
W_H	35.30	35.78 ± 0.30	36.08 ± 0.69	35.77 ± 0.80	35.76 ± 0.75	35.72 ± 0.69	35.75 ± 0.68
W_A	9.10	9.52 ± 0.44	9.67 ± 0.46	9.79 ± 0.50	9.75 ± 0.54	9.72 ± 0.54	9.76 ± 0.32
W_E	8.00	8.64 ± 0.42	8.70 ± 0.50	8.68 ± 0.45	8.49 ± 0.44	8.60 ± 0.43	8.60 ± 0.52
W_{Wr}	6.00	5.58 ± 0.18	5.56 ± 0.35	5.54 ± 0.32	5.51 ± 0.30	5.40 ± 0.35	5.52 ± 0.51
Note: n = 5, 10, 15 denote cumulative sample sets constructed from the first 5, 10, 15, 20,25 and 30 consecutively generated valid AIB images, respectively.							

Table B.2 - Cumulative absolute mean deviations from the real body and overall mean absolute deviation at different sample-size levels

Parameter	n = 5	n = 10	n = 15	n = 20	n=25	n=30
$\lvert MD(S_W)\rvert$	0.14	0.28	0.24	0.21	0.24	0.26
$\lvert MD(C_W)\rvert$	0.5	0.16	0.21	0.24	0.25	0.3
$\lvert MD(W_W)\rvert$	0.96	0.44	0.31	0.33	0.32	0.31
$\lvert MD(H_W)\rvert$	0.48	0.78	0.47	0.45	0.42	0.45
$\lvert MD(A_W)\rvert$	0.42	0.57	0.69	0.65	0.62	0.66
$\lvert MD(E_W)\rvert$	0.64	0.7	0.68	0.69	0.60	0.60
$\lvert MD(WW_r)\rvert$	0.42	0.44	0.46	0.49	0.60	0.48
OMD	**0.509**	**0.481**	**0.438**	**0.435**	**0.436**	**0.437**
Note: MD denotes the difference between the cumulative mean of the generated AIBs and the corresponding real-body value. OMD denotes the overall mean absolute deviation averaged across the seven projection parameters.						

Table B.3 - Incremental changes in cumulative means between adjacent sample-size levels

Parameter	5 → 10	10 → 15	15 → 20	20 → 25	25 → 30
SW	0.14	0.04	0.03	0.03	0.02
CW	0.34	0.05	0.03	0.00	0.06
WW	0.52	0.13	0.02	0.01	0.01
HW	0.3	0.31	0.02	0.03	0.01
AW	0.15	0.12	0.04	0.03	0.04
EW	0.06	0.02	0.01	0.09	0.00
WrW	0.02	0.02	0.03	0.03	0.04

Note: values indicate the absolute change in cumulative mean after adding the next 5 generated samples.

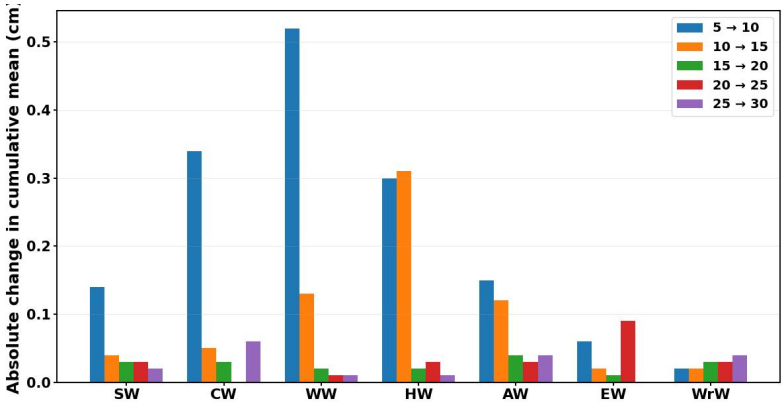

Figure B.1 - Change in the overall mean absolute deviation with increasing sample size

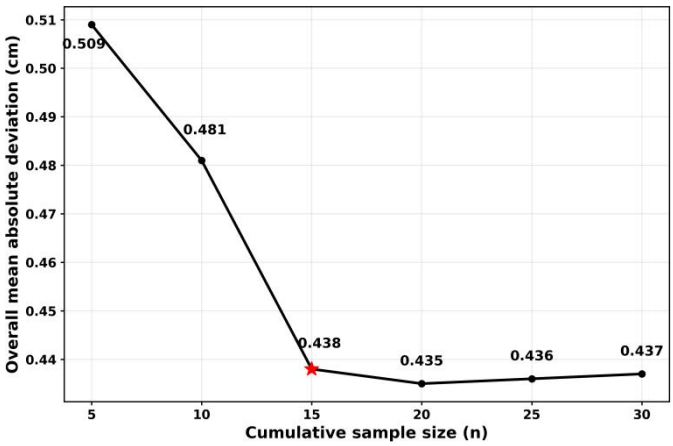

Figure B.2 - Incremental changes in cumulative means of the seven projection parameters at different sample-size levels

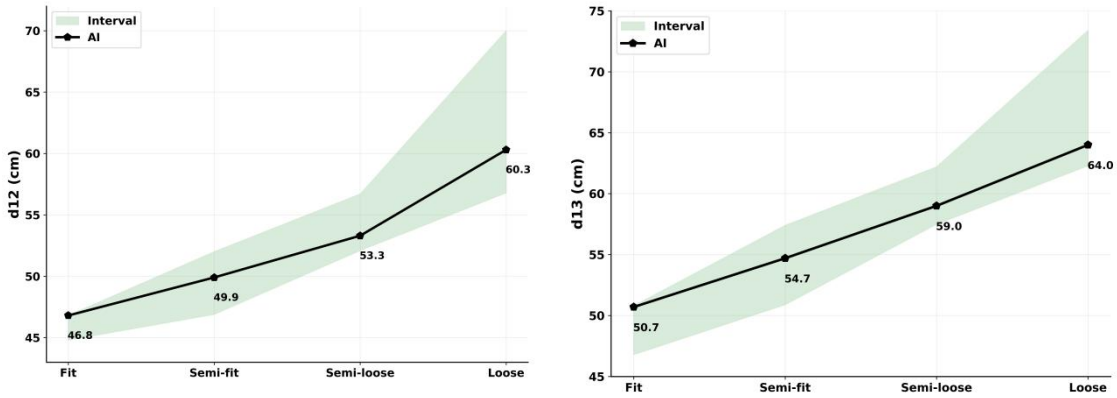

d_{12} d_{13}

Figure B.3 - Volume–silhouette shapes generated at the armhole line (left) and elbow line (right) configurations

E(CG),cm	Cotton	Polyester	Wool	Cotton	Polyester	Wool
12						
16	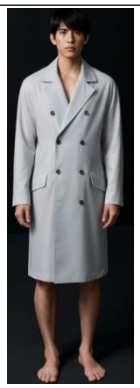					
20			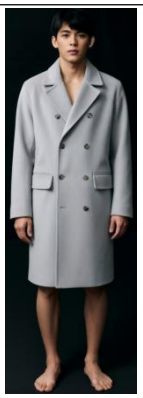			

28					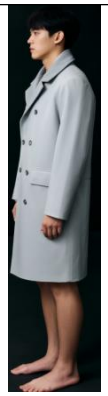	

Figure B.4 - AI-generated raglan coats across cotton, polyester, and wool under four chest-ease levels

Table B.4. - Projection deviations of AIB compared with RB (cm, °)

No.	ΔW_S	ΔW_C	ΔW_W	ΔW_H	ΔW_A	ΔW_E	ΔW_{wr}
1	-0.4	0.5	-0.5	0.7	0.2	0	-0.6
2	0.6	0.8	0.3	0.7	0.9	1	-0.3
3	-0.6	0.7	-1	0.7	-0.1	0.7	-0.2
4	0.2	0.4	-0.8	0.1	0.5	0.5	-0.4
5	0.9	0.1	-0.7	0.2	0.4	1	-0.6
6	0.7	0.7	0.5	1	1.3	1.7	-0.8
7	0.4	-0.3	0	1.7	0.5	0.5	0
8	1.1	-0.5	0.5	1.4	1	0	1
9	-0.2	0.5	0.5	1.7	0.7	0.9	-1
10	0.1	-1.3	-0.7	-0.4	0.1	0.7	-0.6
11	1.2	1.7	0.6	-0.9	1.2	0.2	-0.7
12	-0.2	-0.3	-0.1	0.4	0.2	0.4	-0.2
13	0.2	-0.1	-0.3	-0.4	0.8	0.9	-0.7
14	-0.1	-0.6	-0.7	-0.5	1.1	0.6	-0.7
15	-0.3	0.9	0.3	0.7	0.9	1.1	-0.7
16	0.6	0.7	0.5	0.8	1.3	0	-0.8
17	0.4	0.7	-0.9	-0.6	-0.2	0.4	-0.3
18	-0.1	0.2	-0.6	0.1	0.6	1	-0.6
19	0.1	0.7	-1.1	0.8	-0.1	0.4	-0.8
20	-0.3	-0.3	0.3	0	0	0.2	-0.8
MD	*0.22± 0.24*	*0.26± 0.32*	*–0.20 ± 0.28*	*0.41 ± 0.34*	*0.57 ± 0.23*	*0.61± 0.21*	*–0.49± 0.20*

Table B.5 - Intertemporal comparison of AIB projection parameters generated using the same multimodal prompt

Parameter, cm	RB	Mean, 2025.03.14	Mean, 2026.04.22	Mean difference
S_W	44.6	44.72 ± 0.51	44.74 ± 0.52	0.02
C_W	33.3	33.54 ± 0.68	33.78 ± 0.50	0.24
W_W	29.5	29.17 ± 0.73	29.32 ± 0.58	0.15
H_W	35.3	35.76 ± 0.75	35.79 ± 0.67	0.03
A_W	9.1	9.75 ± 0.54	10.05 ± 0.39	0.3
E_W	8	8.49 ± 0.44	8.69 ± 0.38	0.2
W_{Wr}	6	5.51 ± 0.30	5.66 ± 0.25	0.15

Table B.6 - The deviation of body projection parameters

Parameter, unit (cm,°)	Body dimensions				Deviation between RB dimensions and		
	RB	VB	AIB_A	AIB_B	Δ1	Δ2	Δ3
Heights, cm							
H	182	182	182	182	0	0	0
H_S	149.2	144.2	146.7	150.7	5	2.5	-1.5
H_C	131.6	130.7	136.7	132.6	0.9	-5.1	-1
H_U	84.5	85.8	87	84.8	1.3	3.5	0.3
H_W	114.5	117.4	120.2	116.7	-2.9	-5.7	-0.2
H_H	90.3	93.1	97.6	93	-2.8	-7.3	-2.7
H_F	150.3	150.7	152.8	150.7	-0.4	-2.5	-0.4
H_B	157.9	153.7	155.3	157.2	4.2	2.6	0.7
MD_H					*0.7±2.4*	*-1.5±3.5*	*-0.6±0.9*
Front widths, cm							
W_S	44.6	45.3	42.8	45.2	-0.7	1.8	-0.6
W_C	33.3	32.5	32.7	32.9	0.8	0.6	0.4
W_W	29.3	29.5	27	28.8	-0.2	2.3	0.5
W_H	35.3	35.3	35	35.1	0	0.3	0.2
W_A	9.1	9.4	9.6	9	-0.3	-0.5	0.1
W_E	8	7.7	8.2	8.5	0.3	-0.2	-0.5
W_{Wr}	6	5.7	5.8	5.2	0.3	0.2	0.8
MD_W					*0.1±0*	*0.7±1.*	*0.1±0.*

					.5	*0*	*5*
Profile widths, cm							
D_C	26.7	26.7	26.6	26.6	0	0.1	0.1
D_W	22.7	22.7	21.8	22.4	0	0.9	0.3
D_H	26.2	26.9	26.3	26.4	-0.7	-0.1	-0.2
D_A	11.4	11.4	11.5	11.4	0	-0.1	0
D_E	8.9	8.9	9.4	9	0	-0.5	-0.1
D_{Wr}	6.5	6	6.9	6.2	0.5	-0.4	0.3
MD_D					*-0.03 ±0.4*	*-0.02± 0.5*	*0.07± 0.2*
Angles, ˚							
∠E	165.8	167.8	156.1	167.2	-2	9.7	-1.4
∠1	19	20.7	25.8	17.7	-1.7	-6.8	1.3
∠2	15	11.2	15	10.6	3.8	0	4.4
∠3	19.2	26.9	20.6	20.8	-7.7	-1.4	-1.6
MD_A					*-1.9± 8.5*	*0.4±10 .9*	*0.7±4. 5*

Table B.7 - Accuracy comparison between RC, VC, and AIC (cm, ˚)

Parameter, unit(cm, ˚)	Coat dimensions			Differences between RC and	
	RC	VC	AIC	VC	AIC
				Δ2’	Δ3’
Front widths, cm					
W'_C	37.1	36.8	36.9	-0.3	-0.2
W'_W	37.3	35.8	36.5	-1.5	-0.8
W'_H	38.8	37.8	38.6	-1	-0.2
W'_A	9.0	10.8	9.6	1.8	0.6
W'_E	11.2	10.3	10.8	-0.9	-0.4
W'_{Wr}	11.4	9.5	10.3	-1.9	-1.1
W'_S	48.8	47.9	48.1	-0.9	-0.7
MD'_W				*-0.7±1.1*	*-0.4±0.5*
Profile widths, cm					
D'_C	33.9	28.8	33.7	-5.1	-0.2
D'_W	35	30.7	35.4	-4.3	-0.4
D'_H	35.4	30.3	36.2	-5.1	-0.8
D'_A	18.9	13	18.2	-5.9	-0.7

D'_E	17.3	13	16.4	-4.3	-0.9
D'_{Wr}	15.1	12	12	-3.1	-3.1
MD'_D				-4.6±1.0	-1.0±1.1
Angles, °					
∠S’	23.4	18.5	22.8	-4.9	-0.6
∠A	125.3	122.8	126.4	-2.5	-1.1
MD'_A				*-3.7±15.2*	*-0.9±3.2*

Table B.8 - Accuracy of AIB_C (cm, °)

Parameters, unit(cm，°)	Body dimensions			Differences between RB dimensions and		Differences between
	RB	AIB_B	AIB_C	AIB_B	AIB_C	AIB_B and AIB_C
				Δ3	Δ4	Δ5
Heights, cm						
	182	182	182	0	0	0
H_S	149.2	150.7	146	-1.5	-0.8	0.7
H_C	131.6	132.6	132.2	-1	-0.6	0.4
H_U	84.5	84.8	84.8	0.3	0.3	0
H_W	114.5	116.7	114.1	-0.2	0.4	0.6
H_H	90.3	93	91.4	-2.7	-1.1	1.6
H_F	150.3	150.7	148.4	-0.4	1.9	2.3
H_B	157.9	157.2	157.2	0.7	0.7	0
MD_H				*-0.6±0.9*	*0.1±0.8*	*0.7±0.7*
Front widths, cm						
W_S	44.6	45.2	45.5	-0.6	-0.9	-0.3
W_C	33.3	32.9	33.9	0.4	-0.6	-1
W_W	29.3	28.8	29.5	0.5	-0.2	-0.7
W_H	35.3	35.1	37	0.2	-1.7	-1.9
W_A	9.1	9	9.5	0.1	-0.4	-0.5
W_E	8	8.5	8.5	-0.5	-0.5	0
W_{Wr}	6	5.2	5.6	0.8	0.4	-0.4
MD_W				*0.1±0.5*	*-0.6±0.6*	*-0.7±0.6*
Profile widths, cm						
D_C	26.7	26.6	25.9	0.1	0.8	0.7
D_W	22.7	22.4	22.8	0.3	-0.1	-0.4
D_H	26.2	26.4	26.0	-0.2	0.2	0.4

D_A	11.4	11.4	11.2	0	0.2	0.2
D_E	8.9	9	8.8	-0.1	0.1	0.2
D_{Wr}	6.5	6.2	6.2	0.3	0.3	0
MD_D				*0.1±0.2*	*0.3±0.3*	*0.2±0.4*
Angles, °						
∠S	22.8	23.5	24.3	-0.7	-1.5	-0.8
∠E	165.8	167.2	166.1	-1.4	-0.3	1.1
∠1	19	17.7	17.1	1.3	1.9	0.6
∠2	15	10.6	11	4.4	4	-0.4
∠3	19.2	20.8	16.7	-1.6	2.5	4.1
MD_A				*0.4±3.1*	*1.3±2.7*	*0.9±2.4*

Table B.9 - Accuracy of AICs with different volume-silhouette shapes

Parameters, unit(cm, °)	Shapes											
	Fit			Semi-fit			Semi-loose			Loose		
	S1			*S2*			*S3*			*S 4*		
	RC_{S1}	AIC_{S1}	Δ_{S1}	RC_{S2}	AI_{S2}	Δ_{S2}	RC_{S3}	AIC_{S3}	Δ_{S3}	RC_{S4}	AIC_{S4}	Δ_{S4}
Front widths, cm												
W'_C	35.2	34.8	-0.4	35.6	35.4	-0.2	36.5	36.5	0	38.7	38.6	-0.1
W'_W	32.8	32.2	-0.6	33.4	33	-0.4	34.2	34.3	0.1	38.0	37.8	-0.2
W'_H	35.4	35.8	0.4	36.6	36.5	-0.1	38.0	37.8	-0.2	39.8	39.2	-0.6
W'_A	7.2	6.3	-0.9	7.1	7.3	0.2	9.3	8.5	-0.8	10	11.0	1
W'_E	8.3	7.8	-0.5	9.9	10.3	0.4	11.6	12	0.4	12	13	1
W'_{Wr}	7.7	7.2	-0.5	9.6	9.2	-0.4	10.1	10.5	0.4	11.1	12.1	1
WS	43.3	43.7	0.4	44.2	44.5	0.3	46.3	46.9	0.6	47.5	47.7	0.2
MD_W	*-0.3 ± 0.5*			*-0.03 ± 0.3*			*0.1 ± 0.4*			*0.3 ± 0.6*		
Profile widths, cm												
D'_C	29.3	30.9	1.6	31.9	32.8	0.9	33.2	33.6	0.4	33	33.5	0.5
D'_W	31.4	31.5	0.1	33.4	33.3	-0.1	33.9	34.4	0.5	34.4	34.7	0.3
D'_H	33.2	34.5	1.3	36.1	35.9	-0.2	36	36.4	0.4	36.4	37	0.6
D'_A	13.6	14.3	0.7	14.2	14.9	0.7	15.8	16.1	0.3	16.2	16.7	0.5
D'_E	12.7	12.1	-0.6	13.7	14	0.3	15.4	15.4	0	16.2	16.4	0.2
D'_{Wr}	11	10.7	-0.3	11.7	11.3	-0.4	11.9	11.9	0	13.1	12.9	-0.2
MD_D	*0.5 ± 0.9*			*0.2 ± 0.5*			*0.3 ± 0.2*			*0.3 ± 0.3*		
Angles,°												
∠S'	30.9	32.6	1.7	29.3	29.8	0.5	28.4	27.9	-0.5	26.5	26	-0.5
∠A	127.6	130.5	2.9	127.4	129	1.6	128.0	128.5	0.5	125	128	3
MD_A	*2.3 ± 7.6*			*1.1±7.0*			*0 ± 6.4*			*1.3 ± 22.2*		

Table B.10 - 2.5D projection parameters of AI-generated raglan coats across cotton, polyester, and wool under four predefined chest-ease levels (12, 16, 20, and 28 cm)

Parameters, unit (cm, °)	S1			S2			S3			S4		
	Cotton	Polyester	Wood	Cotton	Polyester	Wood	Cotton	Polyester	Wood	Cotton	Polyester	Wood
W'_C	33.9	34.2	34.8	35	34.9	35.4	36	36.5	36.5	37.9	38.3	38.6
W'_W	32.2	31.8	32.2	33.4	33.8	34	34.7	34.8	34.2	36.9	37.3	37.8
W'_H	36	35.9	35.8	36.9	36.5	36.5	36.3	37.3	38	38.4	38.7	39.2
W'_A	6.2	6.3	6.3	7.8	8.1	7.3	9.2	9.3	9.3	11.2	11.5	11
W'_E	8.3	7.5	7.8	10.7	10.9	10.3	11.2	11.5	11.6	12.8	13.1	13
W'_{Wr}	7.4	7.1	7.2	8.9	9.3	9.2	10.4	11.3	10.1	11.5	11.7	12.1
W_S	43.6	43.2	43.7	43.6	43.7	44.5	45.3	46	46.3	47.4	47.2	47.7
D'_C	29.3	30.6	30.9	30.2	31.4	32.8	32.4	33.1	33.2	33.2	33.4	33.5
D'_W	28.5	29.6	31.5	32.8	32.9	33.3	32.7	33.9	33.9	32.8	33.2	34.7
D'_H	33	33.5	34.5	34.7	35.1	35.9	35.9	36.7	36	36.9	37.3	37
D'_A	14	14.1	14.3	14.7	14.6	14.9	15.2	15.7	15.8	15.8	16.3	16.7
D'_E	12.6	12.6	12.1	12.9	13.4	14	15.0	15.6	15.4	16.1	16.4	16.4
D'_{Wr}	9.9	10.7	10.7	11.7	12.4	11.3	12.3	11.9	11.9	12.7	12.9	12.9
∠S’	30.2	32.2	32.6	27.9	30.1	29.8	27.3	29.3	28.4	25.3	25.9	26
∠A	134.2	140.6	130.5	137	141.1	129.2	134.2	130.2	128	130.4	137.8	128

Table B.11 - Inter-fabric differences in 2.5D projection parameters relative to the wool baseline across S1 – S4

Parameters, unit(cm, °)	S1		S2		S3		S4	
	Cotton-wood	Polyester-wood	Cotton-wood	Polyester-wood	Cotton-wood	Polyester-wood	Cotton-wood	Polyester-wood
W'_C	-0.9	-0.6	-0.4	-0.5	-0.1	0.1	-0.6	-0.2
W'_W	0	-0.4	-0.6	-0.2	-0.2	-0.4	0.2	0.2
W'_H	0.2	0.1	0.4	0	0.1	0.4	-0.4	-0.3
W'_A	-0.1	0	0.5	0.8	-0.8	-0.3	1.1	-0.5
W'_E	0.5	-0.3	0.4	0.6	-0.9	-0.2	0.8	-0.7
W'_{Wr}	0.2	-0.1	-0.3	0.1	-0.2	-0.4	0.5	0.2
WS	-0.1	-0.5	-0.9	-0.8	0.3	-0.1	-0.7	0.4
D'_C	-1.6	-0.3	-2.6	-1.4	1.1	-1.2	-0.2	2.3
D'_W	-3	-1.9	-0.5	-0.4	-1.5	-0.1	-0.3	-1.4
D'_H	-1.5	-1	-1.2	-0.8	-0.2	-0.4	-0.4	0.2
D'_A	-0.3	-0.2	-0.2	-0.3	0.1	0.1	-0.4	0

D’$_E$	0.5	0.5	-1.1	-0.6	1.1	-0.5	-0.1	1.6
D’$_{Wr}$	-0.8	0	0.4	1.1	-1.1	-0.7	1.8	-0.4
∠S’	-2.4	-0.4	-1.9	0.3	-0.7	-2.2	2.5	1.5
∠A	3.7	10.1	7.8	11.9	-1.8	-4.1	16	2.3

Table B.12 - d12 and d13 values of AI-generated raglan coats across cotton, polyester, and wool under four predefined volume – silhouette categories, together with the corresponding interval ranges

Fabric	d12, cm				d13, cm			
	S1	S2	S3	S4	S1	S2	S3	S4
Interval	44.8... 46.8	46.9... 52	52.1... 56.7	56.8... 70	46.8... 50.8	50.9... 57.4	57.5... 62.2	62.3... 73.4
Cotton	45.3	49.1	53.8	60.3	48.8	54.1	58.4	63.4
Polyester	46.8	51.1	53.9	61.3	50.2	55.6	59.5	64.5
Wood	46.8	49.9	53.3	60.3	50.7	54.7	59	64

Table B.13 - Complete projection-parameter datasets of RC, AIC, and VC across *S1...S4*

cm	RC				AIC				VC			
	S1	S2	S3	S4	S1	S2	S3	S4	S1	S2	S3	S4
W'$_S$	22.7	23.5	25.8	26.5	22.7	23.2	24.7	27	21.5	20.8	20.3	26.5
W'$_C$	18.2	18.8	20.5	20.6	18.3	18.9	20	20.7	18.5	18.5	19.6	19.6
W'$_W$	19.3	20.1	20	20.5	18.6	19.3	20	21.2	18.2	19.5	20.1	20.4
W'$_H$	18.4	21.7	22	22.8	18.3	21.4	22	23.2	18.5	20.4	21.3	21.5
W'$_A$	8.7	9	10	11.5	8.8	9.3	10.5	11.7	7.4	8.1	9	9.5
W'$_E$	10.2	10.4	11	12	10.3	11.2	11.9	12.3	10.5	10.5	9.8	11.2
W'$_{wr}$	10.4	11.6	12.5	13.7	9.4	11.4	12	13.8	8.4	9.8	10.6	10.8
∠S'°	22.7	22	23.6	24	25.5	24.5	25	23.6	18.7	19.3	17.4	18.3
∠A°	139.5	140	138.9	138	137.2	138	137.8	139.8	138.7	130.6	130.6	130.6
D'$_C$	30.8	31.4	32.2	32.8	30.9	31.4	32.9	33.6	32.3	30.8	32.2	32.2
D'$_W$	31.8	32.3	33.6	34.7	32.8	33.8	34.1	35.7	33.3	31.9	33.5	32.8
D'$_H$	33.5	34.3	35	36.2	33.8	35.5	36	37.7	32.9	32.7	35.1	35.7
D'$_A$	14.5	15.3	16	18.7	14.8	15.3	16.7	18.3	14.6	15.3	15.2	15.6
D'$_E$	13.2	13	13.9	17.7	13.3	13.7	14.7	17	14.5	16.8	15.7	17.3
D'$_{wr}$	11.9	13.4	14	15.6	11.9	12.5	13.9	15.3	12.7	14.9	13.4	13.8

Table B.14 - Basic structure of prompt for iterative refinement of AIC

No.	Item	Content
1	Role	Defect-guided iterative refinement system for AI-generated raglan-coat images
2	Objective	Refine an already generated AIC image by correcting the specified local structural defects while preserving the valid global silhouette, garment–body relationship, and view consistency.
3	Primary priority	Local structural correction with maximum preservation of the original valid shape. Structural accuracy, sleeve–arm fit logic, and silhouette stability should be prioritized over stylistic variation or decorative effects.
4	Input parameters	The input should include: (1) the original generated image; (2) the target view (front, side, or back, as required); (3) the identified defect type; (4) the textual description of the correction objective; and (5) the requirement to preserve the unchanged regions and the original silhouette category.
5	Structural constraints	The refinement should focus only on the defect-related region. The valid global silhouette, garment category, coat length, sleeve topology, body pose, and view orientation should remain unchanged unless otherwise specified. The refined result should preserve the raglan-sleeve structure and maintain plausible garment–body interaction.
6	Stylization policy	Low stylization and high structural fidelity. The refined image should remain realistic, visually stable, and suitable for evaluation-oriented comparison. Decorative exaggeration and unnecessary redesign should be avoided during refinement.
7	Negative prompt	Do not redesign the garment. Do not change the silhouette category. Do not alter the body pose, coat length, or valid structural regions. Avoid introducing new folds, distorted sleeve geometry, incorrect cuff shape, excessive smoothing, perspective distortion, or unrelated visual changes.
8	Output	A refined AIC image in the same view, with the specified local defect corrected and the valid overall “body+coat” structure preserved, suitable for subsequent visual comparison and projection-based evaluation.

APPENDIX C.

Materials for Verification and Effectiveness Evaluation of the Proposed Raglan Coat Design Method

Table C.1 - Traditional pattern-making of raglan coat, cm

Segment	Rules of construction
94'-940'	Increase back armhole depth (E(CG)-8)/3
12-940"	Back raglan seam line
T10-T11, **T10-T12**,	10cm
T11-T13	Back shoulder-sleeve angle: **T11-T12** /2
T54-T540	Sleeve center line offset at the cuff by 2 cm.
T540-T56'	8cm-**T556'-T50**
94"-940"	Increase front armhole depth(E(CG)-8)/3
27-940'	Front raglan seam line
T10'-T11', **T10'-T12'**	10cm
T11'-T13"	Back shoulder-sleeve angle: **T11'-T12'** /2+3
T54'-T540'	2cm
T52-T540'	8cm- **T50-T52**

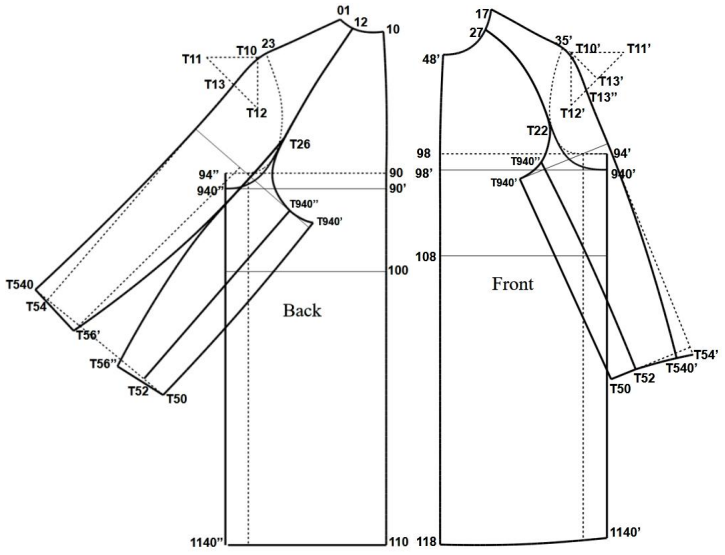

Table C.2 - Accuracy comparison between real coat and real improved coat (cm, °)

Parameter	Coat measurements		
	Real coat	Real improved coat	Δ=Real improved coat - Real coat
Front widths, cm			
W'_C	38.7	38.3	-0.4
W'_W	38.1	38.1	0
W'_H	39.0	38.6	-0.4
W'_A	6.7	8.6	1.9
W'_E	10.1	10.5	0.4
W'_{Wr}	9.1	9.5	0.4
W'_S	44.1	43.6	-0.5
MD'_W			*0.2±0.8*
Profile widths, cm			
D'_C	31.2	30.5	-0.7
D'_W	32.2	31.8	-0.4
D'_H	31.9	31.5	-0.4
D'_A	15 .5	16.2	0.7
D'_E	16.7	15.6	-1.1
D'_{Wr}	14.5	12.1	-2.4
MD'_D			-0.7±1.1
Angles, °			
∠S’	26.0	25.5	0.5
∠A	52.7	57.8	5.1
MD'_A			2.8±29.2
Note: the definition of parameters is in Table 2.7			

Table C.3 - Definition and correspondence of key development links used in the engineering-efficiency comparison

No.	Key development link in the traditional route	Status in the proposed route	Basis for reduction
1	Style analysis and size determination	Retained	A basic input step is required in both routes
2	Basic prototype adjustment	Retained but shortened	Reduced by using the corrected prototype as a stable baseline
3	Raglan division-line trial adjustment	Reduced	Partly replaced by the established pattern-generation logic

4	Sleeve structure trial conversion	Retained but shortened	Reduced by parameterized sleeve-generation procedures
5	Underarm mobility adjustment	Reduced	integrated into controlled pattern-parameter setting
6	Collar and lapel drafting	Retained	Style-dependent fixed step
7	Lining pattern drafting	Retained	Unchanged technical step
8	Interfacing and auxiliary pattern drafting	Retained	Unchanged technical step
9	Pattern matching and consistency check	Retained but shortened	Reduced by earlier verification and more stable pattern relationships
10	Muslim / physical trial correction	Reduced	Partially replaced by virtual and parameter-based pre-correction
11	First fitting modification	Retained	still required for final confirmation
12	Second fitting modification	Removed	Avoided by earlier controlled correction and reduced trial-and-error

Table C.4 - Stage-based time estimation for first-sample development using the traditional and proposed methods

Stage	Traditional method, h	Proposed method, h	Included in the main efficiency index	Note
Style analysis and prototype preparation	4	1	Yes	Reduced by using a corrected prototype baseline
Core structural drafting	8.5	3.5	Yes	Reduced by parameterized raglan drafting
Lining and interfacing pattern drafting	3.5	3.5	Yes	Unchanged technical step
Checking and correction	3	1	Yes	Reduced by earlier verification
Pattern-development subtotal	19	9	Yes	Corresponds to “ pattern-development time” in Section 5.1.5
Fixed garment assembly	7	7.0*	No	Treated as a constant production step
Fitting-related modification	24	12	Yes	Two rounds reduced to one

Development-stage total	43	21	Yes	Main efficiency index used in Section 5.1.5
Overall first-sample cycle	50	28.0*	No	Not used in the main text

Table C.5 - Estimated cost composition for first-sample development under the same material assumption

Cost item	Traditional method, RMB	Proposed method, RMB	Note
Direct material cost	200	200	Same material assumption
Pattern-development fee	400	200	Reduced by parameterized drafting workflow
Sample processing and correction cost	200	100	Reduced due to fewer fitting-related modifications
Estimated first-sample development cost	800	500	Corresponds to Section 5.1.5

APPENDIX D.

Certificates of Industrial Validation of the Proposed Method for Raglan Coat Design

УТВЕРЖДАЮ
Ректор ИВГПУ
Никифорова Е.Н.
"__" _____ 2026 г.

УТВЕРЖДАЮ
Генеральный директор
АО "Сударь" Степанова Е.К.
"05" 05 2026 г.

Акт приема модели
на художественно-техническом совете АО "Сударь"

На художественно-технический совет (далее ХТС) представлена модель пальто с рукавом реглан (мод.PE37R), разработанная Цзя Шуан, аспирантом ИВГПУ. Разработка лекал для мод.PE37R производилась под руководством заведующего кафедрой конструирования швейных изделий ИВГПУ Кузмичевым В.Е.

По предоставленным лекалам на АО "Сударь" было принято решение отшить образец пальто из ткани с высоким содержанием шерсти (70% шерстяное волокно, 30% полиэстр) в коллекцию Осень-Зима 2026 года в размере 100/176.

В процессе подготовки к пошиву были внесены изменения в лекала с целью их адаптации для внедрения в массовое производство. Примерка модели показала удовлетворительную посадку на фигуре. Модель пальто PE37R была презентована на ХТС, по результатам которого рекомендована к показу оптовым покупателем и дальнейшему запуску в массовое производство.

Внедрение данной модели пальто позволит расширить модельный ряд верхней одежды предприятия АО "Сударь" и удовлетворить спрос потребителей различных возрастных групп.

Заведующий кафедрой КШИ ИВГПУ
_____ Кузьмичев В.Е

Руководитель Службы
подготовки производства
_____ Кочетова Т.Ю.

Аспирант ИВГПУ
_____ С.Цзя

Старший инженер-технолог
_____ Гурова И.Ю.

Figure C.1 - The industrial checking records

APPROVEMENT
Polargoose Clothing co.,ltd
Director Zhengfa
24 November 2025

APPROVEMENT
Ivanovo State Polytechnic University
Rector Е.Н.Никифорова
November 2025

An act of results verification
obtained in Jia Shuang' dissertation

We, the undersigned Y. Shuifang, pattern technician S. Liping, technologist, from Polargoose Clothing co.,ltd (China), on the one side, and V. Kuzmichev, Head of Clothing Design Department, and S.Jia, graduate student, from IVGPU (Russia), on the other side, have compiled this act after the validation of the results obtained in the dissertation "Development of male raglan coat design process".

Date of verification July 2025 – September 2025.

The object of implementation is the pattern-making technique for male raglan coat.

Implementation conditions are: (1) software of drawing garments (ET, BUYI Technology, China); (2) software of digital twins simulation (Style 3D, Linctex Co., Ltd., China); (3) a fabric type is melton woolen fabric with next fiber content, %: wool - 60, viscose - 20, polyester - 20; (4) the pattern blocks of coat.

The enterprise was provided four raglan coats with different shapes and the ease allowances of chest girth respectively, cm: 12, 16, 20, and 28. All coats have been designed in terms of the developed pattern blocks.

All produced raglan coats were tested by trying on a men with normal morphology and basic sizes, cm: height - 182, chest girth - 100, waist girth - 84. The try-on result shown that due to developed method of pattern-making all coats produced have optimal fit and accurate shapes.

CONCLUSIONS. (1) The developed pattern-making method allows to produce raglan coat with good fit. (2) The outline shapes of coats met the requirement of enterprise, will use to improve the coat design and to get more high level of consumer satisfaction.

From Polargoose Clothing co.,ltd
Y. Shuifang
S. Liping
www.polargoose.com

From IVGPU
V.Kuzmichev
22 S. Jia
www.ivgpu.com

Figure C.2 - The industrial checking records